Synthesis of Phosphino-Triazole Ligands

By

Yiming ZHAO

UNIVERSITY OF BIRMINGHAM

A thesis submitted to

University of Birmingham

for a degree of

DOCTOR OF PHILOSOPHY

School of Chemistry

College of Engineering and Physical Sciences

University of Birmingham

January 2020

Acknowledgement

I am trying to convey my gratitude to all the people who have helped me to reach this stage, and I find this is one of the most challenging task for the entire thesis because I have received tremendous help from many people. I wish to thank all my friends, family, collaborator, who helped me during my PhD study.

Firstly, great thanks to my supervisors during the last four years. My principal supervisor John Fossey has been a great mentor, allowing me to follow my ideas and guide me when I was struggling in my research. And he also offered me fantastic opportunities to visit different research institutes in Japan and China. I always enjoyed the 'one to one' meeting with John to discuss my project, plan for the next move. We generated lots of new ideas during our discussion, and I always appreciated the moments when we came out with some crazy ideas and John said, "This idea looks cool, let's give it a go". He helped me a lot in proofreading of this thesis and also the paper we published together. I will always be grateful for John's guidance and support during my PhD study. Ben Buckley has also been a great supervisor, and I enjoyed discussing my project during the skype call meeting with him. And I must say thank you to Shinichiro Fuse's hospitability for inviting me to visit Tokyo Institute of Technology, and express my gratitude to Shuli You to allow me to join his group for a three-month visiting programme.

A huge thanks to all the people in the Fossey group who I have worked together. You guys are truly amazing, and I am appreciated by having your guys alongside during my PhD study. I would like to thank a few groups in particular. Huy, you are the best Post-

doc I have ever met, you taught me a lot of new synthetic skills and guided me as a big brother in daily life. I would like to thank you for all the practical help, proofing reading of our papers and this thesis. Daniel, thanks for your essential help when I was a master student in the group, and I wish you all the best in your post-doc research in Japan. William, thanks for the initial help for 'triazole' project. Wenlei and Eric, thanks for keeping send me the relative references for my research. Fernanda, you were always a pleasure to work with, I like discussing reaction mechanism with you, even sometimes, it looks like we are shouting each other in lab. Yixin, thanks for your help in some medicinal chemistry project. Alex(Q) and Órla, thanks for your help in proofreading of my thesis. The other members of the group are also fantastic, Akina, Łukasz, Jonathan, Glenn, Harry, it's my honour to have you guys around during my study.

Visiting and master students, even though we only worked together for a while, the contributions you have made must also be acknowledged. Shun, Winter, Lizzie, Mara, Krzysztof, Andy, Nick, Ryan, Eliot, Chiran, Helena, Josh, Alex(C), Tom, Jing, thanks for your company and I wish your guys all the best in future career. I would especially thank three master students. Tom and Nick, thanks for submitting my sample for biological activity test. A massive thanks to Alex(C), thank for you for hardworking in the synthesis of phosphoramidite type ligand, chapter 4 would not be completed without your effect to the story. And I wish you all the best in your industry career.

I would also like to acknowledge all the members in You group in Shanghai Institute of Organic Chemistry and Nakamura-Fuse group in Tokyo Institute of Technology. During my journey in Japan, I received tremendous help from Matsumura san and Takizawa san. Thank you for making me feel at home in Japan. During my time in Shanghai, I

shared the office with Jicheng Yi, Lu Ding, Ping Yang, Zhijie Wu, Ru Zhang, and they are very friendly and patient to me. Also, thanks to Qing Gu, Chao Zheng and Xiao Zhang for looking after me and making me feel at home.

I would also thanks to Davies, Grainger groups for their help with lending me some chemicals and equipment, and big thanks to Matt from Davies group to test my ligand in his work. The members of the analytical facility of UoB are fantastic. I would like to thank Louise Male, for teaching me knowledge of XRD, which allows me to analyse most of crystal structures from this thesis. And Cécile Le Duff for helping with NMR set up. Lianne Hill, Chi Tsang and Peter Ashton for running all my mass specs and elemental analyst sample, especially big thanks to Chi for teaching me how to operate mass specs machine. Chi never turned me down even one a day when I brought 30 MS samples in one day, and I wish you all the best for setting your own company in Hong Kong. Also, big thanks to Allen Bowden for supporting chromatography when I used 15 bottles of HPLC solvent during a weekend.

And I would like to express my gratitude to all the friends I made in Birmingham, I wish I could list all the name, but there are too many so please don't be offended if your name is not here. Bo, Paige, Ana, Elsa, Dennis, Banksy, YiFei, Xiaoyu, Franklin, Ning Ni, thanks for all the effects from you guys.

I would like to say special thanks to Zoey. Thank you for encouraging me when I was in a low mood. Simply I could not achieve to this stage without your support. Thank you for always standing alongside with me.

Finally, I would like to thank you for all the support from my family. Support from the parents is always pivotal for their kids. I would like to convey my gratitude to my aunt Stella and uncle Alex. Thanks for all the supports.

Abstract

The triazole formation *via* click chemistry has remained a hot topic in recent years. This thesis disclosed the synthesis of triazole containing phosphine ligand for catalysts work. Chapter 1 gives a brief introduction of click chemistry and usage of triazole in various area. Chapter 2 outlines a synthetic strategy to generate triazole-containing phosphine ligands. These triazole ligands are derived from diaryl or dialkyl phosphine and show good catalytic activity in Suzuki-Miyaura cross-coupling. The relationship between bulkiness and catalytic activity of ligand unveiled by *SambVca* webtool. Applications of these ligands into lead-like compound preparation has been conducted with satisfactory result. In Chapter 3, phosphine ligands with different number of triazole units are prepared, and the catalytic activity of corresponding ligand-metal complex screened in Suzuki-Miyaura cross-coupling. In addition, corresponding gold complexes of phosphine ligands also been obtained for activity test. Thirteen single-crystal structures were obtained for the bulkiness study of ligand. Chapter 4 has provided three different strategies towards the synthesis of asymmetric version of triazole ligand. And resulting corresponding gold phosphines have been prepared as well for further activity screening.

Abbreviations

$\%V_{bur}$	Percent Buried Volume
aNHC	Abnormal *N*-Heterocyclic Carbene
Ar	Aryl
BINAP	2,2'-Bis(diphenylphosphino)-1,1'-binaphthyl
BINOL	2,2'-Dihydroxy-1,1'-binaphthyl
Bn	Benzyl
Boc	*tert*-Butoxycarbonyl
Bpy	Bipyridine
Btz	Bis-triazole
calc.	Calculated
CAN	Ceric Ammonium Nitrate
CF	ClickFerrophos
conv.	Conversion
CuAAC	Copper-Catalysed Azide-Alkyne Cycloaddition
Cy	Cyclohexyl
DCM	Dichloromethane
DFT	Density Functional Theory

DG	Directing Group
DMSAuCl	Chloro(dimethylsulfide)gold(I)
Dtzpy	Ditriazole-pyridine
ee	Enantiomeric Excess
equiv.	Equivalents
ESI	Electrospray Ionisation
EtOAc	Ethyl acetate
FBBD	Fragment-Based Drug Discovery
FBLD	Fragment-Based Lead Discovery
et al.	et alia
GC	Gas Chromatography
GSK	GlaxoSmithKline
h	hours
Hex	Hexane
HOMO	Highest Occupied Molecular Orbital
HPLC	High-Performance Liquid Chromatography
ICIQ	Institut Català d'Investigació Química
*i*Pr	Isopropyl

L	Ligand
LEEC	Light-Emitting Electrochemical Cell
LLAMA	Lead Likeness And Molecular Analysis
LUMO	Lowest unoccupied molecular orbital
M	Metal
Me	Methyl
MeOH	Methanol
min	minutes
mol	Moles
m.p.	Melting Point
MW	Microwave
NaAsc	Sodium Ascorbate
*n*Bu	Butyl
NHC	N-Heterocyclic Carbene
NiAAC	Nickel-Catalysed Azide-Alkyne Cycloaddition
NMR	Nuclear Magnet Resonance
obs.	Observed
OLED	Organic Light-Emitting Diode

PDB	Program Database
PMI	Principal Moments of Inertia
Ph	Phenyl
PPh_3	Triphenylphosphine
Pytz	Pyridine-triazole
ppm	parts per million
R	Rectus
rac	Racemic
rt	Room Temperature
RuAAC	Ruthenium Catalysed Azide Alkyne Cycloaddition
s	second
SAR	Structure-Activity Relationship
SIOC	Shanghai Institute of Organic Chemistry
SMC	Suzuki-Miyaura Cross-coupling
TBTA	Tris[(1-benzyl-1*H*-1,2,3-triazol-4-yl)methyl]amine
*t*Bu	tertiary-Butyl
TEA	Triethylamine
Tf	Triflate

THF	Tetrahydrofuran
TLC	Thin Layer Chromatography
TMS	Trimethylsilane
TOF	Time-Of-Flight
TON	Turn Over Number
Tol	Tolyl
Tpy	Terpyridine
UoB	University of Birmingham
UV	Ultraviolet
VT	Variable Temperature
XRD	X-ray Powder diffractometry

Contents

1. Chapter 1 Introduction

1.1 Click Chemistry

Sharpless defined the concept of click chemistry as a series of synthetic methods, with the reaction process being *modular, high yielding, wide in scope*.[1] Besides, it has been postulated by Sharpless that click chemistry should give high yielding product, and reaction could be achieved under non-demanding conditions with non-toxic solvents such as water, and byproducts could be easily removed from the reaction system.[1] Click chemistry also has been widely used in various areas such as pharmacological,[2] biology-oriented synthesis[3] and proteomic applications.[4] Due to these features, click chemistry has become increasingly popular and with several published paper remains an upward trend during the period of 2003-2018.

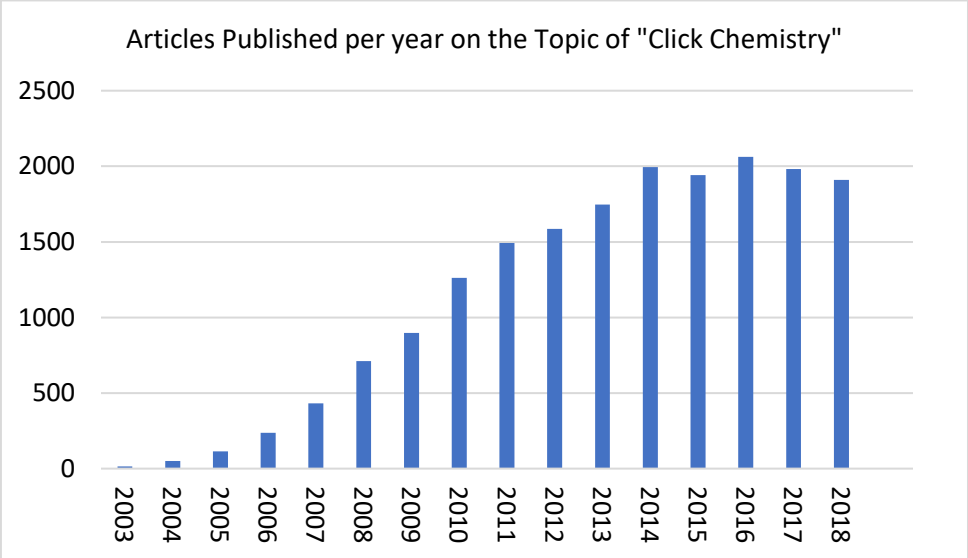

Figure 1. Papers published on the topic of "click chemistry" in the period 2003-2018 (Data from Web of Science, 2019)

As one of the most reliable reactions for making carbon-heteroatom-carbon bonds in aqueous conditions, click chemistry is widely used in a variety of chemical and

biological applications.[1] It is essential to recognise that a high thermodynamic driving force, usually greater than 20 kcal mol^{-1}, is a crucial feature for click reaction to achieve these characteristics, such as rapid process to reaction completion and highly selective for a single product.[1]

One feature of click chemistry is expanding a set of powerful, modular "blocks" that work reliably in both small- and large-scale applications.[1] It has been reported that click chemistry can provide quick access to a large library of compounds and used for high throughput screening, dynamic templated-assisted strategies and fragment-based drug discovery.[5] In addition, click chemistry also has been used in supramolecular chemistry. Fokin *et al.* developed an efficient method to deliver a series of dendrimers *via* click chemistry in high yield and purity with potential metal-binding ability.[6] Additionally, there has been significant progress in using click chemistry in detection, localisation and qualification of biomolecules.[7] Click chemistry provides a modular way to build up complex molecular architecture. These convenience features and reproducibility has led to the overwhelming popularity of click chemistry over recent years.[8]

1.2 Type of Click Reactions

1.2.1 Nucleophilic opening of strained rings.

Molecules contain strained ring systems are high-energy species and could be converted into the corresponding product readily. Sharpless summarised the ring-opening reaction of strained ring molecules such as epoxides **1**,[9] aziridines **2**,[10]

episulfonium ions **3**,[11] cyclic sulphates **4**,[12] cyclic sulphonamides **5**,[13] aziridinium ions **6**,[14] are reliable, stereospecific with nearly quantitative yields (Scheme 1).[1] Due to the stereoelectronically disfavoured competing elimination processes, nucleophilic openings of three-membered rings can be obtained with high yield after simple purification method such as distillation or recrystallisation.[15] Ring-opening reactions with substrates present in Scheme 1 could be conducted in the absence of solvents or just in a solution of alcohol and water.[1]

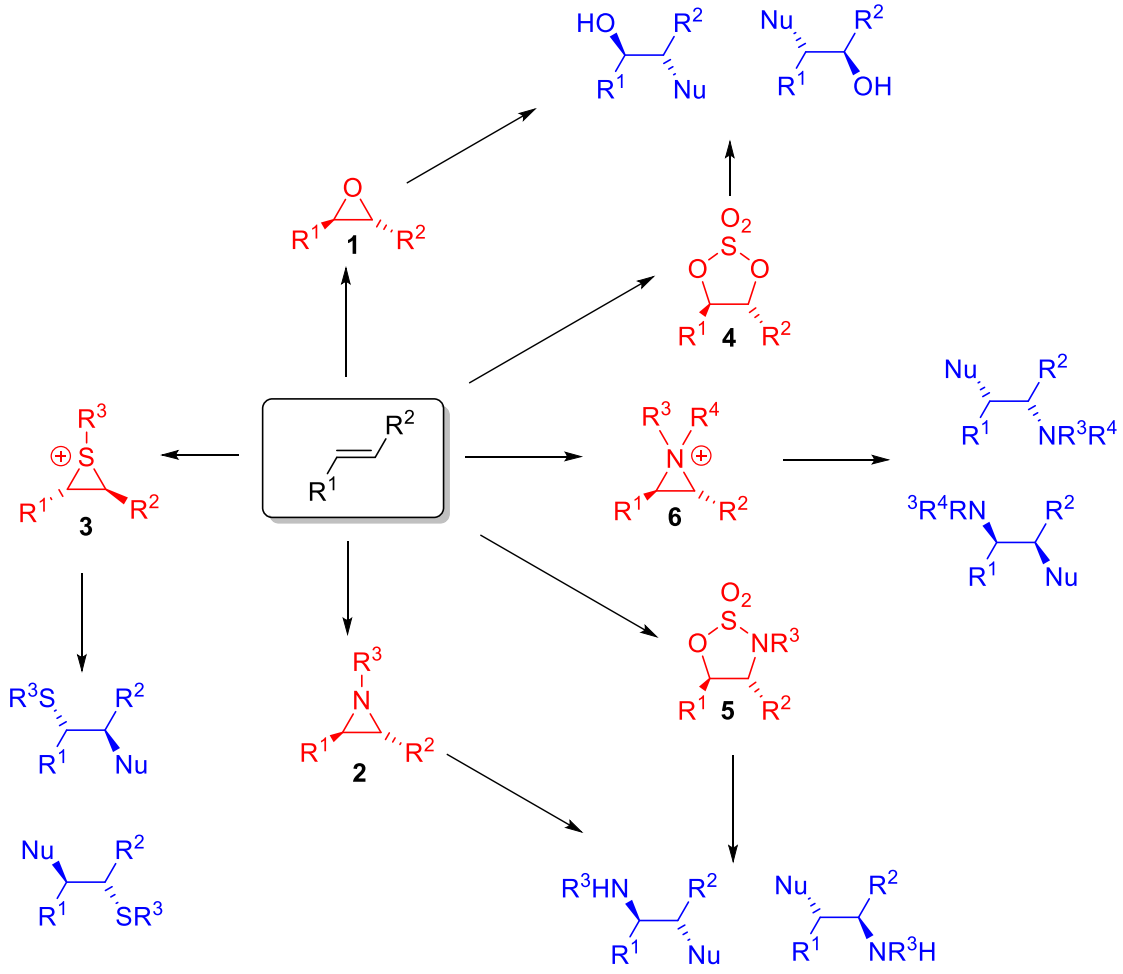

Scheme 1 Generation and ring-opening reaction with molecules containing strain-system(shown in red) and corresponding ring-opening product (shown in blue)[1]

1.2.2 "Protecting Group" Reactions

Acid-catalysed reactions with aldehydes and ketones can provide cyclic 1,3-dioxolane rings in high yields.[1] Instead of common roles as a diol protecting group, Sharpless argued that formation of acetals, ketals, and some of their aza-analogues should be part of click reactions, as they can afford biologically relevant heterocycles that readily appear as critical components in medicinal chemistry.[16] Bioavailability of these molecules can be important as these molecules are stable at physiological pH, have already emerged as components in orally available drugs.[17] These three acetal-like derivatives (**7-9**) are easily prepared in multi-gram scales from corresponding diols and hydroxysulfonamides.[1] Interestingly, due to inductive effects from substituted heteroatoms, these compounds are remained stable in standard acid hydrolysis conditions, all the more so if the azide group is reduced to the amine. Thus, the saturated dioxolane cores are regarded as a new permanent element of structure under most physiological conditions. Besides, these transformations could contribute several hydrogen bond acceptor sites and interesting dipole effects, provide constrained scaffolds with well-defined projections and spatial orientations of their substituents. [1] Sharpless defined these reactions represent one of the rare click chemistry modules based on reversible carbonyl chemistry.[17]

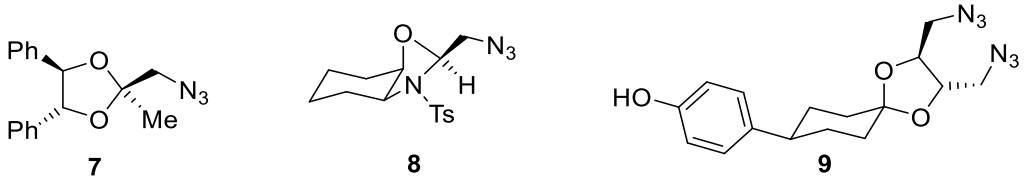

Figure 2. Selected example of acetal-like derivatives

1.2.3 Cycloaddition Reactions

The ideals of click chemistry are perfectly represented among cycloaddition reactions, such as hetero-Diels-Alder reactions and, especially, 1,3-dipolar cycloadditions. These reactions involve the fusion of two unsaturated components and provide a quick way to access a diverse library compounds of five- and six-membered heterocyclic compounds.[18]

The Huisgen dipolar cycloaddition of azides and alkynes has been regarded as the "cream of the crop" in this powerful class of click reactions.[1] In addition, the azide group is one of the most convenient of the 1,3-dipolar components to introduce and to "carry" until needed.[1] It can be introduced from an amino group *via* nucleophilic substitution. What makes azides unique for click chemistry is the extraordinary stability toward water, oxygen, and the majority of organic synthesis conditions.[19] Thus, with the various functionalities displayed by unsaturated components, the Huisgen dipolar cycloaddition provides a robust method for the creation of combinatorial libraries, which can significantly benefit to medicinal chemistry.[1, 20]

1.3 Triazole formation from cycloaddition

The azide-alkyne Huisgen cycloaddition is a 1,3-dipolar (2+3) cycloaddition between an azide and a terminal or internal alkyne to yield 1,5- or 1,4- disubstituted 1,2,3-triazole (Figure 3, **10**, **11**) as products. The scope of this reaction was firstly understood by the Rolf Huisgen.[21] And Sharpless has referred this reaction as "the premier example of a click reaction."[22]

Figure 3. 1,5- or 1,4-disubstituted triazole

1.3.1 Thermal azide-alkyne cycloaddition

The azide-alkyne cycloaddition could be carried out under just thermal conditions without solvent. Heating of azide **12** and alkyne **13** in the absence of solvent can lead to the triazoles mixture of 1,5- and 1,4- regioisomers **10, 11**. This thermally promoted cycloaddition shows very poor regiochemical control, with a 1.2:1 mixture of 1,5- and 1,4-regioisomers respectively when phenylacetylene and azidobenzene are the starting material **(**Scheme 2**)**.[23] This effect due to the HOMO-LUMO energy gap of the two possible regiochemical intermediates being too close to achieve selectivity. In the case of using propargylaldehyde diethyl acetal, the ratio of the product is 2.2:1 mixtures of regioisomers with 1,4-substituted as the major species. This reaction outcome may also be based on the opposing effects of electronic and steric factors.[23, 24] Furthermore, since the difference between HOMO-LUMO energy levels for the azide and alkyne are of a similar magnitude, and these cycloadditions are controlled under both dipole-HOMO- and dipole-LUMO pathways. As a result, a mixture of regioisomer of triazole product is usually isolated when an unsymmetrical alkyne is used as the starting material.[25] Even this reaction is highly exothermic, but the high activation energy barrier is responsible for low reaction rate.[19]

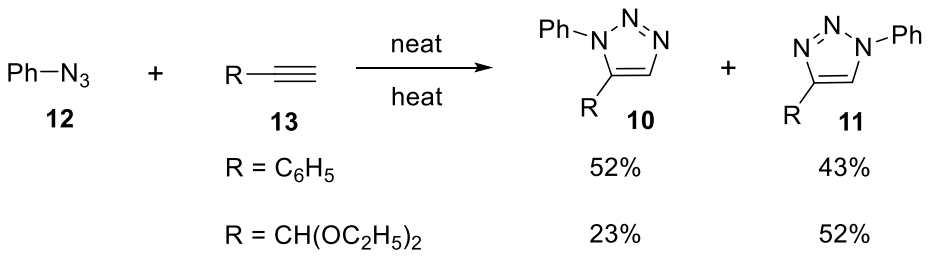

Scheme 2 Thermally promoted azide-alkyne cycloaddition

Although the thermal azide-alkyne cycloaddition shows low regioselectivity, this methodology has still been used in a variety in biological applications, mainly in strained-promoted conditions and where regioisomeric control is not crucial, or substrates are symmetric.[26-29] Thus, the thermal azide and alkyne cycloadditions typically use symmetric alkynes to avoid regioselectivity. In this respect, the classic 1,3-dipolar cycloadditions are not fulfilling the criteria of the click reaction.

1.3.2 Regio-selective triazole formation

Switching the regiochemical outcome is one of the challenging tasks in the formation of carbon-heteroatom bonds. It is important to impart a high-level regiocontrol to the azide-alkyne Huisgen cycloaddition, with ideal atom economy.[30] And there are various success examples of regioselective triazole formation. (Scheme 3).

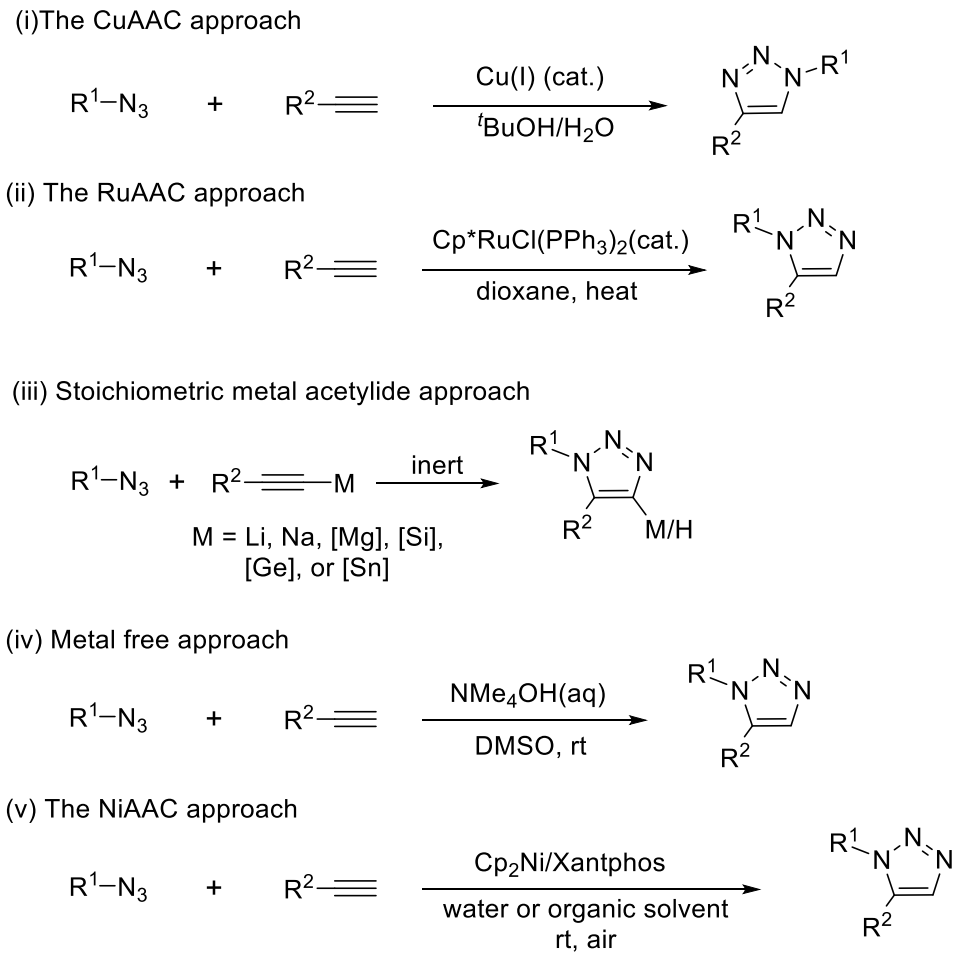

Scheme 3. Selectively triazole formation. (i) Copper catalysed 1,4-triazole formation.[19, 31] (ii) Ruthenium catalysed 1,5-triazole formation.[25] (iii) 1,5-Triazole formation with stoichiometric metal acetylide reagents.[32-34] (iv) Base catalysed 1,5-triazole formation.[35] (v) Nickel catalysed 1,5-triazole formation.[36]

Rapid and regioselective synthesis of 1,4-triazoles has been accomplished by the copper-catalysed azide-alkyne cycloaddition (CuAAC), since the first reported by Sharpless and Meldal. (Scheme 3, (i)).[19, 31]This transformation proceeds not only in organic solvents but also in aqueous media at room temperature. The CuAAC reaction is complemented by the ruthenium-catalysed azide-alkyne cycloaddition (RuAAC) and nickel-catalysed azide-alkyne cycloaddition (NiAAC) reaction, which provides 1,5-triazoles regioselectively (Scheme 3, (ii), (v)).[25] The catalytic CuAAC and RuAAC extended the catalytic activity of metal acetylides with azides. Thus, lithium,[32]

sodium,[32] magnesium,[32] zinc,[33] silicon,[34] germanium[34] and tin[34] acetylides can undergo reactions with azides group to afford 1,4,5-trisubstituted triazoles with metal/metalloid located at the 4-position. Subsequent aqueous quenching can lead to 1,5-triazole formation (Scheme 3, (iii)). A metal-free protocol employing catalytic tetraalkylammonium hydroxide in DMSO also affords 1,5 triazoles exclusively, and is not sensitive to atmospheric oxygen and moisture (Scheme 3,(iv)).[35] Hong *et al.* developed the nickel-catalysed azide-alkyne cycloaddition to access 1,5-triazoles at room temperature. The combination of a Cp_2Ni precatalyst and Xantphos ligand were critical to accomplish the catalytic manifold under atmospheric environment.[36]

1.3.2.1 Formation of 1,4- triazole *via* CuAAC

As mentioned above, a highly regioselective copper-catalysed Huisgen azide-alkyne cycloaddition reaction between azide and alkyne, also known as CuAAC-reaction, independently reported by Meldal[31] and Sharpless[19], can form 1,4-triazoles with simple purification. The introduction of copper(I) catalyst dramatically decreases the activation energy required to form triazole product compared with thermal promoted pathway; thus CuAAC features an enormous reaction rate acceleration, from 10^7 to 10^8.[37] In addition, CuAAC could be conducted at near neutral pH values and very forgiving condition which does not require extra precautions such as exclusion of moisture and oxygen. In other words, CuAAC is a robust catalytic process, and insensitive to usual reaction parameters.[6]

Despite the ubiquitous nature of the CuAAC, the mechanism of this reaction has been widely debated since it discovered. After density functional theory (DFT) calculations, Sharpless *et al*. proposed the first mechanism of CuAAC in 2004 (Scheme 4).[19] It starts with the formation of copper acetylide species **14** from terminal alkyne **13** (since no reaction can be observed with internal alkynes). After the formation of copper acetylide **14**, the nitrogen from the azide also coordinate to the same copper centre to form intermediate **15**. This is followed by reductive elimination of the six-membered metalacyclic transition state of **16** to form the metal-triazole complex **17** and subsequent protonation to release triazole **11** and regeneration of catalyst.

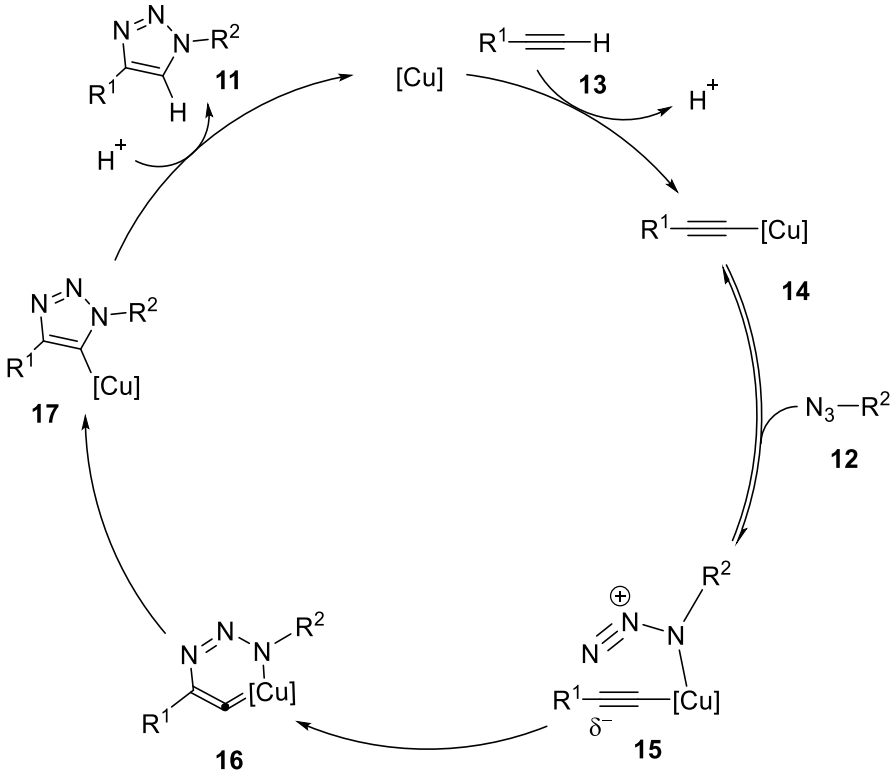

Scheme 4. First proposed mechanism of CuAAC, with a single catalytic active copper centre[19]

By calculating the energies of transition states during cycloaddition and isotope enrichment studies, Worrell *et al.* proposed a revision of the catalytic cycle with the

incorporation of multiple copper atoms in the catalytic process (Scheme 5).[38] First, a copper centre coordinate in a π-fashion with alkyne **18**, followed by formation of a copper acetylide **19**. Then nitrogen of the azide **12** binds to dinuclear copper species **19** forming a metalacyclic intermediate **21**. At this stage, as there is no bias which copper eliminates from the catalytic cycle to form triazolide **17**. Finally, with the protonation of **17** to release triazole product **11** and the regeneration of the copper catalysts.

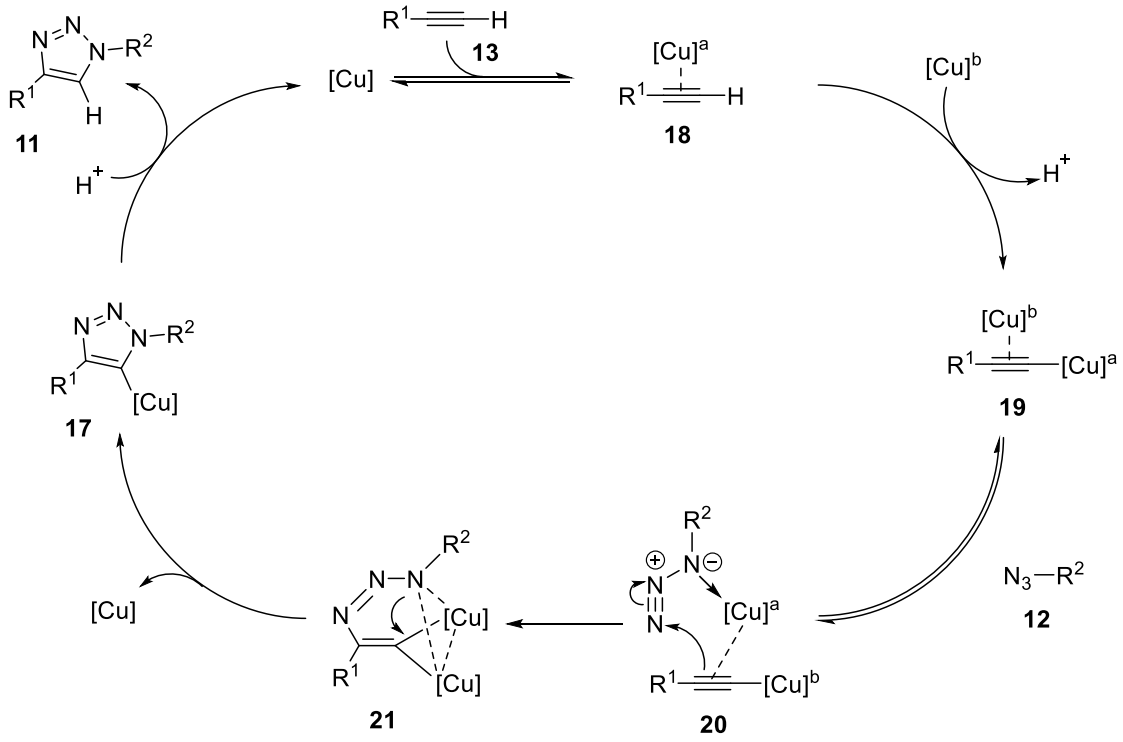

Scheme 5 Proposed catalytic cycle for the CuAAC with dinuclear copper[38]

In addition, dinuclear copper intermediates have been detected *via* mass spectrometry for the first time by Lacobucci *et al.* in 2015.[39] Further mechanistic study of CuAAC has been conducted by Bertand *et al.,* as dinuclear copper NHC coordinated alkyne intermediate has been successfully isolated and analysed in XRD (Figure 4).

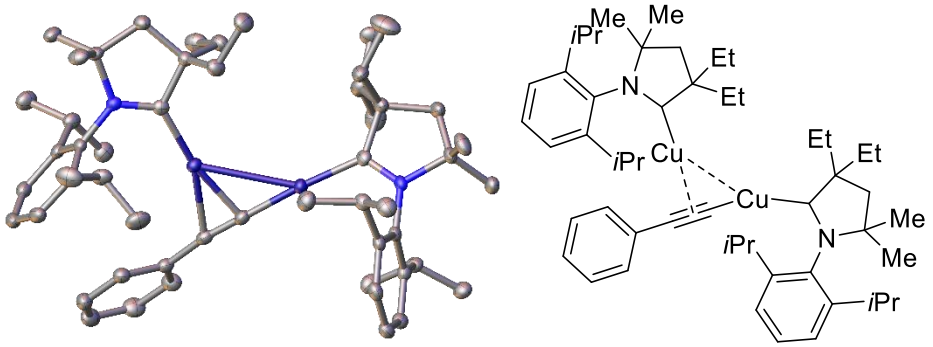

Figure 4. Single crystal structure of a dinuclear copper NHC coordinated terminal alkyne, a proposed intermediate specie from CuAAC.[40] Ellipsoids are drawn at the 50% probability level, protons and anion are omitted for clarity.

Bertrand hypothesises that both mono-and bis-copper pathways are both active in the CuAAC catalytic cycle. However, the bis-copper pathway is much more kinetically favoured.[40] Using the stable NHC copper acetylide intermediates, the mono- and bis-copper acetylide complexes **26** and **22** were isolated by Bertrand *et al.*, which helped confirm the previously proposed dinuclear pathway of the catalytic cycle. The two copper acetylides **26** and **22** were used in stoichiometric amounts to react with benzyl azide. Both reactions proceeded and formed triazole **11** as a product, but a significantly different reaction rate has observed during the process. Thus, a new catalytic cycle is proposed, featuring both possible mono and multinuclear pathways, with superior catalytic activity of the binuclear complex **22** over **26** during the catalytic process (Scheme 6).[40]

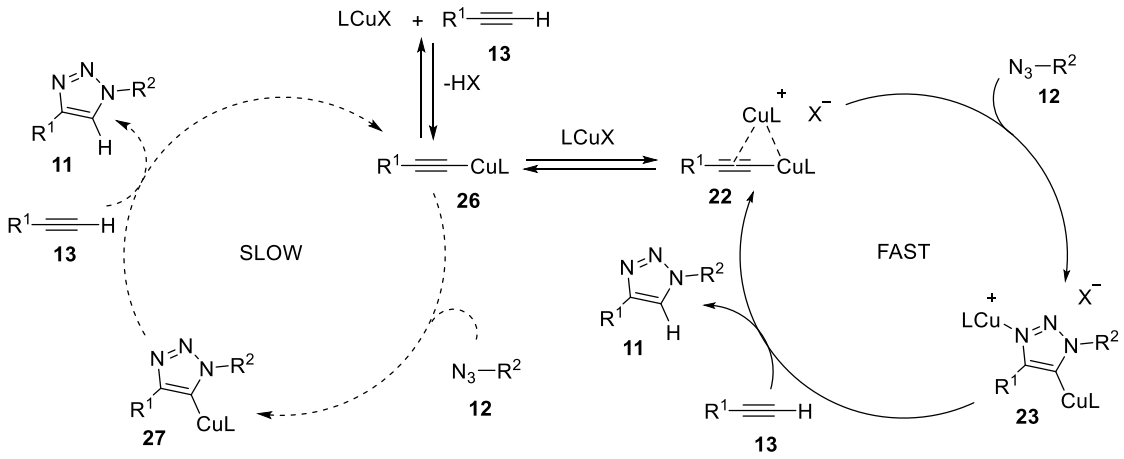

Scheme 6. Proposed CuAAC catalytic cycle by Bertrand *et al.*, with multinuclear pathways followed on kinetic grounds.[40]

In summary, CuAAC provides a robust method to access 1,4-disubstituted triazoles under mild conditions. Considering the complexity nature of copper acetylides,[41] there is still much investigation carried out to elucidate the CuAAC mechanism fully.

1.3.2.2 Formation of 1, 5-triazole

While using copper(I) catalyst provides a reliable method to prepare 1,4-disubstituted triazoles, a general method for the preparation of 1,5-disubstituted triazoles by the reaction between the stoichiometric amount of metal acetylides with azide are well documented.[32-34] The acetylene and azide group are found at the 1, 5 positions, with metal/metalloid located in the 4-position of triazole. [32]

The proposed mechanism (Scheme 7) starts with the nucleophilic attack from magnesium acetylide **28** to the terminal nitrogen of azide **12**, followed by spontaneous ring closed reaction from linear intermediate **29** to yield 4-metallotriazole species **30**. The 1,5-disubstituted triazoles **31** formed after hydrolysis of **30**. Most reactions furnished 1,5-disubstituted triazoles at room temperature after overnight reaction

with quantitative yields without purification since side-product crashed out from the organic phase. Besides, halomagnesiotriazole intermediates **30** also can undergo reactions with suitable electrophiles, resulting in a regioselective way to furnish 1,4,5-trisubstituted triazoles.[33]

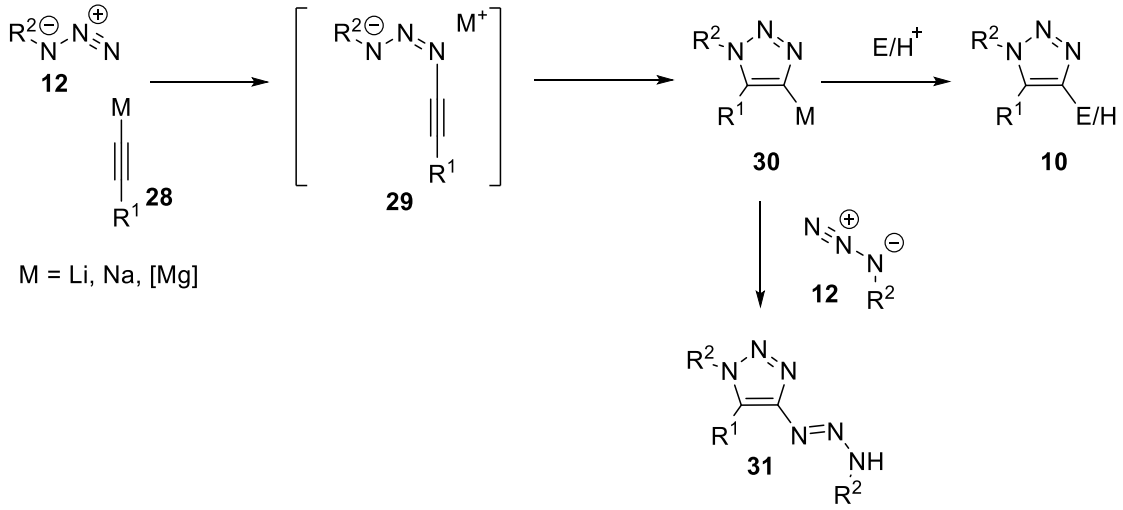

Scheme 7. Proposed mechanism 1,5-triazole formation *via* metal acetylides.[32]

The limitation of this magnesium acetylide method is the substrate scope. Electron poor azides are required to improve the reaction rate, an observation consistent with the proposed nucleophilic attack of the acetylide on the azide. Halomagnesiotriazole intermediates **30** can react with another equivalent of azide **12**, resulting in hydrolysis to form byproduct **31**.[32]

With considerable limitations of magnesium-acetylide method triazole formation, Fokin *et al.* disclosed a more robust approach to prepare 1,5-disubstituted triazole, catalysed by [Cp*RuCl] complexes.[25] Furthermore, by contrast to the CuAAC, this ruthenium-catalysed process, also referred to as RuAAC, can also engage with internal

alkynes in the catalytic cycle, thus provides a method to access 1,4,5-trisubstituted triazole.

A proposed mechanism of RuAAC is presented in Scheme 8. The replacement of the spectator ligand from **32** produces activated complex **33**. Followed by oxidative coupling of azide and alkyne to convert to the ruthenacycle **34**, which is the key step to control the regioselectivity of the overall process. The new C-N bond trends to be more easily formed between the more electronegative and less sterically-demanding nitrogen from the azide and carbon of the alkyne. Reductive elimination of **34** forms metal-triazole complex **35**. Triazole product **10** is then released with the regeneration of the catalyst **32**.[25]

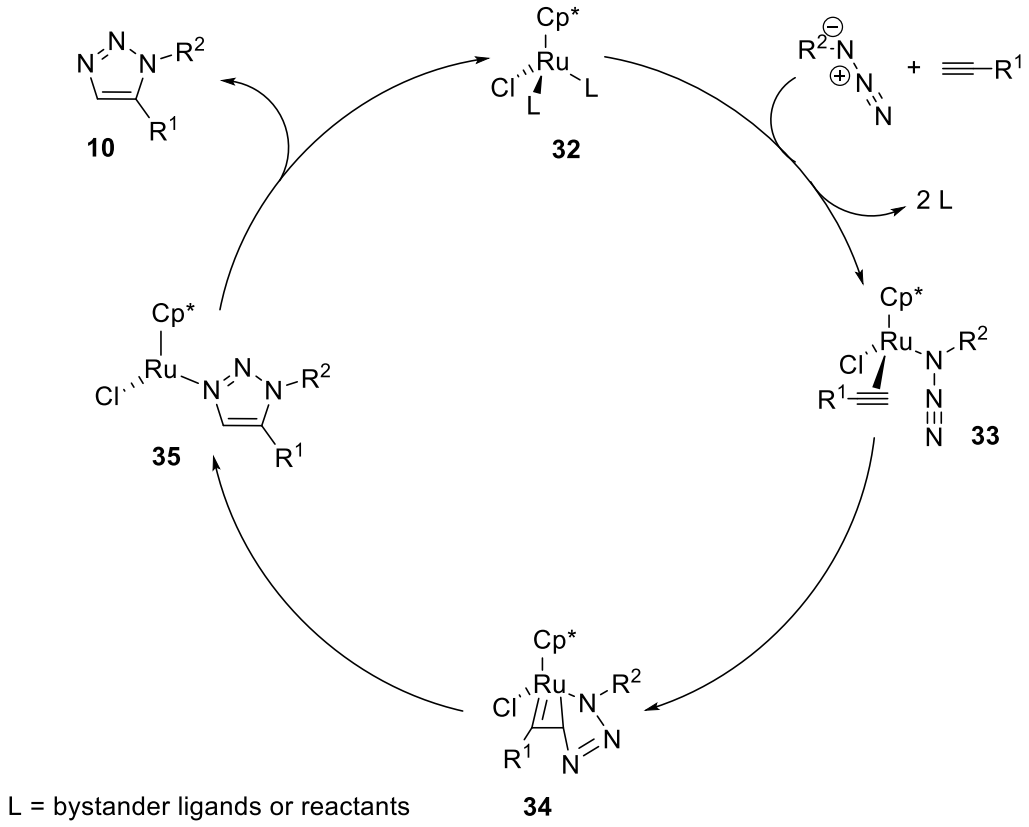

Scheme 8 Proposed RuAAC catalytic cycle[25]

In summary, an irreversible oxidative coupling is involved in the process of RuAAC, then followed by a reductive elimination as the rate-determining step. This RuAAC overcomes the limitations of metal acetylide method to access 1,5-disubstituted triazole and can tolerate a variety of functional group form organic azide and terminal alkynes. However, the RuAAC reaction using [Cp*RuCl] complexes are typically sensitive to moisture, and reaction only proceeds at elevated temperatures. Also, regioselectivity relied on the bulkiness of ligand applied.[42]

Fokin and co-worker reported a base-catalysed approach to synthesise 1,5-triazole without using transition metal, with the proposed mechanism in Scheme 9. The reaction starts with reversible deprotonation of terminal alkyne then generate acetylide, which acts as a nucleophile to attack the terminal nitrogen in the azide unit. Followed by the either *6π*-electrocyclization or *5-endo*-dig cyclisation to form 1,5-triazolyl anion which completes the catalytic cycle by deprotonation a molecule of DMSO, terminal alkyne, or water. This reaction provides mild, transition-metal-free condition to prepare 1,5-triazole, but low conversions of product are observed with steric demanding substrate and alkyl acetylenes.[35]

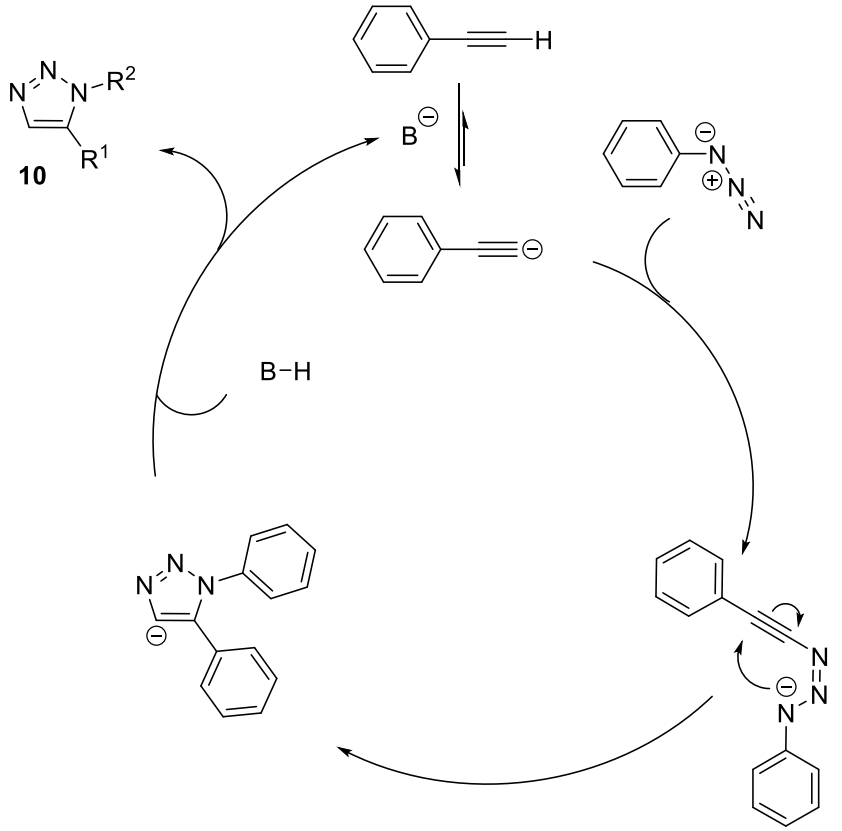

Scheme 9. Proposed intermediates in the base-catalysed synthesis of 1,5 triazoles[35]

Hong *et al.* developed a strategy to access 1,5-triazole by the nickel-catalysis. This nickel-catalyse azide-alkyne cycloaddition (NiAAC) method can tolerate with functionalisation of carbohydrates and amino acids in water and room temperature.[36] The proposed mechanism listed in Scheme 10. Alkyne and azide coordinate to Ni by changing the spectator ligands (Cp and Xantphos) bonding mode. Analogous to the RuAAC pathway, the new C-N bond formation between alkyne and azide to give nickelacycles intermediate to determine 1,5-regioselectivity. Subsequent reductive elimination leads to the formation of 1,5-triazole while regenerating NiL_n for new catalytic cycle.[36]

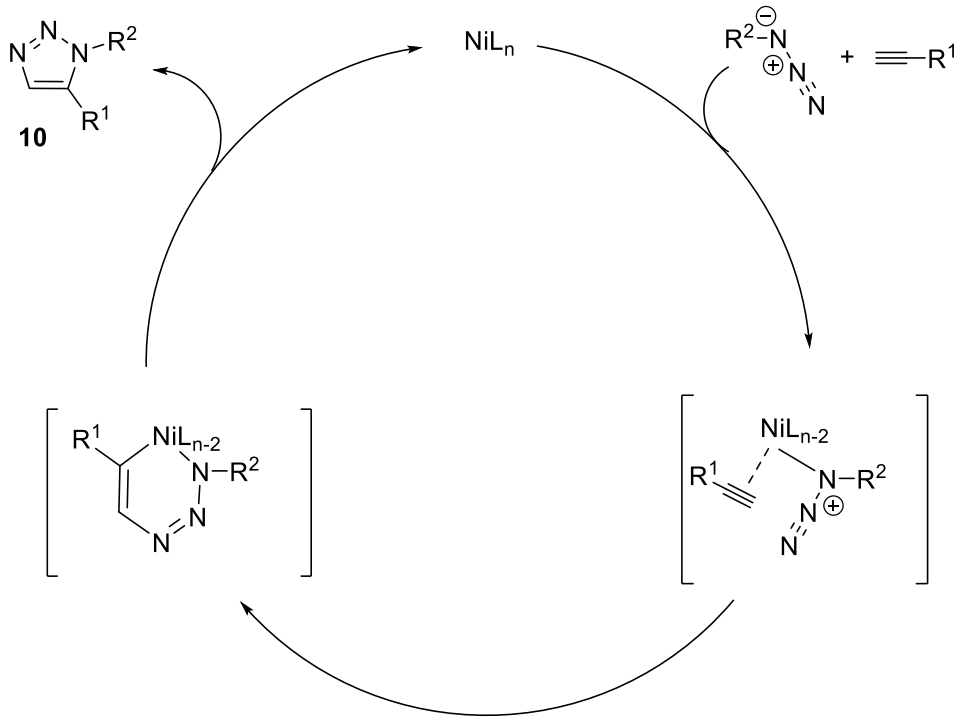

Scheme 10. Tentative reaction mechanism of the NiAAC

1.4 Application of Triazole

CuAAC, as part of click chemistry, is a modular synthetic method to construct carbon-heteroatom bonds. The triazole product from this robust approach has been widely used in most areas of modern chemistry, including drug discovery and material science.[1] All proteins are consists of 20 amino acids *via* heteroatom linkages; besides, following natures lead, CuAAC provides a method by joining small molecules together through heteroatom.[1] In addition, due to the reliability, biocompatibility and regiospecific, CuAAC has become as one of the gold standards of click chemistry.[43]

1.4.1 Triazoles in medicinal chemistry

Sharpless *et al.* applied triazoles as a linkage assembling tool in the femtomolar inhibitor in 2002.[44] Unlike classical linker strategies which can react in an undesired

way under biochemical systems, and triazole are generally compatible with enzymes under physiological condition, which can provide diverse organic building tool.[45]

As 'click reaction' can be achieved in aqueous condition, the potential for facile functionalisation under biomolecular environment has been realised. As a result, various biomolecules including peptides, proteins, DNA, oligosaccharides and glycoconjugates have been labelled with multiple appendages for the exploring biological system.[43]

Carell *et al*. applied click chemistry into high-density functionalisation of modified DNA, with alkyne modified uridine nucleosides **36** and **37** (Figure 5). These studies show that high-density functionalisation of oligodeoxyribonucleotides is made possible by applying the concept of click chemistry.[46] Azides **38-40** are chosen for conjugation. Azido-sugar **38** is used for selectively silver staining, while coumarin contained azide **39** can only emission fluoresces after triazole formation.[47] Fluorescein azide **40** is widely used in biophysical application due to the strong fluorescent.[48]

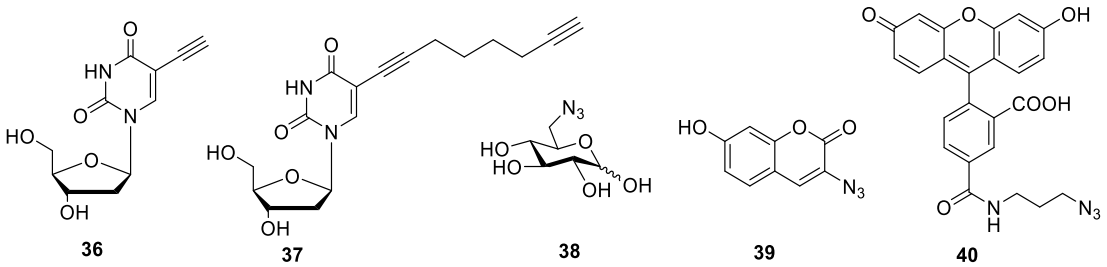

Figure 5. Modified nucleoside and azide labels in DNA study[46]

Lautens *et al*. reported a robust, general method to prepare 1,4,5-trisubstituted 5-acyl-triazoles (Figure 6), which involves a CuAAC triazole formation followed by an intramolecular acylation onto a carbonyl chloride. This domino process can be achieved

in a mild condition with high yield, and directly applied to the synthesis of a series of highly functionalised pharmaceutically related compounds with triazole scaffold.[49]

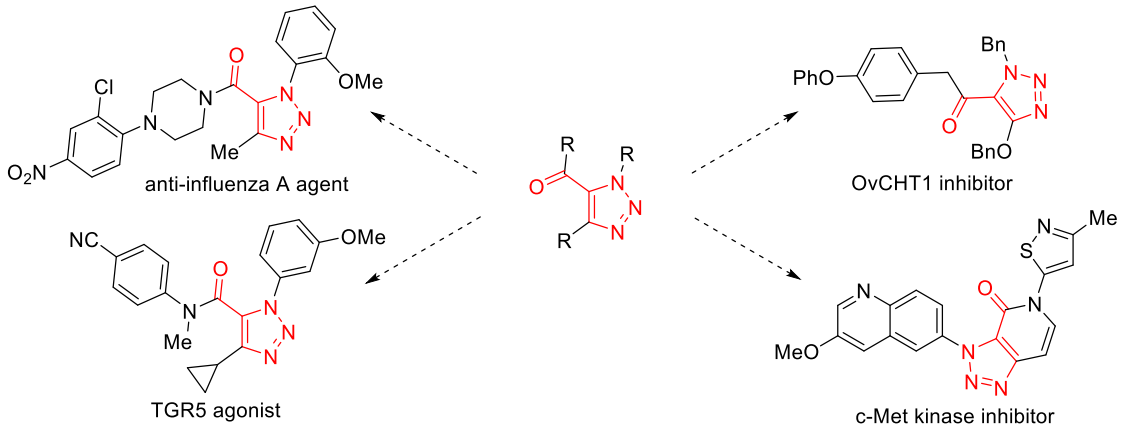

Figure 6. Selected 5-acyl triazoles which display bioactivity.[49]

Artemisinin and quinoline derivatives are the two main classes of antimalarial drugs. Tsogoeva *et al.* combined these privileged antimalarial scaffolds and synthesised a series of artemisinin-quinine hybrid compounds. (Figure 7). They reported these hybrid compounds exhibited potent antimalarial activity in a nanomolar to picomolar range against chloroquine/multidrug-resistant parasite strains, which provide a new strategy to multidrug resistance malaria treatment.[50]

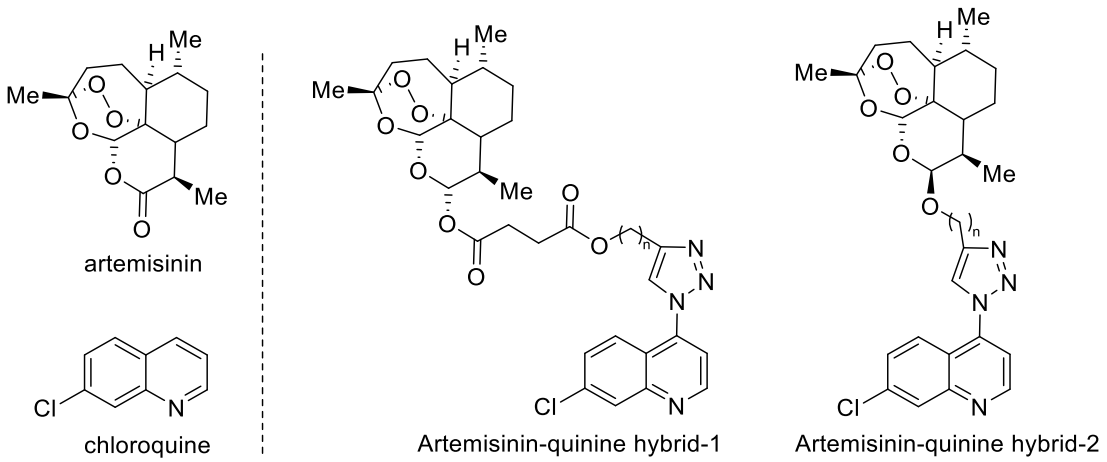

Figure 7. Selected hybrid artemisinin-quinine with anti-malaria activity[50]

In addition, CuAAC has become a key method in Fragment-Based Lead Discovery (FBLD), also known as Fragment-Based Drug Discovery (FBDD). It is desired to find a lead-like compound which can benefit from the early phase of drug discovery. FBDD focused on identifying organic molecules with low molecular weight and small in size and possess biological activity towards the target (even with a weak activity). New molecules were derived from these fragments or combining these fragments to achieve higher affinity to the target. Click chemistry widely used in FBDD by jointing two fragment molecules together *via* triazole linkage for further biological study.[5] As mentioned earlier in (Figure 7), this is one of the examples of click chemistry used in FBDD. Besides, a range of protein phosphatase inhibitors with varying targets, have been synthesised *via* this method.[51-53] There are also a range of antitumor agents that have been developed using click linkage techniques (Figure 8).[54-57] Compound **41** is the derivative of Etoposide, showed significant cytotoxicity, selectively against some human cancer cell lines.[54] Compound **42** is a bidentate inhibitor, where the molecule interacts with two different binding sites of the same target. Compound **42** is identified as protein tyrosine phosphatase (PTP) inhibitor, which contains *N*-phenyloxamic acid as a core group for

primary binding with PTP1, and aromatic rings with different polarity as potential peripheral group for PTP binding.[55, 56] Compound **43,** derivatised from oxazolidinone antibiotic and coumarin acid, is successfully used for live bacterial cell imaging. The widespread using triazole as linkages show the power of click chemistry in FBDD.[57]

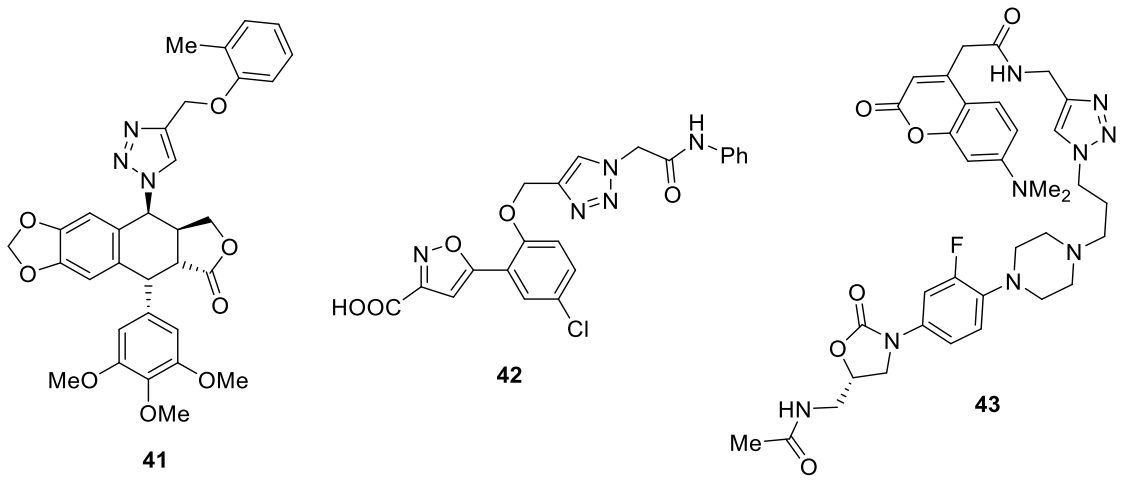

Figure 8. Antitumor and antibiotic agents developed via triazole linkage

1.4.2 Triazoles in material science

Triazoles have also been found in many applications outside of medicinal chemistry. It has been applied in the synthesis of rotaxanes. Leigh *et al.* reported metal-templating pathway to produce rotaxane (Scheme 11). A stoichiometric amount of copper is used with 94% isolated yield of rotaxane [58]

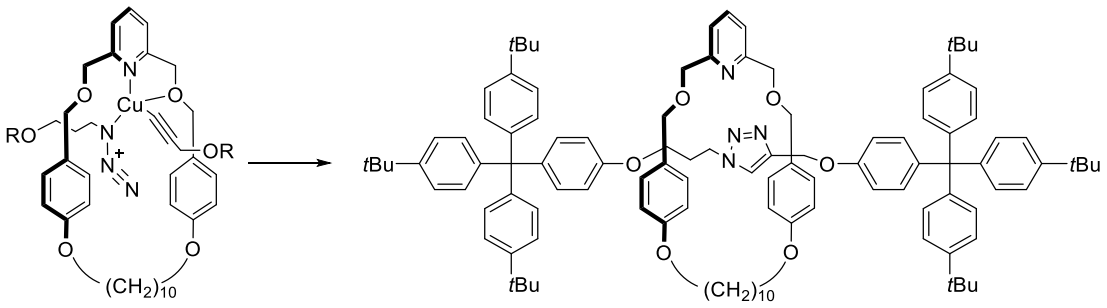

Scheme 11. Copper templated synthesis of a rotaxane compound.[58]

In addition, triazole motif can be applied as directing group (DG) due to the Lewis basic nitrogen, which upon coordination with the metal catalyst can lower the energy barrier for the cleavage of the specific C-H bond.[59] Generally, these processes include the formation of a thermodynamically stable five- or six-membered metallacycle intermediate and allows for the selective activation of its proximal ortho C-H bond. Ackermann *et al.* introduced the triazole motif as a modular and practical directing group in the field of C(sp^2)-H arylation for the first time. The usage of the ruthenium catalyst can achieve C-H arylation regio-selectively in the aryl ring by selectively activated the C-H bond(H_b in Scheme 12).[60] Meanwhile, use of Pd or Cu catalyst can lead to the functionalisation in triazole ring, forming C-5 aryl-substituted product through an electrophilic-activation-type pathway (H_a in Scheme 12).[61-63]

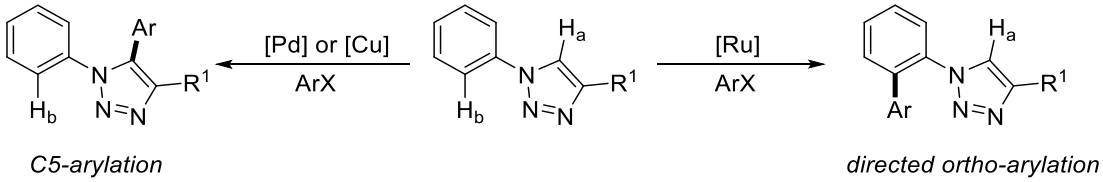

Scheme 12. Regioselectivity of direct arylation in 1-aryl 1,2,3-triazoles[64]

Click chemistry has been applied to the fashionable field of nanotechnology (Figure 9, **A**). Andronov *et al.* reported high functionalised single-walled carbon nanotubes (SWNTs) with well-defined polystyrene *via* click chemistry. These materials exhibited high solubility and stability in the aqueous and organic solution.[65] Triazolo cage (Figure 9, **B**) was designed by Liu *et al*. in 2019. It possessed very strong high attomolar-affinity (10^{17} M^{-1}) which can extract chloride ion from water into DCM solvents.[66]

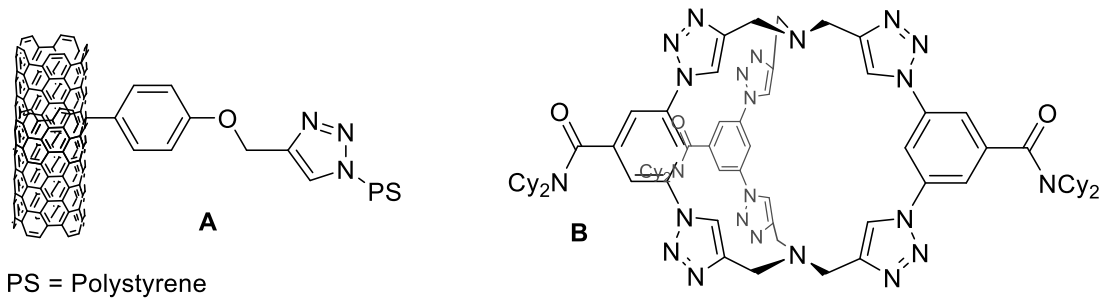

Figure 9.Click chemistry in material chemistry. (A) Triazole as linkage in the functionalisation of carbon nanotubes; (B) Triazolo cage as chloride trap.

Dendrimers are repetitively branched of synthetic molecules and received much attention in medicinal and material chemistry. But the major problem in the preparation of dendrimers is purification, mainly due to the loading side reaction from monomer. Fokin et al. published the first dendrimer preparation via click chemistry with a variety of functional group and high isolate yield. Purifications are greatly simplified due to the absence of side products.[67]

Boronic acid-mediated saccharide sensing has shown encouraging results but still lack of selectivity for higher-order saccharides.[68] Zhai *et al.* has been applying triazole as a linkage unit into saccharides sensor (Figure 10). These results demonstrate that CuAAC can be applied into rapid sensor preparation, screening and discovery.[69]

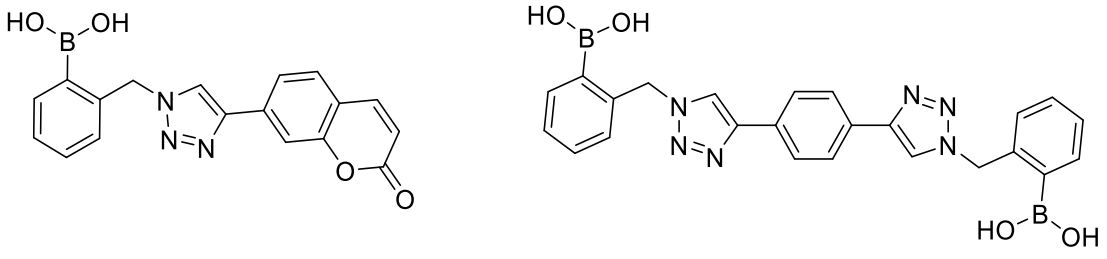

Figure 10. Triazoles in saccharide sensors

1.4.3 Triazoles in catalysis

The 1,2,3-triazole motif, through its ease of preparation and functionalisation, provides an excellent route for ligand designing. Triazoles formed by CuAAC possess two basic nitrogen atoms which are capable to metal coordination, and *N3* nitrogen is more basic then *N2*. (Figure 11).[70] Potentially, other donor functional groups can be introduced both in alkyne and azide precursors, therefore accessing a series of chelating ligands. In addition, the 5-position of C-H can go through C-H activation to form the thiazolidine compound. Since the basicity nature of *N3*-position, once *N3*-position has been alkylated, deprotonation of C-H in 5-position can lead to the formation of new mesoionic N-heterocyclic carbene (NHC). The utilisation of triazole in the designing of a novel ligand system has dramatically increased in recent years.[70, 71]

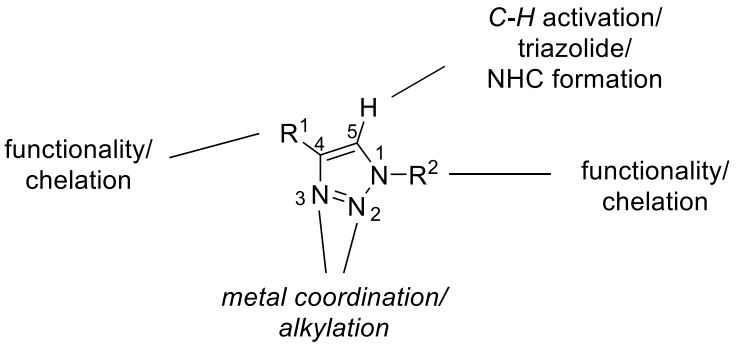

Figure 11. Functional potential of 1,2,3 - triazoles for coordination chemistry.[70]

1.4.3.1 Triazole coordination chemistry

A series of triazole-metal coordination complexes **45** has been prepared from NCN-pincer Pd, or Pt bromide salt **44** followed by bromide extraction *via* silver salt then reacted with appropriate triazole (Scheme 13). These complexes were obtained as a powder with above 90% yield. Due to the board functional group tolerance from click

chemistry, a considerable variety of stable 1,2,3-triazole ligands are readily accessible. In addition, metal coordination to the myriad of triazoles which have been incorporated into molecules as building blocks, could add an extra dimension to these compounds and offer a handle for further, non-covalent functionalisation.[72]

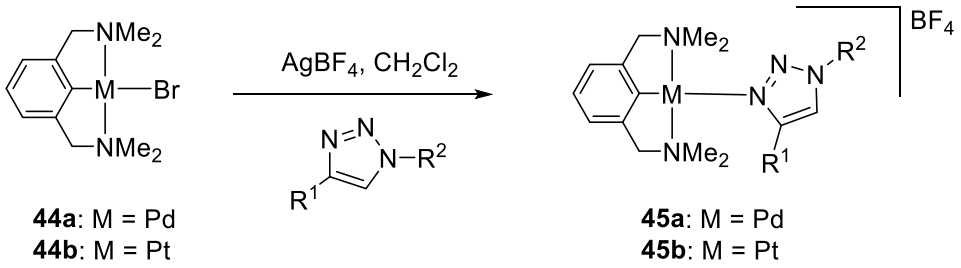

44a: M = Pd
44b: M = Pt

45a: M = Pd
45b: M = Pt

Scheme 13. Preparation of monodentate triazole complex[72]

Suijkerbuijk *et al.* concluded that coordination strength of the triazole toward NCN-Pt complexes could conveniently be tuned both sterically and electronically by verifying functionalisation of azide and alkyne group. In addition, they also reported that these triazole ligands possess similar binding ability compared with pyridine and imidazole-based ligand.[72]

Infrared data for the carbonyl stretching ode indicate that the donor ability of triazole ligands are marginally better than pyridine, Elliott *et al.* unveiled a new series of triazole-rhenium complexes (Scheme 14). Significant structure differences have been observed in solid-state, even a small difference in the alkyl substituents. In addition, these complexes were also found to be highly luminescent, with extended phosphorescent lifetimes in DCM solution.[73] Due to the long luminescent lifetimes as well as the facile CuAAC derivation of many biological activity molecules, potential

applying these complexes as time-gated luminescent imaging agents is still under investigation.[73]

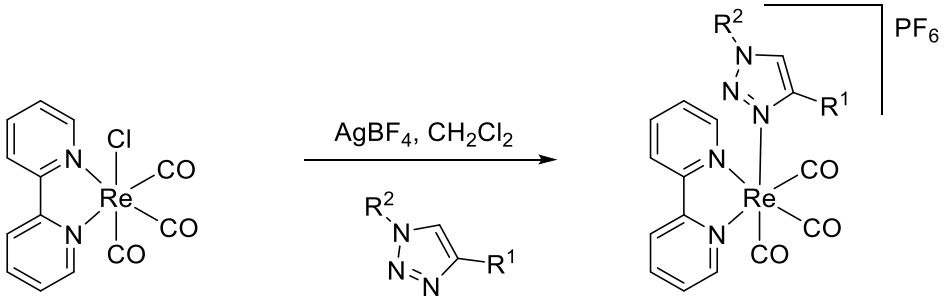

Scheme 14. Preparation of rhenium-triazole complexes[73]

Since bipyridine(bpy) and terpyridine(tpy) can form a stable metal complexes with some unique electrochemical and photophysical properties, a range of triazole containing chelating ligands for transition metals have also been developed.[74, 75] Functionalisation of ligands system is the key feature for the optimisation properties of ligand-metal complex. Due to the ease with which a range of functional groups can be incorporated into the substituents of the triazole moiety, CuAAC have received attention in developing chelating ligand systems. Some analogues (Figure 12) like pyridine-triazole (pytz), bis-triazole (btz), ditriazole-pyridine (dtzpy) have been investigated, various metals complex with these triazole-ligands have been prepared, including rhenium(I), ruthenium(II), iridium(III).[76-79] In addition, the pytz-rhenium complex shows almost three times the luminescent lifetime compared with bpy-rhenium complex under the same condition.[73]

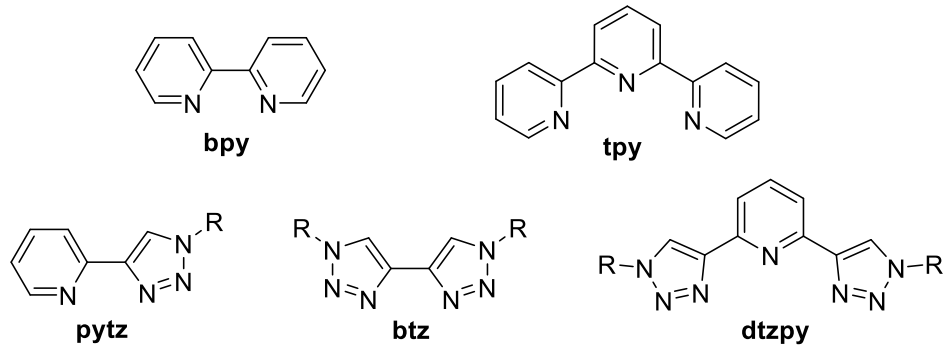

Figure 12. Bpy, tpy, and triazole analogues pytz, btz and dtzpy.[74]

Furthermore, polytriazole ligands such as TBTA were shown to accelerate reactions of CuAAC (Figure 13).[80] It appears to protect copper(I) under aerobic aqueous condition and promoting reaction proceed. The tetradentate binding ability of TBTA is believed to completely envelop the copper(I) centre, which can shields the copper(I) from potential destabilising interactions.[81] A series of analogue of TBTA has been prepared by Zhou *et al.*, with introducing different azide functional group, such as THPTA.[82] These tris-triazole based ligands greatly facilitate CuAAC reaction process.

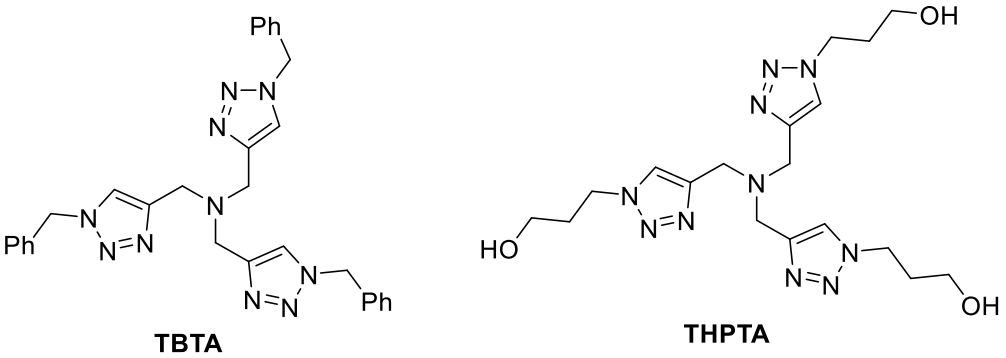

Figure 13. Example of polytriazole ligands, **TBTA** and **THPTA**

1.4.3.2 Cyclometalated complexes

Applying triazole into cyclometalated complexes of iridium and platinum have also attracted enormous interests in the application in Organic Light-Emitting Diode (OLED)

and Light-Emitting Electrochemical Cell (LEEC) devices. The key advantage of triazoles in this area is the ability to tune the emission colour through modification of the ligand of these complexes. Cyclometallation of triazoles were first demonstrated by Schubert *et al.* with good yield (Scheme 15). In addition, the emission was shown to be readily tunable based on the nature of the ancillary ligand, and it also can be monitored through variation of the substituents on the aryl rings of the cyclometalated aryltriazole ligands.[83]

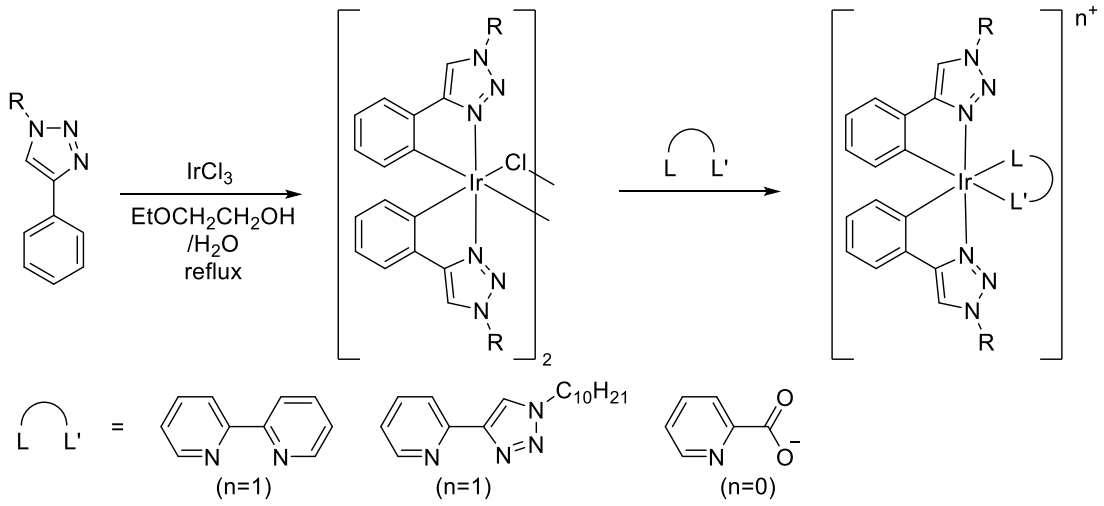

Scheme 15. Synthesis of cyclometalaed iridium triazole complex[83]

1.4.3.3 Triazolylidene ligand complexes

The *N*-heterocyclic carbenes (NHCs) have become ubiquitous in organometallic chemistry since the first isolation of an imidazole-based carbene ligand.[84] The two-electrons of *C2*-donor atom in these neutral imidazolylidene ligands are stabilised by two adjacent nitrogen atoms (Figure 14, **46**).[70] And these carbene ligands generally possess high efficiency in terms of improving catalyst activities.[85] Arduengo-type imidazolylidenes **46** have been widely used due to the free carbene is stabilised by two

nitrogen atoms adjacent to the carbene, which make them easier to handle.[86] Besides, the carbenic centre can be formed in C-4 position, as a result of neutral canonical form carbene, so-called 'abnormal' carbene or mesoionic NHCs **47**.[87] These abnormal NHCs (aNHCs) possess a stronger donor ability than traditional imidazolylidenes. A new sub-class of aNHCs have attached growing interest, and these ligands are derived from triazolium salts have emerged in which the *C2* imidazolylidene group is replaced by a nitrogen atom (Figure 10, **48**).[88]

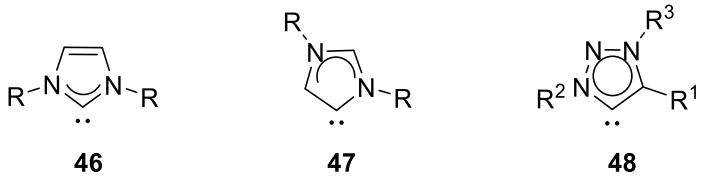

Figure 14. General structure of imidazole and triazole based carbenes

The first example of triazolylidene carbene was demonstrated by Albrecht *et al*. (Scheme 16).[85] Alkylation of CuAAC triazole product to form a triazolium salt **49** that readily to react with silver oxide to obtain the NHC silver complex **50**, followed by the transmetalation of **50** with ruthenium(II), rhodium(I), and iridium(I) precursors to afford the corresponding triazolylidene complex, **51, 53-55**. Besides, direct metal insertion to triazolium salts **49** *via* C-H bond activation protocol has successfully yield palladium complex **52**. Albrecht concluded that this triazolylidene metal system has highly benefited from CuAAC, it can be easily versatile by introducing different substitution group.[88]

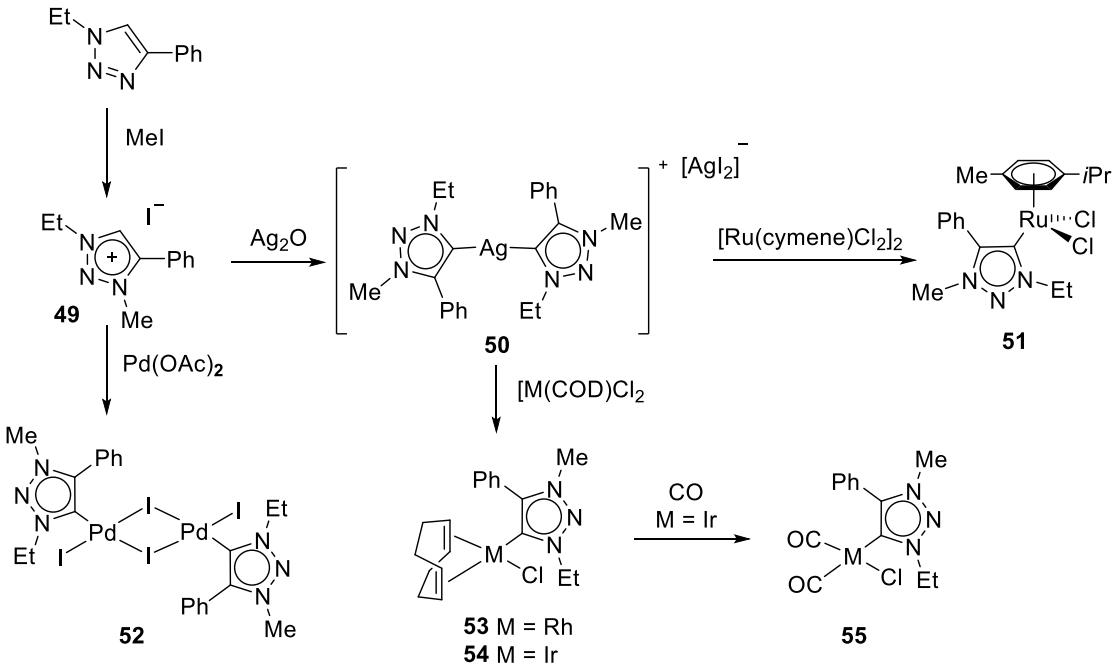

Scheme 16. Synthesis of triazolylidene complexes

The intense usage of NHCs in organometallic chemistry resulted by features as follow: i) relatively high covalent contribution to the M-NHC bond; ii) strong donor ability of M-NHC bond.[88] A series of CuAAC-derived triazole carbenes presented in Figure 15. Copper complex **56** are versatile catalysts for the CuAAC in a wide range of substrate with low loading of catalyst (0.05%). Functional groups with heteroatom are well tolerated, such as alcohols, esters and pyridines, besides, it has been reported then electron-poor phenylacetylenes are converted much faster than electron-rich analogues.[89, 90] Triazolylidene palladium complex **57** can catalyse the hydroarylation of alkynes under low catalysts loadings (0.5%).[91] Inspired by the success of palladium carbene complex, gold(I) carbene complex **58** was demonstrated by Crowley *et al*. This triazolylidene gold complex can catalyse the hydroalkoxylation, and promote carbene insertion cyclisation reactions.[92]

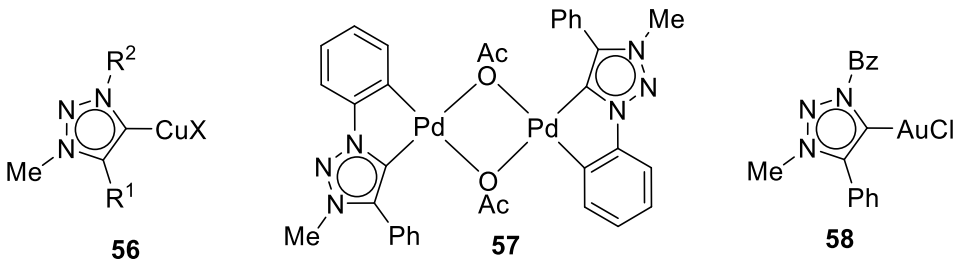

Figure 15. Structure of triazoles based carbene

Number of NHC-palladium complexes have also been investigated as catalyst precursors for Suzuki-Miyaura cross-coupling reaction. The enhanced donor properties of triazolic carbene expected to increase the activity of the oxidative addition step in the catalytic cycle. Complexes **59-63** show high catalytic activity in cross-coupling with 2-5 mol% catalysts loading even in more sterically demanding substrates.[90, 93-95] In addition, complex **63** is also effective in Heck olefin arylation and Sonogashira alkyne arylation reactions.[94]

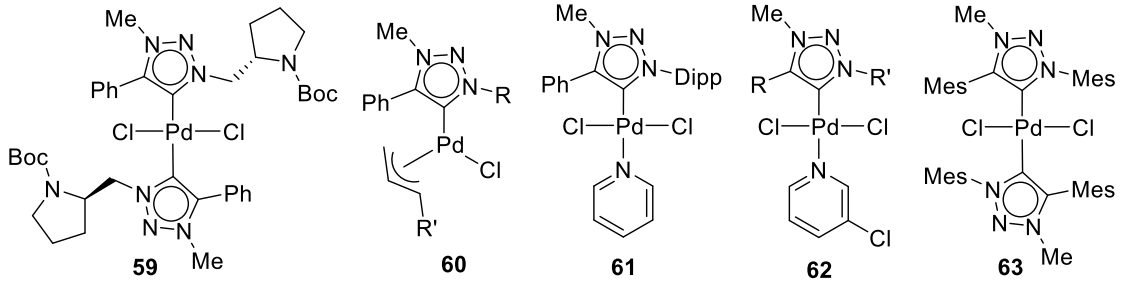

Figure 16. Triazolic palladium complex for cross-coupling reactions.

Bertrand and Grubbs have both explored the application of triazolylidene complexes analogues into Grubbs II's imidazolylidene olefin metathesis catalyst system (Figure 17).[96, 97] Complexes **64** were reported as proficient catalysts for the ring-opening metathesis polymerisation of cyclic olefins and ring-closing olefin metathesis reactions at room temperature.[96] It has been reported that complexes with N3 alkyl-substituted

are less stable compared with *N3* arylated substitution.[96] A binuclear ruthenium(I) complex **65** was developed and applied into the ring-opening metathesis polymerisation of norbornene when activated by trimethylsilyl-diazomethane.[98]

Both iridium and ruthenium triazolylidene complex has shown high activity in water oxidation, which is described as a key technology to utilise the solar energy for fuel generation. For example, complexes **66-68** can lead to efficient oxygen evolution from water in the presence of Ceric ammonium nitrate (CAN) as a sacrificial oxidant.[99, 100]

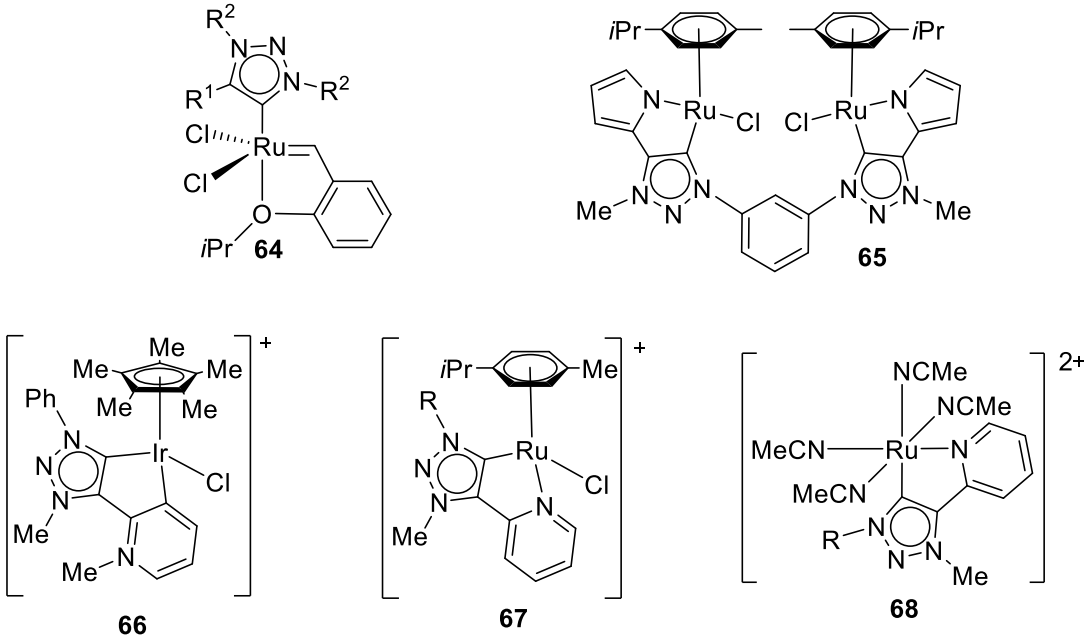

Figure 17. Ruthenium and Iridium-Triazolic carbene complex

1.4.3.4 Triazole-bridged phosphine ligand architectures

Triazole has also been used in the assembly of phosphorous-containing species that can potentially be employed as ligands. Functionalisation of CuAAC derived triazole readily to give access to libraries of triazole for bridging phosphines with another motif. Example of phosphine ligand listed in Figure 18. Phosphinites ligand **69** and **70** are first

demonstrated by Börner *et al.* as a choice for rhodium-catalysed hydroformylation.[101] They designed the methodology which consists of the assembling of hydroxymethyl substituted triazole in one-pot followed by phosphorylation reaction. These electron-deficient P-ligands show activities and regioselectivities in corresponding rhodium catalysed hydroformylation reaction.[101] Gandelman *et al.* used click chemistry to prepare *PCP* (**71**) and *PCN* (**72**) pincer complexes from bis- and mono- phosphino triazoles separately.[102, 103] These triazole based ligands contain two coordination arms in 1 and 4 position, while the relatively acidic C5-H proton of the triazole gives an opportunity of *C5* coordination once binding with the metal atom. The catalytic activity of ligand-palladium complex has been tested in Heck reaction with high TON (turn over number) in low catalyst loading ($7x10^{-4}$ mol%).

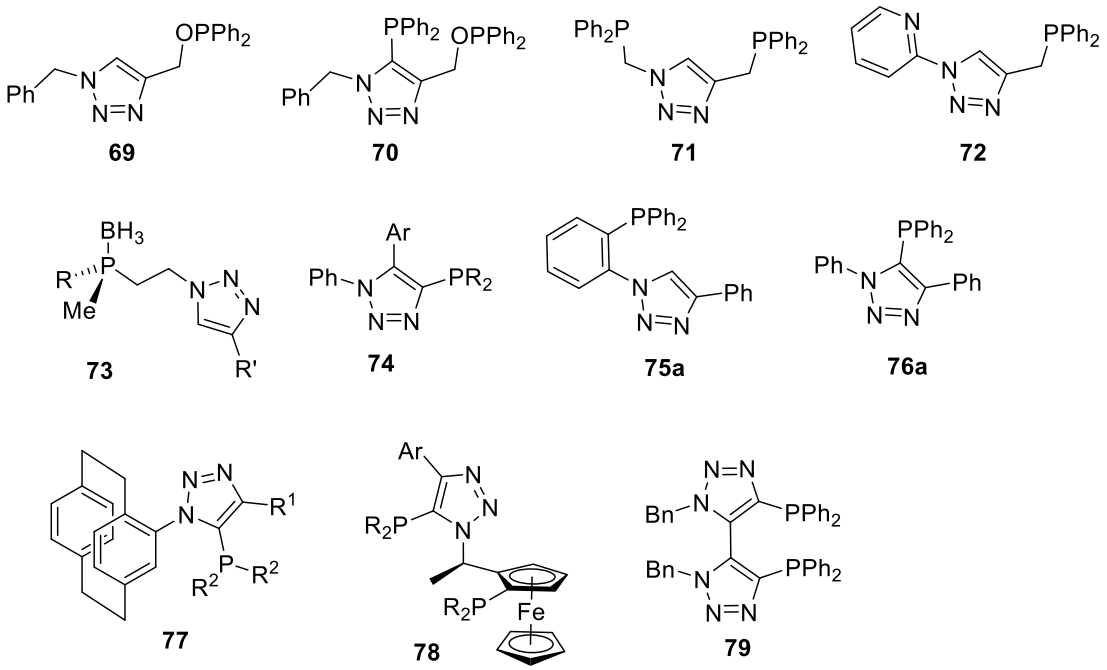

Figure 18. Phosphorus-containing 1,2,3-triazole derivatives

P-chirogenic phosphine ligands are proficient for asymmetric synthesis since the stereogenic centre is positioned near the reaction centre upon coordination to a metal. Kann *et al*. applied triazole moiety into ligand designing to access a series of novel and diverse P-chiral phosphine ligands (Figure 18, **73**) (ChiralClick).[104] Preliminary screening of ligands show that they are effective catalysts for palladium-catalysed asymmetric allylic alkylation although the enantioselectivity was less promising. Zhang *et al.* synthesised a library of triazole based phosphine ligands *via* alkynyl Grignard method. (Figure 18, **74**) (ClickPhos).[105] The features of these ligands are quickly assembled and easily diversified by the benefit of CuAAC reaction, and possess highly catalytic activity in Suzuki-Miyaura coupling and Buchwald-Hartwig amination.[106] In meanwhile, the luminescence properties of ClickPhos have been investigated by the Bräse group.[107] Phosphine ligands **75a** and **76a** were reported by Balakrishna *et al. via* either kinetically or thermodynamically favoured reaction pathway of lithiation of brominated triazole. These two ligands were described as useful chelating ligand with gold, copper, palladium and platinum.[108] The first planar chiral [2.2] paracyclophane derived phosphino triazole compound **77** was reported by Rowlands *et al.* These phosphine ligands show promising result in palladium-mediated cross-coupling reactions.[109] A series of bisphosphine ClickFerrophos(CF) **78**, based on triazoleferrocene scaffold, was demonstrated by Fukuzawa.[110] They also reported that enantiomeric selectivity of hydrogenation reactions of alkenes and ketones could be improved by using more steric demanding phosphine moiety. Bistriazole backbone has been introduced into phosphine ligand **79** by Virieux *et al.*, bisphosphine**79** was tested for imine

hydrogenation and showed good catalytic activities compared with an iridium complex.[111]

1.5 Cross-coupling in drug discovery

Transition metal catalysed cross-coupling reactions are well documented that ligands are widely used to stabilise the transition metal, and have a significant influence on the reaction outcome.[112-117] A series of triazole containing phosphine ligands have been listed in Figure 18, and most of them possess strong catalytic activity in Suzuki-Miyaura cross-coupling.

The Suzuki-Miyaura cross-coupling (SMC) reaction is one of the most studied reactions, which offers ready access to a series of biaryl scaffolds (Scheme 17, **80**).[118] SMC is an extremely powerful method for the preparation of C-C bond, and it possesses advantageous features such as: 1) Organoboron starting materials are generally stable in air and moisture; 2) mild and convenient reaction conditions; 3) less toxic byproducts and easy removal. These aspects make the SMC suitable for drug discovery and industrial applications.[118] Kishi *et al.* reported a route of total synthesis of natural product Palytoxin, which involved a key step achieved by SMC, this demonstrates the potential of the SMC reaction.[119]

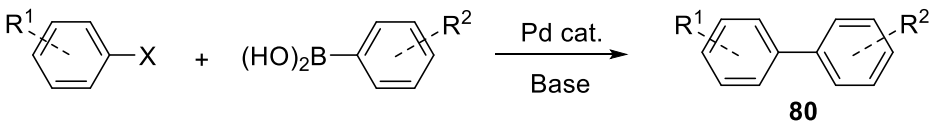

Scheme 17. Outline of a general palladium-catalysed Suzuki-Miyaura cross-coupling

In addition, SMC reaction is an effective method to synthesise biaryls atropisomer compounds[120] The suite of palladium-catalysed cross-coupling chemistry has provided a robust synthetic methodology to the preparation of biologically relevant products that benefited the field of drug discovery, although cross-coupling between sterically hindered, lead-like building blocks and less-active halides reactant, remain as challenge.[121]

1.6 Biaryl and Atropisomer

Since the first resolution of tartaric acid was achieved by Louis Pasteur in 1848, asymmetric synthesis of compound contained one or more stereogenic centres has become one of the challenging tasks in organic chemistry.[122] Atropisomers, by contrast, are enantiomers or diastereoisomers that possesses a stereogenic element arises because of hindered rotation, about σ-bonds with energy barriers exceeding 20 kcal/mol, this results in a half-life of more than 1000s at room temperature.[123] In some cases, atropoisomeric proton can be detected by NMR spectroscopic if the half-life exceed 0.01s.[124] Atropisomerism can often occur from a hindered rotation of bonds connecting two aryl groups with bulky ortho substituents (Figure 19, **A**), or from a barrier in the ring flip of a medium-size ring (Figure 19, **B**).[125] The first enantiomerically enriched atropisomer was isolated by James Kenner in 1992, since then, different chemical, physical and biological properties between atropisomers have been noted. [123, 125, 126]

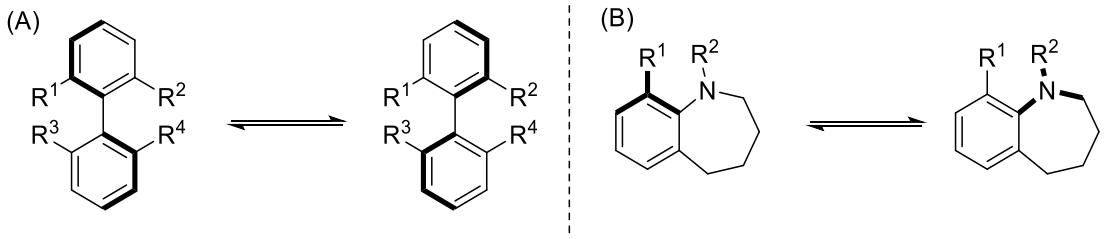

Figure 19. Generic atropisomers. (A) Atropisomer based on biaryls compound with bulky *ortho*-substituted unit. (B) Atropisomer with barrier in the ring flip.

Atropisomers can racemise by bond rotation, and the energy barrier for this process depends on the electron distribution, solvent effect, temperature and demanding steric properties. Conformers with lower activation energy can undergo interconversion freely, which with means it cannot be isolated as a single enantiomer or diastereoisomer. Conversely, Atropisomers with high energy barrier should be easily separable and stable under physiological conditions, which is necessary for chemical characterisation and therefore, biological activity test.[127]

The phenomenon of atropisomer chirality have big impacts on drug discovery and medicinal chemistry.[127] Atropisomers widely occur in natural product and drug design, selected examples are listed in Figure 20. Knipholone firstly isolated in 1984 from roots of *Kniphofia* as traditional medicine, with antimalarial activity and antitumor activities.[128, 129] Natural product Mastigophorene A has the potential to help in the growth of necrotic cell culture.[130] (-)-*N*-acetylallocolchinol has been observed to cause damage to the tumour cell selectively without damaging normal tissue, and has resurrected interest of colchicine-related agent in treatment of cancer chemotherapy. Gossypol is a potent inhibitor of leukaemia cell and that the (*M)*-isomer is more toxic and exhibit significantly great anti-cancer activity then (*P*)-isomer.[131]

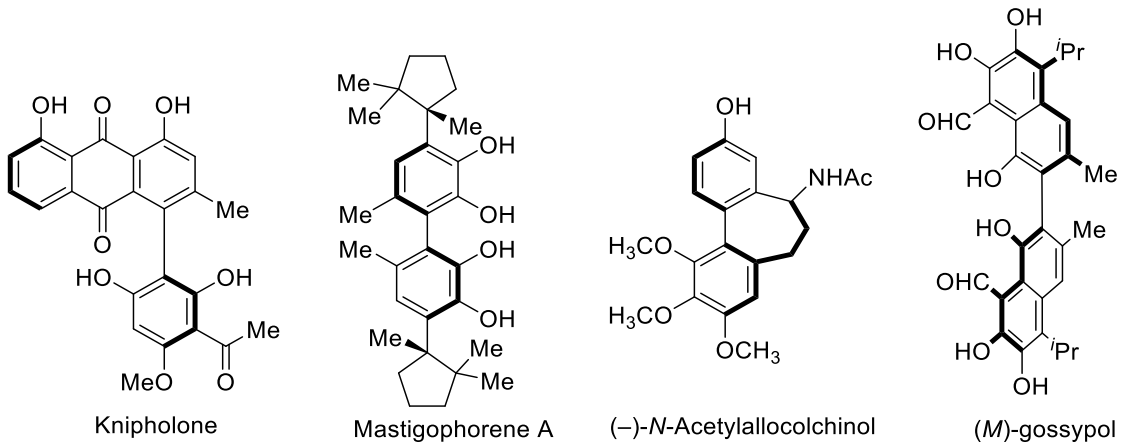

Figure 20. Selected examples of naturally occurring atropisomers and drug designing

The most important class of atropisomers in catalysts are biaryls compounds such as BINOL (Figure 21). BINOL is derivative of naphthalene dimer, where hindered rotation occurs about the naphthalene bridge. BINOL not only be used as a ligand with transition metals for stoichiometric and catalytic asymmetric reaction, but also is efficient organocatalyst for the asymmetric Michael addition.[132, 133] BINAP, which prepared from BINOL *via* its bistriflate derivatives, is a widely used bisphosphine ligand. This chiral bisphosphine ligand is commonly used in asymmetric reactions catalysed by the corresponding complexes with ruthenium, rhodium, and palladium.[134] QUNIAP is the *P*,*N*-chelating analogue of BINAP, with one component carrying a pendant phosphine unit, diaryl substituted, and the other bearing an sp^2-nitrogen adjacent to the biaryls linkage. The QUNIAP-silver complex show the high catalytic activity in the Ag-catalysed (3+2) dipolar cycloaddition reaction, while QUNIAP-palladium complex shows high catalytic activity and regioselectivity in hydroboration and oxidation of arylalkenes.[135, 136] Maruoka catalysts are commercially available phase transfer catalysts for the enantioselective alkylation.[137]

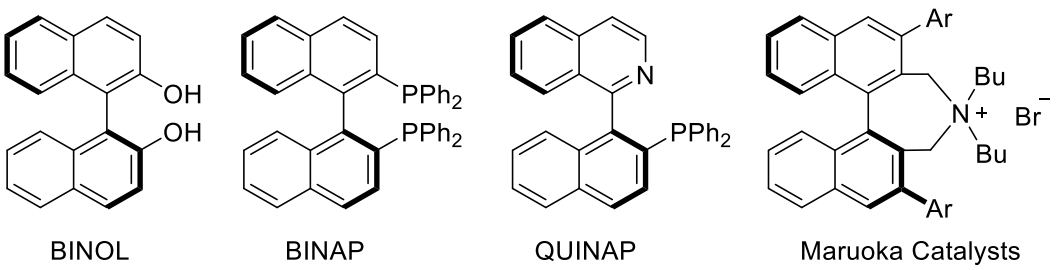

Figure 21. Selected examples of atropisomer in catalysts.

1.7 Summary

The triazole motif from CuAAC reaction has become a mainstay in areas such as drug discovery, biological methodology and catalysts design. The simple preparation and potential of functionalisation features of triazole have thus been embraced by researchers in different disciplines. Triazole can serve as an efficient linker between two molecular species, the mild reaction condition and multiple functional groups toleration features of CuAAC have offered a new strategy in synthetic chemistry.

1.8 Aims and objectives

Although triazole containing ligands or catalysts have been widely reported, rapid assembly of diverse ligand systems are still important for the development of effective catalysts. The experiment detailed in future chapters will show the strategy of developing a new series of triazole containing phosphine ligand for palladium or gold catalysed reaction. In addition, the potential usage of triazole containing ligand for the synthesis of lead-like molecules. Works in later chapter also presented three different ways to achieve asymmetric triazole containing ligand.

2. Chapter 2 Mono Triazole Phosphine Ligands

The triazole product from copper-catalysed azide-alkyne cycloaddition (CuAAC) has been widely used in a range of scenarios.[138] In addition, 1,2,3-triazole derived nitrogen-chelating ligands have been widely used, e.g. in *N*,*N*'-,[139-145] *N*,*S*-,[139] *N*,*Se*-[139] and cyclometallated[146-148] bidentate coordination complexes. As discussed in the previous chapter, triazole containing ligand has been widely applied in transition metal catalysed reaction.

Developments in palladium-catalysed chemistry have been heavily influenced by ligand design and optimisation. Bulky phosphine ligands are among the superior ligands for palladium mediated cross-coupling reactions, such as Buchwald type SPhos **81** and XPhos **82** (Figure 22). Palladacycle as precatalysts have been developed as well, which can enhance stability and improve reaction outcome.[149-151]

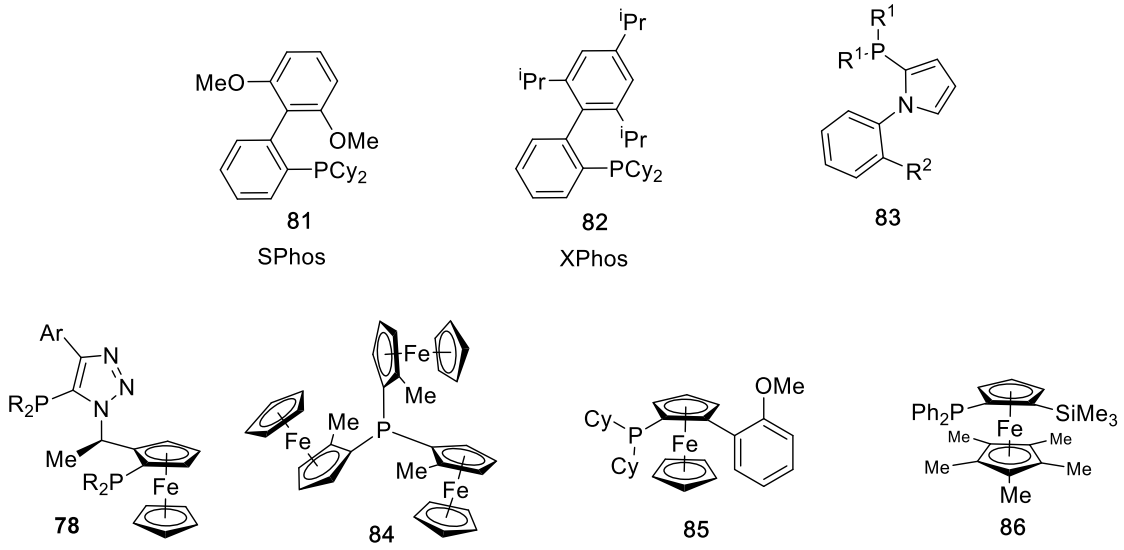

Figure 22. Selected examples for bulky phosphine ligands

Beller *et al*. developed the pyrrole-contained phosphine ligand **83**, which is commercially available as 'cataCXium series', these have been proven to be robust

ligands for palladium catalysed cross-coupling to furnish lead-like and drug-like structures.[152] Furthermore, ferrocene-appended phosphines ligands have been reported by Fukuzawa (Figure 22, **78**), Richards (Figure 22, **84**), Johannsen (Figure 22, **85**), Fu (Figure 22, **86**), and their respective co-workers provide access to highly active palladium-ligand conjugates for cross-coupling some of the least active substrates. [153-155]

Bulky, or sterically hindered phosphine contained ligand can also be applied outside of palladium catalysed reactions; steric feature can be important in a series gold-catalysed reaction.[156-158] Steric and electronic properties of phosphine ligand have been studied for more than 40 years. Tolman's cone angle θ is used to measure the steric bulkiness of ligand with metal complex; it is defined as the solid angle of a cylindrical cone, with metal in the vertex and fixed bond length with phosphine and metal. The steric parameter θ for symmetric ligands (all three substituents the same) is the apex angle of a cylindrical cone, centred 2.28 Å from the centre of the P atom, which just touches the van der Waals radii of the outermost atoms of the model (Figure 23, A). Cone angle θ can be rapidly and confidently measured for ligand with fixed geometry, but less accurate with complex ligands.[159]

Most recent contributions have built upon Tolman's concept of cone angle as a descriptor of the steric bulk a ligand imparts about a metal, resulting in a parameter known as percent buried volume ($\%V_{bur}$). It is defined as the percent of the total volume of a sphere around metal occupied by a ligand (Figure 23, B).[160] The sphere has a metal in the centre with a defined radius.[161] The concept of percent buried volume is initially

used to describe the steric pressure brought about by the use of NHC ligands, but it can also be applied in theory to tertiary phosphine ligands. Cavallo *et al.* have developed a free web-based tool for the calculation of $\%V_{bur}$, named SambVca.[162] The volume represents the potential coordination of ligand, which refer to the bulkiness of ligand/metal fragment, has facilitated exceptional ligand design across a range of catalysed reactions.

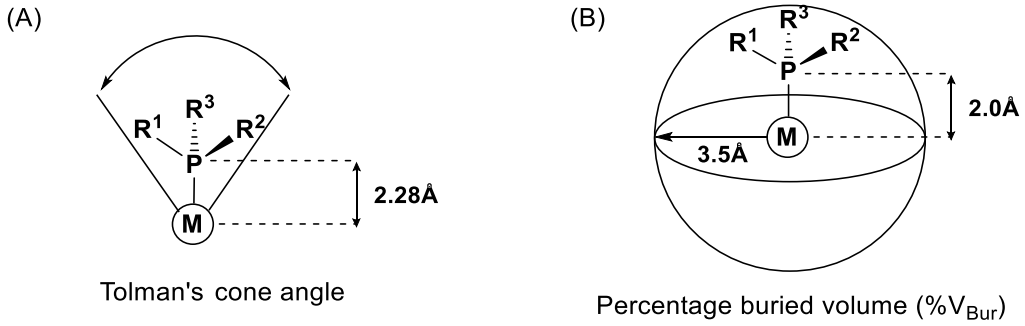

Figure 23. Legend of Tolman's cone angle(**A**) and percent buried volume ($\%V_{bur}$) (**B**)

While many useful phosphine ligands have been reported, quick construction of diverse ligand system *via* efficient synthetic methods such as CuAAC, is still a hot topic in the development of catalysts across the various application, especially in cross-coupling reactions and novel catalysts preparation. Furthermore, cross-coupling reaction can provide a synthetic route to 'three-dimensional' products and directly delivering small molecules with drug-like or lead-like properties may be reduced the introducing protection group.[163, 164]

2.1 1,4,5-Trisubstituted triazole containing phosphine

To avoid the Staudinger ligation between phosphine compounds and azides during the process of triazole formation, an order of reaction with phosphine installation step

after CuAAC is required. A potential synthetic route that masking phosphine to phosphine oxide during synthesis, then reduce back to phosphine after assemble triazole scaffold is possible.[111]

The initial approach chosen in this project is using triazole as directing group for *ortho*-lithiation or directly halogen-lithium exchange reaction then quenching with electrophile chlorodiphenylphosphine to access **75a-b** separately. To test if triazole directed *ortho*-lithiation could deliver the required intermediate for phosphine installation, **11a** was prepared as for the model reaction to test whether **75a** or **75b** could be given as resulting product. Over numerous reaction attempts with various condition, **76a** was isolated as the main product from these reactions. This indicated that acidic proton from *C5* position had been taken off by the alkyl lithium reagent, as a result of giving the major product of **76a**. In order to avoid the formation of unanticipated triazole phosphine compound **76a**, brominated triazoles **87a-b** were prepared for further test, followed by the same lithiation protocol with varying equivalent of *n*-butyllithium reagent to introduce the phosphine sidearm. In all cases, the same 5-phospino triazole product **76a** was isolated as a major product (Scheme 18). In the case of **87a**, desired phosphine compound **75a** isolated from the reaction mixture with 44% yield if using diethyl ether as a reaction solvent. But compound **75b** has not been detected in the same reaction condition with **87b** as starting material. Both structures of **76a** and **75a** have been confirmed by X-ray crystal structure analyses, as shown in Figure 24.

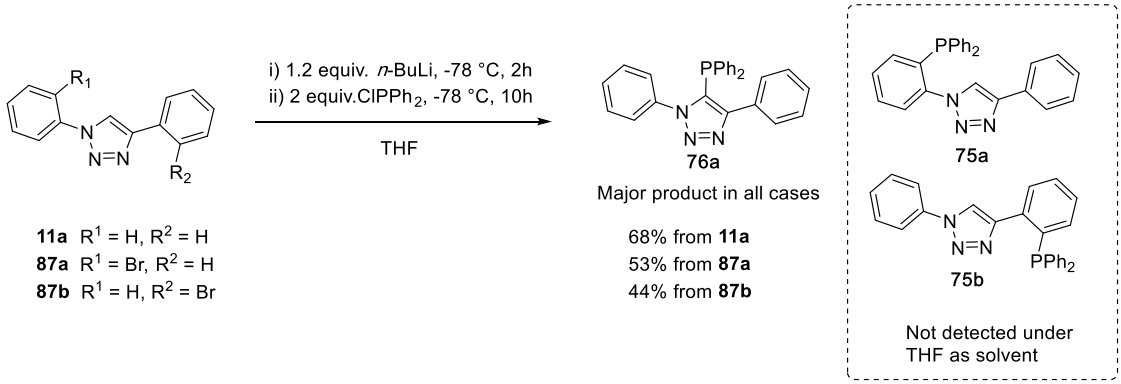

Scheme 18. Reaction of 1,2,3-triazole **11a**, **87a-b** with *n*-BuLi and chlorodiphenylphosphine lead to formation of **76a**

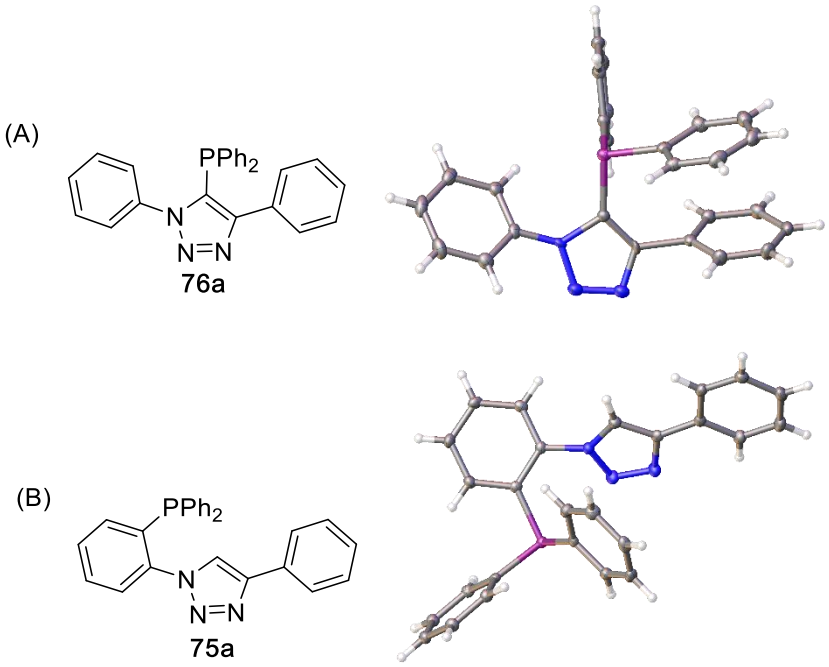

Figure 24. Crystal structures of **76a** and **75a**, ellipsoids were drawn at the 50% probability level. For **76a** the central triazole unit is disordered such that the triazole ring occupies two opposing orientations, related by a 180° rotation of the triazole ring about the phosphorus-triazole bond. For **75a** the x-ray structure contains two independent molecules in one unit cell, only one has been shown for clarity.

These observations should not have been at all unanticipated.[108, 109] Balakrishna *et al.* have previously investigated the reaction from **87b** to **75a** and **76a** in more detail than us under analogous conditions.[108] and determined a "kinetic" and "thermodynamic" relationship between lithium-halogen exchange alone, versus lithium-halogen

exchange followed by lithium (triazole-) proton exchange leading to products **75a** and **76a** respectively. (Scheme 19).

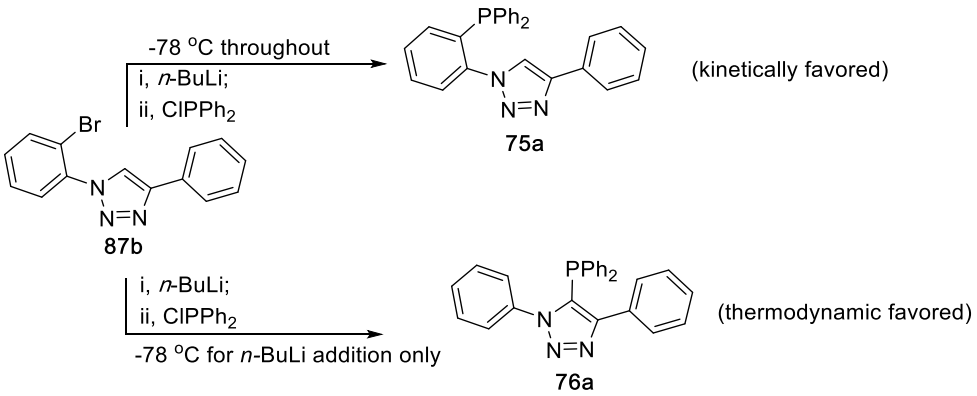

Scheme 19. Previously reported lithiation and phosphorus addition to brominated triazole **87b**.[72]

Attempts to block the triazole 5-H position, using the deuterium masking approach deployed by Richards *et al.* in the preparation of ferrocene derivatives. A high value of k_H/k_D has been observed in the lithiation of ferrocene derivatives.[165] Deuterium labelled triazole **87a'** was prepared, followed by the same reaction condition at Scheme 18, afford a phosphino-triazole **76a'** with phosphine group still be introduced in the 5-position of triazole instead of the phenyl ring, which suggested reaction was still directed with thermodynamically favoured pathways (Scheme 20). In addition, triazole **11c'** has been prepared as well, followed by deprotonation and phosphine installation, to yield **76e** with 54% yield while 35% triazole has been recover with 25% deuterium labelled. These results suggested this deuterium masking approach has not dramatically modify reaction outcomes in this case.

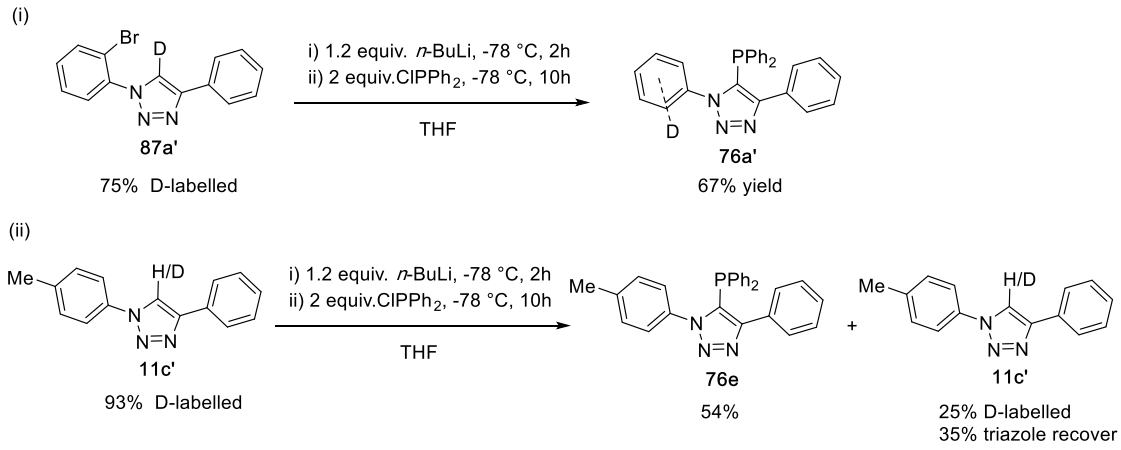

Scheme 20. Deuterium masking approaching study, phosphine group has still been introduced into 5-position of triazole even with deuterium labelled starting material.

Since the scope of **76a**-like compounds had not been tested as ligands in cross-coupling reaction, we choose to focus attention on *C-5* direct lithiation reaction to deliver a range of triazole containing phosphine compounds for cross-coupling catalysis. Thus, azides **12a-h** were synthesised from the corresponding anilines with moderate to good yield (Scheme 21). And then azides **12a-g** reacted smoothly with alkynes **13a** and **13b** to furnish triazole **11a-i** in a good to acceptable yield (Scheme 22).

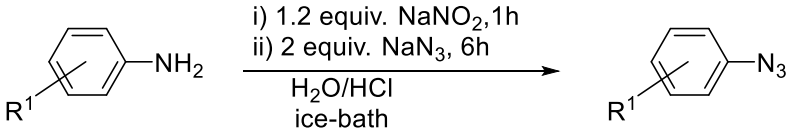

	R^1	Yield/%
12a	H	77
12b	4-Me	55
12c	4-OMe	93
12d	2,6-OMe	84
12e	2-Ph	95
12f	C_4H_4*	72
12g	4-CF_3	58
12h	3,5-OMe	73

*Meaning 1-naphthyl azide

Scheme 21. Preparation of azides **12a-h** via diazonium salts.

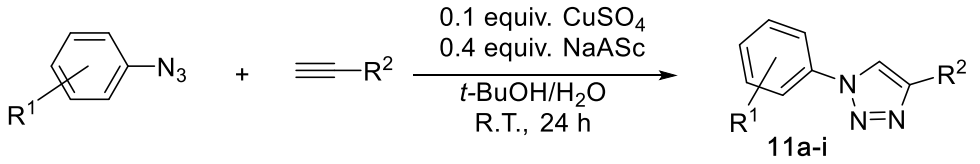

	R^1
12a	H
12b	4-Me
12c	4-OMe
12d	2,6-OMe
12e	2-Ph
12f	C_4H_4*

*Meaning 1-naphthyl azide

	R^2
13a	Ph
13b	Cy

	R^1	R^2	Yield/%
11a	H	Ph	93
11b	H	Cy	54
11c	4-Me	Ph	92
11d	4-OMe	Ph	81
11e	2,6-OMe	Ph	64
11f	2,6-OMe	Cy	83
11g	2-Ph	Ph	95
11h	C_4H_4*	Ph	83
11i	C_4H_4*	Cy	71

*Meaning 1-naphthyl triazole

Scheme 22. CuAAC reaction to form 1,4-disubstituted triazole derivatives.

The isolated triazole **11a-i** were then treated with aforementioned lithiation protocol and quenching with different phosphine species such as diphenyl-, di-isopropyl and dicyclohexyl phosphorus chloride to furnish the targeted *C-5* substituted phosphino triazole set **76a-l** with acceptable to good yields (Scheme 23).

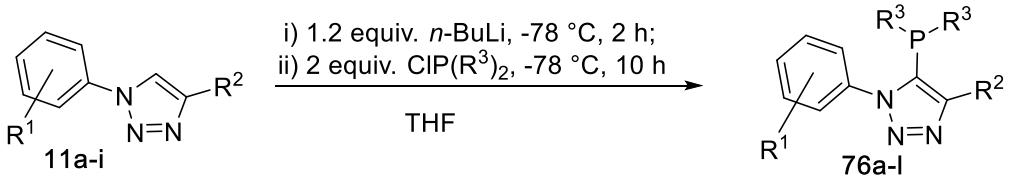

	R^1	R^2	R^3	Yield/%
76a	H	Ph	Ph	68
76b	H	Ph	*i*-Pr	68
76c	H	Ph	Cy	52
76d	H	Cy	Ph	27
76e	4-Me	Ph	Ph	63
76f	4-OMe	Ph	Ph	42
76g	2,6-OMe	Ph	Ph	97
76h	2,6-OMe	Cy	Ph	42
76i	2-Ph	Ph	Ph	68
76j	2-Ph	Ph	Cy	91
76k	C_4H_4*	Ph	Ph	42
76l	C_4H_4*	Cy	Ph	91

*Derived from 1-naphthyl azide

Scheme 23. Lithiation and phosphorus installation to deliver **76a-l**

In order to benchmark the catalytic activity of the triazole ligand series, all the ligands were tested in palladium catalysed Suzuki-Miyaura cross-coupling between the 2-bromo-*m*-xylene **88** and *ortho*-tolylboronic acid **89** under standard conditions(1 mol % palladium, 2 mol % ligand, three equivalents of base, 10 h, toluene, 90 °C) was compared. The catalysed formation of biaryl product **90** represented a challenging but achievable cross-coupling: while an aryl bromide is employed in the reaction, the product (a triply ortho-substituted biaryl) is sterically congested about the formed bond. Diphenyl aryl phosphine **75a** and C5-phosphine substituted triazole **76a-l** were employed as ligands in this reaction (Table 1).

The use of **75a** as ligand resulted in 29% conversion to product **90**. (Table 1, entry 1) The C-5 isomer of **75a**, **76a** shows moderate activity but still lower than 50%. As may be expected, switching the diphenylphosphine part of **76a** to dialkylphosphine groups

such as di-*iso*-propyl (**76b**) and dicyclohexyl (**76c**) improved the reaction outcomes, resulting in 62% and 75% conversion, respectively (Entries 3,4). Changing the alkyne derived part of the triazole from phenyl to cyclohexyl group (**76d**) significantly boost catalytic activity, delivering product with 86% conversion. Modification in the *ortho* position of azide unit could dramatically increase the reaction outcome. Meanwhile, **76m** gave to 99% conversion of starting material.

Table 1. Ligand screening: 1,4 disubstituted triazole derived phosphine ligands in Suzuki-cross-coupling

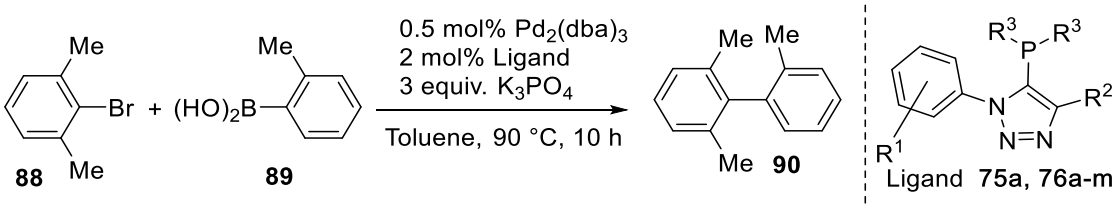

Entry	R^1	R^2	R^3	Ligand	Conversion [%][b]
1	-	-	-	**75a**	29
2	H	Ph	Ph	**76a**	47
3	H	Ph	*i*-Pr	**76b**	62
4	H	Ph	Cy	**76c**	75
5	H	Cy	Ph	**76d**	86
6	4-Me	Ph	Ph	**76e**	69
7	4-OMe	Ph	Ph	**76f**	83
8	2,6-OMe	Ph	Ph	**76g**	92
9	2,6-OMe	Ph	Cy	**76h**	72
10	2,6-OMe	Cy	Ph	**76i**	90
11	2-Ph	Ph	Ph	**76j**	84
12	2-Ph	Ph	Cy	**76k**	92
13	C_4H_4[c]	Ph	Ph	**76l**	91
14	C_4H_4[c]	Cy	Ph	**76m**	99

[a] Reaction conditions: 2-Bromo-*m*-xylene (0.4 mmol), *o*-tolylboronic acid (0.6 mmol), potassium phosphate (1.2 mmol), $Pd_2(dba)_3$ (0.5 mol%), ligand (2 mol%), toluene (3 mL), 10 h, 90 °C. [b] Conversion determined by inspection of the corresponding ^1H NMR spectra of crude reaction isolates. [c] Meaning derived from 1-naphthyl azide.

While good result has been observed from this series of phosphine ligands in Suzuki cross-coupling, but generally this type of ligands has suffered from low solubility. Thus,

ligand modification with retained catalytic activity with better physical properties and readily synthesised are still required.

2.2 1,5-disubstituted triazole containing phosphine

From briefly surveying the results in Table 1, it was concluded that changes in the R^2 (alkyne-derived) part (e.g., entry 8 versus entry 10) were less influential on the reaction outcome than changes in the R^1 (azide-derived) part (e.g., entry 5 versus entry 14). Reasoning that smaller ligands may benefit from enhanced the solubility and tractability, a strategy to retain the *N*-substituents (azide-derived parts) while minimising the alkyne-derived parts was chosen for further elaboration.

Gevorgyan *et al.* have already reported that 1,5-disubstituted 1,2,3-triazoles can be accessed by selective reaction at the 5-position of 1-substituted triazoles (Figure 25 shows the electrostatic potentials of the triazole-carbons they determined). In combination with synthetic strategies for mono-substituted triazole reported by Banerjee, this led to the conclusion that 1-substituted triazoles may be readily converted to a library of 1-substituted, 5-phosphino 1,2,3-triazoles.[61]

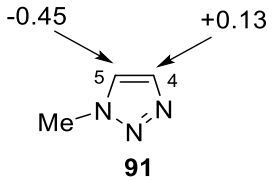

91

Figure 25. Electrostatic potential charges at C-4 and C-5 position.[166]

Following the optimised CuAAC protocol by Banerjee, a range of 1-substitute triazole has been prepared.[61] Specifically, trimethylsilylacetyleneacetylene (**13c**) and various azides (**12a-i**) were exposed to desilylation CuAAC reaction, that led to effectively

triazole formation and desilylation in one pot, afford triazole series **92a-i** with acceptable to good yields (Scheme 24).

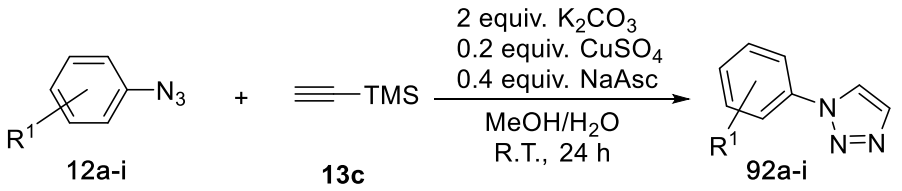

12a-i + 13c → 92a-i

	R^1
12a	H
12b	4-Me
12c	4-OMe
12d	2,6-OMe
12e	2-Ph
12f	C_4H_4*
12g	4-CF_3
12h	3,5-OMe
12i	2,6-*i*-Pr

*Derived from 1-naphthyl azide

	R^1	Yield/%
92a	H	71%
92b	4-Me	84%
92c	4-OMe	85%
92d	2,6-OMe	64%
92e	2-Ph	28%
92f	C_4H_4*	40%
92g	4-CF_3	72%
92h	3,5-OMe	85%
92i	2,6-*i*-Pr	40%

*Derived from 1-naphthyl triazole

Scheme 24. Reaction between trimethylsilylacetylene (**13c**) and arylazides (**12a-i**) to furnish monosubstituted triazole **92a-i**.

Then triazoles **92a-i** were reacted with *n*-butyllithium to remove *C-5* proton, then quenching with different chloroalkylphosphine reagent to furnish desired phosphino triazole ligands **93a-m** in acceptable to good yields (Scheme 25). The X-ray crystal structure of **93g** has been determined and also confirmed the installation of phosphine at the *C-5* position (Figure 26). The orientation of molecule (in solid-state) is such that, the lone pair of phosphine is oriented to the same direction as the 1-aryl substituent of triazole. In turn, this orientation about a central five-membered ring describes a relatively wide binding pocket for metals with potential for arene-metal interactions alongside primary phosphorus–metal ligation.

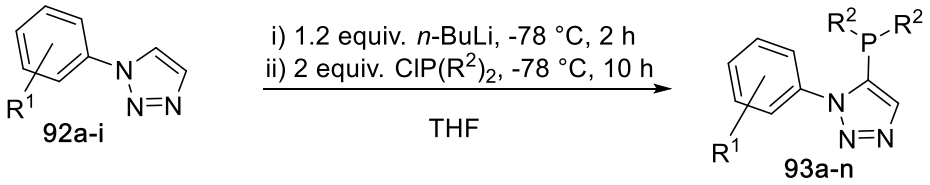

	R^1	R^2	Yield/%
93a	H	Ph	47
93b	H	Cy	73
93c	4-Me	Ph	36
93d	4-OMe	Ph	49
93e	2,6-OMe	Ph	82
93f	2,6-OMe	*i*-Pr	88
93g	2,6-OMe	Cy	73
93h	2,6-OMe	*t*-Bu	72
93i	2-Ph	Ph	27
93j	C_4H_4*	Ph	37
93k	4-CF_3	Ph	68
93l	3,5-OMe	Ph	72
93m	2,6-*i*-Pr	Cy	89
93n	2,6-*i*-Pr	*t*-Bu	88

*Derived from 1-naphthyl azide

Scheme 25.Lithiation and phosphorus installation to deliver **93a-n**

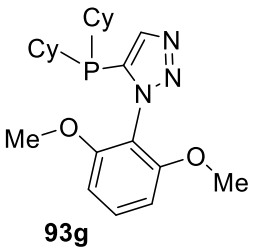

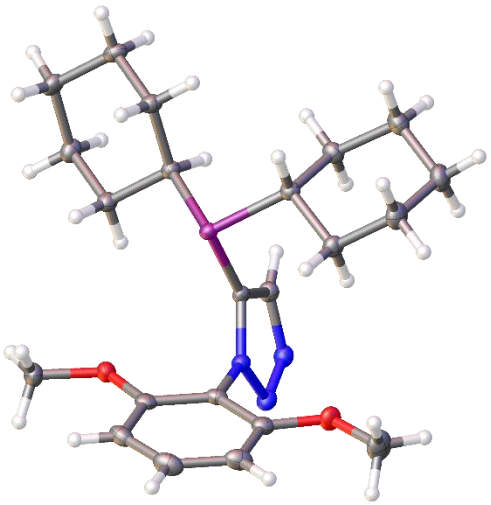

Figure 26. Representation of the crystal structure of **93g**, ellipsoids are drawn at the 50 % probability level.

Ligands **93a-n** were then tested in the aforementioned benchmark SMC reaction of **88** with **89** catalysed by a palladium-phosphine complex, to produce biaryl **90** (Table 2). Under the same conditions, commercially sourced ligands, SPhos (7) and XPhos (8)

were also used for comparison (Table 2, entry 15, 16). As can be observed from Table 2, diphenylphosphine ligand series offer lower catalytic activity then dialkylphosphine substituted version. In addition, dialkyl-phosphino triazole derived ligands **93b, 93f, 93g, 93h, 93m,** and **93n** gave universally excellent conversion, equal to the commercially sourced SPhos and XPhos in performance, under these conditions.

Table 2. Ligand screening: 1- substituted triazole containing phosphine ligand in Suzuki-cross-coupling

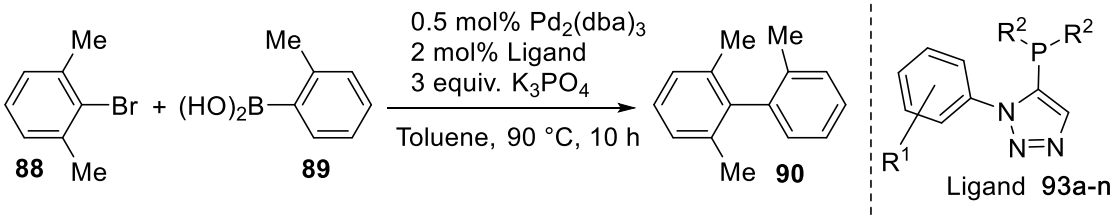

Entry	R^1	R^2	Ligand	Conversion [%] [a, b]
1	H	Ph	**93a**	20
2	H	Cy	**93b**	98
3	4-Me	Ph	**93c**	54
4	4-OMe	Ph	**93d**	28
5	2,6-OMe	Ph	**93e**	90
6	2,6-OMe	*i*-Pr	**93f**	99
7	2,6-OMe	Cy	**93g**	99
8	2,6-OMe	*t*-Bu	**93h**	98
9	2-Ph	Ph	**93i**	82
10	C_4H_4[c]	Ph	**93j**	29
11	4-CF_3	Ph	**93k**	83
12	3,5-OMe	Ph	**93l**	51
13	2,6-*i*-Pr	Cy	**93m**	99
14	2,6-*i*-Pr	*t*-Bu	**93n**	99
15	-	-	SPhos (**81**)	98
16	-	-	XPhos (**82**)	99

[a] Reaction conditions: 2-Bromo-*m*-xylene (0.4 mmol), *o*-tolylboronic acid (0.6 mmol), potassium phosphate (1.2 mmol), $Pd_2(dba)_3$ (0.5 mol%), ligand (2 mol%), toluene (3 mL), 10 h, 90 °C. [b] Conversion determined by inspection of the corresponding ^1H NMR spectrums of crude reaction isolates. [c] Meaning derived from 1-naphthyl azide.

To further probe the utility of 1-aryl 5-phosphino 1,2,3-triazoles as ligands in Suzuki–Miyaura cross-coupling, the synthesis of compound **90** from aryl chloride **97** and

boronic acid **89** was investigated (Table 2). Ligand **76m**, **93b**, **93f-n** were selected for this reaction since these ligands showed good reaction outcome with aryl bromide substrate in Suzuki cross-coupling. (Table 1, Table 2) The reaction conditions mirrored those used earlier for cross-coupling with bromide analogue **88** in Table 2, but in order to ensure good reaction conversions, the reaction temperature was increased slightly (toluene at reflux).

Table 3. Ligand screening of **76m, 93b, 93f-n**, SPhos and XPhos in Suzuki-cross-coupling with **97** and **89**.

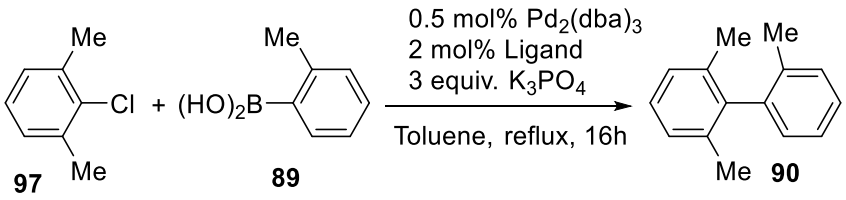

Entry	Ligand	Conversion [%] [a, b]	Isolated yield [%]
1	**76m**	5	-
2	**93b**	6	-
3	**93f**	77	75
4	**93g**	99	93
5	**93g**[c]	99	92
6	**93h**	99	82
7	**93m**	99	92
8	**93n**	70	-
9	SPhos (**81**)	33	25
10	XPhos (**82**)	99	90

[a] Reaction conditions: 2-Chloro-*m*-xylene (1.0 mmol), *o*-tolyboronic acid (1.5 mmol), potassium phosphate (3.0 mmol), $Pd_2(dba)_3$ (0.5 mol%), ligand (2 mol%), toluene (3 mL), 16 h, reflux. [b] Determined by GC analysis with *n*-dodecane as internal standard. [c] $Pd_2(dba)_3$ (0.25 mol%), ligand (1 mol%) was used.

Under the conditions employed in Table 3, catalysts derived from triazole-containing ligands **76m** and **93b** showed low catalytic activity to deliver product **90**, and moderate activity observed by using **93f** as ligand. Catalysts system derived from **93g**, **93h** and **93m** deliver compound **90** in quantitative yield. Using **93g** as ligand at a lower catalyst

loading of 0.5 mol% of palladium proportionally, quantitative conversion to **90** (isolated yield 92%) was achieved. In this comparison, the use fo SPhos as ligand gave 33% conversion and use of XPhos as ligand gave quantitative conversion to compound **90** (isolated yield 90%).

While pleased to have created ligands offering good performance in a benchmark reaction, the reaction itself did not provide enough diversity of outcomes to evaluate dialkyl-phosphino ligand performances against each other nor against readily available commercial ligands SPhos and XPhos. Next, a more sterically demanding test-reaction was chosen to evaluate the ligands further. The formation of biaryl C–C bonds where the formed bond is flanked by four ortho-substituents presents a particularly challenging yet attractive transformation, not in the least due to the apparent three-dimensional nature of the cross-coupled products.[163] The cross-coupling between arylbromide **94** and boronic acid **95** were selected to probe catalyst effectiveness further (Table 4). Conversion to product **96** may be monitored by gas chromatographic analysis, facilitating ready comparison of reactions performed in parallel. Having given quantitative conversions to product **90** (Table 3), and being both relatively easy to synthesise and available in sufficient quantities, ligands **93g-n** were selected for further investigation. These ligands are triazole-analogues of leading phenylene ligands SPhos and XPhos; thus, in order to probe any specific advantages of triazole-core ligands, they were compared directly against SPhos and XPhos phenylene ligands. (For retained and compared ligands, see Figure 27)

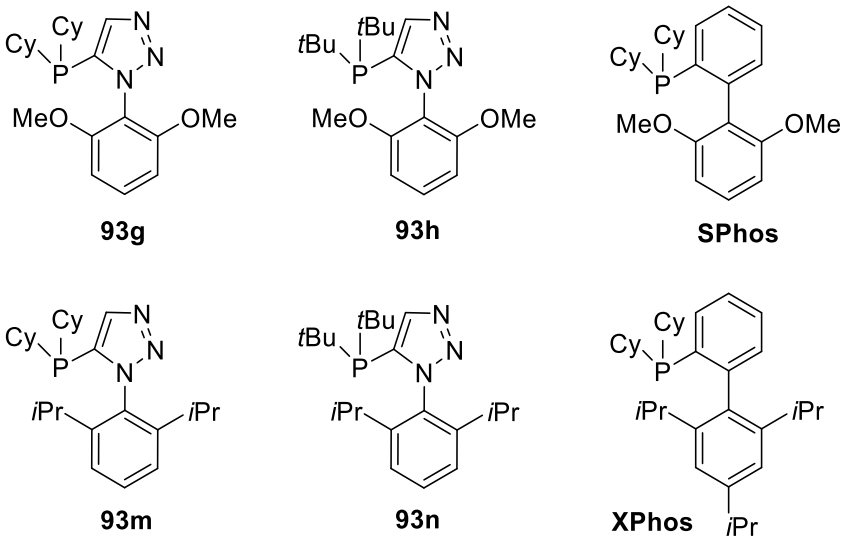

Figure 27. Ligands used in further catalytic test.

Table 4. Ligand screening of **93g, h, m, n**, SPhos and XPhos in Suzuki-cross-coupling with **94** and **95**.

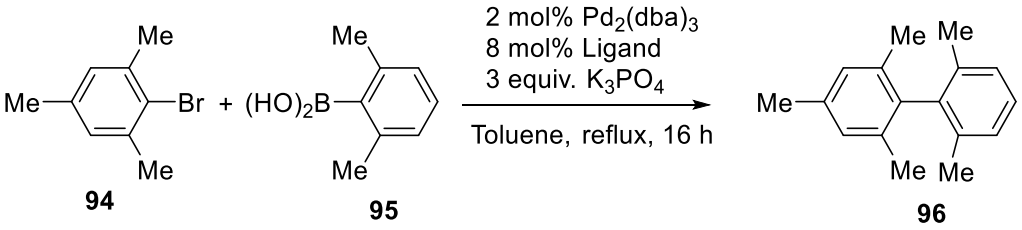

Entry	Ligand	Conversion [%] [a, b]	Isolated yield [%]
1	**93g**	99	85
2	**93g**[c]	84	71
3	**93h**	47	-
4	**93m**	60	-
5	**93n**	13	-
6	SPhos (**81**)	87	79
7	SPhos (**81**)[c]	74	-
8	XPhos (**82**)	50	-

[a] Reaction conditions: 2-Bromomesitylene (0.5 mmol), 2,6-xylylboronic acid (1.0 mmol), potassium phosphate (2 mmol), $Pd_2(dba)_3$ (2 mol%), ligand (8 mol%), toluene (3 mL), 16 h, reflux. [b] Determined by GC analysis with *n*-dodecane as internal standard. [c] $Pd_2(dba)_3$ (0.5 mol%), ligand (2 mol%) was used.

In order to ensure good reaction conversions, reaction time, temperature and catalysts loading were all increased compared with the initial benchmark reaction condition in Table 1 and Table 2. Under the new reaction conditions (Table 4), cyclohexyl

substituted ligands **93g** and **93m** achieved higher conversions with *tert*-butyl substituted ligands **93h** and **93n**. Under these conditions, SPhos gave better conversion compared with XPhos. Since **93g** already gave the best conversion under the condition employed, catalyst loading was then reduced to 1 mol% of palladium loading (in the form of 0.5 mol% $Pd_2(dba)_3$, and under these conditions, a conversion of 84% (isolated yield) was achieved. While SPhos achieved 74% conversion under with this low catalysts loading condition.

Next, a demanding palladium-catalysed reaction between 2-chloro-meta-xylene (**97**) and 2,4,6-trimethylphenylboronic acid (**98**) leading to product **96** was attempted. Two triazole ligand-based catalyst systems were compared against catalyst systems derived from SPhos and XPhos (Table 5).

Table 5. Ligand screening of **93g, 93m**, SPhos and XPhos in Suzuki-cross-coupling with **97** and **98**.

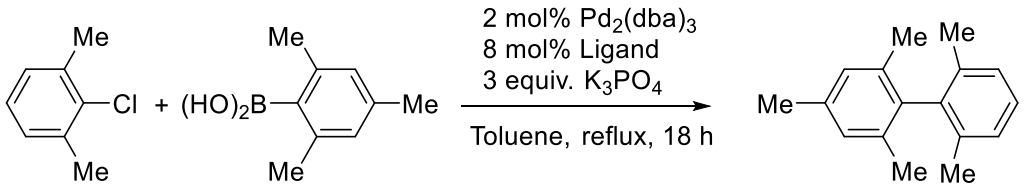

Entry	Ligand	Conversion [%] [a, b]
1	**93g**	49
2	**93m**	37
3	SPhos (**81**)	55
4	XPhos (**82**)	5

[a] Reaction conditions: 2-Chloro-*m*-xylene (0.5 mmol), 2,4,6-trimethylphenylboronic acid (1.0 mmol), potassium phosphate (2 mmol), $Pd_2(dba)_3$ (2 mol%), ligand (8 mol%), toluene (3 mL), 18 h, reflux. [b] Determined by GC analysis with *n*-dodecane as internal standard.

Under the conditions employed in Table 5, the four catalyst systems compared produced only moderate conversion. That is not to say that these reactions could not be optimised further, but the side-by-side comparison revealed, SPhos shows slightly better than triazole derived phosphine ligand **93g**. Slightly lower conversions were obtained when 29m or X-Phos were used as ligands.

One potential problem with Suzuki–Miyaura catalysed reactions, particularly evident when using less reactive aryl chlorides in cross-coupling, is homocoupling of the boronic acid-containing reaction partner.[167] In order to test our routine reaction protocols and our four selected triazole ligands for their propensity to lead to undesired homocoupled product, the following reaction was probed. Chlorotoluene **99** was reacted with 1.5 equivalent of phenylboronic acid **100**. Catalyst loading was about 2 mol % palladium and 4 mol % ligand. The reactions were conducted in toluene at 90 °C with 3 equivalent of potassium phosphate as base (Scheme 26). Set up like this, we can judge a reaction to be successful, i.e., not suffering from an adventitious homocoupling side reaction leading to product composition, if conversion of aryl chloride **99** is high (near 100%) and the amount of formed byproduct **102** is low. Choosing 1.5 equivalent of boronic acid gives a chance for the formation of **102**, thus evidencing the cross- versus homo-coupling potential of the ligands in the chosen Suzuki–Miyaura reaction under the conditions described.

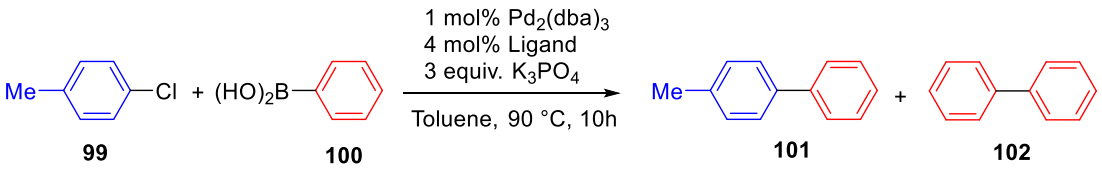

Ligand	Cross-coupled	Homo-coupled
	Conversion 99 [%]	Percent 102 [%][b]
93g	96	10%
93g[a]*	99	0%
93h	99	10%
93m	94	12%
93n	99	6%

[a] $Pd_2(dba)_3$ (0.5 mol%), ligand (2 mol%) was used.
[b] Caculated from GC ratio between **102:101**

Scheme 26. Percentage of homo-coupled product **102** under described reaction conditions when 1.5 equiv. boronic acid applied. The results were determined by GC analysis with *n*-dodecane as internal standard.

All four of the tested ligands (**93g, h, m** and **n**) gave good conversion of starting material **99**. In this case, the most bulky ligand, **93n**, performed best giving just 6% (mol/mol) homocoupled product (**102**); the other three ligands gave rise to only slightly elevated amounts of homocoupled side product (10–12% (mol/mol)). Additional, it has also been noticed that with lower palladium and ligand loading, **93g** can achieve 99% conversion without forming side product. Thus, demonstrating that under the conditions employed, reaction protocols used throughout this study do not suffer appreciably from loss of halide-containing starting materials through unwanted homocoupling.

2.3LLAMA & Lead like compounds

While the results discussed thus far have exemplified the effectiveness of ligands **93g** and **93m** to catalyse sterically demanding cross-coupling reactions, the ability to catalyse the cross-coupling of functionalities relevant to medicinal chemistry, to give a lead- and drug-like products remains a critical need in the agrochemical and

pharmaceutical sectors.[121] To this end, a range of biaryl products, containing motifs which are commonly encountered in drug discovery, were identified and ready for preparation.[167-169] The virtual product of SMC reaction of 48 aromatics halides and 44 aromatic boronic acids from (i) a collection held within the lead research group; (ii) those collated within the UoB scaffold resource and (III) boronic acid *via* GSK free building block resource; were enumerated and analysed by online research tool named LLAMA (Figure 28).[164]

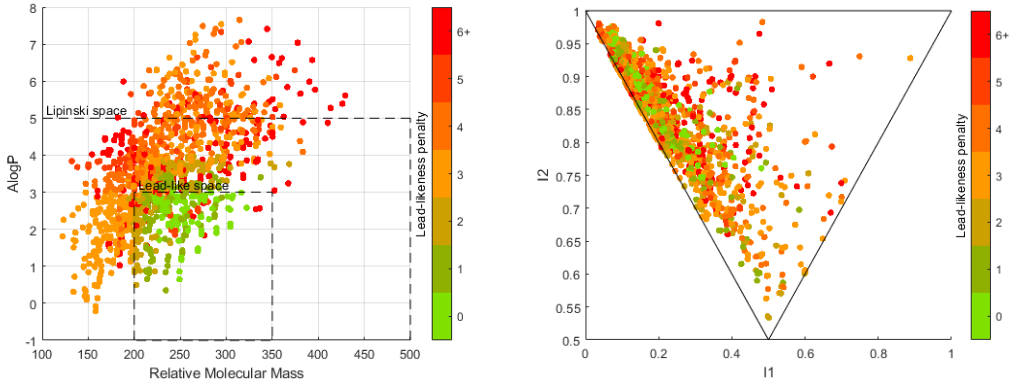

Figure 28. Virtual SMC product analysed in the LLAMA with lead-likeness (left) and PMI table (right)

LLAMA is an open-access web tool that allows users to upload the chemical structure and conduct virtual reaction to build their library compound.[164] The LLAMA tool can analyse the library and provide a series of molecular properties such as Alog P, molecular weight, and 3D character. A virtual library with 1661 small molecules was created by virtual SMC reaction has been analysed and presented in Figure 28. It has been observed that the majority of the product fall within the Lipinski space (Mw <500, Alog P <5), but only approx. 20% of fit within so-called 'lead-like' space, defined by Churcher *et al.* (200 < Mw <350, -1 < Alog P < 3).[164] The average of lead-likeness penalty scores of these compound is about 3.47. This penalty scoring system is developed by

LLAMA to visualise the distance between an ideal lead-like compound with the compound from visual synthesised and incorporates all determined molecular features into one scoring system. Principal moments of inertia (PMI) plot represent the geometry of the molecule, with top left-hand corner stand for a linear molecule, the top right-hand corner represents a spherical molecule, and the bottom corner represents a disc-like molecule (benzene). With the PMI plot (Figure 28, right), as can be observed that majority of the compound from virtual library are resides close to the right side of chart, which representing flat compounds.

From the 1661 virtual compounds constructed by the LLAMA tool, 14 possible products that accessed preferably lead-like chemical space were selected to explore the full potential of **93g** as ligand in SMC reaction (Scheme 27). The screening reaction condition, in this case, were modified to one hour in sealed-tube microwave heating at 100 °C in acetonitrile. The possible products include challenging heteroatom-containing and/or ortho substituents, representing both a set of possible products displaying favourable characteristics for drug discovery and a robust challenge for road-testing ligand **93g**. Desiring products **105a-j** has been successfully prepared with most of the reactions attempted gave greater than 50% isolated yield by utilising **93g** as ligand.

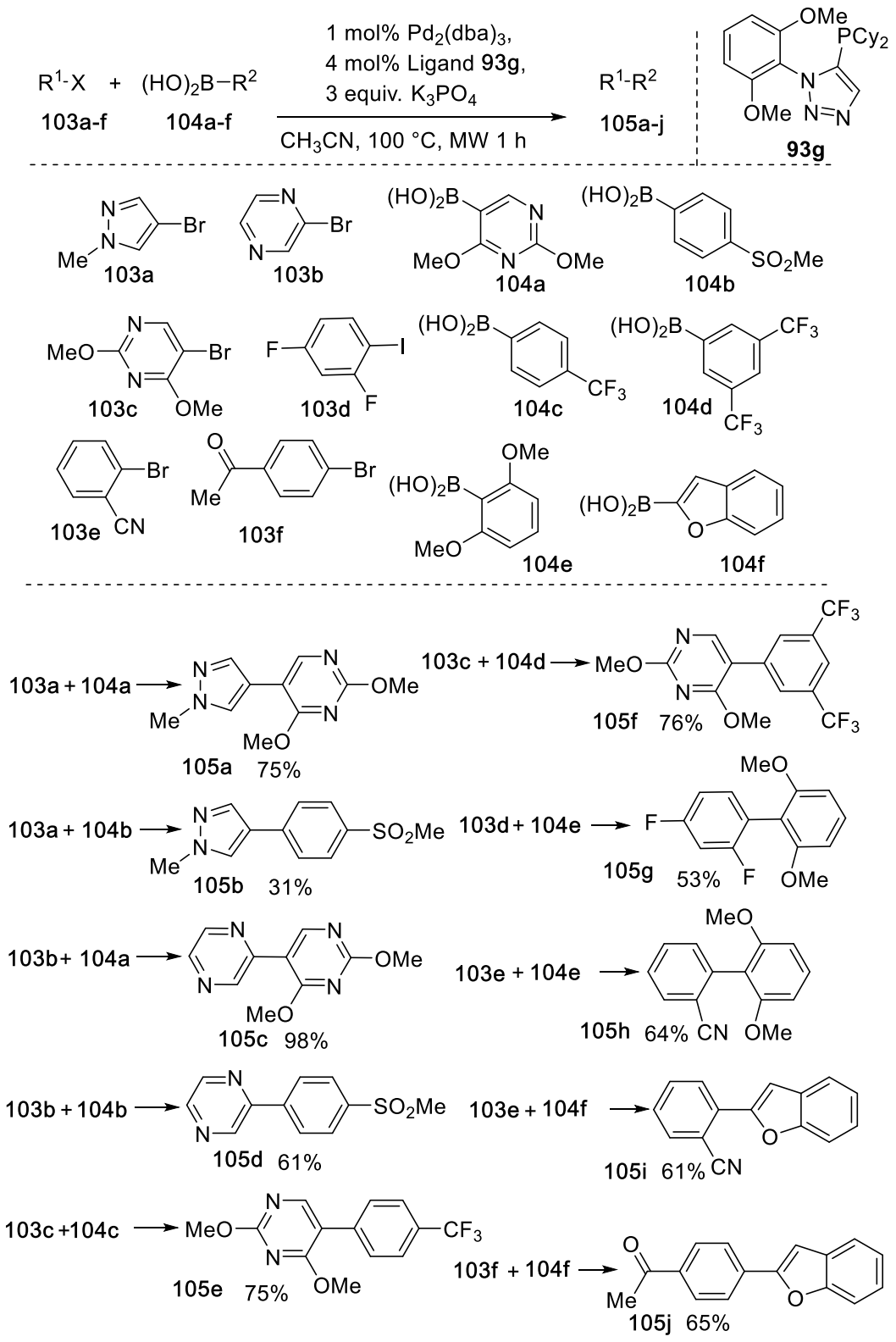

Scheme 27. Preparation of ten lead-like compounds via SMC with ligand **93g.**

To determine the lead-like properties of products synthesised in Scheme 27, these ten compounds have been load to LLAMA web tool for analyses (Figure 29). As can be observed from LLAMA plot, all the compounds are lying within the Lipinski rule, while four of them are fitting with lead-like space. This illustrates the potential for this catalytic system to synthesis compound, which are potential benefit to medicinal chemistry. PMI analysis of products demonstrate a capability of this catalytic system in making no-flat SMC products.

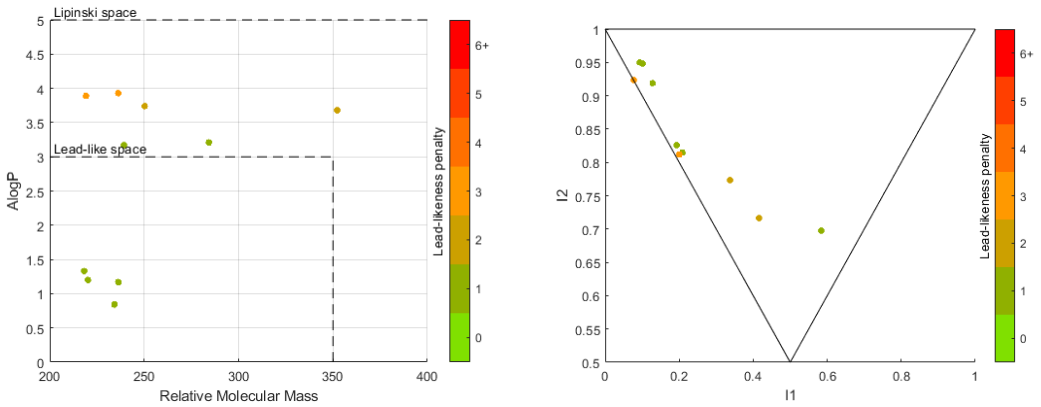

Figure 29. LLMA analyses result for selected synthesis product, with lead-likeness (left) and PMI table (right)

These analyses provide evidence that triazole ligand system can make the drug-like product to benefit in medicinal chemistry. And these ten compounds are still under evaluation of biological activity across a range of targets.

2.4 XRD structure &Bulkiness of phosphine ligand

During this project, numerous attempts to growing single crystals of ligand-palladium complex for X-ray study were made; thus, palladium phosphine complexes have been achieved, by using ligand **93e** and **93h** and palladium(II) precursor.

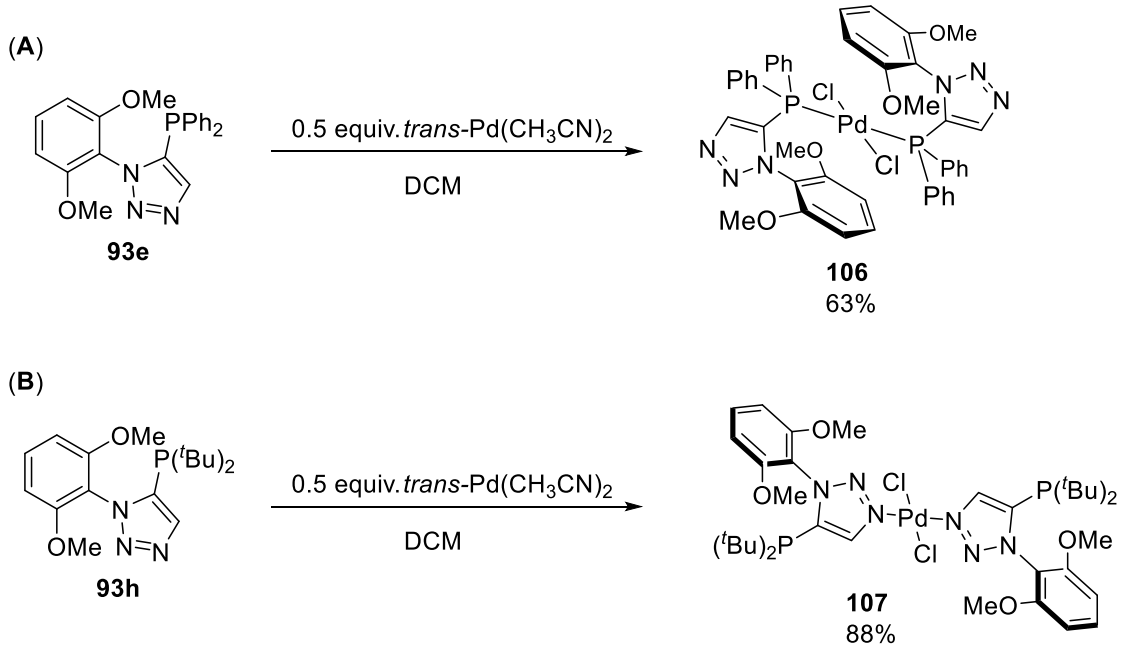

Scheme 28. Preparation of phosphine-palladium complexes

The mixture of **93e** and 0.5 equivalent of *trans*-$Pd(CH_3CN)_2Cl_2$ were dissolved in DCM solution at room temperature to form phosphine ligand metal complex in *situ*. Then pentane was added to the resulting solution to precipitate complex **106** with 63% yield. (Scheme 28, A). The obtained solid **106** was then recrystallised from DCM and hexane, and a single crystal has been obtained for x-ray analysis, with data presented in Figure 30. A 2:1 ligand: metal square planar trans palladium (II) dichloride complex has been observed. The structure features of complex **106** may unveil the structure-activity relationship with di-*ortho*-substituted **93** series. The five-membered 1,5-disubstituted 1,2,3-triazole core presents the triazole 2,6-dimethoxy aryl fragment oriented toward the metal with an aryl-centroid···Pd distance of 3.843(2) Å, in this solid-state structure. The triazole phosphine ligand offers a distinct geometric difference to phenylene core ligands (c.f. SPhos and XPhos), being more akin to other five-membered ring core

ligands (c.f., Figure 22, **83, 84**), generating a slightly wider metal-binding pocket while still offering a stabilising shield about the metal centre.

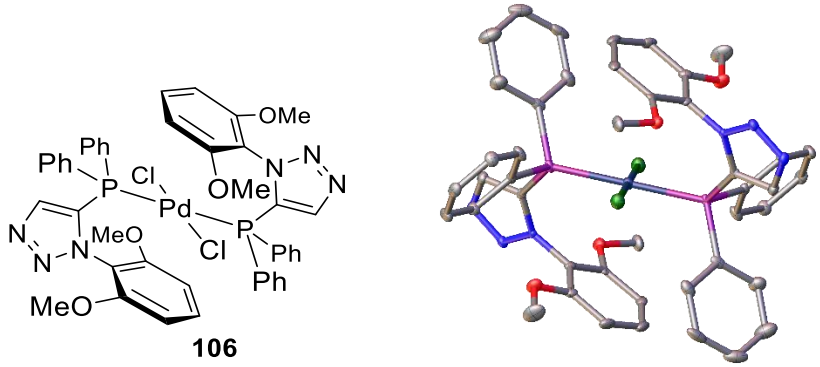

106

Figure 30. Representation of the crystal structure of **106**, ellipsoids are drawn at the 50 % probability level. The palladium complex was located on an inversion centre. Hydrogen and dichloromethane are omitted for clarity.

The mixture of **93h** and 0.5 equivalent of *trans*-$Pd(CH_3CN)_2Cl_2$ were dissolved in DCM solution at room temperature to form phosphine ligand metal complex in *situ*. Then pentane was added to the resulting solution to precipitate complex **107** with 88% yield. (Scheme 28, B). The obtained solid **107** was then recrystallised from DCM and hexane, and a single crystal has been obtained for XRD analysis, with data presented in Figure 31. Unexpected nitrogen-palladium coordination has been observed from X-ray analyses, with two *N-3* from triazole ring ligations are present in a *trans*-dichloride palladium (II) metal centre.

Since **93h** still functions as expected in the aforementioned catalysed reactions, it is suggested that a more crystalline and readily formed (kinetic) complex is formed under the crystallisation conditions employed. Similar nitrogen coordination has been observed from literature as well, but **107** is unique due to the phosphine is present.[170] However, this stable complex also reminds us of another potentially important feature of the triazole ligands, called a rear-side ancillary coordination, such as TBTA (Figure

13). It is conceivable that lone pair from nitrogen may offer some unique properties in some reaction such as aggregation suppression for example. Suffice it to say, the sterically encumbered phosphine face of ligand **93h**, as evidenced by the isolation of **107**, bodes well for understanding differing catalysis modes of action on steric rationales as well as opportunities for divergence from phenylene core ligands.

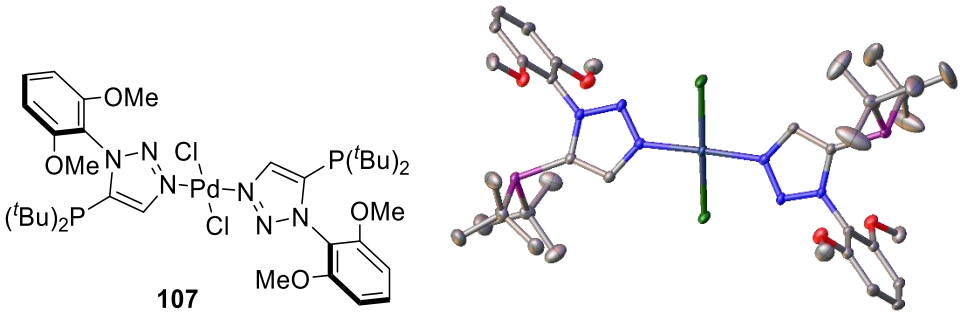

Figure 31. Representation of the crystal structure of **107**, ellipsoids are drawn at the 50 % probability level. The palladium complex is located on an inversion centre. Hydrogen and two molecules of dichloromethane are omitted for clarity.

The phosphine-Pd complexes **106** and **107** were also tested in benchmark cross-coupling reaction (Table 6). Under the reaction employed, **106** and **107** maintained catalytic activity compared with **93e** and **93h**. Triazole **92h** was also tested in this reaction with no conversion of starting material observed. This also suggested the phosphine unit is necessary to achieve a good catalytic activity in the ligand **93** series.

Table 6. Complex screening of **106, 107** and **92h** in Suzuki cross-coupling with **88** and **89**

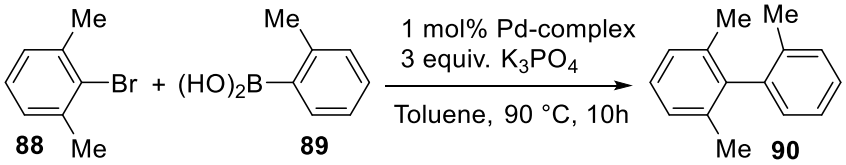

Entry	Complex	Conversion [%] [a, b]	Isolated yield [%]
1	**106**	88	79
2	**107**	94	85
3	**92h, $Pd_2(dba)_3$**[c]	7	-

[a] Reaction conditions: 2-Bromo-*m*-xylene (0.4 mmol), *o*-tolylboronic acid (0.6 mmol), potassium phosphate (1.2 mmol), palladium-phosphine complex (1 mol%), toluene (3 mL), 10 h, 90 °C. [b] Conversion determined by inspection of the corresponding ^{1}H NMR spectrums of crude reaction isolates.[c] 2 mol% **92h** and 0.5 mol% $Pd_2(dba)_3$ were used

There is a growing body of literature discussing the importance of various parameters including steric effects of bulky phosphines relating to suitability and efficacy in catalysis.[171-174] Tolman's cone angle was an effective descriptor about bulkiness of ligand.[159] But it has been complemented more by recently by Nolan's percent buried volume, ($\%V_{bur}$).[175] Thus, $\%V_{bur}$ of our phosphine ligands have been determined by SambVca web tool.[176]

The crystal structure of the free ligand **93g** was first investigated, the PDB file corresponding to the XRD of **93g** was modified in Spartan software, by virtually adding a palladium to phosphorus with a standard bond length of 2.280 Å to generate a palladium-coordination model. The new PDB file was uploaded SambVca 2.0 web tool for analysis without further minimised or edited. The added palladium was set as the centre then deleted during the calculation process. Thus, a summary of the analysis was generated (Figure 32). A steric map generated from this analysis is shown in, and

a 47.0%V_{bur} was calculated with default SambVca settings. The topographic steric maps highlight the surface of interaction between the catalytically active metal and the substrate, shaped by the spectator ligands in the complex.

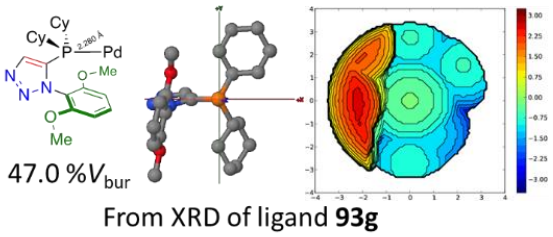

Figure 32. Steric map of phosphine-palladium complex: derived from the crystal structure of free ligand **93g** with a P-Pd distance of 2.280 Å applied, resulting in a 47.0% V_{bur}.

Follow this analysis, the only successfully obtained palladium phosphine complex **106** with XRD structure has been analysed by the same protocol. It should be noticed that **106** is a square planar palladium (II) complex of ligand **93e** and as such does not necessarily represent the catalytically relevant species, the determined %V_{bur} of 36.2% (Figure 33, A) may not the best comparator across with rest of ligands. In order to find an appropriate comparison to fairly evaluate relative steric parameters of triazole phosphine ligand **93** series. Crystal structure file of **106** was edited in Spartan and P-Pd length adjusted to 2.280 Å as same with **93g** at Figure 32. And the new determined of %V_{bur} of 36.9% (Figure 33, B) was essentially the same as that for the slightly longer, crystallographically determined, Pd–P bond length in the earlier analysis. Since a model to allow for comparison of ligands where crystallographically determined data is not available was ultimately sought two further analyses were conducted.

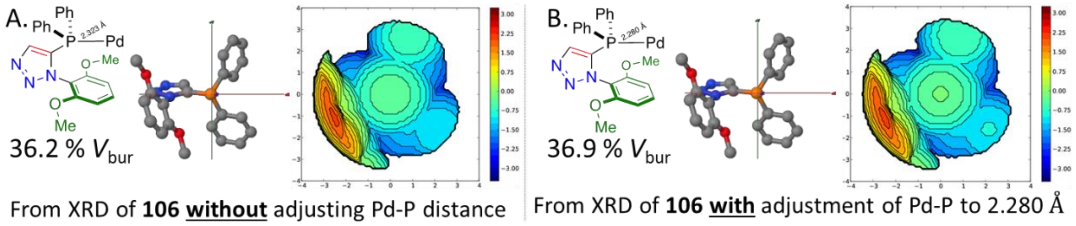

Figure 33. Steric map of phosphine-palladium complex: Derived from crystal structure of **106**. A, without adjusting Pd-P distance, B, fixed Pd-P to 2.280 Å

It has been reported by Sigman *et al.* that using phosphine oxides as computational models for structural minimisation proxies of ligand-metal complex.[177] Thus, it was reasoned by using in silico-generated phosphine oxides for computational minimisation might be a sensible method to characterise bulkiness of **93** ligand series. Two approaches were compared for optimisation and determining the $\%V_{bur}$ of ligand **93e** as an example (Figure 34). In the first case, a phosphine oxide with geometric restrictions was used, and dihedral geometries of atoms 1 to 6 were restricted presenting the aryl group directly and orthogonally aligned to the vector of phosphine (Figure 34, left).; in the second case, there is no geometries restriction of phosphine oxide (Figure 34, right). This two model were adopted the same minimisation and optimisation cascade. The lowest energy structure was obtained from both model, thus edited to replace the oxygen (from phosphine oxide) with a palladium atom with fixed bond length of 2.280 Å. (Figure 34, centre).

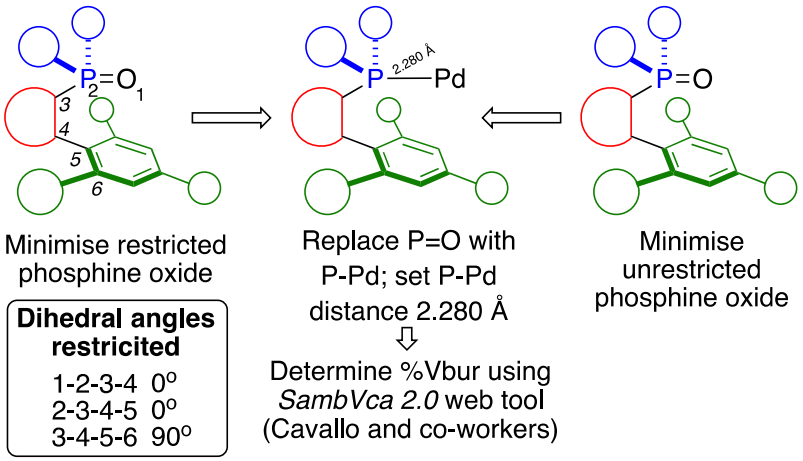

Figure 34. The minimisation protocol for obtaining structures for comparison of steric parameters *via* an unrestricted (right) and a dihedral angle restricted model (left).

The procedure outlined in Figure 34, was first applied to ligand **93e**, and $\%V_{bur}$ 44.2 for restricted and 47.3% for unrestricted geometries model, respectively (Figure 35). Although this method gives slightly higher values of $\%V_{bur}$, the restricted geometry model is more closely aligned to the XRD-derived file than the unrestricted one. It should be noticed that with only one example, it is difficult to confirm whether this model provides the best approach for assessing the bulkiness of ligands when single crystal data are not available for exploring. Furthermore, the XRD-derived **106** $\%V_{bur}$ are based on palladium (II) from solid-state might not offer the best cross-ligand comparison. As such, the most active ligands of our study were examined using both protocols shown below (Figure 35).

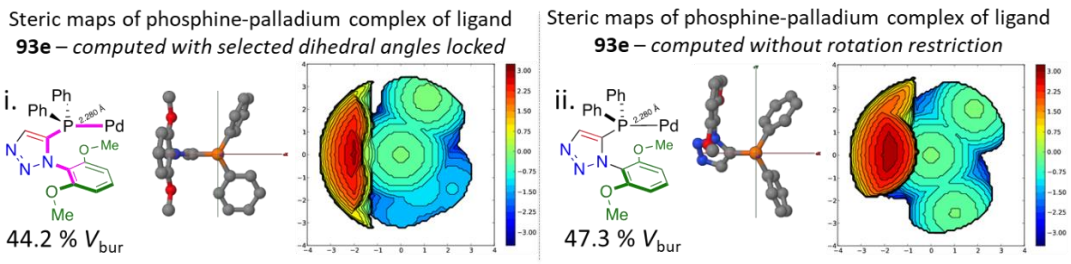

Figure 35. Steric map of phosphine-palladium complex: Derived from **93e** in silico with restricted dihedra angle (left) and unrestricted (right).

The $\%V_{bur}$ and steric maps of four triazole derived ligand and Buchwald ligand of Figure 27, are shown in Figure 36. The left column represented data with restriction of dihedral angle and none restriction on right column. It is interesting and confounded our expectation that unrestricted geometry gives a higher $\%V_{bur}$ than the restricted one. While the geometry-unrestricted structures of triazole ligands bear a striking resemblance (by rudimentary visual inspection) to any XRD-derived structures, the buried volume determinations of previously reported SPhos and XPhos (by derived from phosphine oxide) complexes more closely match the geometry-restricted models employed

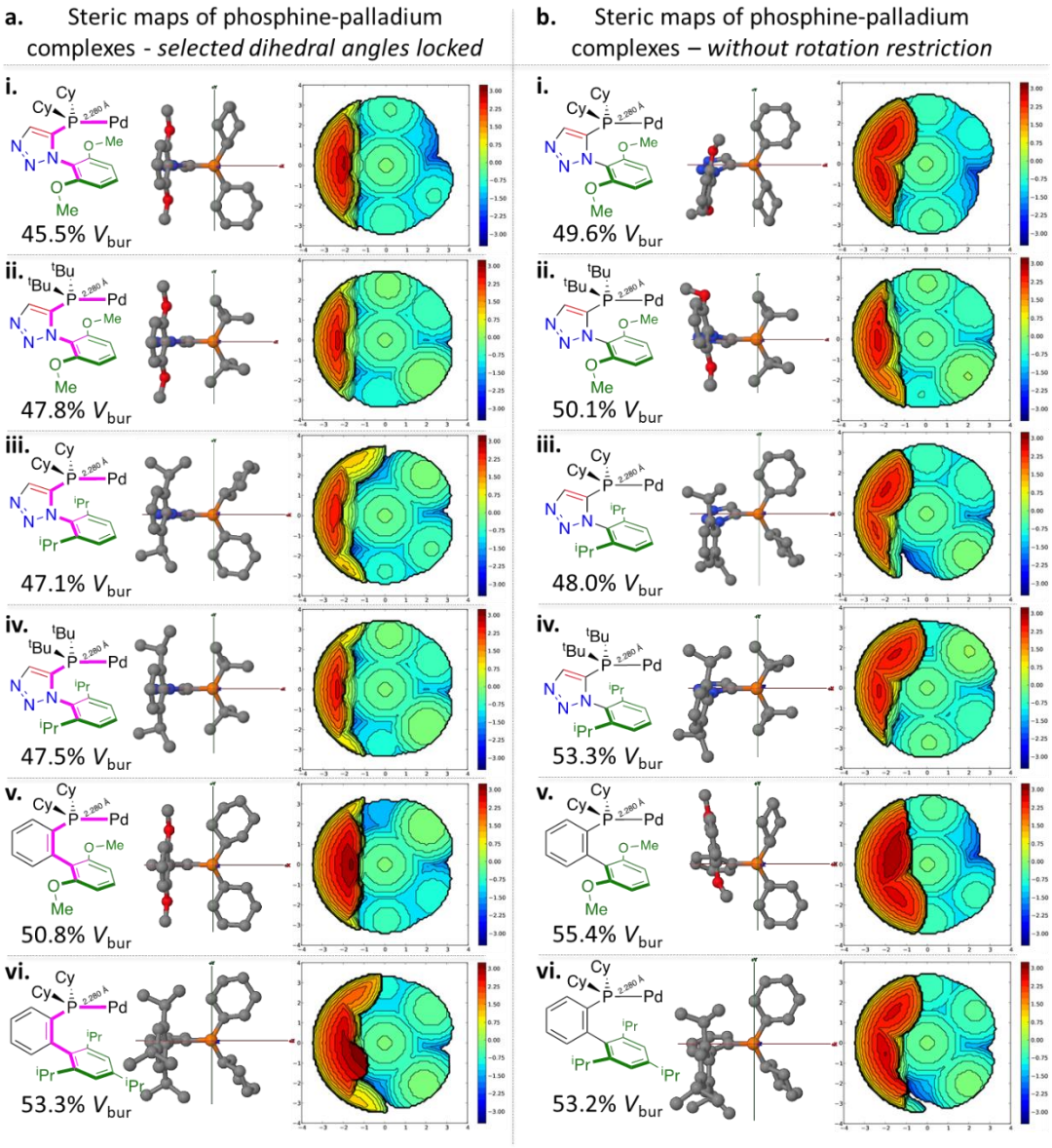

Figure 36. The SambVca 2.0 derived %V_{bur} and steric maps for the: i. **93g**; ii. **93h**; iii. **93n**; iv. **93m**; v. SPhos; vi. XPhos, derived palladium complexes of structures derived in silico

Further analysis **93a-n** side by side by using restricted dihedral angle minimisation protocol and plotting the %V_{bur} and conversion from Table 2 together (Figure 37). A strong relationship between bulkiness and conversion has been observed. Essentially any %V_{bur} value above 46% leads to quantitative conversion to products, under the prescribed conditions.

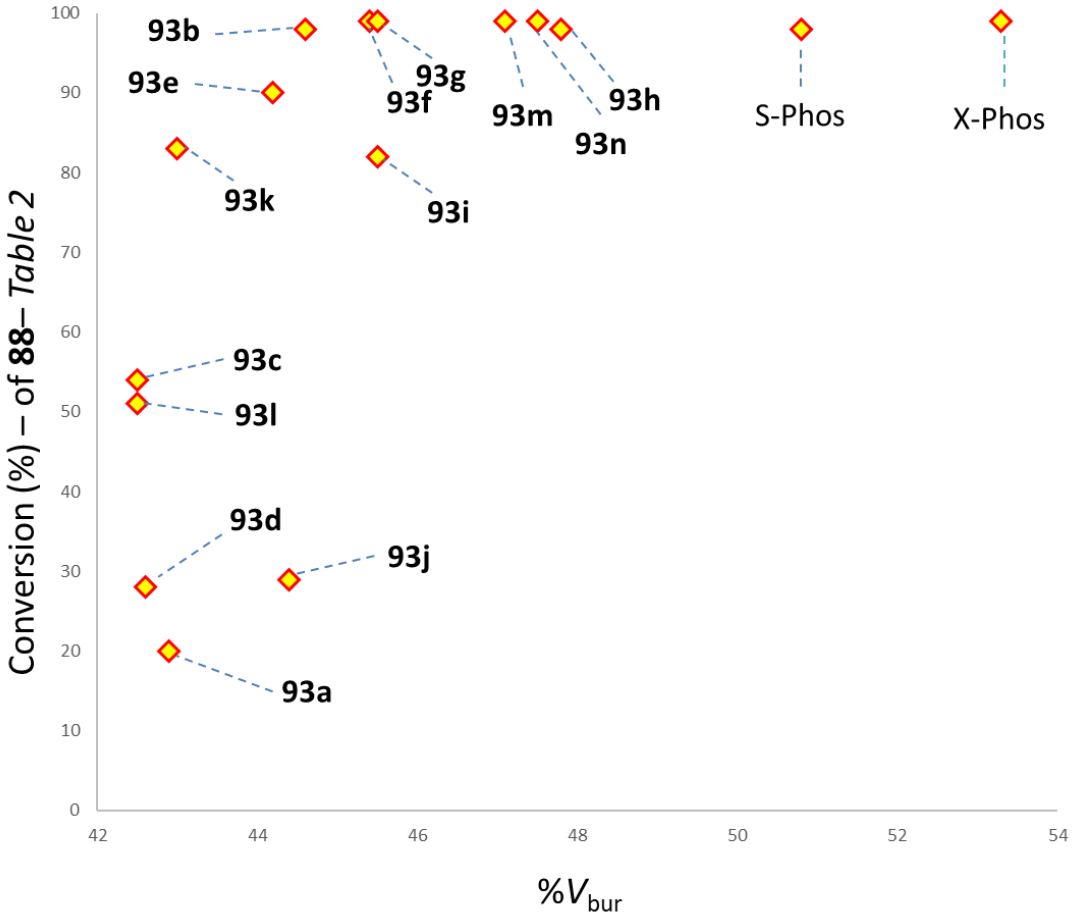

Figure 37. Conversion to **80** versus computed %V_{bur} as determined by the same protocol.

Further analysis of the data obtained for conversion in reactions catalysed by **93** ligands series is only against small datasets, and significant correlations of variances in conversion might lead to no meaningfully comparable correlations.

2.5 Conclusion

Two series of triazole-containing phosphine ligands were synthesised and tested in SMC reaction with bulky and heteroatom-containing substrates. The bulkiness of **93** ligand series were determined by a restricted dihedral angle with phosphine oxide in silico. And a general protocol for measuring phosphine ligand bulkiness via SambVca has been established in this project. Furthermore, a trend between the bulkiness of

ligand and catalytic in bulky substrate has been observed. Notably, triazole nitrogen's may not be entirely innocent in the coordination environment since a nitrogen-palladium coordination has been observed with the presence of phosphine motif. The ligand series are compatible with commercially available Buchwald ligand. The phosphine ligand reported in this chapter could use in preparation of lead-like compound throughout cross-coupling reaction.

Experiment work in Scheme 27 was carried out jointly between the author of this thesis and Huy Nguyen (UoB). Figure 32-37 were generated by John Fossey (UoB), and data of this chapter were initially published in Organometallics.[20]

3. Chapter 3 Balancing Bulkiness in Phosphino-Triazole Catalysis

3.1 Design and Preparation

As mentioned in the earlier chapter, bulky phosphine ligands can offer significant and well-documented advantages in transition-metal catalysed reactions.[149] The landmark contribution of Buchwald *et al.* have led to a deeper understanding of the properties required for highly active ligands. [116]

The first generation of phosphine contained triazole has been synthesised and achieving promising result in palladium catalysed Suzuki-Miyaura cross-coupling (Figure 38). Analysis of the steric parameter of ligand has led to the primary conclusion that the catalytic activity of phosphine ligand was enhanced with the increasing of the bulkiness of ligand.[20] Thus, to push this concept even further, bulkier ligands are required.

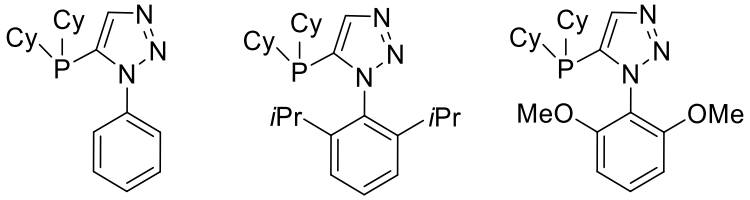

93b **93m** **93g**

Figure 38. Selected example of ligand in Chapter 2.

The 1-aryl triazole phosphine ligand series, such as **93g** (Figure 38), the 1-aryl fragment was presented in the same orientation as the phosphorus lone pair and potentially the same direction of metal when coordinated, thus significantly impacting the determined buried volume. As been observed in chapter 2, the bulkiness of ligand can be modified

by different phosphorus substituted units (such as di-cyclohexyl or di-*tert*-butyl group) or other functional groups of aryl unit from triazole. This offered a new strategy in ligand designing with the phosphorous atom flanked by up to three, rather than one triazole unit. A series of ligands ranging from zero to three triazoles, for comparison of the manifested bulk about the phosphorus centre by 1,5 - disubstituted - triazole motif(s), was proposed. (Figure 39). As changing the triazole number attached to the phosphorous atom, various buried volume results could be occurred and can impart favourable properties as ligands in catalysis. In this study, a series of phosphines comprising of triphenylphosphine (**108a**) and tricyclohexylphosphine (**108b**) along with mono-triazole-appended phosphines **93a** and **93b** from chapter 2, and previously unprepared bis-triazole **109a**, **109b** and tris-triazole **110a** was investigated.

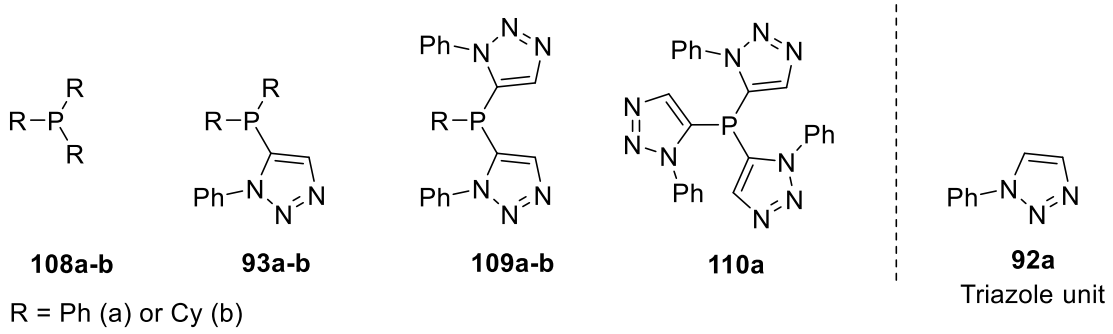

Figure 39. Proposed structure with different number of triazole **92a** in phosphorous ligand.

The substituents attached to phosphorus and the triazole nitrogen, could in principle be varied significantly. To provide a benchmark reaction in this initial investigation, phenyl triazole (**92a**) was selected as only triazole motif, while functional group attached to phosphorus has been restricted to phenyl- and cyclohexyl- groups (Figure 39). As such, two series of aryl- and alkyl-substituted phosphines were planned for synthesis.

Preparation of triazole unit **92a**, ligand **93a** and **93b** has already been synthesised and fully characterised in chapter 2. Similar protocol was taken into the synthesis of **109a-b** and **110a**. Triazole unit **92a** was selectively deprotonated at the *C-5* position, followed by quenching with electrophile phenyl- or cyclohexyl phosphorous dichloride to furnish **109a** and **109b** respectively. When a third equivalent of phosphorus trichloride was added to deprotonated **92a**, resulted and was subsequently isolated in 77% yield of **110a**.

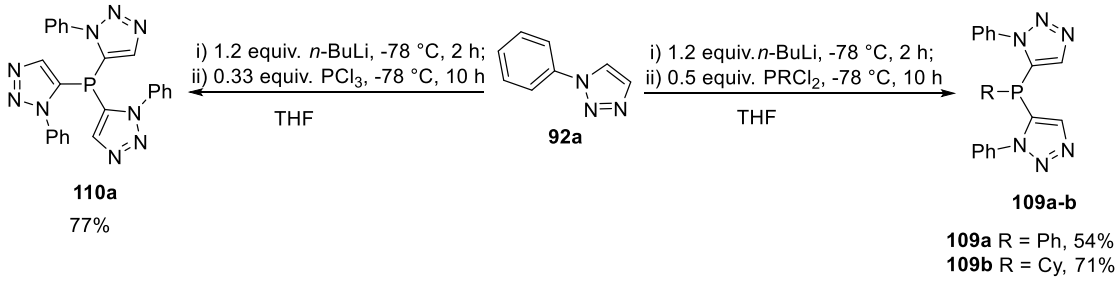

Scheme 29. Preparation of bis-triazole and tris-triazole substituted phosphorous ligand.

The proton and carbon NMR of **110a** (in $CDCl_3$ at room temperature) show a single set of well-defined resonance, corresponding to the three equivalent triazole arms of **110a**, suggesting a high degree of symmetry in solution on the NMR time scale. In addition, with increasing the number of triazole motif, an increasing high-shielding ^{31}P-NMR signal has been observed (*Table 7*).

Table 7. ^{31}P-NMR shift (δ ppm) for triphenylphosphine, tricyclohexylphosphine and triazole containing ligands

	108a-b	**93a-b**	**109a-b**	**110a**
(**a**)Ph	-5.5	-35.5	-64.3	-93.5
(**b**)Cy	11.2	-30.2	-65.9	

^{31}P-NMR signals in $CDCl_3$, data recorded as (δ ppm), all the result was obtained from P-H decoupled method

The structure of **109a** and **109b** were confirmed by X-ray structure, a single crystal suitable for analysis were isolated from recrystallisation from slow evaporation of DCM solution, respectively (Figure 40). In the solid-state structure of **109a**, only one of the aryl group from triazole unit points in the same direction as the lone pair of phosphorous, while in the case of **109b**, both aryl groups point broadly in the same direction as the phosphorus lone pair, thus boding well for a systematic study of the effect of modulating the steric crowding or bulkiness about a coordinated metal in a catalytically relevant complex.

(i)

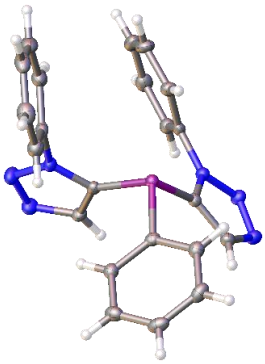

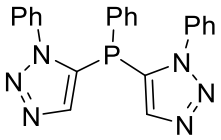

109a

(ii)

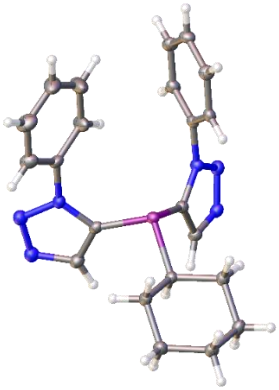

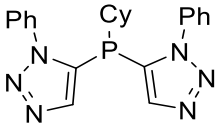

109b

Figure 40. X-ray determined structure of **109a (i)** and **109b (ii)**, ellipsoid are drawn at the 50 % probability level.

In the case of compound **110a**, a suitable single crystal was obtained from the recrystallisation of **110a** by slow evaporation from acetone solution. The solid-state configuration contains two unique molecules in the unit cell, both of which show the aryl arms of the triazole are directed along the same orientation as the phosphorus lone pair, creating a bowl-shaped ligand.

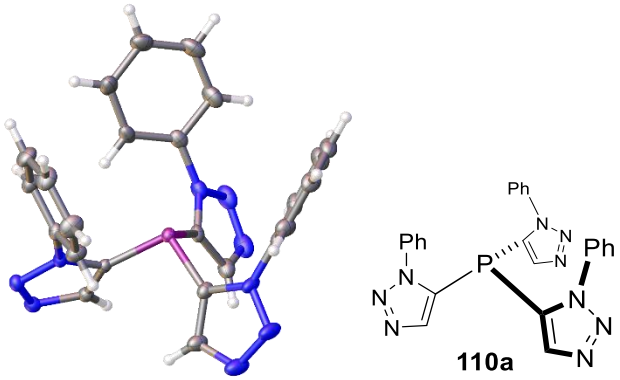

Figure 41. Determined X-ray structure of **110a,** ellipsoid are drawn at the 50 % probability level. Each until cell contained two molecules of **110a** and a molecule of acetone was omitted for clarity.

3.2 Gold(I) complex synthesis and structural analysis

Since a potential binding pocket has been observed in X-ray structure analysis of **110a**, instead of using square binding pattern metal like palladium(II), gold(I) has been selected for coordination due to the potential linear binding pattern with phosphine-gold(I) chloride. In addition, gold(I) phosphine complexes have achieved tremendous success as catalysis.[178] Complemented by commercially available sourced, triphenylphosphine **108a** and tricyclohexylphosphine **108b**, two ligand sets corresponding to Figure 39 were therefore available for comparison in the complexation of a chosen metal. The X-ray structure of gold(I) chloride complexes of **108a** and **108b** have been previously reported by other research groups.[179, 180]

Phosphine-gold complexes of the rest ligands have been prepared by the similar protocol, with moderate to good isolated yields, as presented in Scheme 30. Triphenylphosphine gold(I) chloride (**111a**) and tricyclohexylphosphine gold chloride (**111b**) has been purchased from commercially available suppliers.

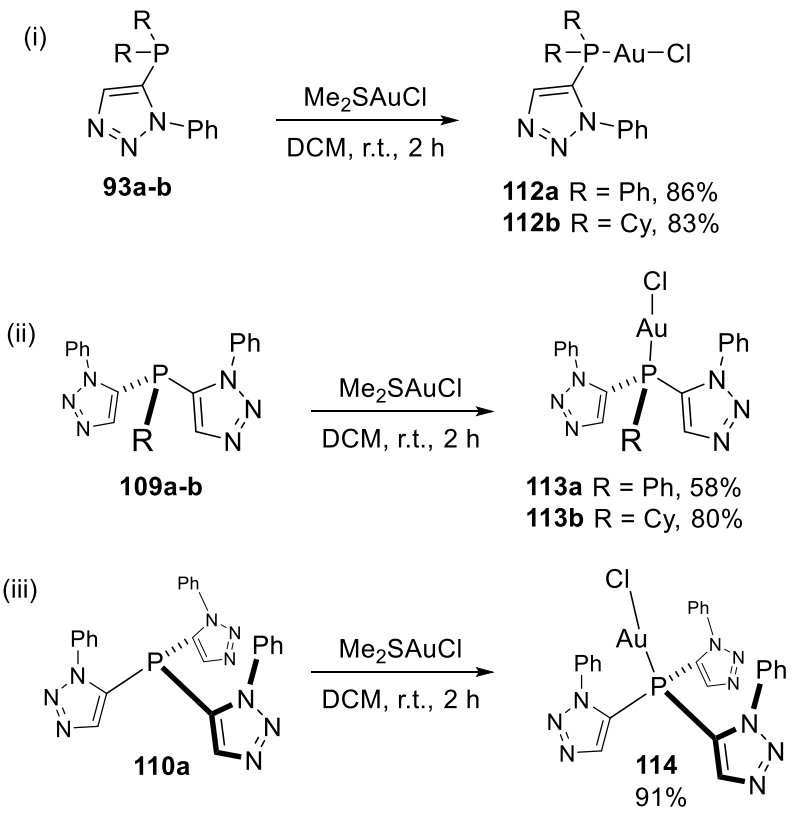

Scheme 30. Preparation of gold(I) chloride phosphine complex with different number of triazole motif.

The single-crystal X-ray structures of gold(I) chloride complexes **111a** and **111b** have been previously reported in the literature. The deposited PDB files were used to render images (Figure 42) and determine the percentage buried volume by using SambVca (2.0). Triphenylphosphine gold(I) chloride **111a** has a 30.8%V_{bur} whereas the tricyclophenylphosphine gold(I) chloride complex **111b** has a 33.9%V_{bur}. The single-crystal X-ray diffraction structures of **112a** (Figure 43), **112b** (Figure 43), **113a** (Figure 44), **113b** (Figure 44), **114** (Figure 45) were obtained from the complexes synthesised

herein, and same analytical studies have been conducted, and %V_{bur} were listed below. The crystal structures of the gold-phosphorus bond lengths used in the buried volume determinations were those obtained crystallographically.

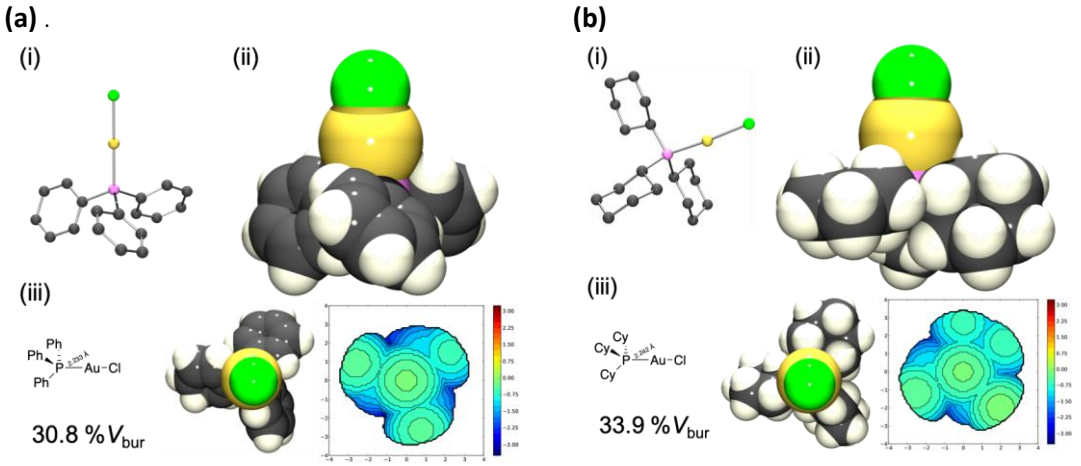

Figure 42. (a) (i)X-ray study of literature deposited CIF file of **111a**, ellipsoid are drawn at the 50 % probability level, hydrogen omitted for clarity;(ii)space-filling model; (iii) %V_{bur} of **111a** (30.8%),steric map; (b) (i)X-ray study of literature deposited CIF file of **111b**, ellipsoid are drawn at the 50 % probability level, hydrogen omitted for clarity;(ii)space-filling model; (iii) %V_{bur} of **111b** (33.9%),steric map

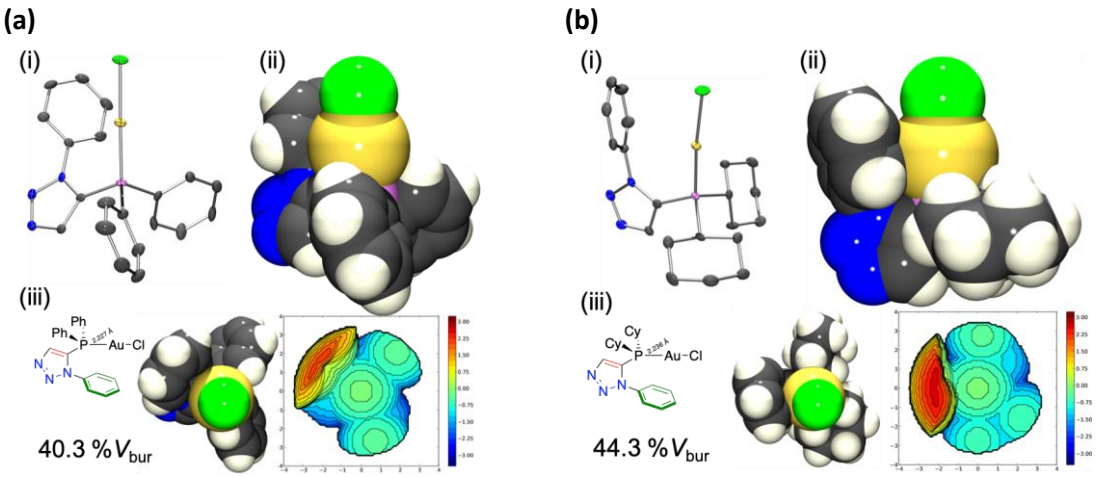

Figure 43. (a) (i)X-ray study **112a** ellipsoid are drawn at the 50 % probability level, hydrogen omitted for clarity;(ii) space-filling model; (iii) %V_{bur} of **112a** (40.3%), steric map; (b) (i)X-ray study of **112b**, ellipsoid are drawn at the 50 % probability level, hydrogen omitted for clarity;(ii) space-filling model; (iii) %V_{bur} of **112b** (44.3%), steric map

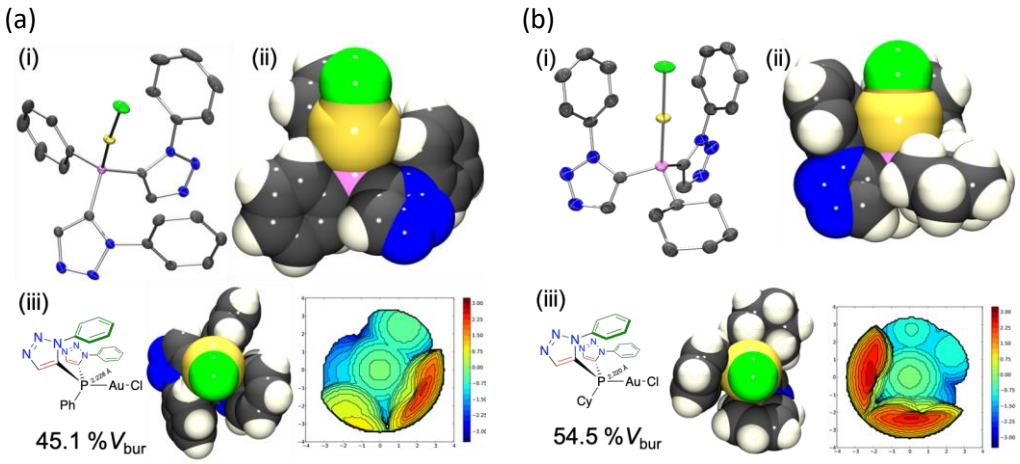

Figure 44. (a) (i)X-ray study **113a**, ellipsoid are drawn at the 50 % probability level, hydrogen omitted for clarity;(ii) space-filling model; (iii) $\%V_{bur}$ of **113a** (45.1%), steric map; (b) (i)X-ray study of **113b**, ellipsoid are drawn at the 50 % probability level, hydrogen omitted for clarity;(ii) space-filling model; (iii) $\%V_{bur}$ of **113b** (54.5%), steric map

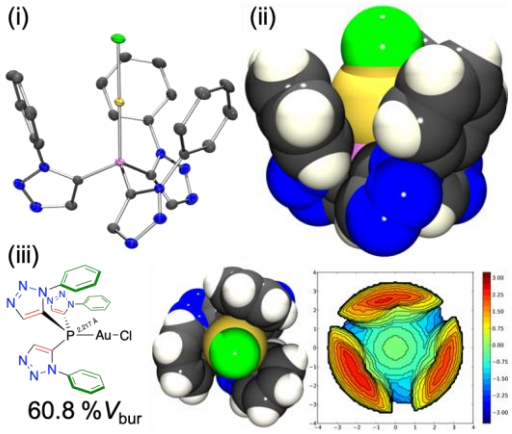

Figure 45. (i)X-ray study **114**, ellipsoid are drawn at the 50 % probability level, hydrogen omitted for clarity;(ii) space-filling model; (iii) $\%V_{bur}$ of **114** (60.8%), steric map.

The summary of $\%V_{bur}$ has been listed in Table 8, and it shows that cyclohexyl substituted group confer higher bulkiness compared with phenyl substituted group, and with the increasing number of triazole, the buried volume increased as well, with tris-triazole substituted phosphine ligand reach to 60.8% in $\%V_{bur}$.

Table 8. Summary of percent buried volume of phosphine gold complex (determined from x-Ray result)

	111a-b	**112a-b**	**113a-b**	**114**
(**a**)Ph	30.8%	40.3%	45.1%	60.8%
(**b**)Cy	33.9%	44.3%	54.5%	

Percent buried volume (%V_{bur}) have been determined from x-ray structure via SambVca web tool, Au-P bonds length are taken from XRD without further modification.

Since previously prepared mono-triazole-containing phosphines **93e** and **93g** were readily available to this programme of study (chapter 2), and as **93g** was shown previously to have been among the superior ligands of the mono-triazole set in earlier palladium-mediated Suzuki-Miyaura catalysis, the synthesis of gold(I) chloride complexes thereof was also attempted. The phosphine gold(I) chloride of **93g** was prepared with the same protocol, by mixing equal equivalent of **93g** and dimethyl sulphide gold chloride, and precipitation of complex **115** with hexane (Scheme 31).

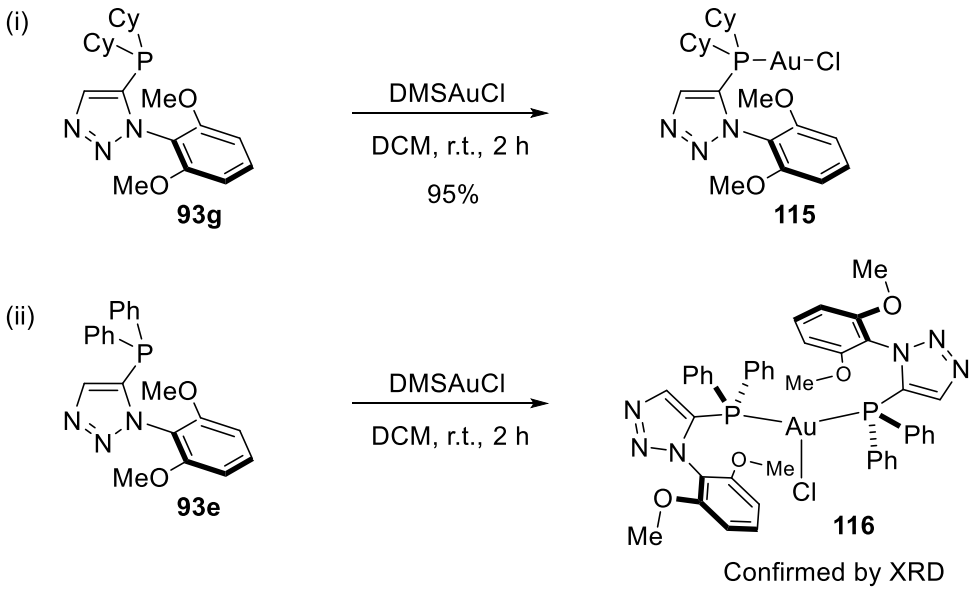

Scheme 31. Preparation of gold complex **115** and **116**

A single crystal XRD structure of **115** was observed (Figure 46). The calculated %V_{bur} of **115** was equal to 46.0%, which was match quite well with our restricted rotation model

in Figure 36 (Chapter 2). Attempts to prepare a 1:1 complex of **93e** and gold(I) chloride under the same conditions were inconclusive. However, a trigonal 2:1 ligand/gold(I) chloride complex **12** was identified by single-crystal X-ray diffraction crystal structure determination (Figure 46, B) from a mixture of otherwise unidentified products. A 76.6% $\%V_{bur}$.was determined from the obtained crystal structure. Attempts to prepared **116** by using two equivalents of ligand **93e** still give inconclusive results. It is noteworthy that this 2:1 phosphine: gold complex has been similarly reported for $(PPh_3)_2Au(I)Cl$ and $(PPh_3)_2Au(I)SCN$. [181-183] Therefore, the crystal structure of 12 is included for completeness. Attempts to prepare two and three 2,6 dimethoxy phenyl triazole-containing variants of **109**(**a** or **b**) and **5** failed to deliver any desired products.

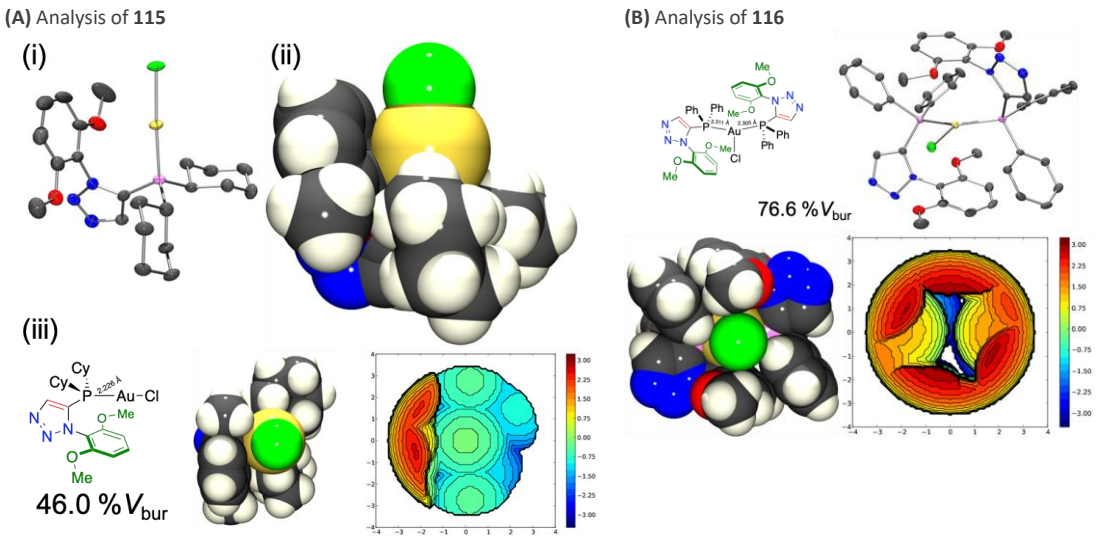

Figure 46. A (i) X-ray study **115**, ellipsoid are drawn at the 50 % probability level, hydrogen omitted for clarity;(ii) space-filling model; (iii) $\%V_{bur}$ of **115** (46.0%), steric map; B (i) X-ray study **116**, ellipsoid are drawn at the 50 %probability level, hydrogen omitted for clarity;(ii) space-filling model; (iii) $\%V_{bur}$ of **116** (76.6%), steric map.

3.3 Catalytic screening

With the set of new phosphine compounds in hand, their effectiveness as phosphine ligands in palladium catalysed SMC reaction was tested (Table 9), in order to distinguish the efficiency of ligand, more challenging reaction condition was selected with less

palladium loading (0.2 mol%), the conversion has been monitored with GC in 6-hour and 24-hour time point. As the data listed in Table 9, catalyst systems with cyclohexyl substituted ligands provide activity compared with the phenyl substituted ligands. In the phenyl substituted phosphine ligands, **93a** with one triazole unit shows best activity (Entries 1-3). Solubility of tris-triazole ligand **110a** was very poor in toluene, thus no conversion has been observed in entry 4. **109b**, **93b**, **93g** possess good activity in this reaction, with quantitative conversions obtained.

Table 9. Ligand screening: triazole containing phosphine ligand in Suzuki-cross-coupling

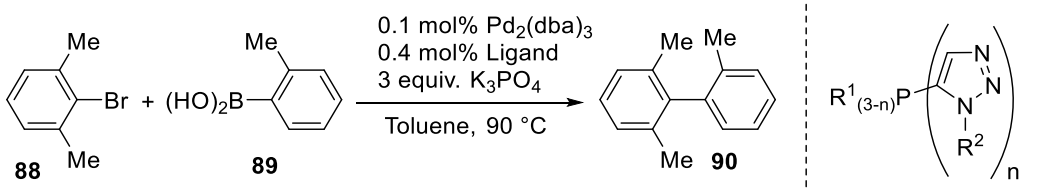

Entry	R^1	R^2	Ligand	Triazole No.(n)	Conversion [%] [a, b] 6h	24h
1	Ph	-	**108a**	**0**	37	45
2	Ph	Ph	**93a**	**1**	56	63
3	Ph	Ph	**109a**	**2**	44	68
4	-	Ph	**110a**	**3**	0[c]	0[c]
5	Cy	Ph	**109b**	**2**	100	100
6	Cy	Ph	**93b**	**1**	100	100
7	Cy	-	**108b**	**0**	80	80
8	Cy	2,6-DMP[d]	**93g**	**1**	100	100

[a] Reaction conditions: 2-Bromo-*m*-xylene (0.4 mmol), *o*-tolylboronic acid (0.6 mmol), potassium phosphate (1.2 mmol), $Pd_2(dba)_3$ (0.1 mol%), ligand (0.4 mol%), toluene (3 mL), 10 h, 90 °C. [b] Determined by GC analysis with *n*-dodecane as internal standard. [c] Solubility of ligand **110a** is very poor. [d] 2,6-DMP = 2,6-dimethoxyphenyl

In the case of gold complexes, the effectiveness as precatalysts for gold-catalysed hydration of terminal alkyne has been tested (Table 10). Catalytically active cationic gold(I) species were generated by silver mediated chloride abstraction, and choice of appropriate counter‑anion showed moderate catalytic effects.[184-186] In this study,

silver triflate was selected as a chloride abstraction reagent. Initially, the gold-catalysed hydration of 1-decyne **117a** was performed with 0.5 mol% gold complex loading and 1 mol% of silver triflate to activate the catalyst. Starting material **117a** was dissolved in methanol, followed by the addition of precatalyst solution. Since complex **114** was not well solubilised in methanol, a protocol of activation in dichloromethane and dilution in methanol was deployed. To facilitate comparison in the subsequent reactions with lower catalyst loadings (0.25 and 0.05 mol% of gold complex), the dichloromethane activation and methanol dilution protocol was used in those cases. Following the addition of water (2 equiv.), all reactions were heated at 80 °C in a sealed tube for two hours, and conversions to ketone **118a** were determined by gas chromatography.

Table 10. Screening of ligand in hydration of alkyne **106a** to ketone product **107a**.

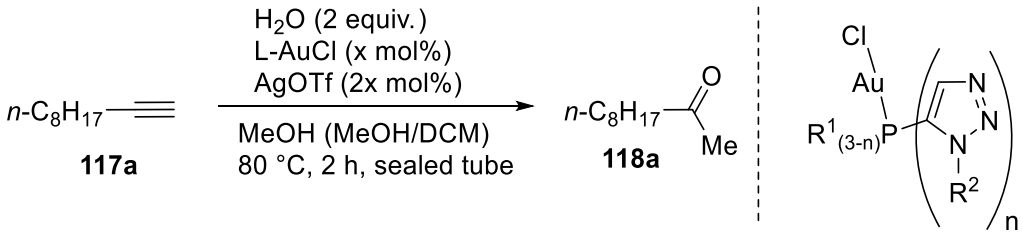

Entry	R^1	R^2	L-AuCl	Triazole No. (n)	Conversion (%) (x mol%)		
					0.50[a]	**0.25**[b]	**0.05**[b]
1	Ph	-	**111a**	0	>99	52	3
2	Ph	Ph	**112a**	1	>99	57	4
3	Ph	Ph	**113a**	2	>99	26	2
4	-	Ph	**114**	3	32[b]	11	4
5	Cy	Ph	**113b**	2	>99	46	3
6	Cy	Ph	**112b**	1	>99	>99	9
7	Cy	-	**111b**	0	>99	86	10
8	Cy	2,6-DMP[c]	**105**	1	>99	>99	10

[a] Methanol used as solvent, unless otherwise stated; [b] Catalyst precursor initially solubilised in dichloromethane and dispersed in methanol, such that the resulting solvent composition was 10% CH_2Cl_2 and 90% MeOH; [c] 2,6-DMP = 2,6-dimethoxyphenyl. Conversion was determined by GC with n-dodecane as internal standard.

With 0.5 mol% loading of catalysts, most reactions including triphenylphosphine gold chloride **111a** and tricycohexylphosphine gold chloride **111b**, achieved in high conversion except the bulkiest complex **114**, only reaching 32% conversion of starting material. When lower catalyst loadings were probed, 0.05 mol% of gold(I) complexes proved to be too insufficient to achieve satisfactory conversion with two hours (the maximum conversion observed across the set was 10% under these conditions). Good gradation across the test series was seen at a 0.25 mol% catalyst loading (Table 10) and confirmed the superior ligands, for this gold-catalysed transformation, to be those with one triazole substituent. The dicyclohexylphosphine-containing complex **112b** afforded the completeness conversion, while phenyl-version **112a** only delivered 57% conversion. The tris-triazole gold complex **114** gave only 11% conversion under the same condition. Pleasingly, however, catalysts derived by halide abstraction in the same manner from complex **115** delivered quantitative conversion in the terminal alkyne hydration (Table 10, Entry 8).

Synthetic modification of phosphorus-containing ligand can result in a significant difference in the outcomes of reactions catalysed by their corresponding cationic gold(I) complexes.[187] The regioselectivity of hydration of unsymmetrical internal alkynes has been previously investigated by Nolan *et al*. who reported anti-Makovnikov selective gold(I) carbene catalysed hydration.[175] As such, a model reaction, namely the hydration of unsymmetrical internal alkyne **119** has been selected to probe selectivity that might arise from the structural modifications across the series of gold(I) complexes of phosphino-triazoles prepared in this study (Table 11). Addition of water in benzylic

position to form **120a** represents the generally expected (Markovnikov) outcome, with selective reaction at the alternate alkyne position (**120b** anti-Markovnikov) are more challenging.

Table 11. Screening of ligand in hydration of alkyne **119** to ketone product **120a** and **120b**.

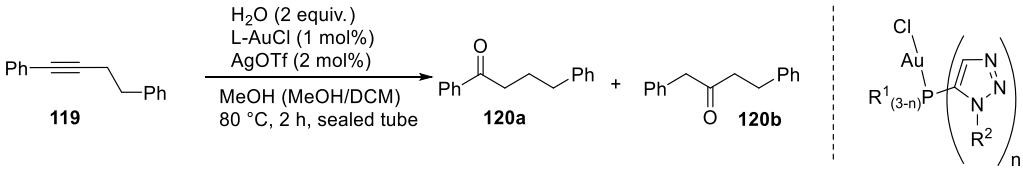

Entry	R^1	R^2	L-AuCl	Triazole No. (n)	Conv. (%)	Ratio[a] (120a: 120b)
1	Ph	-	**111a**	0	>99	4.0:1
2	Ph	Ph	**112a**	1	>99	4.2:1[b]
3	Ph	Ph	**113a**	2	>99	3.3:1[b]
4	-	Ph	**114**	3	64	3.8:1
5	Cy	Ph	**113b**	2	>99	4.3:1
6	Cy	Ph	**112b**	1	>99	3.2:1
7	Cy	-	**111b**	0	>99	3.5:1
8	Cy	2,6-DMP[c]	**115**	1	95[c]	2.3:1

[a] Ratio determined by GC analysis of reaction mixture; [b] Ratio determined by analysis of the proton NMR spectrums of mixtures of **120a** and **120b** obtained from the reactions; [c] Complete consumption of **119** was observed, the product mixture contained 5% of a dimethyl acetal adduct as determined by GC/GC-MS; [d] 2,6-DMP = 2,6-dimethoxyphenyl.

Alkyne **119** was added to a mixture of catalysts precursor (1 mol%) which, followed by silver triflate (2 mol%) to abstract chloride in a mixture solution of water and methanol. Conversion of **119** and the ratio of the product of **120a** and **120b** were monitored by ^{1}H-NMR or GC. Quantitative conversion has been observed in most ligand except tris-triazole phosphine gold complex **114**, and this share a similar outcome in the hydration of terminal alkyne (Table 10). While all complex showed a preference in the Markovnikov addition (**120a**) at the benzylic position of an alkyne, it is noteworthy that

use of complex **113b** leading to a greater proportion of Markovnikov product, with ratio 4.3:1 of **120a**:**120b**.

From the result above, **112b** and **115** derived phosphine gold complex possess an excellent activity for gold(I) catalysed hydration of alkyne. **115** was deployed in a brief substrate scope survey (Scheme 32). Most reactions are conducted in two hours with 0.25 mol% loading of catalyst **115** (substrate **117j-l** were conducted with 1 mol% catalyst loading). Linear alkyl-alkynes **117a** and **117f** gave slightly higher yields than the cyclic alkane ethynylcyclohexane **117b**, 79 and 89% *vs.* 64% respectively. 1-Ethynylcyclohexene **118c** gave a similar yield (69%) compare to **117b**. Phenylacetylene **117d** gave 58% yield, with the yield for the methylnaphthyl derivative **117e** being somewhat better (80% yield). The yield for use a of *para*-methoxy phenylacetylene **117g** was better than for phenylacetylene (88 *vs.* 58% yield). Pleasingly an arylboronic ester substituted substrate gave 81% isolated yield under the reaction condition employed, as was thiophene derivative alkynes **117i**, albeit in a slightly lower isolated yield. Quaternary oxindoles containing alkynes have been of interest to co-authors of this report, and their availability to this programme allowed **117j-l** to be probed as substrates for gold(I) catalysed hydration. In order to obtain appreciable conversion of isolatable oxindole contained product, catalyst loading has been increased to 1 mol%. The nitrogen unprotected substrate **117j** was converted to product **118j** with relatively low yield. Then *N*-benzyl analogue **117k** gave fared better yield, improved to 85%. A major side reaction has been observed from *N*-boc substrate **117l**, with deprotection *in situ*, with 30% isolated yield of desired *N*-boc product **118l**, and 61% isolated yield of

deprotected product **118j**. The reaction of **117m** gave the dimethyl acetal of overall reaction with 94% isolated yield. In addition, nitroarene **117n**, aryl ester **117o**, aryl bromide **117p-q**, pyridinio **117r-s**, *tert*-butyl **117t** substituted substrate failed to give any detectable hydration product under the reaction condition employed. Further optimisation to facilitate these transformations were not conducted.

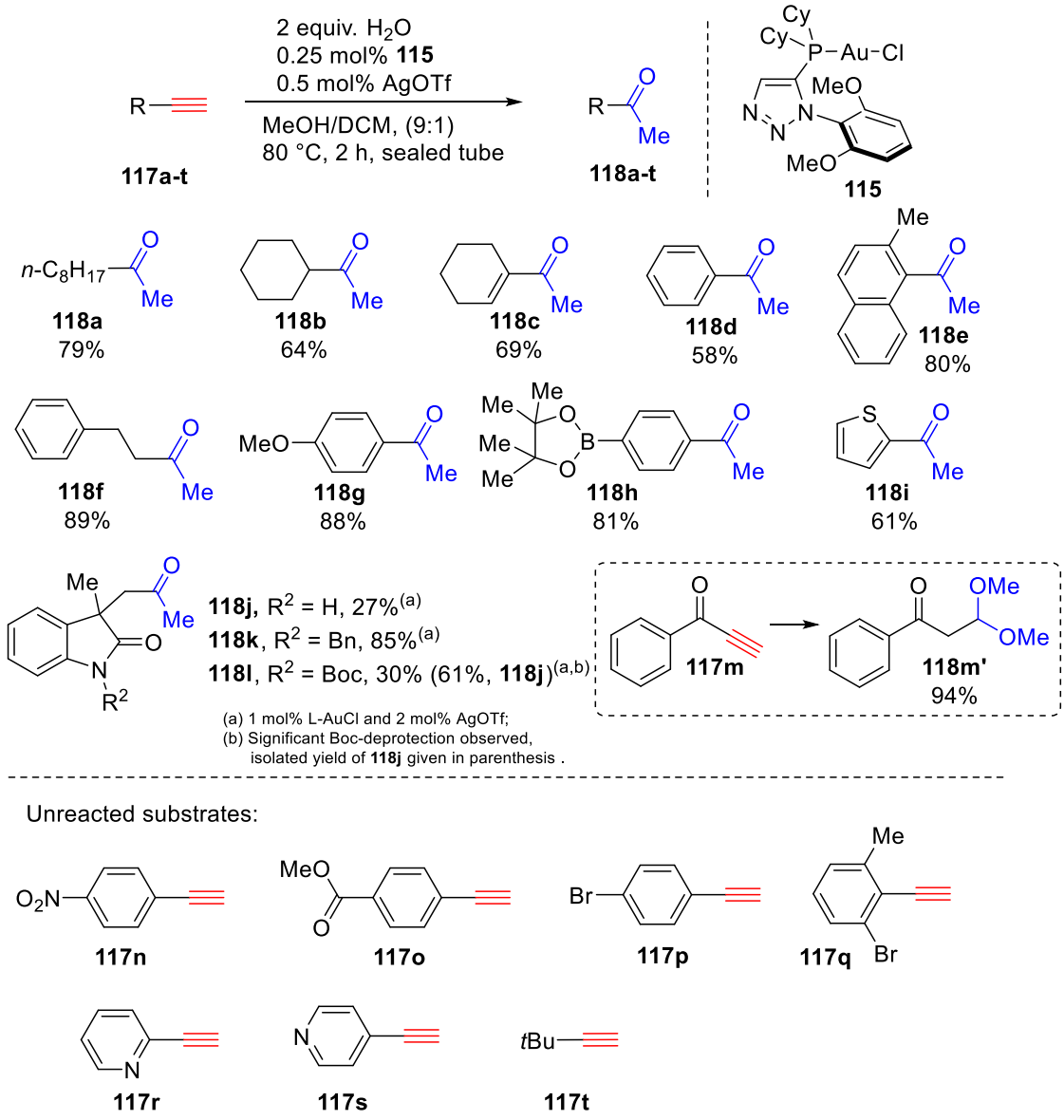

Scheme 32. Substrate scope for triazole phosphine gold complex in hydration of terminal alkyne.

3.4 Analogue of tris-triazole compound **110** series

Despite tris-triazole phosphine compound **110a** did not show a promising catalytic activity in the palladium and gold mediated reaction, but the unique 'bowl' shape pocket still evokes great interest. Thus, a small list of **110a** analogues prepared *via* the similar protocol. Electronic properties of aryl triazole has been considered as the main feature in the case of choosing the functional group, with electron-donating, electron-withdrawing group. Attempting to make tris triazole version of 2,6-dimethoxyl triazole **92d** tried without a successful result, this might due to the bulky demanding of the *ortho*-substitution feature.

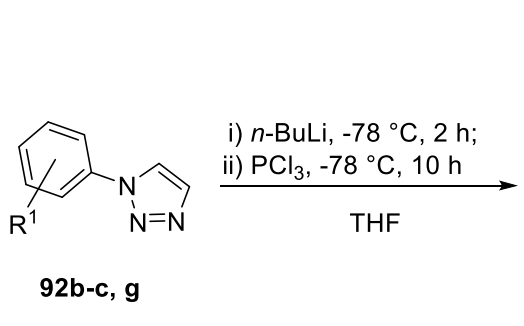

92b-c, g

110b-c, g-h

	R^1	Yield/%
110b	4-Me	77%
110c	4-OMe	8%
110g	4-CF_3	89%

Scheme 33. Preparation of tris-triazole phosphine

The suitable single crystal for X-ray analysis obtained with the data presented in Figure 47. It has been noticed that during the solid-state study, **110b, 110c, 110g** are fully cylinder symmetric like **110a**. From top view of phosphorus atom, two aryl group are pointed in the same direction with the phosphorus lone pair, with one aryl unit pointed to flank side.

(i)

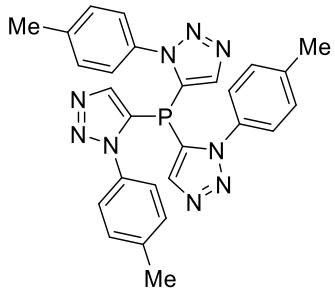

110b

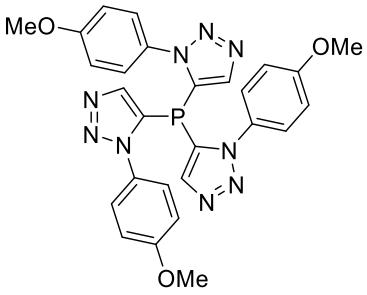

110c

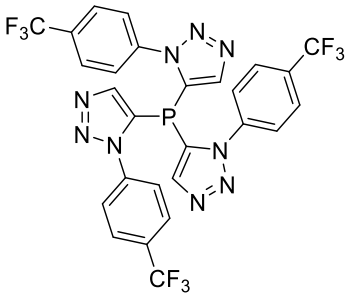

110g

(ii)

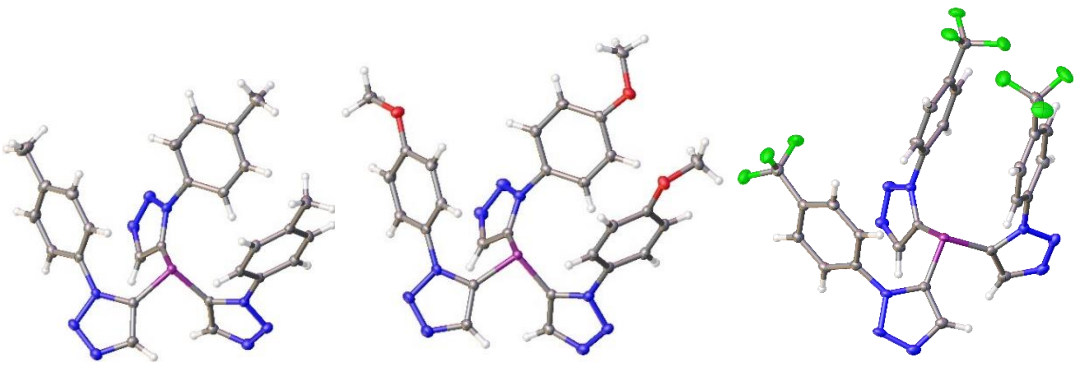

(iii)

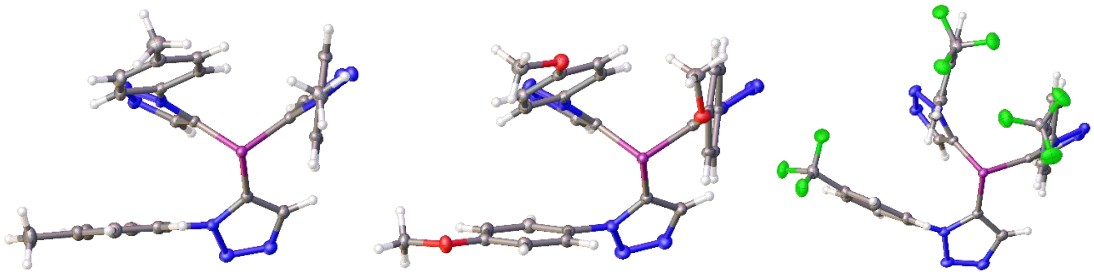

Figure 47. (ii), (iii) XRD structure of **110b, 110c, 110g**, with different orientation. Ellipsoid are drawn at the 50 % probability level. A molecule of acetone was omitted from **110b.**

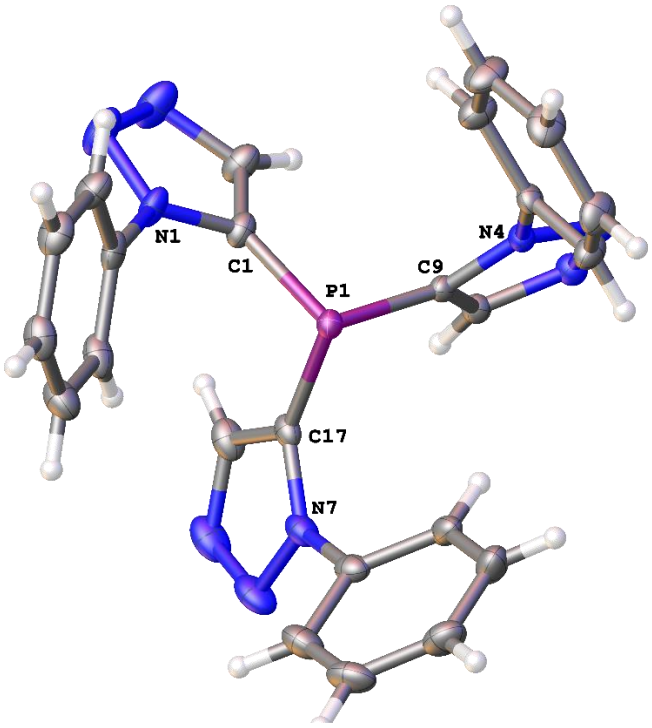

Figure 48. XRD structure of **110a.** Ellipsoid are drawn at the 50 % probability level. A molecule of acetone has been omitted for clarity.

In order to evaluate the symmetric of **110**s bowl-shape ligands, a series of torsions angles have been measured from XRD structures. Phosphorous bond angles C1-P1-C17, C17-P1-C9 and C9-P1-C1, torsion angles of N1-C1-P1-C17, N4-C9-P1-C1 and N7-C17-P1-C9 have been taken to verify the symmetric of the ligand to create potential binding pocket for metal. Similar protocol has also been applied into **110b, 110c**, **110d** and metal complex **114**. The results are presented in Table 12. Ligand **110a** shows the best symmetric compared with rest ligand, since three triazole torsions angles have been located around 97-105°. It also has been noticed gold complex **114** process smaller triazole torsions angles and P-bond angles compared with **110a**, this suggested 'bind pockets' has been narrowed down after gold atom attached to the phosphorous atom.

Following metal-binding study is still under investigation, but **110a** and **114** unveiled the binding ability of this bowl-shaped ligand.

Table 12. Triazole torsions angles and P-bond angels of bowl-shape compound, measured via Mercury

	Triazole Torsions angles			**P-Bond angles**		
110a	103.34°	97.59°	104.97°	98.98°	97.83°	99.49°
110b	-158.73°	124.57°	144.19°	97.59°	101.81°	97.90°
110c	-166.66	118.06	147.96	96.51	103.81	97.64
110g	-167.36	113.86	157.30	99.54	101.18	98.64
104	87.05	97.42	97.30	103.13	102.83	101.422

3.5 Conclusions

Aryl and 5-phosphino functionalised triazole has been prepared, wherein the phosphorous atom was connected with one, two or even three triazole motifs. In addition, corresponding gold(I) chloride complexes triazole phosphine has been prepared, and their bulkiness has been determined by SambVca with term $\%V_{bur.}$ Two more gold(I) complexes have also been prepared from ligand derived with substituted aryl-triazole group which prepared in the previous chapter. These free ligands and complexes set along with triphenylphosphine and tricyclphexylphosphine set, have been all tested in an SMC and gold(I) mediated hydration of alkyne. As such, the increasing number of triazole motif have not significantly boost the activity of ligand, the mono-triazole containing ligand confirmed as a superior ligand in these reactions been tested.

In summary, the derived from the reaction above show that **93g** and corresponding gold(I) complex **115** are to be the most promising ligand and catalysts in this study. The ease of synthesis and modification of triazole framework should prove useful in future ligand designing, preparation and optimisation.

Experiment work in this chapter was mainly carried out by the author of this thesis and date from Table 11 was generated by Matthew Wakeling (UoB). Figure 42-46 were developed by John Fossey (UoB), and data of this chapter were initially published in the European Journal of Organic Chemistry.[188]

4. Chapter 4 Preparation of Asymmetric Phosphino-Triazole

Chiral phosphine ligands have played pivotal roles in transition metal-mediated asymmetric reaction. An asymmetric environment around the reaction site can be created by the coordination of metal and chiral ligands, which eventually affect the enantioselectivity and reaction rate.[189] Asymmetric catalytic performance is not only determined by the centre metal, but also by the chiral ligand selected as well. Thus, the designing and synthesis of chiral phosphine ligands have been an active research subject, for the production of useful optically active compounds.[190]

Triazole containing phosphine ligand has been successfully prepared in the previous chapter, and it has shown to be as competitive as well know ligands in the palladium catalysed SMC reaction and gold catalysed hydration of alkynes. It has been concluded that with the increasing the number of triazole motif, the catalytic outcome has not been significantly improved through the condition employed. Thus, one triazole unit has been mainly focused for the further development to the asymmetric version of the ligand.

Chiral phosphine ligands are generally categorised into two general classes: backbone chirality and P-chirogenic phosphine ligands.[190] BINAP is a typical example of backbone chirality phosphine ligands since the restricted rotation of bis-naphenyl unit (*Figure 49*). The most well-known example of P-chirogenic phosphine ligands is DIPMAP, which was first reported by Knowles *et al.* in 1975 (Figure 49). DIPAMP is C_2-symmetric phosphine ligand, with three different substituents at phosphorous centre. Rhodium complex of

DIPAMP has been widely use in asymmetric hydrogenation reaction of dehydroamino acid with high enantioselectivities. In addition, DIPAMP also has been applied to industry-level production of L-Dopamine, which is a key agent in the treatment of Parkinson's disease.[191, 192] Feringa proposed a new series of chiral monodentate phosphine ligand based on phosphoramidite scaffold, which were widely used for enantioselective synthesis. The remarkable effect of phosphoramidite ligands in enones' 1,4 addition give 93% yield and *ee* value greater than 98%. The unique feature of this ligand is the incorporation of two chiral structure units, that is, the sterically demanding bis-phenylethylamine and BINOL unit in a 'matched combination' (with mismatched ligand (*S,S,S*) afforded lower yield and worse ee%).[193]

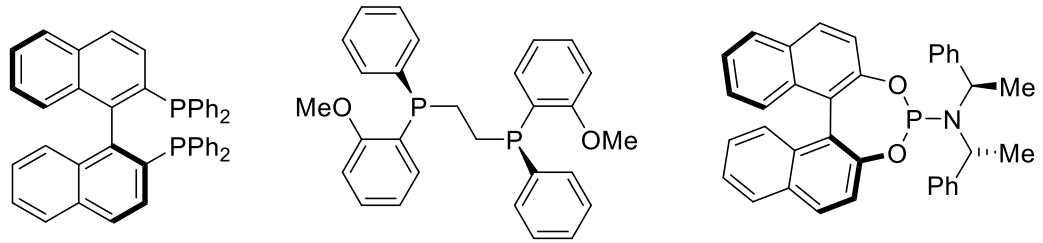

(*S*)-BINAP (*R,R*)-DIPAMP Feringa type ligand (Phosphoramidite)

Figure 49. Selected examples of asymmetric ligands

4.1 "Backbone chiral" triazole containing phosphine

Previous group member Dr Brittain developed a series of triazolium salts as for the potential carbene ligand.[194] He reported that triazolium salts **121** and **122** are both chiral species due to the restricted rotation of the highlight bonds (Figure 50). It has been noticed that the benzylic protons in both compounds appeared to be diastereotopic from ^{1}H-NMR spectra, suggest that both enantiomers are stable under the NMR timescale. After further variable temperature (VT)-NMR study, **122** is a stable

atropisomer, even at 110 °C. This proves that the rotation of this triazolium system is highly restricted and stable even at high temperature. Since both triazolium salt **121** and **122** is the alkylated product of triazole **123**, methyl-naphthyl substituted motif are selected as pre-chiral backbone of asymmetric triazole phosphine ligand design.

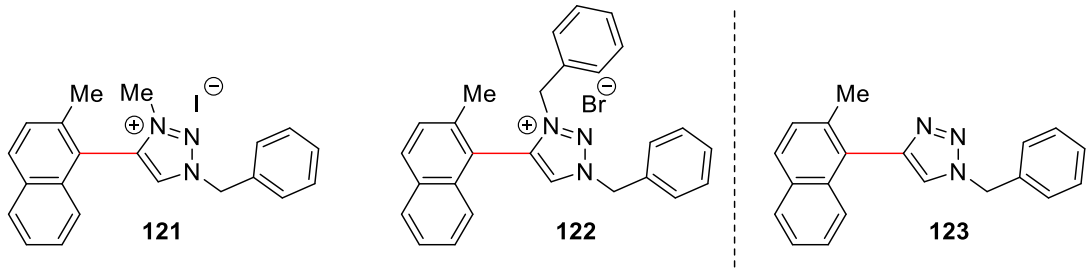

Figure 50. Examples of chiral triazolium salt and triazole before the alkylation

Due to acidity of benzylic proton, direct phosphine installation is unsuitable with triazole **123**. Thus, a new pro-chiral triazole backbone **126** was designed and successfully prepared (Scheme 34). 2-Methyl-1-naphthylamine was treated under standard diazotisation then react with sodium azide to form azide **125**, followed by triazole formation with TMS-acetylene to yield triazole **126** with moderate yield.

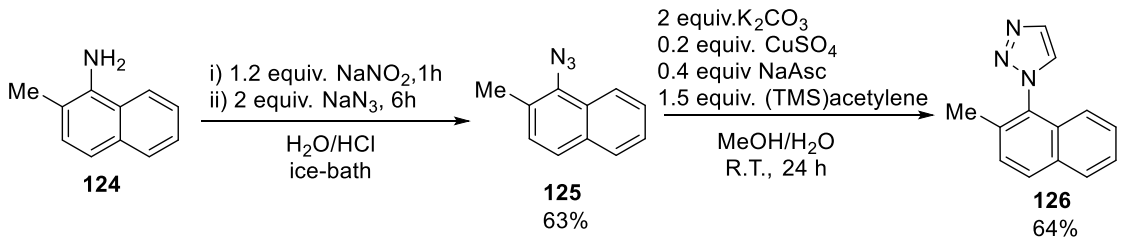

Scheme 34. Preparation of chiral backbone triazole

Triazole **126** is a new analogue of mono-substituted triazole from chapter 2. Existing phosphine installation protocol were employed, di-*tert*-butyl substituted phosphine compound **127a** was initially designed to for chirality studies. There are two reasons for choosing *tert*-butyl substituted phosphorus group: i) bulkiness nature of *tert*-butyl

group; ii) a diastereotopic signal could be identified in ^{1}H-NMR spectra once rotation is restricted. Compound **127a** was successfully prepared by the method presented in chapter 2 with a 65% yield.

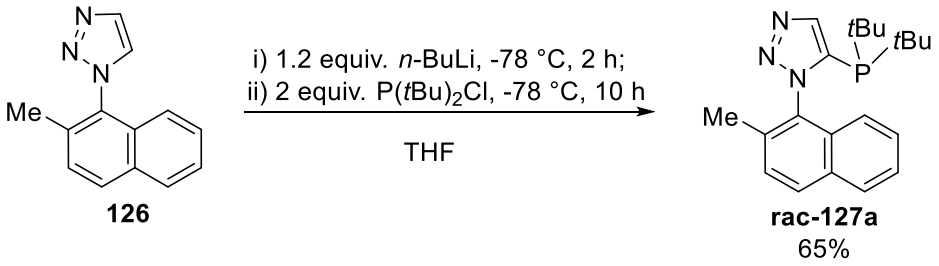

Scheme 35. Preparation of triazole phosphine with chiral backbone.

The proton NMR spectrum of **127a** presented in Figure 51. Upon inspection of the ^{1}H-NMR spectra of **127a**, it can be noticed that the *tert*-butyl groups attached to the phosphorous appeared to be diastereotopic, with a set of peak at 1.21,1.17 and 1.06, 1.02 respectively. This was encouraging, as it showed the rotation around the single bond between the triazole motif and naphthyl moiety was restricted after installation of phosphine. A single crystal of rac-**127a** has been obtained and analysed. From the X-ray study, both enantiomers could be obtained from one unit cell (Figure 52).

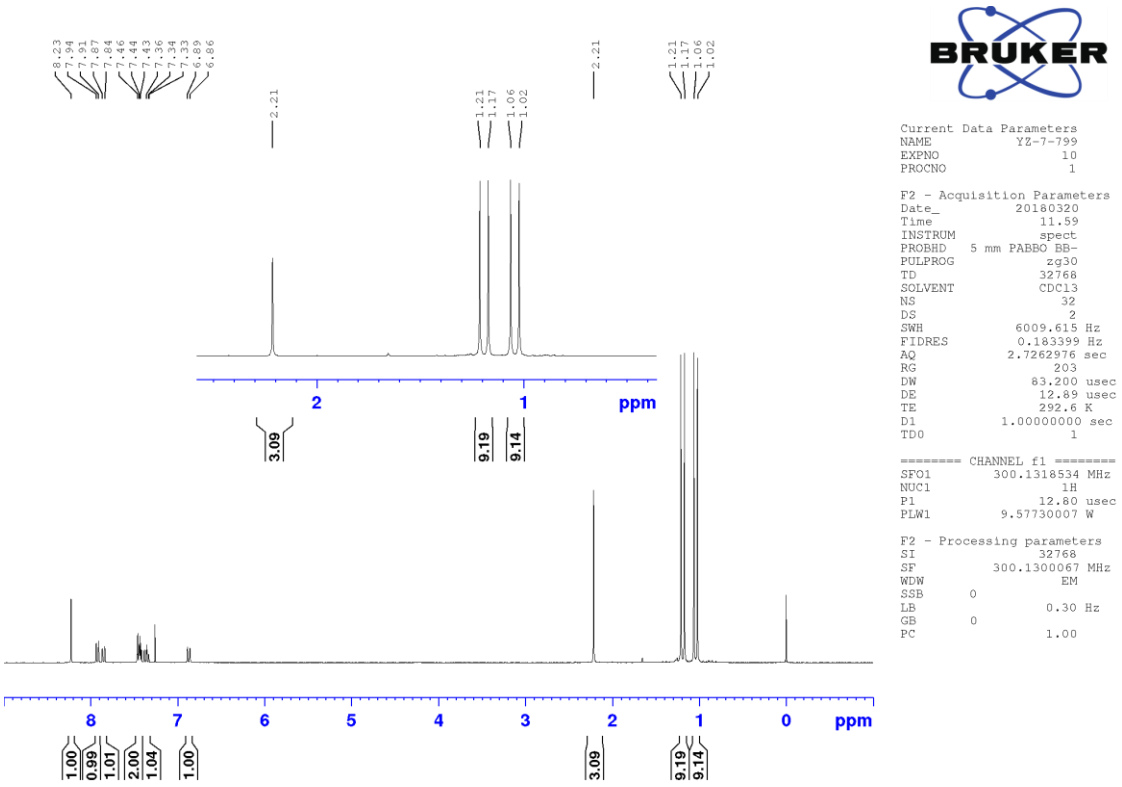

Figure 51. ^{1}H-NMR of **127a**, data collected in ambient temperature with d-chloroform as solvent.

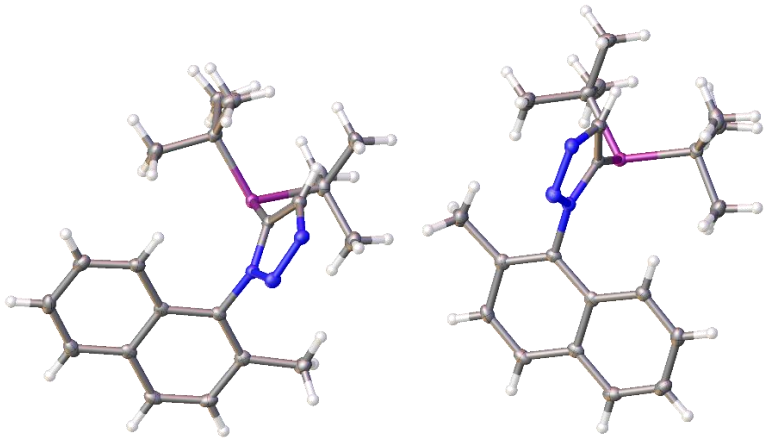

Figure 52. X-ray structure of triazole phosphine rac-**127a,** ellipsoid are drawn at the 50% probability level. Both enantiomers can be observed in the same unit cell.

To measure the stability of this locked configuration, variable temperature (VT)-NMR was initially targeted. Racemate triazole phosphine **127a** was dissolved in *d*-toluene, and a clear diastereotopic splitting patterns could be observed from 0.8-1.0 ppm, and these signals did not coalesce even at 105 °C (Figure 53), this suggested the system was

highly restricted and stable even at high temperature, which confirmed this chiral backbone is suitable for ligand designing.

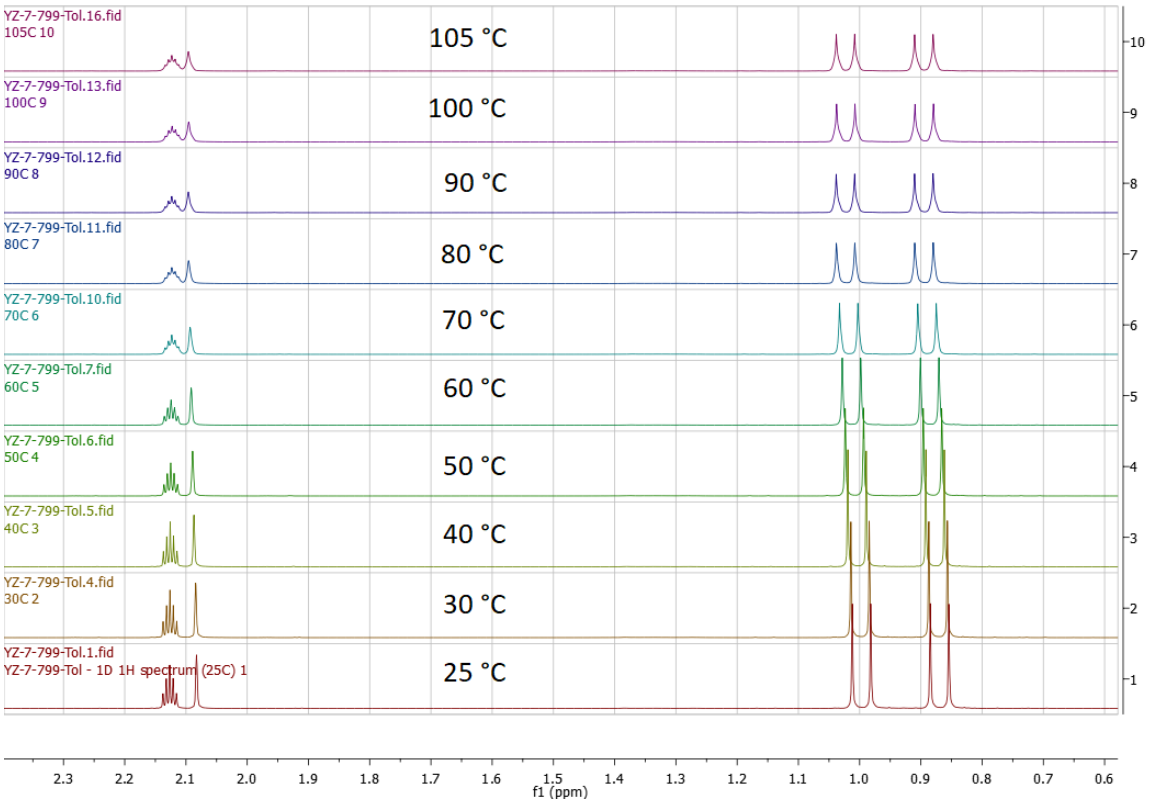

Figure 53. VT-NMR spectroscopic study of **127a**. Data collected in various temperature with *d*-toluene as solvent. Temperature was increased up to 105 °C shows no coalescence in the resonance centre 0.94 ppm.

The attempt to isolate enantioenriched compound **127a** by *via* Staudinger reaction to prepare phosphinimide and phosphine oxide has been tested without successful results (Scheme 36).[195] The ideal situation was that a Staudinger reaction between a racemic phosphine **127a** and an enantiopure organoazide should provide a 1:1 mixture of diastereomeric phosphinimines, and these diastereomers would be separable by column chromatography or crystallisation. But in the reaction presented in **Scheme *36***, no reaction could be observed between **127** and azidoethyl benzene after 6 hours reaction.

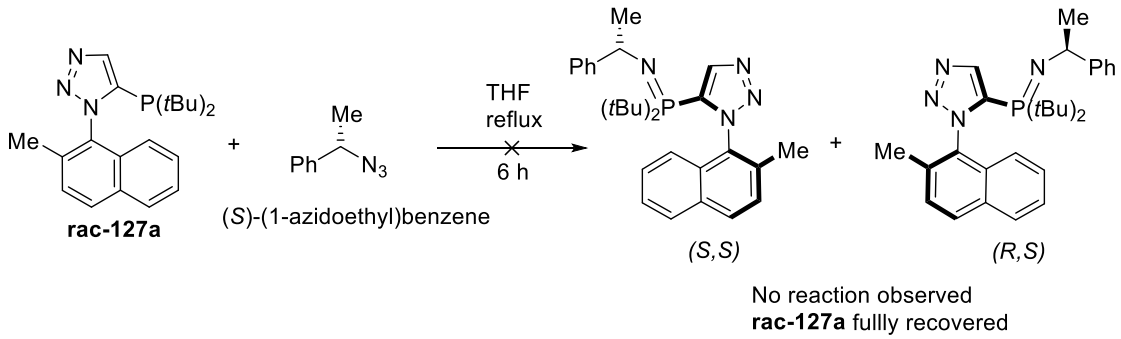

Scheme 36. Resolution of **127a** with (S)-(1-azidoethyl)benzene.

Chiral HPLC resolution of **127a** was conducted with Cellulose-1 column. A baseline separation of both enantiomers had been achieved with 60% isocratic acetonitrile in water solution (Figure 54). This was encouraging, which suggested that **127a** is possible to be separated by prep-chiral HPLC to obtain enantioenriched sample. Enantiopure **127a** was obtained by chiral preparative HPLC, and the isolated material was eluted through analytical HPLC to confirm its enantiopurity (Figure 55). The single crystal of early fraction of **127a** has been obtained, and absolute confirmation has been determined by single-crystal X-ray diffraction, which confirmed the first fraction is (*R*) configuration by anomalous dispersion with a Flack parameter of -0.013(8). In addition, the space group of the crystal lattice was found to be $P2_1$, as a non-centrosymmetric space group, which strengthened the evidence of a single enantiomer form (Figure 56).

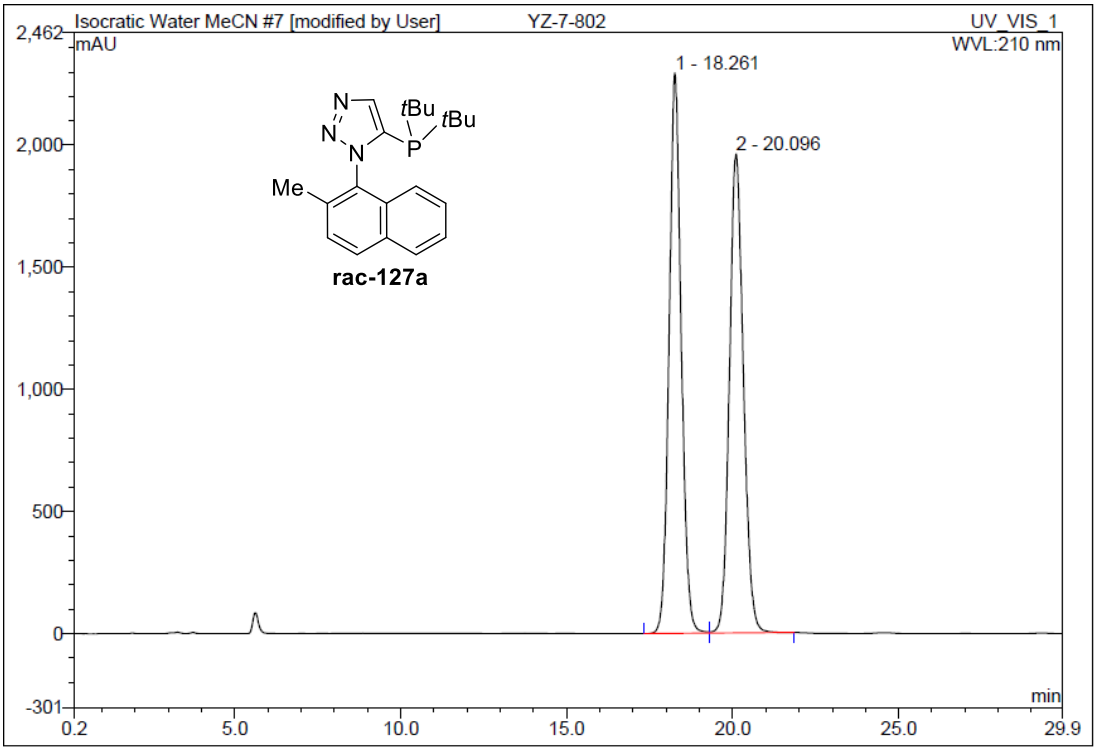

No.	Ret.Time min	Peak Name	Height mAU	Area mAU*min	Rel.Area %	Amount	Type
1	18.26	n.a.	2294.586	973.678	50.42	n.a.	BM
2	20.10	n.a.	1961.034	957.301	49.58	n.a.	MB
Total:			4255.620	1930.979	100.00	0.000	

Figure 54. Chiral HPLC separation of rac-**127a**, Cellulose-1 column with isocratic 60% MeCN in Water

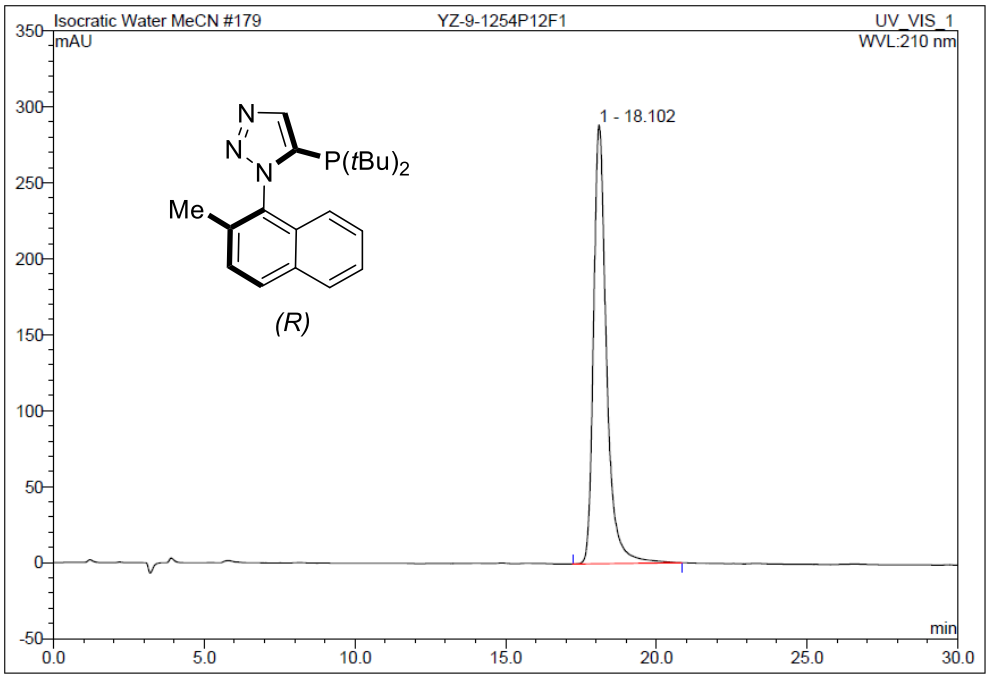

No.	Ret.Time min	Peak Name	Height mAU	Area mAU*min	Rel.Area %	Amount	Type
1	18.10	n.a.	288.712	144.535	100.00	n.a.	BMB
Total:			288.712	144.535	100.00	0.000	

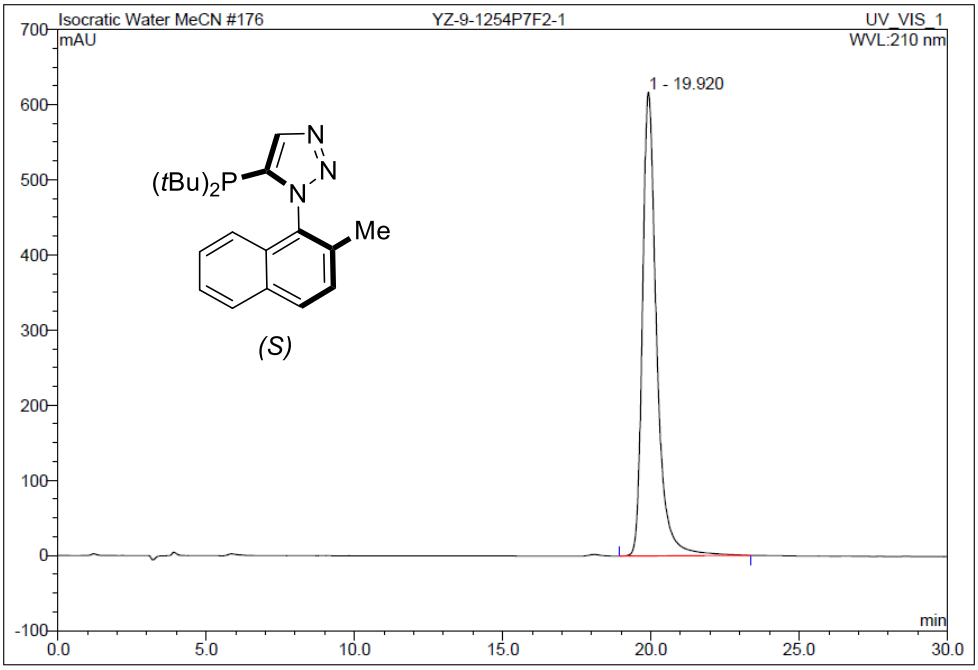

No.	Ret.Time min	Peak Name	Height mAU	Area mAU*min	Rel.Area %	Amount	Type
1	19.92	n.a.	617.064	341.332	100.00	n.a.	BMB
Total:			617.064	341.332	100.00	0.000	

Figure 55. HPLC separation of a single enantiomer of **127a**, with enantiomeric pure of the first fraction (F1) and enantiomeric pure of the second fraction (F2).

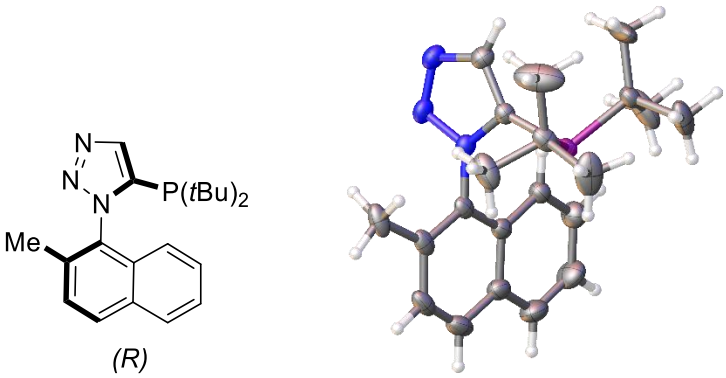

Figure 56. Configuration of early fraction (F1) **127a** has been confirmed by X-ray structure with R configuration, ellipsoid are drawn at the 50% probability level, space group = $P2_1$, with a flack parameter of -0.013(8).

This crucial crystal structure allows the determination of the absolute configuration of the atropisomer isomer ligand. From knowing which enantiomer was analysed, it was straightforward to deduce the configuration of the ligand-metal complex during the catalysis study.

A small portion (5mg) of (*R*)-**127a** has been tested to prepare gold complex, by co-crystallising equal equivalent of (*R*)-**127a** and (DMS)AuCl in DCM and hexane mixed solution, a suitable single crystal for XRD analysis has been obtained, and structure has been solved in space group $P2_1$ with Flack parameter -0.007(7). (Figure 57)

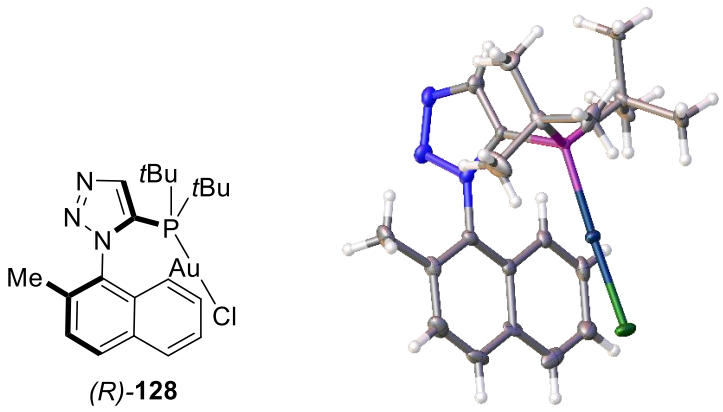

Figure 57. **(R)-128**, the structure has been confirmed by X-ray structure with (S) configuration, ellipsoid are drawn at the 50% probability level, space group = $P2_1$, with a flack parameter of -0.007(7). A molecule of DCM has been omitted for clarity.

Enantiomerically pure phosphine gold complex (*S*)-**128** has been prepared by reacting with equal equivalent of (*S*)-**127a** and (DMS)AuCl with 82% isolated yield. A suitable single crystal for x-ray structure has been obtained from recrystallisation by slow evaporation from DCM/Hexane mixed solvent. (Scheme 37) The determined structure is (*S*) configuration by anomalous dispersion with a Flack parameter of -0.034(4). In addition, the space group of the crystal lattice was found to be $P2_1$.

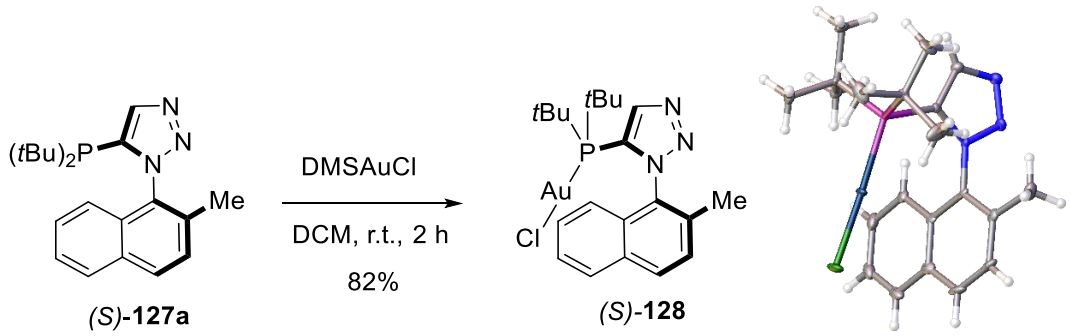

(S)-**127a** *(S)*-**128**

Scheme 37. Synthesis of gold complex (*S*)-**128**, structure has been confirmed by X-ray structure with (S) configuration, ellipsoid are drawn at the 50% probability level, space group = $P2_1$, with a flack parameter of -0.034(4). A molecule of DCM has been omitted for clarity.

To expand ligand option and test the stability of this pro-chiral backbone, phenyl and *iso*-propyl group in phosphorous has been selected for ligand design. **127b** and **127c** has been synthesised with a similar protocol, by quenching lithium triazole species with diphenylphosphine chloride and di-isopropylphosphine chloride to furnish **127b** and **127c** in 45% and 65% yield respectively. (Scheme 38)

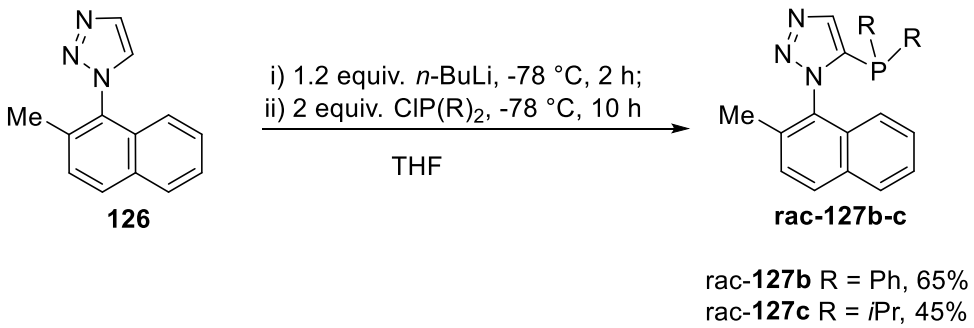

Scheme 38. Synthesis of phosphine substituted analogue

A single crystal for racemate **127b** has been obtained after slow evaporation of **127b** DCM/Hexane mixture solution. During XRD analyses, both enantiomers can be observed from the same unit cell. (Figure 58) Besides, pi-pi interaction has been observed between phenyl unit from phosphorous and naphthyl ring, with a shift of centroid-centroid distance of 1.210 Å.

Chiral HPLC resolution of **127b** has been achieved using Cellulose-1 column with isocratic 60% acetonitrile in water solution, the result was presented in Figure 59, and suggested **127b** is an atropisomer.

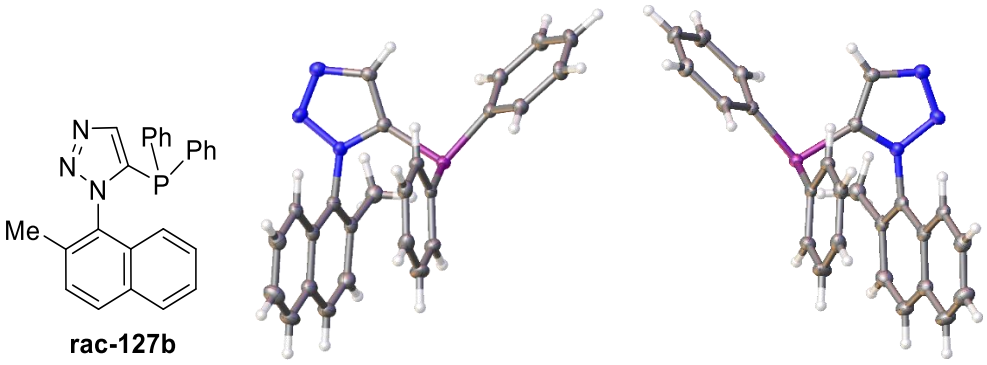

Figure 58. X-ray structure of triazole phosphine rac-**127b**, ellipsoid are drawn at the 50% probability level. Pi-Pi interaction has been observed from phenyl ring and naphthyl ring.

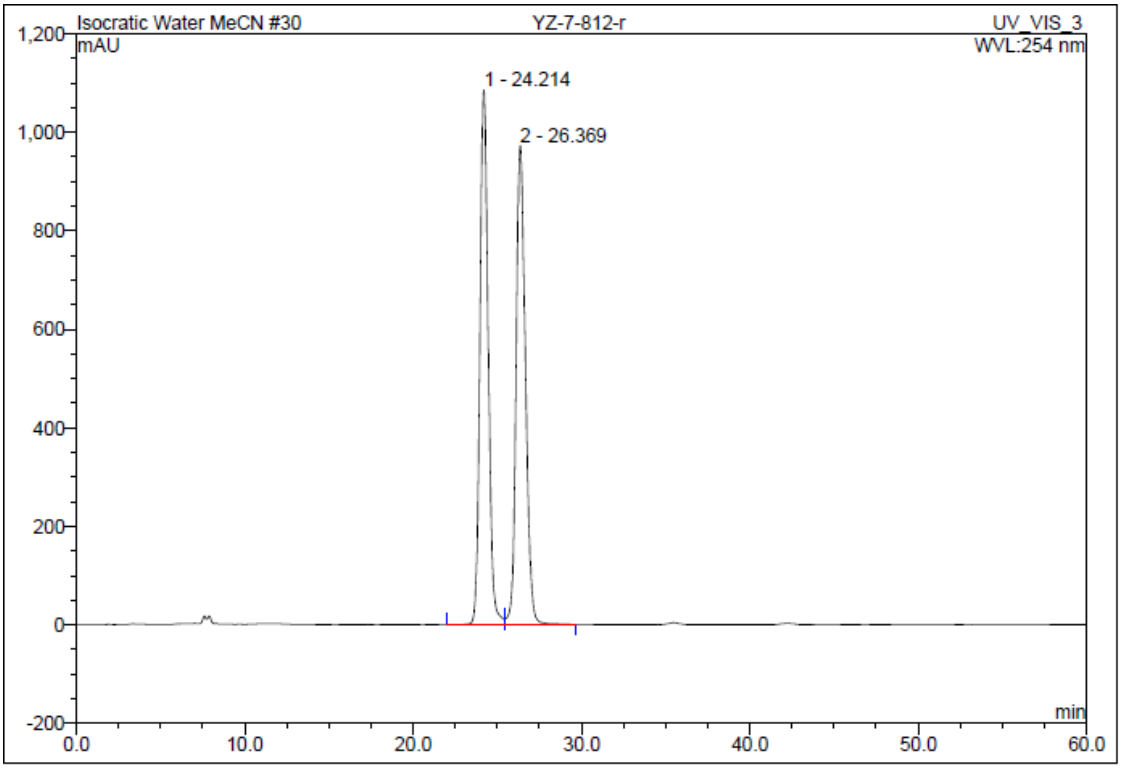

No.	Ret.Time min	Peak Name	Height mAU	Area mAU*min	Rel.Area %	Amount	Type
1	24.21	n.a.	1084.380	621.069	49.80	n.a.	BM
2	26.37	n.a.	971.867	626.038	50.20	n.a.	MB
Total:			2056.247	1247.107	100.00	0.000	

Figure 59. Chiral HPLC separation of rac-**127b**, Cellulose-1 column with isocratic 60% MeCN in Water

A small amount of rac-**127b** has been tested to prepare gold complex, by co-crystallising equal equivalent of rac-**127b** and DMSAuCl in DCM and hexane mixed solution; a suitable single-crystal X-ray analyst has been obtained with data presented in Figure 60. A trigonal gold complex of **129** has been observed with similar coordination pattern of **116** in Figure 46 (B). The gold complex consists of two ligands unit and Au(I) chloride. Besides, both (*R*) and (*S*) configuration of ligand have been observed through the same unit cell, but only homo-chiral of gold complex of **129** has been obtained. Further exploring the catalytic activity of complex **129** has not been conducted**.**

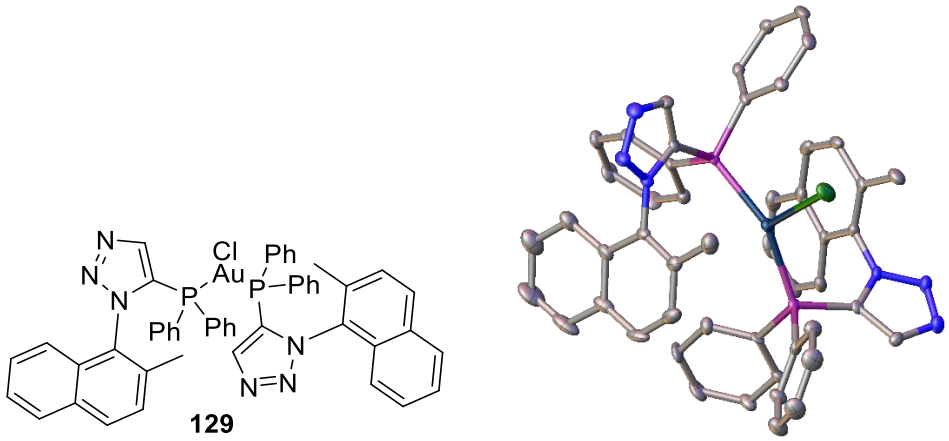

129

Figure 60. X-ray structure of triazole phosphine **129**, ellipsoid are drawn at the 50% probability level, hydrogen atoms have been omitted for clarity. Pi-Pi interaction has been observed

Isopropyl substituted version of ligand has also been prepared with only 45% isolated yield (Scheme 38). Upon inspection of the ^{1}H-NMR spectra of **116c**, it was shown that the isopropyl groups attached to the phosphorous appeared to be diastereotopic, with the split into two sets of doublet of septets C*H* signal from isopropyl group. (Figure 61). This suggested, the restricted bond rotation between the triazole ring and naphthyl ring. Chiral-HPLC resolutions of single-enantiomer of **116c** have been attempted but unable to achieve baseline HPLC separation by various conditions.

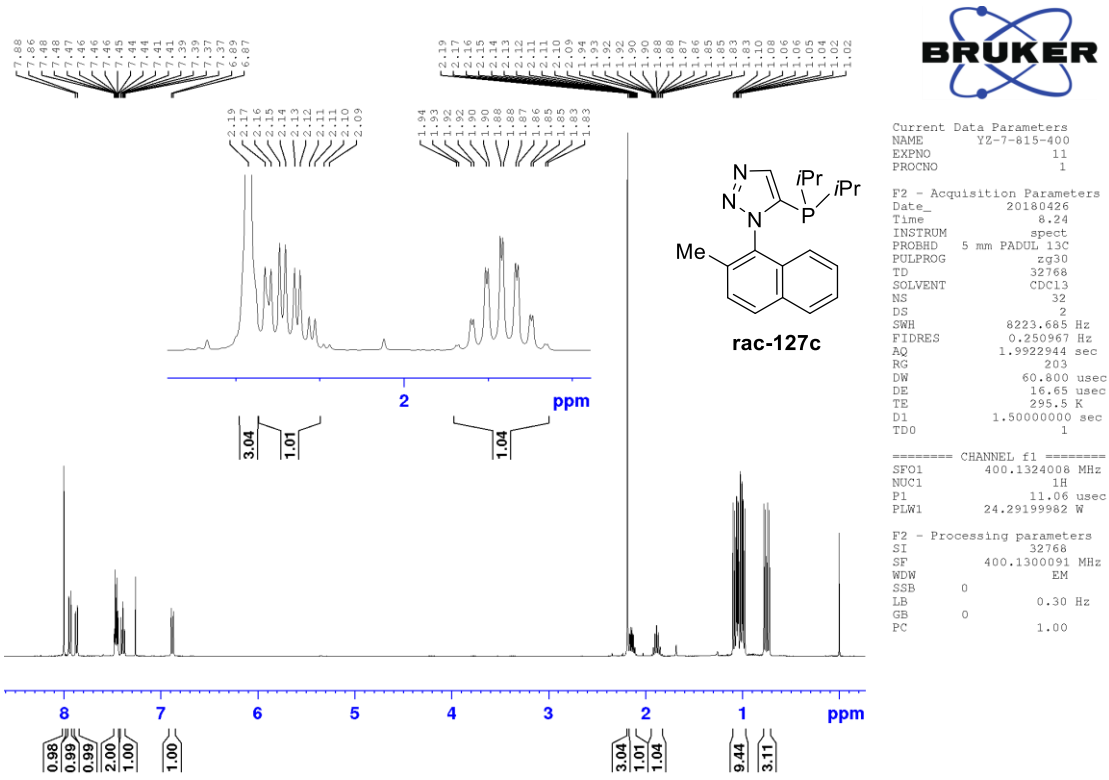

Figure 61. [1]H-NMR of **127c**, data collected in ambient temperature with d-chloroform as solvent.

4.2 P-Chirogenic phosphine ligand

The greatest enantioselectivity of P-chirogenic phosphine ligand is applying DIPAMP-Rh catalyst system allowed the industrial production of (*S*)-3,4-dihydroxylphenylalanine (L-DOPA), used to treat Parkinson's disease (Scheme 39).[196] [192] However, despite this important application, P-chirogenic phosphine ligand, including DIPAMP, have not been widely used, due to the difficulty of the synthesis *via* phosphine oxides as a key intermediate.[197]

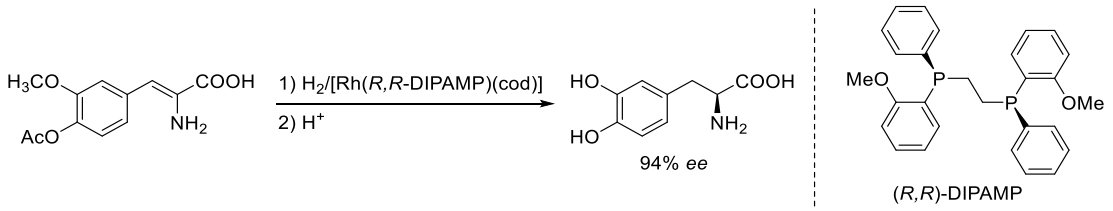

Scheme 39. Synthesis of L-DOPA via hydrogenation with the DIPAMP

In this project, the initial strategy to deliver P-chirogenic phosphine ligand is a combination of chiral phosphine chloride to lithium triazole species. Thus, **92h** was selected as the triazole unit, since the most efficient ligand in this project was built on triazole motif **92h**. Followed by lithiation protocol then react with rac-chloro(*tert*-butyl)phenylphosphine to furnish phosphine compound **130** with 74% yield. (Scheme 40)

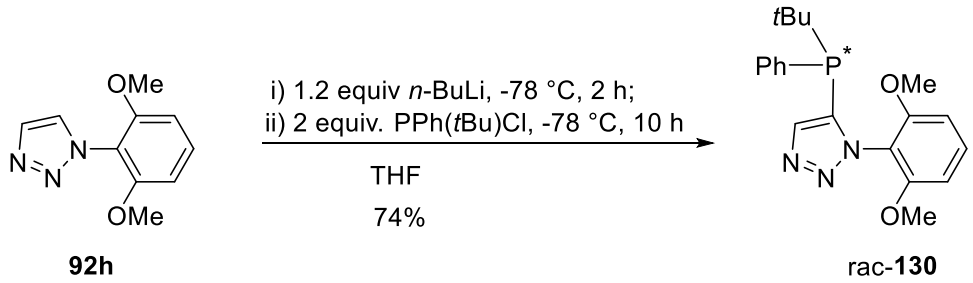

Scheme 40. Synthesis of P-chirogenic phosphine ligand

The proton NMR spectrum of rac-**130** presented in Figure 62. Upon inspection of the ^{1}H-NMR spectrum of **130**, it can be seen that the two methoxy groups from aryl triazole and a proton from 3 and 5 position from aryl group are diastereotopic, with a set of peaks at 3.78, 3.09 and 6.67. 6.41 respectively.

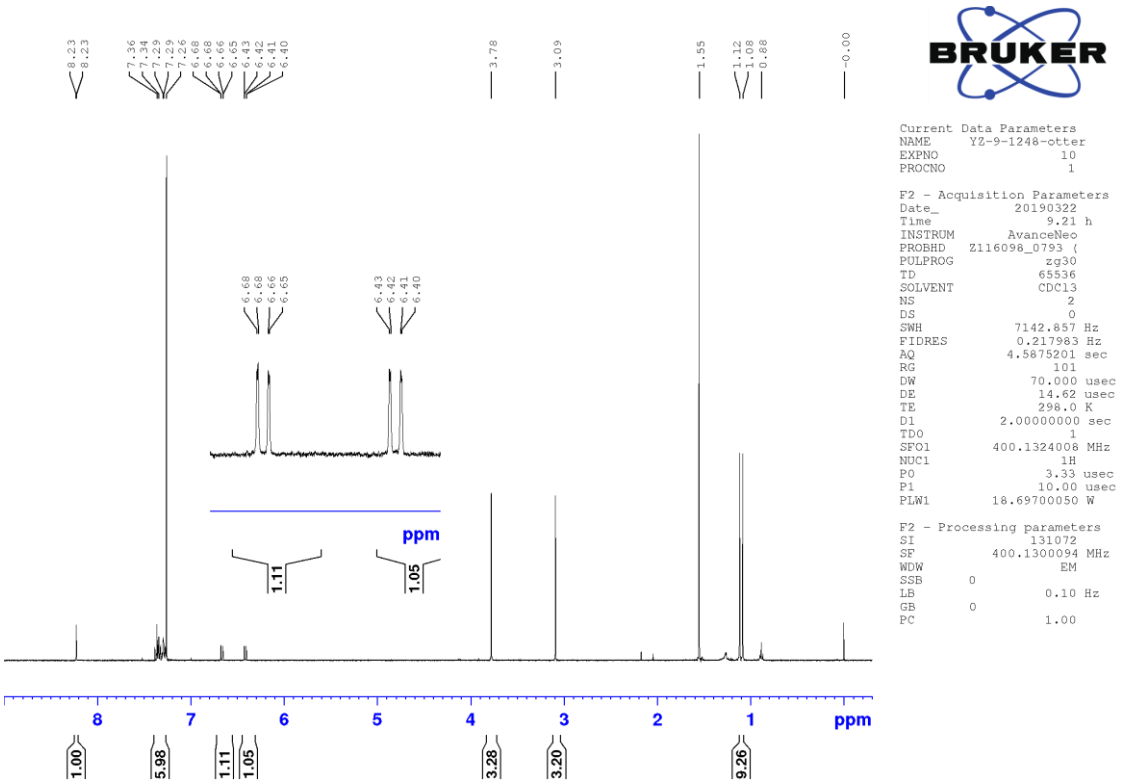

Figure 62. ^{1}H-NMR spectrum of **130**, data collected in ambient temperature with d-chloroform as solvent.

Chiral HPLC analyses of **130** was conducted with Cellulose-1 column with isocratic 50% acetonitrile and water, achieved nearly baseline isolation of two enantiomer (Figure 63). This suggested rac-**130** was a stable atropisomer in both NMR and HPLC time scale, but the direct resolution of **130** *via* prep-HPLC could be a challenging task since unable to get fully baseline separation during current condition. The attempt to isolate enantioenriched compound **130** by using the Staudinger reaction to prepare phosphine oxide has been tested without success.[195] Thus, chiral resolution was finally achieved with multiple resolution processes *via* prep-HPLC, and isolated material was eluted through analytical HPLC to confirm its enantiopurity (Figure 64).

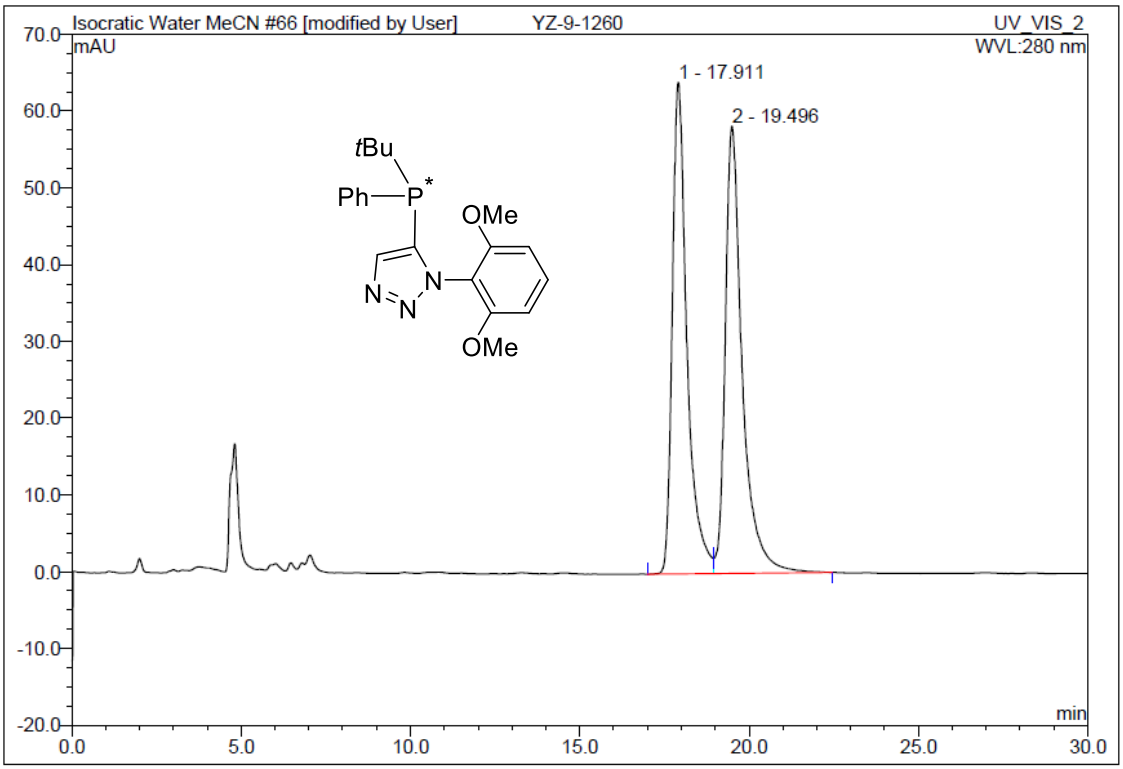

No.	Ret.Time min	Peak Name	Height mAU	Area mAU*min	Rel.Area %	Amount	Type
1	17.91	n.a.	64.053	32.189	48.59	n.a.	BM
2	19.50	n.a.	58.279	34.063	51.41	n.a.	MB
Total:			122.332	66.251	100.00	0.000	

Figure 63. Chiral HPLC separation of rac-**130**, Cellulose-1 column with isocratic 50% MeCN in Water

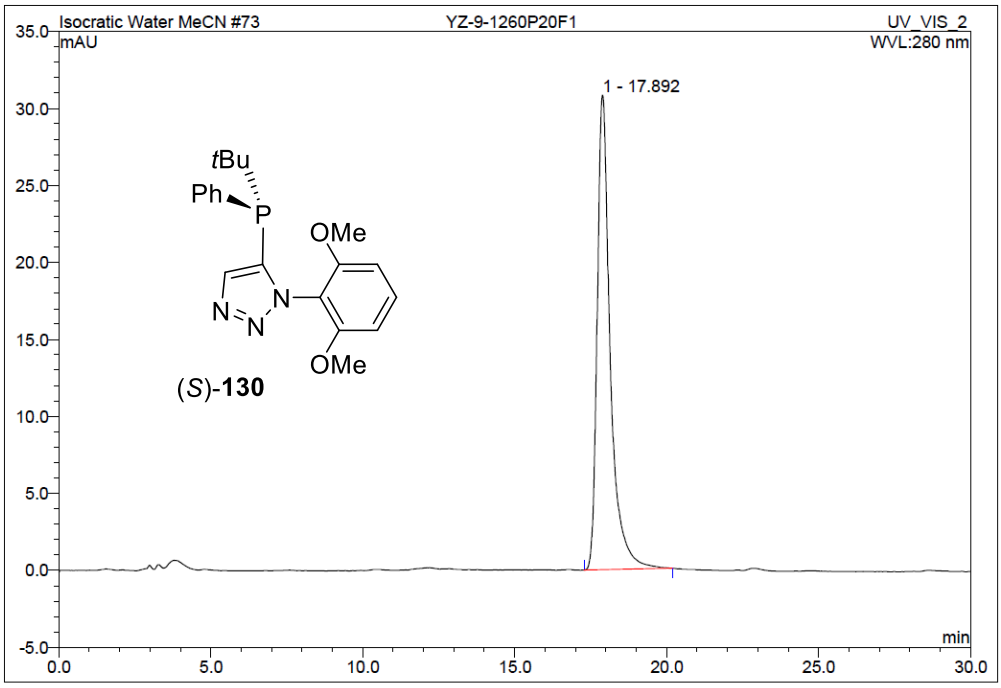

No.	Ret.Time min	Peak Name	Height mAU	Area mAU*min	Rel.Area %	Amount	Type
1	17.89	n.a.	30.818	15.307	100.00	n.a.	BMB
Total:			30.818	15.307	100.00	0.000	

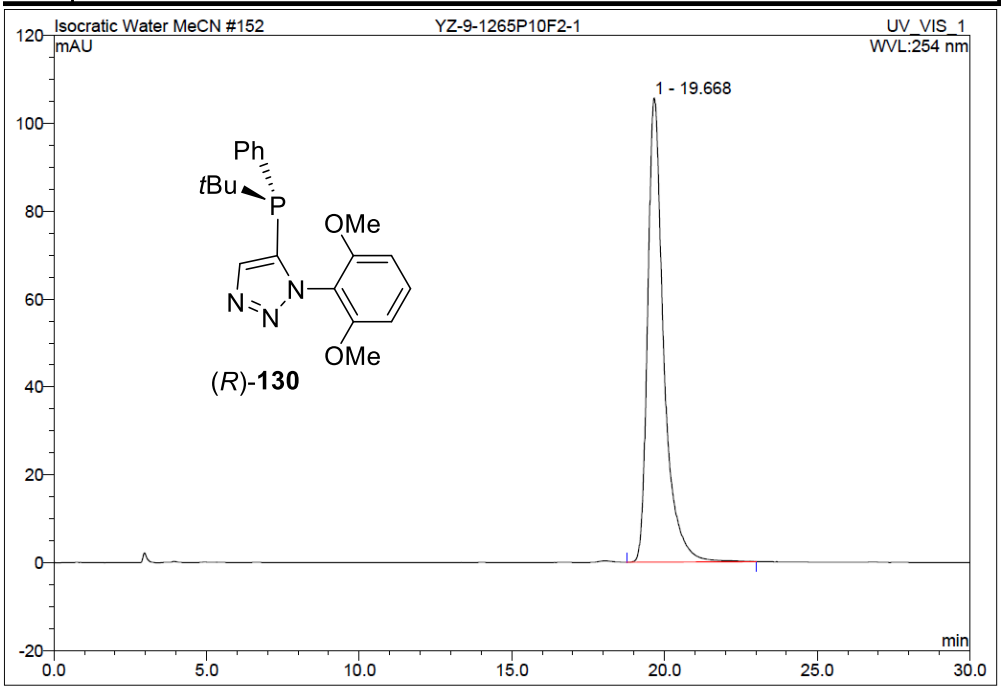

No.	Ret.Time min	Peak Name	Height mAU	Area mAU*min	Rel.Area %	Amount	Type
1	19.67	n.a.	105.668	64.302	100.00	n.a.	BMB
Total:			105.668	64.302	100.00	0.000	

Figure 64. HPLC separation of a single enantiomer of **130**, with enantiomeric pure of the first fraction (F1) on left and enantiomeric pure of the second fraction (F2) on the right.

Phosphine compound **130** was quite hygroscopic, thus unable to obtain a suitable crystal for XRD study to determine the absolute configuration. Instead, gold complex of the second fraction (t_{min}=19.50) was prepared, and a single crystal was successfully obtained after recrystallisation in DCM/Hexane, the XRD result has been presented in Scheme 41. The XRD study has confirmed (*S*) as absolute configuration by anomalous dispersion with a Flack parameter of -0.050(5), and the space group of the crystal lattice was found to be $P2_1$. From knowing which enantiomer was analysed, it was straightforward to deduce the configuration of the opposite enantiomer.

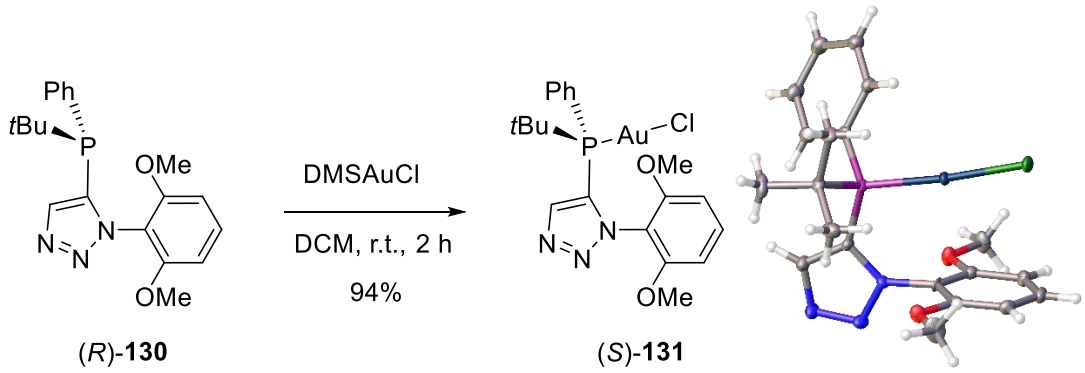

Scheme 41. Synthesis of gold complex (S)-**131**, structure has been confirmed by X-ray structure with (S) configuration; ellipsoid are drawn at the 50% probability level, space group = $P2_1$, with a Flack parameter of -0.050(5).

4.3 Preparation of phosphoramidite type triazole containing phosphine

Phosphoramidite ligand were first introduced by Feringa *et al*., the enantiomeric control was controlled by both BINOL backbone and amine moiety (Figure 65). The BINOL backbone of phosphoramidite are prepared *via* the chlorophosphite.

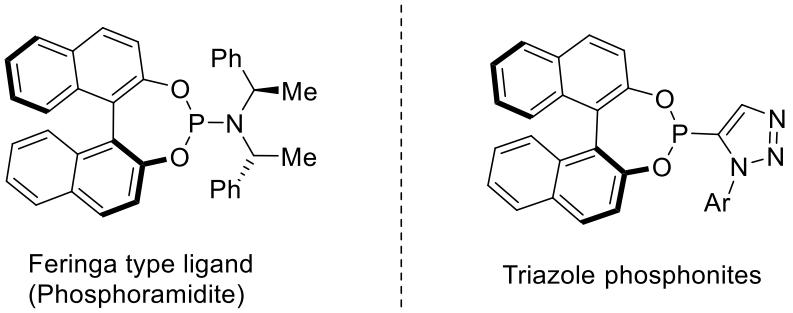

Figure 65. typical examples of Feringa type Phosphoramidite ligand, derived triazole phosphonite

Inspired by the preparation procedure of phosphoramidite, a brand new chiral triazole phosphonite compound has been designed, with the chirality introduced by BINOL backbone of phosphonites. (*S*)-**132** has been successfully prepared by quenching lithium triazole species with PCl(sBINOL), to furnish (*S*)-**132** with only 26 % yield (Scheme 42), the side reaction will be discussed later in this chapter. But since enantiomeric pure (*S*)-BINOL derivatives have been used as a reactant, the absolute configuration of BINOL are expected remain as same as the reactant.

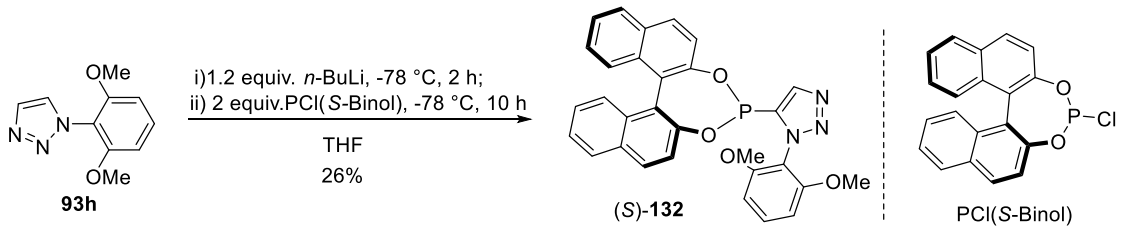

Scheme 42. Synthesis of triazole phosphonite

Enantiomeric pure phosphonite gold complex (*S*)-**133** was prepared by reacting with the same equivalent of (*S*)-**132** and DMSAuCl with 87% isolated yield. A suitable single crystal for X-ray diffractometry analyst was obtained from recrystallisation in DCM/Hexane mixed solvent (Scheme 43). The determined structure is (*S*) configuration

by anomalous dispersion with a Flack parameter of -0.038(3). In addition, the space group of the crystal lattice was found to be C2 (Scheme 43).

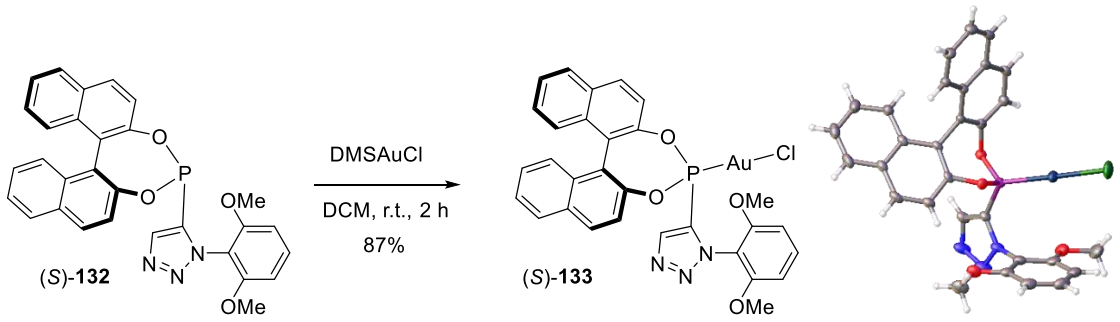

Scheme 43. Synthesis of gold complex (*S*)-**133**, structure has been confirmed by X-ray structure with (*S*) configuration; ellipsoid are drawn at the 50% probability level, space group = C2, with a Flack parameter of -0.038(3). A molecule of DCM has been omitted for clarity.

Since the lower yields of product obtained continuously from the formation of the phosphonite compound, further investigation of reaction has been conducted. One of the reason is due to the unstable nature of chlorophosphonite reagent; it is highly moisture sensitive. Besides, there is a major side product has been formed from the reaction as different peak could be observed from ^{31}P-NMR spectroscopy. Attempt to isolate this byproduct has been conducted but unable to get pure material for characterisation.

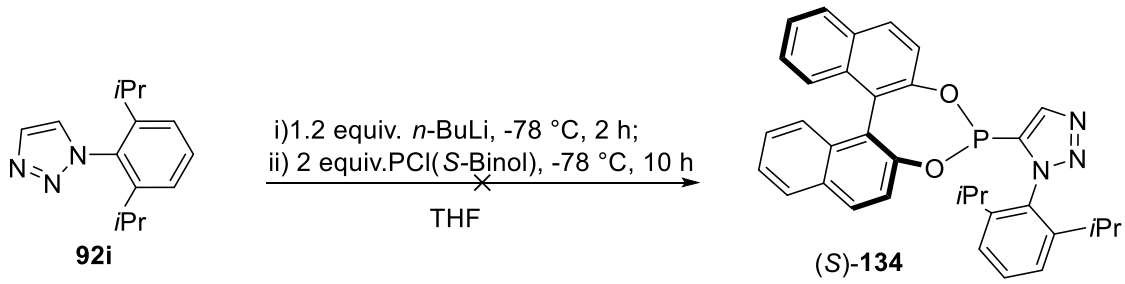

Scheme 44. Failed in attempted to synthesis (*S*)-**134**, with no product formation during the reaction.

Synthesis of **(S)-134** via the similar reaction protocol from triazole **92i** attempted without successful results (Scheme 44). Besides, a white solid byproduct **135** has been

isolated. The structure of formed byproduct of (*S,S*)-**135** has been confirmed by an X-ray analyst since the single crystal has been obtained by recrystallisation from DCM and hexane solution (Figure 66). The absolute configuration of **135** has been determined as (*S,S*), which matched with the (*S*)-BINOL derived chlorophosphonite reactant. Also, the structure has been solved in $P2_1$ space group with Flack parameter equal to -0.02(3). This highly confirmed enantiopurity of the formed crystal.

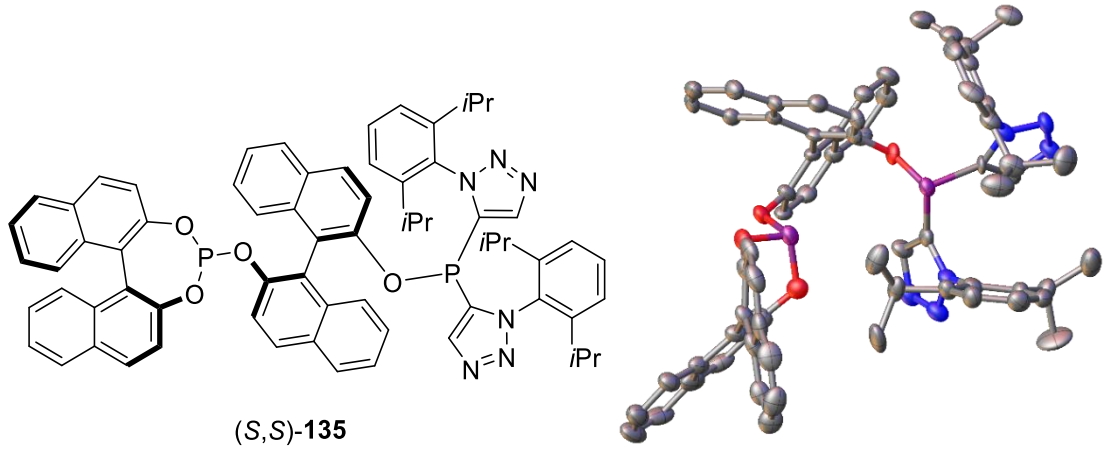

Figure 66. **(*S,S*)-135**, the structure has been confirmed by X-ray structure with (S,S) configuration, ellipsoid are drawn at the 50% probability level, space group = $P2_1$, with a Flack parameter of -0.02(3). Hydrogen has been omitted for clarity.

A proposed structure of unknown byproduct and mechanism has been proposed in Scheme 45. Initially, triazole **92i** was deprotonated by *n*-BuLi and then reacted by chlorophosphonite to form the desired product (S)-**134**. However, the formed (*S*)-**134** can still be attacked by another equivalent of lithium-triazole species, P-O was opened and reacted with another equivalent of chlorophosphonite species to formed **(*S,S*)-135**. This proposed mechanism also suggests that order of addition is critical in this reaction, to test this, the reaction was reperformed by employing deprotonated triazole transferred via cannula into a THF solution of Chlorophosphonite. The result for the alternative order of the addition, giving the promising result since only one triazole

phosphonite signal has been observed from ^{31}P-NMR, with similar value of (S)-**132**. Despite promising result, the purification of (S)-**134** still remained as a challenging task, thus the pure form of product (*S*)-**134** still have not been obtained from this project.

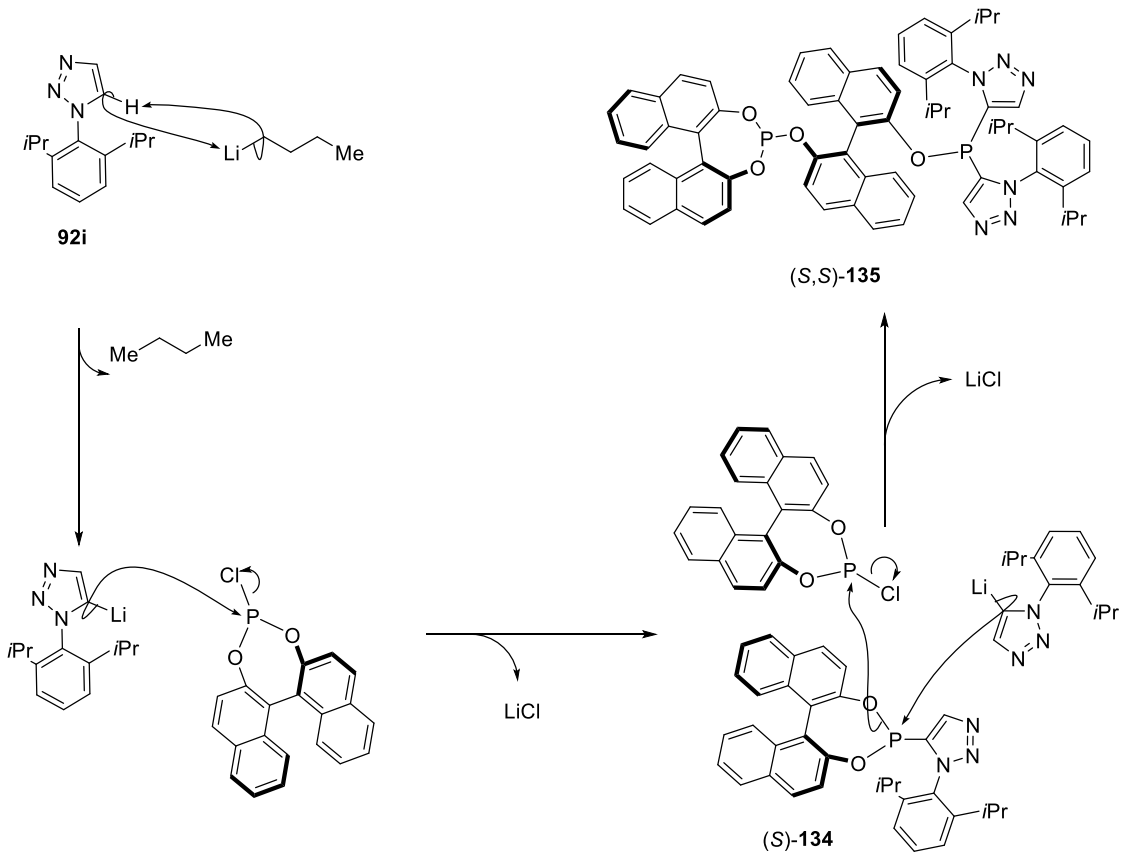

Scheme 45. Proposed mechanism and structure of bi-phosphorus species **(*S,S*)-135.**

4.4 Summary

This section detailed preliminary studies into the asymmetric version of triazole containing phosphine ligand with three different features: (i) chiral backbone; (ii) P-chirogenic phosphine; (iii) BINOL-derived phosphonite. The enantiomeric resolution was conducted by the prep-HPLC. Separation of enantiomeric pure ligands was found to be difficult, and due to time constraint; this project was not progressed further. The

activity of these ligands and complexes are conducted in the different research group at SIOC(China) and ICIQ(Spain), which are not included in this thesis. It is hoped that these preliminary results can be built upon further ligand derivation.

Experiment work in this chapter was mainly carried out by the author of this thesis, and compound **132** was prepared by Alexander Conner (UoB).

5. Chapter 5 Conclusion and Future work

Various triazole containing phosphine ligands have been prepared throughout this thesis. Ligand series **76** and **93** have all been tested in the benchmark SMC reaction against commercially available ligand SPhos and XPhos (*Scheme 46*). During the reaction condition employed, ligand series **93** generally shows better catalytic activity against the ligand series **76** and compatible activity against SPhos and XPhos. It was notable that **93g** shows the best activity not only in the benchmark palladium catalysed reaction, but also in further reaction to the synthesis of four *ortho*-substituted bi-aryl compounds. Since ligand **93g** shows the best activity in SMC reaction to synthesise bis-aryl substrate, and to fully explore catalytic potential, **93g** has been introduced to the synthesis of ten lead-like compounds which virtual selected by LLAMA programme. These lead-like products have been sent for biological tests.

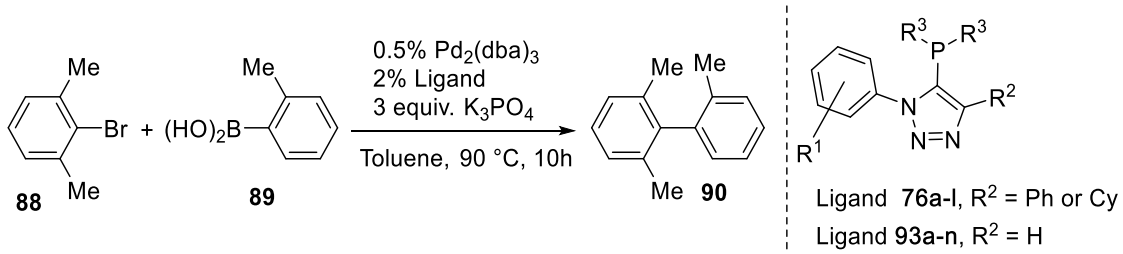

Scheme 46. Ligand series in the benchmark SMC reaction.

The X-ray structure of **93g** has been analysed for unveiling the structure-activity relationship, and these parameters were obtained by restricted dihedral angle *via* phosphine oxide surrogate methods. The analysis shows the strong relationship between the bulkiness features and catalytic activity in palladium chemistry. Besides, triazole-nitrogen might not be entirely 'innocent' in the coordination environment since an XRD structure of nitrogen-palladium has been observed. (**107**) And there will

be more transitional metal catalysed need to be screened to check whether nitrogen atom offers the unique property to this series of ligand.

To verify the relationship between the bulkiness of ligand and catalytic activity, phosphine ligand with different number of triazole units has been designed and successfully prepared (Figure 67).

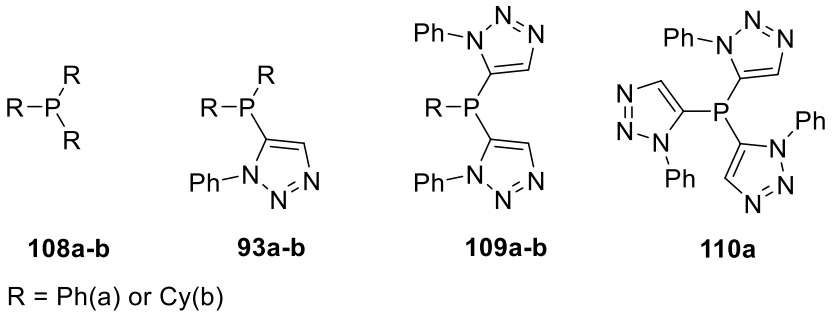

Figure 67. Phosphorous compound with different number of triazole unit.

It has been noticed that although increasing bulkiness of ligands shows positive effects to catalytic outcome in one-triazole ligand model. But the catalytic activity in palladium catalysed SMC reaction has been decreased with the increasing number of triazole motifs under the reaction condition employed. Besides, the corresponding phosphino triazole gold complexes have been prepared, and bulkiness of these ligands were determined by *SambVca* web tool. The corresponding gold complexes, as well as tricyclohexyl phosphine gold chloride and triphenylphosphine gold chloride have been tested as alkyne hydration catalysts, and this led to the conclusion that the mono-

triazole containing phosphine compound is the most effective ligands for gold(I) catalysed hydration of alkynes under the employed condition.

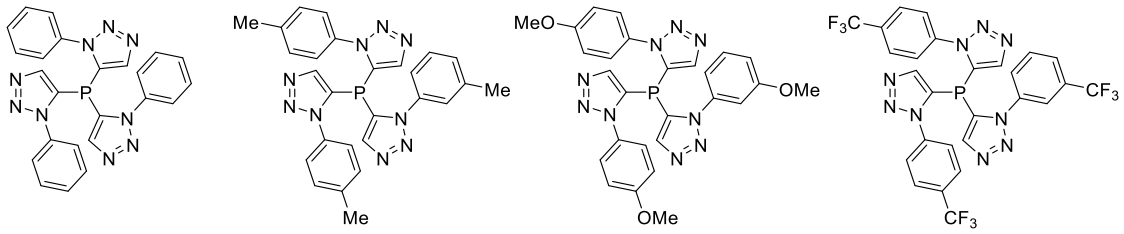

Figure 68. Tris-triazole phosphine compound with different functional groups in aryl-triazole.

A series of tris-triazole phosphine compound has been prepared and initially for bulkiness study (Figure 68). Although the catalytic outcome of these ligands were not fantastic, the potential metal-binding ability were still under investigation.

Additionally, since the **93g** to be the most promising ligands for palladium catalysed SMC reaction, the usage of gold complex of **93g** (**115**) shows encouraging result in the hydration of alkynes (Scheme 47). The ease of synthesis and modification of the triazole ligand framework should prove useful in future ligand design, synthesis and screening.

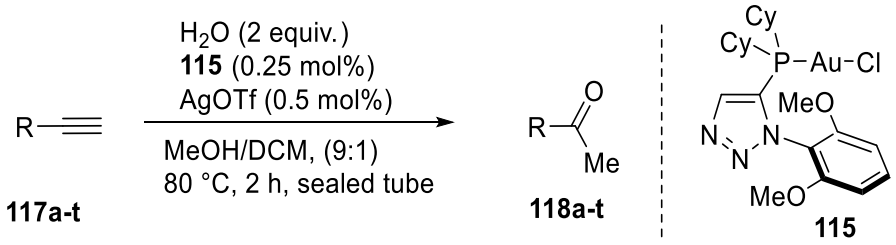

Scheme 47. Hydration of terminal alkyne by using complex **115**

Finally, the asymmetric version of triazole containing phosphine ligands have also been successfully achieved in this thesis. The chirality of ligand has been introduced with

different ways; i) chiral triazole backbone; ii) P-chirogenic with achiral triazole iii) phosphonite with chiral motif (Figure 69).

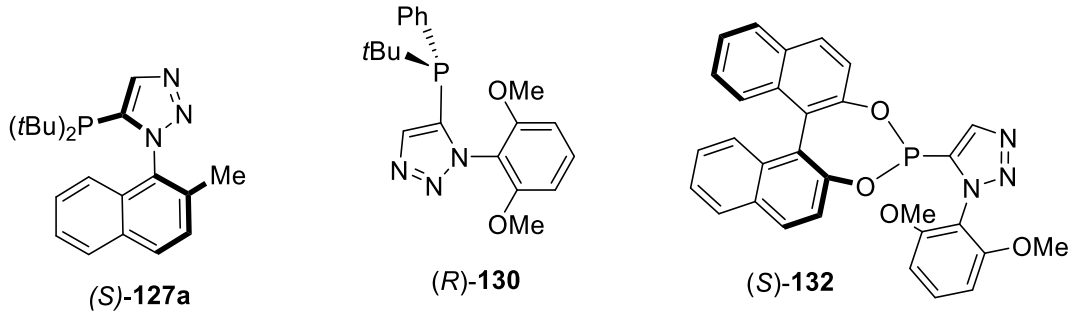

Figure 69. Asymmetric phosphino triazole compound

The enantiomeric pure of these ligand has been successfully separated by prep-HPLC and *ee*% re-checked by analytical HPLC. Besides, the enantiomeric pure phosphine gold complex has also been prepared under standard condition. The reactivity of these ligands were tested in collaborator in SIOC(Shanghai) and ICIQ(Spain).

Future work in this area could be designing different pro-chiral triazole backbone and applying these ligands and corresponding gold complexes into series asymmetric reactions. Since the XRD structure of these ligands and gold-complexes are already available, it would be much easier to study SAR from the crystal structure.

6. Appendix 1 Experimental

6.1General

Unless otherwise stated, commercially available solvents and reagents were used as obtained, without further purification. Proton NMR spectrums were recorded on Bruker AVIII300/400/500 NMR spectrometers at 300, 400 and 500 MHz respectively. Proton decoupled ^{19}F NMR spectrums were recorded on a Bruker AVIII300 NMR spectrometer at 282 MHz. Both proton-coupled and proton-decoupled ^{31}P NMR spectrums were recorded on a Bruker AVIII300 NMR spectrometer at 131 MHz. The ^{31}P chemical shift is reported as, unless otherwise stated, obtained from the proton decoupled spectrum relative to external 85% phosphoric acid (δ = 0.0 ppm). Proton decoupled ^{13}C NMR spectrums were recorded at room temperature on Bruker AVIII300, AVIII400 and AVIII500 NMR spectrometers at 75, 101 and 126 MHz respectively.[198] The proton decoupled ^{13}C NMR signal quality was superior when using the UDEFT pulse sequence, as such all ^{13}C NMR signals are reported as obtained from UDEFT experiments.[199] Furthermore, assignments of ^{13}C NMR spectroscopy signals in some cases was facilitated by obtaining spectrums using the J-MOD pulse sequence, the sign relating to proton substitution as follows: positive *C*H and *C*H_3 (denoted [+]) and negative C_{quat} and *C*H_2 (denoted [-]), relative in this case to solvent *C*DCl_3 [-].[200] The UDEFT pulse sequence was also used to enhance the signal intensity of ^{13}C signals in some cases, where a signal was observed utilising UDEFT but not observed with J-MOD the signal is given designation [u]. Coupling constants (*J*) are expressed in Hertz (Hz).[201] Multiplicities are reported as singlet (s), doublet (d), triplet (t), quartet (q), septet (sept),

multiplet (m) and broad (br), the designation app is used to describe the *apparent* appearance of a signal believed to consist of overlapping signals or displaying other phenomena to reveal an apparent signal inconsistent with expected multiplicity. NMR spectroscopic data was processed using *Mestrenova v10.02.-15465* and/or *Topspin v3.5*. The chemical shifts for each signal in the proton NMR spectrums are reported as chemical δ (ppm) relative to either tetramethylsilane (TMS) where $\delta_{(TMS)}$ = 0.00 or the residual solvent peak.[202] The chemical shifts for each signal in the ^{13}C NMR spectrums are reported relative to signals of the solvent employed.[202] Mass spectrometry was conducted using a Waters LCT Time of Flight mass spectrometer (electrospray) or by using a *Waters GCT Premier Time of Flight Mass Spectrometer* (EI GC/MS). Infrared spectra were recorded at room temperature on either a *PerkinElmer 100FT-IR* spectrometer or a *Varian 660-IR* spectrometer with ATR attachments; a corresponding thin film was obtained by evaporation of dichloromethane solvent from a given sample. Melting points are uncorrected and were carried out in triplicate using a *Stuart SMP10* melting point apparatus and average values reported as a range using. Microwave heating of reactions was conducted, where specified, using a *CEM Discover S* microwave reaction heating system. Column (flash) chromatography was carried out using an *Isco Combiflash EZ Prep* or *Interchim PuriFlash XS 420+* automated chromatography apparatus. Mobile and stationary phases are described in the general methods or the experimental procedures. Chromatographic traces were recorded at two wavelengths (254 nm and 288nm). Neighbouring tubes identified as pure were double-checked by separate TLC analysis, prior to being combined into single fractions and evaporated to dryness *in vacuo*. Compounds synthesised that have been previously

reported compounds gave satisfactory correlation with spectroscopic observations given in the literature and cited herein.

6.2Experimental for Chapter 2

General Procedure 1: Preparation of aryl azides **12a-i**

To a solution of a mixture of substituted aniline compound (10 mmol) and aqueous HCl solution (5 M, 10 mL) in a round-bottom flask at 0 °C, sodium nitrite (12 mmol, in water, 30 mL) was added dropwise in the ice bath. The reaction mixture was stirred at 0 °C for one hour. After which, a solution of sodium azide (20 mmol, in water, 5 mL) was added dropwise, and the reaction mixture stirred at 0 °C for a further hour, upon which time the flask and its contents were allowed to warm room temperature. After consumption of starting material was judged complete through (TLC analysis), the reaction mixture was extracted three times with ethyl acetate, and the combined organic fractions were washed with water to neutral pH. The organic layer was dried over anhydrous magnesium sulphate, filtered, and the solvent removed in vacuo to deliver a crude residue. The crude residues were purified by flash chromatography (Isco CombiFlash, silica 50-60 µm, 4 or 12 g size column, hexane (100%) to hexane (80%): ethyl acetate (20%) gradient elution, detection 254 and 288 nm absorption) to afford the corresponding aryl azides.[203]

General procedure 2: Preparation of 1,4-disubstituted triazoles **11a-l, 87a-b**

In a round-bottom flask, the corresponding alkyne (1 mmol, 1.0 equiv.) and azide (1.1 equiv.) were suspended in the appropriate amount of water:*t*-butanol (50:50) mixture,

to deliver a substrate concertation of 0.2 M. Copper(II) sulphate (0.1 equiv., 10 mol%) and sodium ascorbate (0.4 equiv., 40 mol%) were added. The reaction mixture was stirred at room temperature for 24 h. After which time aqueous ammonium chloride solution was added, the resulting mixture was extracted with ethyl acetate (at least three times), the combined organic layers were dried over anhydrous magnesium sulphate, filtered and concentrated in vacuo to deliver a crude residue. The residues thus obtained were purified by flash chromatography (Isco CombiFlash, silica 50-60 µm, 4 or 12 g column, hexane (100%) to hexane (50%): ethyl acetate (50%) gradient elution, detection 254 and 288 nm absorption) to afford the corresponding 1,4-triazole products.

General procedure 3: Preparation of mono-substituted 1-triazole derivatives **92a-i**

In a round-bottom flask the corresponding azide (1 equiv.) and trimethylsilyl acetylene (1.5 equiv.) were suspended in a water: methanol (1:1) mixture, to deliver a substrate concentration of 0.1 M. Copper(II) sulphate (0.2 equiv., 20 mol%), sodium ascorbate (0.4 equiv., 40 mol%) and Potassium carbonate (2 equiv.). The reaction mixture was stirred at room temperature for 24 h. After which time aqueous ammonium chloride solution was added, the resulting mixture was extracted with ethyl acetate at least three times, and the combined organic layers were dried over anhydrous magnesium sulphate, filtered and concentrated in vacuo to deliver a crude residue. This crude residue was purified by flash chromatography (Isco CombiFlash, silica 50-60 µm, 4 or 12 g column, hexane (100%) to ethyl acetate (100%) gradient elution, detection 254 and 288 nm absorption) to afford the corresponding triazole products.

General procedure 4: Preparation of triazole-containing phosphines 76a-i and 93a-n

Under anhydrous conditions and protected from air, a solution of the corresponding triazole (1 equiv.) in tetrahydrofuran (0.04 M) was stirred at -78 °C. And n-butyl lithium (1.2 equiv., 2.0 M in tetrahydrofuran) was added dropwise. The reaction mixture was stirred for two hours at this temperature. Upon which time the corresponding aryl- or alkyl- phosphine chloride (2 equiv.) was added. After addition was complete, the reaction mixture was allowed to slowly warm to room temperature. After stirring at room temperature for a further 10 h, the volatiles were removed in vacuo to afford a crude residue. The residue thus obtained, was purified by flash chromatography (Isco CombiFlash, silica 50-60 µm, or Interchim XS 420, 20 µm, 4 or 12 g column, hexane (100%) to hexane (50%): ethyl acetate (50%) gradient elution, detection 254 and 288 nm absorption) to afford the corresponding product.

General procedure 5: Preparation of lead-like compounds 105a-j via Suzuki-Miyaura cross-coupling

Tripotassium phosphate (2 equiv.), the corresponding boronic acid (1.5 equiv.), if solid the corresponding halide derivative (1 equiv.), $Pd_2(dba)_3$ (1 mol%, corresponding to 2 mol% palladium), and ligand **93g** (4 mol%) were combined in a 10 mL microwave reactor tube. Acetonitrile was added (3 mL), if halide derivative was liquid, it was added with solvent. The microwave reactor vessel was purged with argon (10 s). The reaction vessel was placed into a microwave reactor heat at 100 °C in dynamic mode for 1 h. After the vessel has cool to room temperature, the mixture was diluted with ethyl acetate (20 mL) and washed with brine (10 mL). The aqueous layer was extracted

further with ethyl acetate (15 mL). The combine organic fractions were dried over anhydrous sodium sulphate, filtered and the solvent removed in vacuo. The crude material thus obtained analysed by proton NMR spectroscopy to determine the level of conversion. If NMR spectroscopy reveals a less than 20% conversion, the reaction was abandoned at this point. For reactions with great than 20% conversion isolation and purification by flash chromatography (Interchim XS 420, 20 μm, 4 or 12 g column, hexane (100%) to ethyl acetate (100%) or dichloromethane (100%) to or dichloromethane (90%): methanol (10%) gradient elution, detection 254 and 288 nm absorption), afforded the corresponding products.

General procedure 6: Preparation of palladium(II) complexes for study by single-crystal X-ray diffraction analysis

To a flame dry round-bottom flask, *trans*-$Pd(CH_3CN)_2Cl_2$ (0.05 mmol) and a corresponding ligand (0.1 mmol) were combined in dichloromethane (2 mL). The mixture was stirred at room temperature under argon for 10 h. After this time, pentane (10 mL) was added, resulting in precipitation of yellow-coloured material. The precipitate was collected *via* filtration and washed with pentane.

General procedure 7: Analysis of catalysed reactions (compound 90, 96 and 101)

The equivalent of reactants, reaction time, temperature were referred to the table in the main text individually.

To a flame dry carousel tube, tripotassium phosphate, the corresponding boronic acid halide derivative, $Pd_2(dba)_3$, triazole phosphine ligand were combined, and aryl halides

added with toluene solvent under the protection of argon. The carousel tube was purged with argon three times and heated at listed temperature and time in the table from the main text. After the vessel has cool to room temperature, the mixture was diluted with toluene. A drop of the reaction mixture was taken for the GC analysis.

Conversions of starting materials to Suzuki-Miyaura reaction products compound **90** (Table 2, 3, 6 and 9 in the main text); compound **96** (Table 4 and 5 in the main text) and compound **101** (**Scheme *26*** in the main text) were determined by GC analysis using the same method in each case. Internal standard *n*-dodecane in toluene, injection temperature 260 °C, oven temperature gradient from 100 to 200 °C over 20 min maintain temperature for another 5 min (minimum), column ZB-5. Typical run time 25 min, peaks determined using FID.

For the isolated yield, the reaction mixture was then filtered *via* Celite, and the volatiles were removed *in vacuo* to afford a crude residue. The residue thus obtained, was purified by flash chromatography with 100% hexane to afford the corresponding products.

Synthetic Protocols and Experimental Details

Synthesis of 1,4-diphenyl-1H-1,2,3-triazole (11a)

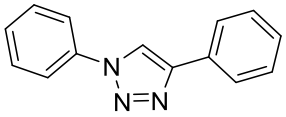

11a

Prepared following *General Procedure 2* on a 2.2 mmol azide scale.[108] Isolated as an off-white solid (411 mg, 93%) ^{1}H NMR (400 MHz, $CDCl_3$) δ 8.20 (s, 1H, Trz*H*), 7.92 (dd, *J* 8.2 & 1.2, 2H), 7.80 (dd, *J* 8.5 & 1.2, 2H), 7.61-7.50 (m, 2H), 7.50-7.42 (m, 3H), 7.40 – 7.33 (tt, *J* 8.0 & 1.4, 1H); ^{13}C NMR (101 MHz, $CDCl_3$) δ 148.42 [-], 137.08 [-], 130.26 [-], 129.78 [+], 128.92 [+], 128.77 [+], 128.42 [+], 125.86 [+], 120.53 [+], 117.60 [+]; IR ν (cm^{-1}) 3120, 1504, 1465; TOF MS ES+ m/z: 222.1 $[M+H]^+$, 244.1 $[M+Na]^+$.

Synthesis of 4-cyclohexyl-1-phenyl-1H-1,2,3-triazole (11b)

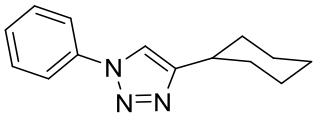

11b

Prepared following *General Procedure 2* on a 2.2 mmol of azide scale.[204] Obtained as a white solid (291 mg, 64%); ^{1}H NMR (300 MHz, $CDCl_3$) δ 7.77-7.68 (m, 3H), 7.54-7.47 (m, 2H), 7.44-7.37 (m, 1H), 2.91-2.80 (m, 1H, Cy*H*), 2.23-2.01 (m, 2H, Cy*H*), 1.93-1.62 (m, 3H, Cy*H*), 1.58-1.21 (m, 5H, Cy*H*); ^{13}C (101 MHz, $CDCl_3$) δ 154.42 [-], 137.38 [-], 129.63 [+], 128.33 [+], 120.41 [+], 117.49 [+], 35.31 [+], 33.01 [-], 26.14 [-], 26.05 [-]; IR ν (cm^{-1}) 2926, 2845, 1503, 1448; TOF MS ES+ m/z: 228.2 $[M+H]^+$; HRMS calc. $[C_{14}H_{18}N_3]^+$ 228.1495, obs. 228.1502.

Synthesis of 4-phenyl-1-(p-tolyl)-1H-1, 2, 3-triazole (11c)

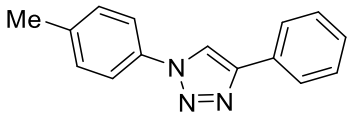

11c

Prepared following *General Procedure 2* on a 2.2 mmol azide scale.[205] Isolated as an off-white solid (436 mg, 92%) ^{1}H NMR (300 MHz, $CDCl_3$) δ 8.16 (s, 1H, Trz*H*), 7.96-7.82 (m, 2H), 7.67 (d, *J* 8.5, 2H), 7.46 (t, *J* 7.1, 2H), 7.40-7.31 (m, 3H), 2.44 (s, 3H, C*H*$_3$); ^{13}C NMR (101 MHz, $CDCl_3$) δ 148.27 [-], 138.90 [-], 134.80 [-], 130.34 [u], 130.26 [+], 128.90 [+], 128.35 [+], 125.84 [+], 120.45 [+], 117.61 [+], 21.12 [+]; IR ν (cm^{-1}): 3126, 1520, 1454; TOF MS EI+ m/z: 235.1 $[M]^+$, 207.1 $[M-N_2]^+$.

Synthesis of 1-(4-methoxyphenyl)-4-phenyl-1H-1, 2, 3-triazole (11d)

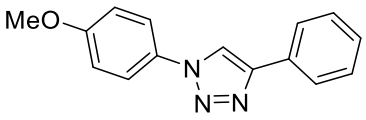

11d

Prepared following *General Procedure 2* on a 2.2 mmol azide scale.[205] Isolated as a light yellow solid (405 mg, 81%);^{1}H NMR (300 MHz, $CDCl_3$) δ 8.11 (s, 1H, Trz*H*), 7.90 (d, *J* 7.1, 2H), 7.68 (d, *J* 9.1, 2H), 7.46 (t, *J* 7.1, 2H), 7.40-7.36 (tt, *J* 7.1 & 1.4, 1H, Ar*H*), 7.04 (d, *J* 9.1, 2H), 3.87 (s, 3H, OC*H*$_3$); ^{13}C NMR (101 MHz, $CDCl_3$) δ 159.87 [-], 148.24 [-], 130.57 [-], 130.41 [-], 128.91 [+], 128.33 [+], 125.84 [+], 122.21 [+], 117.83 [+], 114.82 [+], 55.66 [+]; IR ν (cm^{-1}) 3121, 1518, 1480, 1460; TOF MS ES+ m/z: 252.2 $[M+H]^+$.

Synthesis of 1-(2,6-dimethoxyphenyl)-4-phenyl-1H-1,2,3-triazole (11e)

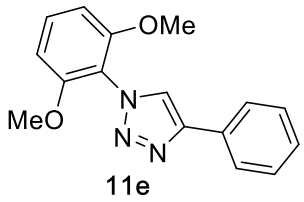

11e

Prepared following *General Procedure 2* on a 1.1 mmol azide scale isolated as a light brown solid (182 mg, 64%); ^{1}H NMR (400 MHz, $CDCl_3$) δ 7.92 (d, *J* 8.3, 2H), 7.86 (s, 1H, Trz*H*), 7.47-7.38 (m, 3H), 7.36-7.29 (m, 1H), 6.69 (d, *J* 8.5, 2H), 3.77 (s, 6H, OC*H*$_3$). ^{13}C NMR (101 MHz, $CDCl_3$) δ 155.98 [-], 146.78 [-], 131.39 [+], 130.92 [-], 128.75 [+], 127.88 [+], 125.79 [+], 123.10 [+], 115.41 [-], 104.36 [+], 56.21 [+]; IR ν (cm^{-1}) 1599, 1219, 1481; TOF MS ES+ m/z: 282.1 $[M+H]^+$, 304.1 $[M+Na]^+$; HRMS calc. $[C_{16}H_{16}N_3O_2]^+$ 282.1237, obs. 282.1245.

Synthesis of 4-cyclohexyl-1-(2,6-dimethoxyphenyl)-1H-1,2,3-triazole (11f)

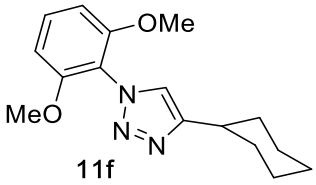

11f

Prepared following *General Procedure 2* on a 1.1 mmol azide scale, isolated as a brown solid (240 mg, 83%); m.p. 89-92 °C; ^{1}H NMR (400 MHz, $CDCl_3$) δ 7.37 (t, *J* 8.5, 1H, CHC*H*CH), 7.32 (s, 1H, Trz*H*), 6.65 (d, *J* 8.5, 2H, C*H*CHC*H*), 3.73 (s, 6H, OC*H*$_3$), 2.94-2.78 (m, 1H), 2.26-2.12 (m, 2H), 1.86-1.79 (m, 2H), 1.77-1.70 (m, 1H), 1.57-1.35 (m, 4H), 1.34-1.23 (m, 1H); ^{13}C NMR (101 MHz, $CDCl_3$) δ 155.96 [-], 152.42 [-], 131.05 [+], 122.58 [+], 115.72 [-], 104.33 [+], 56.16 [+], 35.34 [+], 32.96 [-], 26.21 [-], 26.13 [-]. TOF MS ES+ m/z: 288.2 $[M+H]^+$, 310.2 $[M+Na]^+$; HRMS calc. $[C_{16}H_{22}N_3O_2]^+$ 288.1707, obs. 288.1715.

Synthesis of 1-([1,1'-biphenyl]-2-yl)-4-phenyl-1H-1,2,3-triazole (11g)

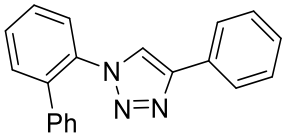

11g

Prepared following *General Procedure 2* on a 2.2 mmol azide scale[206], obtained as a light yellow solid (450 mg, 95%).^{1}H NMR (300 MHz, $CDCl_3$) δ 7.72-7.64 (m, 3H), 7.60-7.50 (m, 3H), 7.41-7.33 (m, 3H), 7.33-7.26 (m, 4H), 7.19-7.10 (m, 2H); ^{13}C NMR (101 MHz, $CDCl_3$) δ 147.42 [-], 137.32 [-], 136.97 [-], 135.08 [-], 131.15 [+], 130.35 [-], 129.89 [+], 128.78 [+], 128.75 [+], 128.62 [+], 128.52 [+], 128.16 [+], 128.06 [+], 126.51 [+], 125.76 [+], 121.70 [+]; IR ν (cm-1) 1478, 1440; TOF MS ES+ m/z: 298.1 $[M+H]^+$, 320.1 $[M+Na]^+$.

Synthesis of 1-(naphthalen-1-yl)-4-phenyl-1H-1,2,3-triazole (11h)

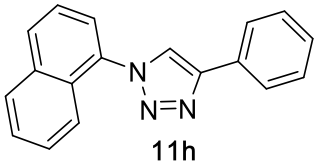

11h

Prepared following *General Procedure 2* on a 2.2 mmol azide scale,[206] in contrast to the physical state reported in the literature the product was obtained here as a red solid (450 mg, 83%); m.p. 89-91 °C (lit. brown oil at r.t.); ^{1}H NMR (400 MHz, $CDCl_3$) δ 8.14 (s, 1H, Trz*H*), 8.03 (d, *J* 8.0, 1H), 7.99-7.93 (m, 3H), 7.72-7.67 (m, 1H), 7.64-7.51 (m, 4H), 7.51-7.44 (m, 2H), 7.38 (tt, *J* 8.1 & 1.2, 1H, Ar*H*); ^{13}C NMR (101 MHz, $CDCl_3$) δ 147.76 [-], 134.20 [-], 133.75 [-], 130.45 [+], 130.33 [-], 128.98 [+], 128.61 [-], 128.43 [+], 128.31 [+], 127.94 [+], 127.12 [+], 125.90 [+], 125.03 [+], 123.57 [+], 122.40 [+], 122.30 [+]; IR

ν (cm^{-1}) 1597, 1470, 1428; TOF MS ES+ m/z: 272.1 $[M+H]^+$, 294.1 $[M+Na]^+$; HRMS calc. $[C_{18}H_{14}N_3]^+$ 272.1182, obs. 272.1186.

Synthesis of 4-cyclohexyl-1-(naphthalen-1-yl)-1H-1,2,3-triazole (11i)

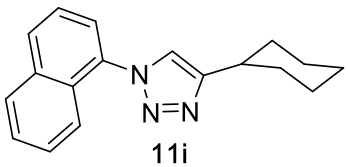

11i

Prepared following *General Procedure 2* on a 2.2 mmol azide scale, obtained as a red oil (392 mg, 71%); ^{1}H NMR (400 MHz, $CDCl_3$) δ 8.03-7.97 (m, 1H), 7.97-7.93 (m, 1H), 7.67-7.61 (m, 2H), 7.62-7.50 (m, 4H), 2.98-2.88 (m, 1H), 2.34-2.15 (m, 2H), 1.99-1.71 (m, 3H), 1.69-1.42 (m, 4H), 1.37-1.19 (m, 1H); ^{13}C NMR (101 MHz, $CDCl_3$) δ 153.64 [-], 134.16 [-], 130.07 [+], 128.69 [-], 128.21 [+], 127.72 [+], 126.96 [+], 124.99 [+], 123.48 [+], 122.53 [+], 122.10 [+], 35.35 [+], 33.09 [-], 26.19 [-], 26.08 [-] (15 of 16 expected signals observed, as judged by the J-MOD spectra an expected [-] C_{quat} signal is not observed); IR ν (cm^{-1}) 2924, 2851, 1597, 1512, 1471, 1447; TOF MS ES+ m/z: 278.2 $[M+H]^+$, 300.2 $[M+Na]^+$; HRMS calc. $[C_{18}H_{20}N_3]^+$ 278.1652, obs. 278.1656.

Synthesis of azidobenzene (12a)

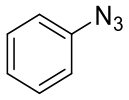

12a

Prepared following *General Procedure 1* on a 20 mmol scale.[204] Obtained as brown oil (1.84 g, 77%); ^{1}H NMR (400 MHz, $CDCl_3$) δ 7.33 (t, *J* 7.9, 2H, Ar*H*), 7.12 (t, *J* 7.4, 1H, Ar*H*), 7.04-6.94 (m, 2H, Ar*H*); ^{13}C NMR (101 MHz, $CDCl_3$) δ 140.05 [-], 129.78 [+], 124.89 [+],

119.06 [+]; IR ν (cm^{-1}) 2921, 2123, 2091, 1593, 1491; TOF MS EI+ m/z: 119.0 $[M]^+$, 91.0 $[M-2N]^+$.

Synthesis of 1-azido-4-methylbenzene (12b)

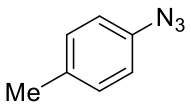

12b

Prepared following *General Procedure 1* on a 20 mmol scale.[207] Obtained as an orange oil (1.47 g, 55%) ^{1}H NMR (300 MHz, $CDCl_3$) δ 7.14 (d, *J* 8.4, 2H, Ar*H*), 6.91 (d, *J* 8.4, 2H, Ar*H*), 2.32 (s, 3H, C*H*$_3$); ^{13}C NMR (75 MHz, $CDCl_3$) δ 137.13 [-], 134.62 [-], 130.35 [+], 118.84 [+], 20.85 [+]; IR ν (cm^{-1}) 2098, 1503, 1294; TOF MS EI+ m/z: 133.1 $[M]^+$, 105.1 $[M-2N]^+$.

Synthesis of 1-azido-4-methoxybenzene (12c)

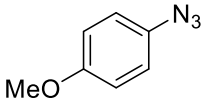

12c

Prepared following *General Procedure 1* on a 20 mmol scale.[207] Obtained as a brown oil (2.77 g, 93% yield) ^{1}H NMR (300 MHz, $CDCl_3$) δ 6.95 (d, *J* 9.2, 2H, Ar*H*), 6.88 (d, *J* 9.2, 2H, Ar*H*), 3.79 (s, 3H, OC*H*$_3$).^{13}CNMR (101 MHz, $CDCl_3$) δ 157.00 [-], 132.34 [-], 119.98 [+], 115.12 [+], 55.55 [+]; IR ν (cm^{-1}) 2097, 1500, 1239; TOF MS EI+ m/z: 149.1 $[M]^+$, 121.1 $[M-2N]^+$.

Synthesis of 2-azido-1,3-dimethoxybenzene (12d)

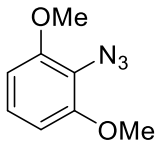

12d

Prepared following *General Procedure 1* on a 10 mmol scale.[207] Obtained as a yellow oil (1.52 g, 84%); ^{1}H NMR (400 MHz, $CDCl_3$) δ 7.03 (t, *J* 8.4, 1H, CHC*H*CH), 6.54 (d, *J* 8.4, 2H, C*H*CHC*H*), 3.86 (s, 6H, OCH_3). ^{13}C NMR (101 MHz, $CDCl_3$) δ 153.26 [-], 125.13 [+], 116.50 [-], 104.82 [+], 56.18 [+]; IR ν (cm^{-1}) 2102, 1590, 1475; TOF MS EI+ m/z: 151.1 $[M-2N]^+$.

Synthesis of 2-azido-1, 1'-biphenyl (12e)

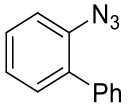

12e

Prepared following *General Procedure 1* on a 20 mmol scale.[208] Obtained as an orange oil (3.52 g, 95% yield) ^{1}H NMR (300 MHz, $CDCl_3$) δ 7.46 – 7.30 (m, 7H), 7.26-7.15 (m, 2H); ^{13}C NMR (101 MHz, $CDCl_3$) δ 138.20 [-], 137.17 [-], 133.84 [-], 131.30 [+], 129.49 [+], 128.74 [+], 128.17 [+], 127.57 [+], 124.97 [+], 118.81 [+]; TOF MS EI^+: 167.1 $[M-2N]^+$.

Synthesis of 1-azidonaphthalene (12f)

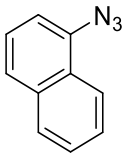

12f

Prepared following *General Procedure 1* on a 20 mmol scale.[209] Obtained as a red oil (2.45 g, 72% yield) ^{1}H NMR (300 MHz, $CDCl_3$) δ 8.14- 7.98 (m, 1H), 7.86-7.71 (m, 1H), 7.57 (d, *J* 8.3, 1H), 7.58-7.32 (m, 3H), 7.18 (dd, *J*-7.4, 1.0, 1H); ^{13}C NMR (101 MHz, $CDCl_3$) δ 136.56 [-], 134.40 [-], 127.77 [+], 126.92 [+], 126.48 [-], 126.17 [+], 125.68 [+], 124.73 [+], 122.61 [+], 113.95 [+]; IR ν (cm^{-1}) 2103, 1573,1390; TOF MS EI+: 169.1 $[M]^+$.

Synthesis of 1-azido-4-(trifluoromethyl) benzene (12g)

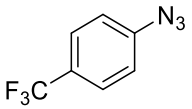

12g

Prepared following *General Procedure 1* on a 20 mmol scale.[210] Obtained as a light brown oil (2.17 g, 58%); ^{1}H NMR (300 MHz, $CDCl_3$) δ 7.60 (d, *J* 8.5, 2H, Ar*H*), 7.11 (d, *J* 8.5, 2H, Ar*H*); ^{19}F NMR (282 MHz, $CDCl_3$) δ -62.18; ^{13}C NMR (101 MHz, $CDCl_3$) δ 143.75 ([-], Ar *C*-N_3) 127.06 ([-], q, $^{2}J_{CF}$ 33.0, Ar 4-*C*-CF_3), 126.99 ([+], q, $^{3}J_{CF}$ 3.8, Ar 3- & 5-*C*(H)CCF_3), 123.91 ([-], q, $^{1}J_{CF}$ 271.5, *C*F_3), 119.20 ([+], Ar 2- & 6- *C*(H)CN_3); IR ν (cm^{-1}) 2101, 1327, 1287; TOF MS EI+ m/z: 186.9 $[M]^+$.

Synthesis of 2-azido-3,5-dimethoxybenzene (12h)

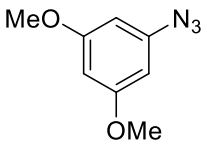

12h

Prepared following *General Procedure 1* on a 6 mmol scale.[211] Obtained as a yellow solid (793 mg, 73%); ^{1}H NMR (400 MHz, $CDCl_3$) δ 6.25 (t, *J* 2.2, 1H, COC*H*CO), 6.19 (d, *J* 2.1, 2H, C*H*CNC*H*), 3.78 (s, 6H, OC*H*$_3$); ^{13}C NMR (101 MHz, $CDCl_3$) δ 161.67 [-], 141.96

[-], 97.52 [+], 97.29 [+], 55.44 [+]; IR ν (cm^{-1}) 2102, 1589, 1472. TOF MS EI+ m/z: 179.1 $[M]^+$, 151.1 $[M-2N]^+$.

Synthesis of 2-azido-1,3-diisopropylbenzene (12i)

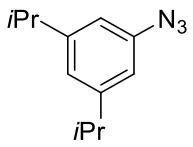

12i

2,6-Diisopropylaniline (5.0 mmol, 886 mg) was dissolved in acetonitrile (10 mL) and cooled to 0 °C in the ice bath. *t*-Butyl nitrite (7.5 mmol, 0.89 mL) and azidotrimethylsilane (6 mmol, 0.79 mL) were added dropwise. After addition was complete, the reaction mixture was allowed warm to room temperature and stirred for a further two hours. Evaporation of the solvent *in vacuo* afforded a crude residue which was purified by flash chromatography(*Isco CombiFlash*, silica 50-60 μm, 4 or 12 g column, hexane to hexane (80%):ethyl acetate (20%) gradient elution, detection 254 and 288 nm) to afford product **24i**.[212] Obtained as a yellow oil (930 mg, 89%); ^{1}H NMR (400 MHz, $CDCl_3$) δ 7.22-7.17 (m, 1H, Ar*H*), 7.15-7.11 (m, 2H, Ar*H*), 3.36 (sept, *J* 6.9, 2H, C*H*$(CH_3)_2$), 1.27 (d, *J* 6.9, 12H, CH(C*H*$_3$)$_2$); ^{13}C NMR (101 MHz, $CDCl_3$) δ 143.12 [-], 135.30 [u], 126.81 [+], 123.92 [+], 28.80 [+], 23.50 [+]; IR ν (cm^{-1}) 2963, 2120, 2098; TOF MS EI+: 175.1 $[M-2N]^+$

Synthesis of 1-(2-(diphenylphosphanyl)phenyl)-4-phenyl-1H-1,2,3-triazole (75a)

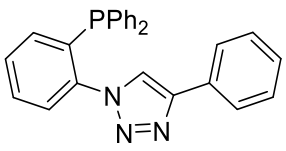

75a

A synthetic procedure akin to that utilised by Choubey *et al*. was employed, and spectroscopic data obtained were consistent with the same material being isolated, on 0.6 mmol scale.[108] Isolated as a white solid (105 mg, 44%); mp. 135-136 °C; ^{1}H NMR (400 MHz, $CDCl_3$) δ 7.81-7.67 (m, 3H), 7.60-7.48 (m, 2H), 7.46-7.23 (m, 14H), 7.12 (m, 1H); ^{31}P NMR (121 MHz, $CDCl_3$) δ -15.53; ^{13}C NMR (101 MHz, $CDCl_3$) δ 147.18, 140.91 (d, J_{CP} 21.6), 135.40 (d, J_{CP} 10.4), 134.65 (d, J_{CP} 21.6), 134.62, 134.05, (d, J_{CP} 20.7), 130.47, 129.82 (d, J_{CP} 8.5), 129.30, 128.77 (d, J_{CP} 2.9), 128.71, 128.09, 126.58, 125.83, 122.11 (d, J_{CP} 5.5); IR ν (cm^{-1}) 1475, 1434; TOF MS ES+ m/z: 406.1 $[M+H]^+$, 428.1 $[M+Na]^+$; HRMS calc. $[C_{26}H_{21}N_3P]^+$ 406.1468, obs. 406.1468.

Synthesis of 5-(diphenylphosphanyl)-1,4-diphenyl-1H-1,2,3-triazole (76a)

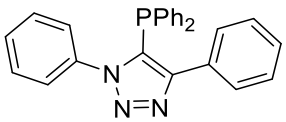

76a

Prepared following *General Procedure 4* on a 0.4 mmol scale.[108] Obtained as a white solid (106 mg, 68%); mp. 166-167 °C; ^{1}H NMR (400 MHz, $CDCl_3$) δ 7.46-7.39 (m, 2H), 7.35 (tt, *J* 7.7 & 2.2, 1H), 7.28-7.11 (m, 17H); ^{31}P NMR (121 MHz, $CDCl_3$) δ -30.15 , (t, *J* 4.41); ^{13}C NMR (101 MHz, $CDCl_3$) δ 154.27 (d, $^{2}J_{CP}$ 9.6), 137.31, 132.64 (d, $^{2}J_{CP}$ 19.8), 132.42 (d, $^{1}J_{CP}$ 8.0), 130.76, 129.44, 129.11 (d, J_{CP} 2.8), 128.95, 128.84, 128.55, 128.48, 128.01, 127.81, 126.42 (d, J_{CP} 2.5); IR ν (cm^{-1}) 3055, 1497, 1434. TOF MS ES+ m/z: 406.1 $[M+H]^+$, 428.1 $[M+Na]^+$; HRMS calc. $[C_{26}H_{21}N_3P]^+$ 406.1468, obs. 406.1470.

Synthesis of 5-(diisopropylphosphanyl)-1,4-diphenyl-1H-1,2,3-triazole (76b)

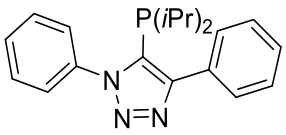

76b

Prepared following *General Procedure 4* on a 0.4 mmol scale. Obtained as a white solid (92 mg, 68%); mp. 120-122 °C;^{1}H NMR (400 MHz, $CDCl_3$) δ 7.69-7.62 (m, 2H), 7.60-7.53 (m, 3H), 7.52-7.41 (m, 5H), 2.04 (sept, *J* 6.8, 2H, PC*H*), 1.01 (dd, *J* 17.2$_{(HP)}$ & 6.8, 6H, CHC*H$_3$*), 0.87 (dd, *J* 13.6$_{(HP)}$ & 6.8, 6H, CHC*H$_3$*); ^{31}P NMR (121 MHz, $CDCl_3$) δ -14.34; ^{13}C NMR (101 MHz, $CDCl_3$) δ 153.23, 137.89, 132.26, 131.75 (d, $^{1}J_{CP}$ 36.9), 129.83, 129.62, 128.96, 128.56, 128.23, 127.50 (d, $^{4}J_{CP}$ 3.1), 24.82 (d, $^{1}J_{CP}$ 9.6), 21.44 (d, J_{CP} 19.1), 21.25 (d, J_{CP} 3.7); IR ν (cm^{-1}) 2952, 2925, 1497, 1465; TOF MS ES+ m/z: 338.2 $[M+H]^+$, 360.2 $[M+Na]^+$; HRMS calc. $[C_{20}H_{25}N_3P]^+$ 338.1781, obs. 338.1787.

Synthesis of 5-(dicyclohexylphosphanyl)-1,4-diphenyl-1H-1,2,3-triazole (76c)

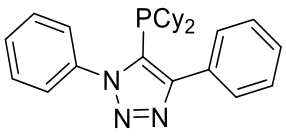

76c

Prepared following *General Procedure 4* on a 0.4 mmol scale. Obtained as a white solid (85 mg, 52%); mp. 168-169 °C; ^{1}H NMR (400 MHz, $CDCl_3$) δ 7.68-7.60 (m, 2H), 7.59-7.53 (m, 3H), 7.52-7.41 (m, 5H), 1.78 (m 2H), 1.68-1.55 (m, 8H), 1.40 (m, 2H), 1.19-0.91 (m, 10H); ^{31}P NMR (121 MHz, $CDCl_3$) δ -25.77; ^{13}C NMR (101 MHz, $CDCl_3$) δ 153.42, 137.94, 132.27, 130.79 (d, $^{1}J_{CP}$ 38.0), 129.80, 129.62 (d, J_{CP} 1.6), 128.93, 128.52, 128.16, 127.40 (d, J_{CP} 3.0), 34.88 (d, J_{CP} 10.0), 31.85 (d, J_{CP} 22.9), 30.69 (d, J_{CP} 8.5), 26.66, 26.56 (d, J_{CP}

= 6.1), 25.92; IR ν (cm^{-1}) 28924, 2849, 1497, 1446; TOF MS ES+ m/z: 418.2 $[M+H]^+$, 440.2 $[M+Na]^+$, 456.2 $[M+K]^+$; HRMS calc. $[C_{26}H_{33}N_3P]^+$ 418.2407, obs. 418.2409.

Synthesis of 4-cyclohexyl-5-(diphenylphosphanyl)-1-phenyl-1H-1,2,3-triazole (76d)

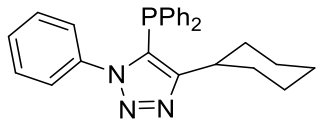

76d

Prepared following *General Procedure 4* on a 0.2 mmol scale. Obtained as a white solid (22 mg, 27%); mp. 130-132 °C; ^{1}H NMR (400 MHz, $CDCl_3$) δ 7.51-7.03 (m, 15H), 1.98 (tt, *J* 11.8 & 3.3, 1H, CH_2CHCH_2), 1.75-1.47 (m, 4H), 1.43-1.08 (m, 4H), 0.82 (m, 2H); ^{31}P NMR (121 MHz, $CDCl_3$) δ -34.81 (t, *J* 7.0); ^{13}C NMR (101 MHz, $CDCl_3$) δ 158.73, 137.30, 133.12 (d, $^1J_{CP}$ 7.0), 132.83 (d, $^2J_{CP}$ 19.8), 129.41, 129.19, 128.88, 128.76 (d, $^3J_{CP}$ 6.9), 127.83 (d, $^1J_{CP}$ 20.7), 126.38 (d, J_{CP} 3.9), 35.13, 32.60, 26.43, 25.72; IR ν (cm^{-1}) 2924, 22852, 1497, 1434; TOF MS ES+ m/z: 412.2 $[M+H]^+$, 434.2 $[M+Na]^+$; HRMS calc. $[C_{26}H_{27}N_3P]^+$ 412.1937, obs. 412.1952.

Synthesis of 5-(diphenylphosphanyl)-4-phenyl-1-(p-tolyl)-1H-1,2,3-triazole (76e)

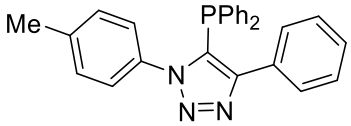

76e

Prepared following *General Procedure 4* on a 0.2 mmol scale. Obtained as a white solid (53 mg, 63%); mp. 178-179 °C; ^{1}H NMR (400 MHz, $CDCl_3$) δ 7.41-7.38 (m, 2H), 7.25-7.11 (m, 13H), 7.05 (s, 4H, Ar*H*), 2.34 (s, 3H, C*H*$_3$); ^{31}P NMR (121 MHz, $CDCl_3$) δ -30.34; ^{13}C NMR (101 MHz, $CDCl_3$) δ 154.10 (d, J_{CP} 8.9), 139.63, 134.81, 132.66 (d, $^2J_{CP}$ 19.6), 132.50,

130.84, 129.42, 129.11, 129.09, 128.87, 128.46 (d, $^{3}J_{CP}$ 6.9), 127.94, 127.76, 126.18 (d, J_{CP} 2.5), 21.19; IR ν (cm^{-1}) 3052, 1513, 1467, 1434; TOF MS ES+ m/z: 420.2 $[M+H]^{+}$; HRMS calc. $[C_{27}H_{23}N_3P]^{+}$ 420.1624, obs. 420.1634.

Synthesis of 5-(diphenylphosphanyl)-1-(4-methoxyphenyl)-4-phenyl-1H-1,2,3-triazole (76f)

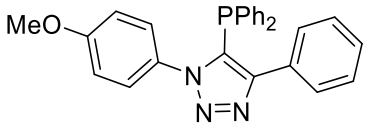

76f

Prepared following *General Procedure 4* on a 0.2 mmol scale. Obtained as a white solid (36 mg, 42%); m.p. 172-173 °C; ^{1}H NMR (300 MHz, $CDCl_3$) δ 7.49-7.37 (m, 2H), 7.30-7.09 (m, 13H), 7.06 (d, *J* 9.0, 2H), 6.72 (d, *J* 9.0, 2H), 3.79 (s, 3H, OC*H*$_3$) ; ^{31}P NMR (121 MHz, $CDCl_3$) δ -30.41; ^{13}C NMR (101 MHz, $CDCl_3$) δ 160.24, 154.08 (d, J_{CP} 10.2), 132.64 (d, $^{2}J_{CP}$ 19.7), 132.58, 132.52, 130.83, 130.25, 129.07 (d, J_{CP} 3.0), 128.91, 128.49 (d, $^{3}J_{CP}$ 6.9), 127.95, 127.79, 127.69 (d, J_{CP} 2.3), 113.98, 55.53; IR ν (cm^{-1}) 3063, 1513, 1467, 1434, 1412; TOF MS ES+ m/z: 436.2 $[M+H]^{+}$; HRMS calc. $[C_{27}H_{23}N_3OP]^{+}$ 436.1573, obs. 436.1578.

Synthesis of 1-([1,1'-biphenyl]-2-yl)-5-(diphenylphosphanyl)-4-phenyl-1H-1,2,3-triazole (76g)

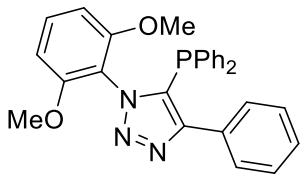

76g

Prepared following *General Procedure 4* on a 0.2 mmol scale. Obtained as a white solid (90 mg, 97%); m.p. 152-154 °C; ^{1}H NMR (400 MHz, $CDCl_3$) δ 7.52-7.43 (m, 2H), 7.30-7.09 (m, 14H), 6.40 (d, *J* 8.5, 2H, COC*H*CHC*H*CO), 3.55 (s, 6H, OC*H*$_3$); ^{31}P NMR (121 MHz, $CDCl_3$) δ -29.90; ^{13}C NMR (101 MHz, $CDCl_3$) δ 156.30, 152.48 (d, $^{2}J_{CP}$ 8.7), 132.99 (d, $^{2}J_{CP}$ 20.1), 132.72 (d, $^{1}J_{CP}$ 7.8), 131.54, 131.20, 129.91 (d, $^{1}J_{CP}$ 28.3), 128.91 (d, J_{CP} 3.1), 128.59, 127.96 (d, $^{3}J_{CP}$ 6.9), 127.67, 127.63, 115.08, 103.68, 55.47; IR ν (cm^{-1}) 2938, 1481, 1433; TOF MS ES+ m/z: 466.17 $[M+H]^+$; HRMS calc. $[C_{28}H_{25}N_3O_2P]^+$ 466.1679, obs. 466.1680.

Synthesis of 4-cyclohexyl-1-(2,6-dimethoxyphenyl)-5-(diphenylphosphanyl)-1H-1,2,3-triazole (76h)

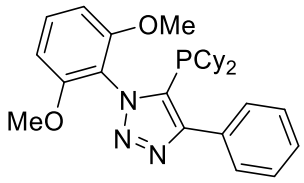

76h

Prepared following *General Procedure 4* on a 0.2 mmol scale. Obtained as a white solid (78 mg, 94%); m.p. 178-180 °C; ^{1}H NMR (400 MHz, $CDCl_3$) δ 7.60-7.56 (m ,2H), 7.48-7.41 (m, 4H), 6.67 (d, *J* 8.5, 2H, COC*H*CHC*H*CO), 3.75 (s, 6H, OC*H*$_3$), 1.86-1.75 (m, 2H), 1.66-1.47 (m, 10H), 1.12-0.98 (m,10H); ^{31}P NMR (121 MHz, $CDCl_3$) δ -23.14; ^{13}C NMR (101 MHz, $CDCl_3$) δ 156.32, 151.29 (d, $^{2}J_{CP}$ 4.9), 133.08, 132.80 (d, $^{1}J_{CP}$ 27.40), 131.55, 129.74, 128.27, 128.01, 115.47, 103.83, 55.61, 34.38 (d, *J* 9.1), 31.64 (d, *J* 21.6), 30.39 (d, *J* 9.4), 26.88, 26.77 (d, *J* 6.5), 26.16; IR ν (cm^{-1}) 2924, 2848, 1600, 1482, 1446, 1302,

1262, 1114; TOF MS ES+ m/z: 478.3 $[M+H]^+$; HRMS calc. $[C_{28}H_{37}N_3O_2P]^+$ 478.2618, obs. 478.2626.

Synthesis of 4-cyclohexyl-1-(2,6-dimethoxyphenyl)-5-(diphenylphosphanyl)-1H-1,2,3-triazole (76i)

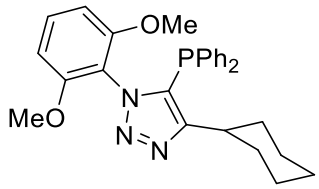

76i

Prepared following *General Procedure 4* on a 0.2 mmol scale. Obtained as a white solid (39 mg, 42%); m.p. 156-158 °C; ^{1}H NMR (400 MHz, $CDCl_3$) δ 7.38-7.21 (m, 11H), 6.56 (d, *J* 8.5, 2H, C*H*CHC*H*), 3.56 (s, 6H, OC*H*$_3$), 2.05 (tt, *J* 11.8 & 3.3, 1H, CH_2CHCH_2), 1.73-1.46 (m, 5H), 1.40-1.10 (m, 2H), 0.82 (m, 2H); ^{31}P NMR (121 MHz, $CDCl_3$) δ -35.85. ^{13}C NMR (101 MHz, $CDCl_3$) δ 157.23, 156.49, 133.69 (d, $^1J_{CP}$ 6.9), 132.60 (d, $^2J_{CP}$ 19.3), 131.43, 129.60 (d, $^1J_{CP}$ 12.2), 128.60, 128.29 (d, $^3J_{CP}$ 6.8), 115.20, 103.91, 55.62, 35.37, 32.39, 26.51, 25.77; IR ν (cm^{-1}) 2928, 2849, 1599, 1481; TOF MS ES+ m/z: 472.2 $[M+H]^+$, 494.2 $[M+Na]^+$; HRMS calc. $[C_{28}H_{31}N_3O_2P]^+$ 472.2148, obs. 472.2156.

Synthesis of 1-([1,1'-biphenyl]-2-yl)-5-(diphenylphosphanyl)-4-phenyl-1H-1,2,3-triazole (76j)

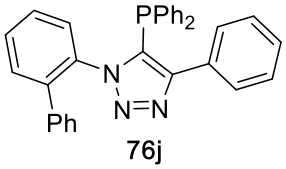

76j

Prepared following *General Procedure 4* on a 0.15 mmol scale. Obtained as a white solid (65 mg, 68%); mp. 208-210 °C; ^{1}H NMR (400 MHz, $CDCl_3$) δ 7.60-7.49 (m, 2H), 7.34 (td, *J* 7.9, 1.9, 1H), 7.31-7.13 (m, 9H), 7.13-6.74 (m, 10H), 6.45 (s, br, 2H); ^{31}P{^{1}H} NMR (121 MHz, $CDCl_3$) δ -31.23; ^{31}P NMR (121 MHz, $CDCl_3$) δ -31.23 (br pent, *J* 7.7); ^{13}C NMR (101 MHz, $CDCl_3$) δ 152.63, 140.01, 137.72, 134.90, 132.66 (br), 131.99 (br), 130.93, 130.84, 130.69, 130.64, 129.05, 128.97, 128.72, 128.42, 128.01, 127.71, 127.59, 127.41 [overlapping signals resulted in observed broadening of some peaks]; IR ν (cm^{-1}) 3054, 1481, 1435; TOF MS ES+ m/z: 482.6 $[M+H]^+$; HRMS calc. $[C_{32}H_{25}N_3P]^+$ 482.1781, obs. 482.1783.

Synthesis of 1-([1,1'-biphenyl]-2-yl)-5-(dicyclohexylphosphanyl)-4-phenyl-1H-1,2,3-triazole (76k)

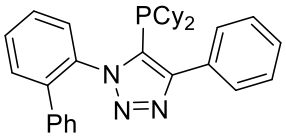

76k

Prepared following *General Procedure 4* on a 0.2 mmol scale. Obtained as a white solid (90 mg, 91%); mp. 140-142 °C; ^{1}H NMR (400 MHz, $CDCl_3$) δ 7.66-7.55 (m, 2H), 7.51 (td, *J* 7.5 & 1.7, 1H), 7.43-7.35 (m, 6H), 7.28-7.19 (m, 5H), 1.84-1.21 (m, 11H), 1.21-0.66 (m, 11H); ^{31}P{^{1}H} NMR (121 MHz, $CDCl_3$) δ -24.64; ^{31}P NMR (121 MHz, $CDCl_3$) δ -24.87 to -24.36 (br s, ^{3}J coupling not discernible); ^{13}C NMR (101 MHz, $CDCl_3$) δ 151.61 (d, $^{2}J_{CP}$ 7.4), 139.90, 138.02, 135.27, 132.60, 132.33, 130.97, 130.50, 129.70, 129.57, 129.26, 128.49, 128.42, 128.03, 127.65, 127.56, 31.57, 26.69 (d, J_{CP} 13.5), 25.85, 22.64, 14.10 [overlapping signals resulted in observed broadening of some peaks]; IR ν (cm^{-1}) 2923,

2849, 1483, 1444; TOF MS ES+ m/z: 494.3 $[M+H]^+$, 517.26 $[M+Na]^+$, 595.40 $[M+C_6H_{15}N]^+$; HRMS calc. $[C_{32}H_{37}N_3P]^+$ 494.2720, obs. 494.2719.

Synthesis of 5-(diphenylphosphanyl)-1-(naphthalen-1-yl)-4-phenyl-1H-1,2,3-triazole (76l)

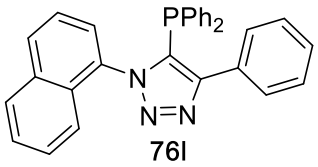

76l

Prepared following *General Procedure 4* on a 0.2 mmol scale. Obtained as a white solid (37 mg, 42%); mp. 140-141 °C; ^{1}H NMR (400 MHz, $CDCl_3$) δ 7.81 (dd, *J* 7.4, 1.9, 1H), 7.73 (d, *J* 8.2, 1H), 7.70-7.61 (m, 2H), 7.42 (ddd, *J* 8.2, 6.8 & 1.2, 1H), 7.37-6.65 (m, 17H); ^{31}P{^{1}H} NMR (121 MHz, $CDCl_3$) δ -31.07; ^{31}P NMR (121 MHz, $CDCl_3$) δ -30.87 to -31.28 (app br s, ^3J coupling not discernible); ^{13}C NMR (101 MHz, $CDCl_3$) δ 153.90 (d, $^2J_{CP}$ 14.7), 133.84, 133.76, 132.56 (br), 130.79, 130.62, 130.44, 130.11, 130.06, 129.05 (d, J_{CP} 4.1), 128.65, 128.19, 128.05, 127.70, 127.28, 126.67, 125.57, 124.29, 122.76 [overlapping signals resulted in observed broadening of some peaks]; IR ν (cm^{-1}) 3053, 1467, 1434, 1412; TOF MS ES+ m/z: 456.2 $[M+H]^+$; HRMS calc. $[C_{30}H_{23}N_3P]^+$ 456.1624, obs. 456.1631.

Synthesis of 4-cyclohexyl-5-(diphenylphosphanyl)-1-(naphthalen-1-yl)-1H-1,2,3-triazole (76m)

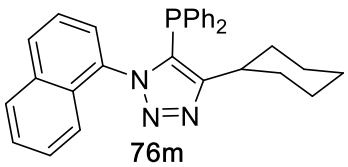

76m

Prepared following *General Procedure 4* on a 1.3 mmol scale. Obtained as an off-white solid (540 mg, 91%); mp. 200-202 °C; ^{1}H NMR (300 MHz, $CDCl_3$) δ 7.94 (d, *J* 8.3, 1H), 7.86 (d, *J* 8.6, 1H), 7.49 (ddd, *J* 8.2, 6.9 & 1.2, 1H), 7.43-7.35 (m, 2H), 7.32-7.23 (m, 7H), 7.18 (td, *J* 8.0, 1.6, 4H), 7.07 (d, *J* 8.4, 1H), 2.18 (tt, *J* 11.9 & 3.4, 1H, CH_2CHCH_2), 1.89-1.43 (m, 7H), 1.34-1.16 (m, 1H), 1.06-0.74 (m, 2H); ^{31}P{^{1}H} NMR (121 MHz, $CDCl_3$) δ -35.93; ^{31}P NMR (121 MHz, $CDCl_3$) δ -35.93 (br pent, *J* 7.4); ^{13}C NMR (101 MHz, $CDCl_3$) δ 158.29, 133.89, 133.78, 132.68 (d, $^{2}J_{CP}$ 20.0), 130.52, 130.42, 130.05 (d, $^{1}J_{CP}$ 21.4), 129.00, 128.53 (d, $^{3}J_{CP}$ 6.9), 127.93, 127.47, 126.78, 125.79 (d, J_{CP} 3.1), 124.50, 122.64, 35.28, 32.73, 26.50, 25.76 [overlapping signals resulted in observed broadening of some peaks]; IR ν (cm^{-1}) 2925, 2850, 1434, 1413; TOF MS ES+ m/z: 462.2 $[M+H]^+$, 484.2 $[M+Na]^+$; HRMS calc. $[C_{30}H_{29}N_3P]^+$ 462.2094, obs. 462.2100.

1-(2-bromophenyl)-4-phenyl-1H-1,2,3-triazole (87a)

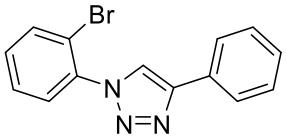

87a

Prepared following *General Procedure 2* on a 3.3 mmol azide scale. Isolated as a yellow solid (730 mg, 73%); ^{1}H NMR (400 MHz, $CDCl_3$) δ 8.17 (s, 1H), 7.96 – 7.88 (m, 2H), 7.78 (d, *J* 8.0, 1H), 7.61 (d, *J* 8.0, 1H), 7.56 – 7.33 (m, 5H); ^{13}C NMR (101 MHz, $CDCl_3$) δ 147.55[-], 136.61[-], 133.96[+], 131.20[+], 130.22[-], 128.93[+], 128.55[+], 128.42[+], 128.22[+], 125.91[+], 125.89[+], 121.66[+], 118.59[+]; IR ν (cm^{-1}) 3052, 1589, 1452, 1266; TOF MS ES+ m/z: 300.2 $[M+H]^+$.

4-(2-bromophenyl)-1-phenyl-1H-1,2,3-triazole (87b)

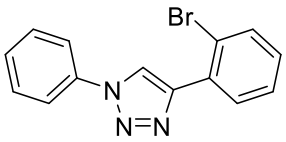

87b

Prepared following *General Procedure 2* on a 1.0 mmol azide scale. Isolated as a yellow solid (148 mg, 55%); ^{1}H NMR (400 MHz, $CDCl_3$) δ 8.66 (s, 1H), 8.19 (d, *J* 7.8, 1H), 7.84 – 7.76 (m, 2H), 7.67 (d, *J* 8.1, , 1H), 7.60 – 7.49 (m, 2H), 7.51 – 7.39 (m, 2H), 7.22 (d, *J* 8.0, 1H); ^{13}C NMR (101 MHz $CDCl_3$) δ 145.95[-], 137.01[-], 133.63[+], 130.96[-], 130.78[+], 129.80[+], 129.57[+], 128.85[+], 127.78[+], 121.26[+], 121.04[+], 120.68[+]; IR ν (cm^{-1}) 3050, 1594, 1472; TOF MS ES+ m/z: 300.2 $[M+H]^+$.

2,2',6-Trimethyl-1,1'-biphenyl (90)

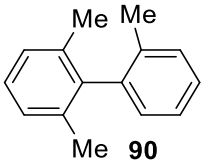

90

Product of catalysed reaction, see *General Procedure 7* for analysis protocol, data collected are consistent with that reported in the literature[213]:

Isolated from **Table *2***, entry 7. Colourless oil. ^{1}H NMR (400MHz, CDCl3) δ 7.30-7.21 (m, 3H), 7.19-7.14 (m, 1H), 7.13-7.08 (m, 2H), 7.03-7.00 (m, 1H), 1.97 (s,3H, CH_3), 1.94 (s, 6H, 2 × CH_3). ^{13}C NMR (101MHz, $CDCl_3$) δ 141.10 [-], 140.55 [-], 135.88 [-], 135.63 [-], 129.98 [+], 128.85 [+], 127.22 [+], 127.00 [+], 126.92 [+], 126.05 [+], 20.35 [+], 19.42 [+]. TOF MS EI+ m/z: 196.1 $[M]^+$, 181.1 $[M-CH_3]^+$.

Synthesis of 1-phenyl-1H-1,2,3-triazole (92a)

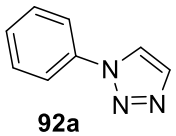

92a

Prepared following *General Procedure 3* on a 1.0 mmol scale of azide.[61] Obtained as a light yellow solid (104 mg, 71%); ^{1}H NMR (300 MHz, $CDCl_3$) δ 8.01 (d, *J* 1.1, 1H, Trz*H*), 7.86 (d, *J* 1.2, 1H, Trz*H*), 7.79-7.71 (m, 2H), 7.59-7.50 (m, 2H), 7.50-7.39 (m, 1H); ^{13}C NMR (101 MHz, $CDCl_3$) δ 137.08 [-], 134.47 [+], 129.77 [+], 128.77 [+], 121.71 [+], 120.69 [+]; IR ν (cm^{-1}) 3146, 3139, 1503, 1463; TOF MS EI+ m/z: 145.1 $[M]^+$, 117.1 $[M-2N]^+$.

Synthesis of 1-(p-tolyl)-1H-1,2,3-triazole (92b)

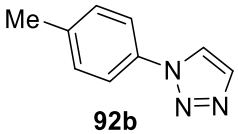

92b

Prepared following *General Procedure 3* on a 1.0 mmol scale of azide.[61] Isolated as a brown solid (134 mg, 84%); ^{1}H NMR (300 MHz, $CDCl_3$) δ 7.96 (d, *J* 1.1, 1H, Trz*H*), 7.83 (d, *J* 1.1, 1H, Trz*H*), 7.62 (d, *J* 8.5, 2H, Ar*H*), 7.29 (d, *J* 8.5, 2H, Ar*H*), 2.43 (s, 3H, CH_3). ^{13}CNMR (101 MHz, $CDCl_3$) δ 138.88 [-], 134.77 [-], 134.32 [+], 130.25 [+], 121.68 [+], 120.59 [+], 21.08 [+]; IR ν (cm^{-1}) 3132,1520; TOF MS EI+ m/z: 159.1 $[M]^+$, 131.1 $[M-2N]^+$.

Synthesis of 1-(4-methoxyphenyl)-1H-1,2,3-triazole (92c)

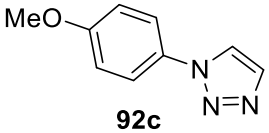

92c

Prepared following *General Procedure 3* on a 1.0 mmol scale of azide.[214] Isolated as a light yellow solid (149 mg, 85%) ^{1}H NMR (400 MHz, $CDCl_3$) δ 7.92 (d, *J* 1.1, 1H, Trz*H*), 7.82 (d, *J* 1.1, 1H, Trz*H*), 7.64 (d, *J* 9.0, 2H, Ar*H*), 7.03 (d, *J* 9.0, 2H, Ar*H*), 3.87 (s, 3H, OC*H*$_3$); ^{13}C NMR (101 MHz, $CDCl_3$) δ 159.83 [-], 134.26 [+], 130.52 [-], 122.31 [+], 121.85 [+], 114.78 [+], 55.62 [+]; IR ν (cm^{-1}) 3142, 1518; TOF MS EI+ m/z: 175.0 $[M]^+$.

Synthesis of 1-(2,6-dimethoxyphenyl)-1H-1,2,3-triazole (92d)

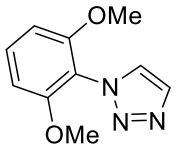

92d

Prepared following *General Procedure 3* on a 1.0 mmol scale of azide. Obtained as an off-white solid (132 mg, 64%); mp. 105-108 °C; ^{1}H NMR (400 MHz, $CDCl_3$) δ 7.84 (d, *J* 1.1, 1H, Trz*H*), 7.66 (d, *J* 1.1, 1H, Trz*H*), 7.41 (t, *J* 8.5, 1H, CHC*H*CH), 6.68 (d, *J* 8.5, 2H, C*H*CHC*H*), 3.76 (s, 6H, OC*H*$_3$). ^{13}C NMR (101 MHz, $CDCl_3$) δ 155.93 [-], 132.82 [+], 131.32 [+], 126.80 [+], 115.28 [-], 104.32 [+], 56.19 [+]; IR ν (cm^{-1}) 1589, 1483; TOF MS EI+ m/z: 205.0 $[M]^+$; HRMS calc. $[C_{10}H_{11}N_3O_2]^+$ 205.0846, obs. 205.0850.

Synthesis of 1-([1,1'-biphenyl]-2-yl)-1H-1,2,3-triazole (92e)

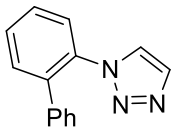

92e

Prepared following *General Procedure 3* on a 1.0 mmol scale of azide. Obtained as an off-white solid (60 mg, 28%); ^{1}H NMR (400 MHz, $CDCl_3$) δ 7.67-7.61 (m, 1H), 7.61-7.50 (m, 4H), 7.32-7.25 (m, 3H), 7.21 (d, *J* 1.1, 1H, Trz*H*), 7.11-7.05 (m, 2H); ^{13}C NMR (101

MHz, $CDCl_3$) δ 137.34 [-], 137.12 [-], 135.07 [-], 133.47 [+], 131.12 [+], 129.86 [+], 128.67 [+], 128.57 [+], 128.48 [+], 127.93 [+], 126.65 [+], 125.68 [+]; IR ν (cm^{-1}) 1487, 1444; TOF MS AP+ m/z: 222.1 $[M]^+$.

Synthesis of 1-(naphthalen-1-yl)-1H-1,2,3-triazole (92f)

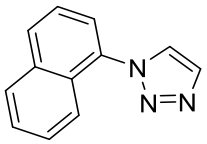

92f

Prepared following *General Procedure 3* on a 1.0 mmol scale of azide.[61] Obtained as a brown solid (78 mg, 40%); ^1H NMR (400 MHz, $CDCl_3$) δ 8.04-7.99 (m, 1H), 7.98-7.92 (m, 3H), 7.61-7.49 (m, 5H). ^{13}C NMR (101 MHz, $CDCl_3$) δ 134.16 [-], 133.74 [+], 130.41 [+], 128.65 [-], 128.30 [+], 127.90 [+], 127.09 [+], 126.25 [+], 125.00 [+], 123.61 [+], 122.28 [+] (11 of 12 expected signals observed, as judged by the J-MOD spectra an expected [-] C_{quat} signal is not observed); IR ν (cm^{-1}) 3132. 3060, 1597, 1513; TOF MS EI+ m/z: 195.0 $[M]^+$.

Synthesis of 1-(4-(trifluoromethyl)phenyl)-1H-1,2,3-triazole (92g)

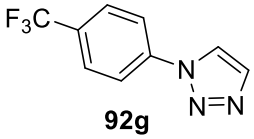

92g

Prepared following *General Procedure 3* on a 1.0 mmol scale of azide. Isolated as an off white solid (154 mg, 72%); ^1H NMR (400 MHz, $CDCl_3$) δ 8.07 (d, *J* 1.2, 1H, Trz*H*), 7.92 (d, *J* 8.4, 2H, Ar*H*), 7.90 (d, *J* 1.2, 1H, Trz*H*), 7.82(d, *J* 8.4, 2H, Ar*H*); ^{13}C NMR (126 MHz, $CDCl_3$) δ 139.45 [u], 134.94 [+], 130.81 (q, $^2J_{CF}$ 33.2), 127.16 (q, $^3J_{CF}$ 3.7) [+], 123.54 (q, $^1J_{CF}$

272.3), 121.61 [+], 120.60 [+]; ^{19}F NMR (282 MHz, $CDCl_3$) δ -62.64; IR ν (cm^{-1}) 3157, 3124, 1617, 1324; TOF MS EI+ m/z: 213.1 $[M]^+$.

Synthesis of 1-(3,5-dimethoxyphenyl)-1H-1,2,3-triazole (92h)

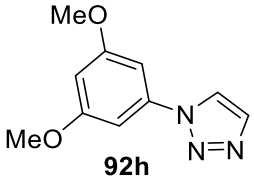

92h

Prepared following *General Procedure 3* on a 1.0 mmol scale of azide. Isolated as an off white solid (174 mg, 85%); mp. 89-91 °C; ^{1}H NMR (400 MHz, $CDCl_3$) δ 7.97 (d, *J* 1.1, 1H, Trz*H*), 7.83 (d, *J* 1.1, 1H, Trz*H*), 6.91 (d, *J* 2.2, 2H, C*H*CNC*H*), 6.51 (t, *J* 2.2, 1H, MeOC*C*(H)COMe), 3.86 (s, 6H, OC*H*$_3$); ^{13}C NMR (101 MHz, $CDCl_3$) δ 161.53 [-], 138.54 [-], 134.35 [+], 121.80 [+], 100.51 [+], 99.11 [+], 55.72 [+]; IR ν (cm^{-1}) 1599, 1475; TOF MS ES+ m/z: 206.1 $[M+H]^+$, 228.1 $[M+Na]^+$; HRMS calc. $[C_{10}H_{12}N_3O_2]^+$ 206.0924, obs. 206.0929.

Synthesis of 1-(2,6-diisopropylphenyl)-1H-1,2,3-triazole (92i)

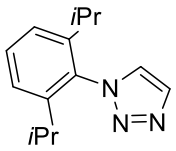

92i

Prepared following *General Procedure 3* on a 5.0 mmol scale of azide.[214] Isolated as a white solid (470 mg, 40%); mp. 112-114 °C ; ^{1}H NMR (400 MHz, $CDCl_3$) δ 7.90 (d, *J* 1.0, 1H, Trz*H*), 7.66 (d, *J* 1.0, 1H, Trz*H*), 7.50 (t, *J* 7.8, 1H, CHC*H*CH), 7.29 (d, *J* 7.8, 2H, C*H*CHC*H*), 2.19 (sept, *J* 6.9, 2H, C*H*$(CH_3)_2$), 1.15 (d, *J* 6.8, 6H, C*H*$_3$), 1.11 (d, *J* 6.9, 6H, C*H*$_3$); ^{13}C NMR (101 MHz, $CDCl_3$) δ 146.15 [-], 133.42 [+], 133.15 [u], 130.75 [+], 126.44 [+],

123.80 [+], 28.32 [+], 24.07 [+]; IR ν (cm^{-1}) 3102, 2964, 1466; TOF MS ES+ m/z: 230.2 $[M+H]^+$, 252.1 $[M+Na]^+$; HRMS calc.$[C_{14}H_{20}N_3]^+$ 230.1652, obs. 230.1658.

Synthesis of 5-(diphenylphosphanyl)-1-phenyl-1H-1,2,3-triazole (93a)

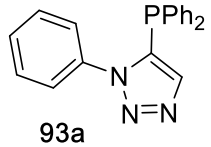

93a

Prepared following *General Procedure 4* on a 0.2 mmol scale. Obtained as a white solid (31 mg, 47%); mp. 112-115 °C; ^{1}H NMR (400 MHz, $CDCl_3$) δ 7.47-7.27 (m, 16H); ^{31}P NMR (121 MHz, $CDCl_3$) δ -35.46; ^{13}C NMR (101 MHz, $CDCl_3$) δ 140.63, 136.91, 135.89 (d, 20.2), 133.74 (d, 7.1), 133.54 (d, $^2J_{CP}$ 21.0), 129.83, 129.45, 129.16, 128.94 (d, $^3J_{CP}$ 7.7), 125.11 (d, $^4J_{CP}$ 4.5); IR ν (cm^{-1}) 3052, 1596, 1498, 1434; TOF MS EI+ m/z: 329.2 $[M]^+$, 301.2 $[M-2N]^+$; HRMS calc. $[C_{20}H_{16}N_3P]^+$ 329.1076, obs. 329.1091.

Synthesis of 5-(dicyclohexylphosphanyl)-1-phenyl-1H-1,2,3-triazole (93b)

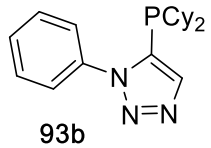

93b

Prepared following *General Procedure 4* on a 0.4 mmol scale. Obtained as a white solid (100 mg, 73%); mp. 110-111 °C; ^{1}H NMR (400 MHz, $CDCl_3$) δ 7.86 (s, 1H, Trz*H*), 7.54-7.48 (app br s, 5H, Ar*H*), 1.87 (tt, *J* 11.9 & 3.1, 2H, CH_2CHCH_2), 1.78-1.56 (m, 10H, Cy*H*), 1.32-1.02 (m, 8H, Cy*H*), 0.94 (m, 2H, Cy*H*); ^{31}P NMR (121 MHz, $CDCl_3$) δ -30.22; ^{13}C NMR (101 MHz, $CDCl_3$) δ 138.82 (d, $^2J_{CP}$ 5.3), 137.30, 134.07 (d, $^1J_{CP}$ 29.7), 129.40, 128.91, 126.65 (d, $^4J_{CP}$ 5.0), 33.55 (d, $^1J_{CP}$ 10.2), 29.99 (d, J_{CP} 15.9), 28.96 (d, J_{CP} 6.9), 26.97 (d,

J_{CP} 12.8), 26.78 (d, J_{CP} 7.7), 26.15; IR ν (cm^{-1}) 2923, 2849, 1497, 1447; TOF MS ES+ m/z: 342.2 $[M+H]^+$, 364.2 $[M+Na]^+$, 380.2 $[M+K]^+$; HRMS calc. $[C_{20}H_{29}N_3P]^+$ 342.2094, obs. 342.2101.

Synthesis of 5-(diphenylphosphanyl)-1-(p-tolyl)-1H-1,2,3-triazole (93c)

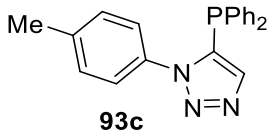

93c

Prepared following *General Procedure 4* on a 0.2 mmol scale. Obtained as a white solid (25 mg, 36%); mp. 136-138 °C; ^1H NMR (400 MHz, $CDCl_3$) δ 7.45-7.28 (m, 13H), 7.20 (d, *J* 8.2, 2H), 2.38 (s, 3H, C*H*$_3$). ^{31}P NMR (121 MHz, $CDCl_3$) -35.89; ^{13}C NMR (101 MHz, $CDCl_3$) δ 140.57, 139.62, 135.73 (d, $^1J_{CP}$ 18.8), 134.43, 133.91 (d, $^1J_{CP}$ 6.7), 133.51 (d, $^2J_{CP}$ 20.8), 132.67, 129.73 (d, $^4J_{CP}$ 4.1), 128.90 (d, $^3J_{CP}$ 7.6), 124.93 (d, $^4J_{CP}$ 4.0), 21.20; IR ν (cm^{-1}) 2947, 1726, 1435; TOF MS ES+ m/z: 344.1 $[M+H]^+$, 366.1 $[M+Na]^+$, 382.1 $[M+K]^+$; HRMS calc. $[C_{21}H_{19}N_3P]^+$ 344.1311, obs. 344.1320.

Synthesis of 5-(diphenylphosphanyl)-1-(4-methoxyphenyl)-1H-1,2,3-triazole (93d)

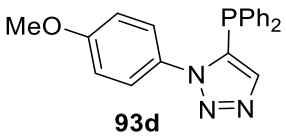

93d

Prepared following *General Procedure 4* on a 0.2 mmol scale. Obtained as a white solid (35 mg, 49%); mp. 112-114 °C; ^1H NMR (400 MHz, $CDCl_3$) δ 7.42-7.27 (m, 13H), 6.89 (d, *J* 9.0, 2H), 3.82 (s, 3H, OC*H*$_3$); ^{31}P NMR (121 MHz, $CDCl_3$) δ -35.88; ^{13}C NMR (101 MHz, $CDCl_3$) δ 160.25, 140.37, 135.97 (d, $^1J_{CP}$ 18.6), 133.87 (d, $^1J_{CP}$ 6.7), 133.52 (d, $^2J_{CP}$ 20.8), 129.78, 129.87, 128.91 (d, $^3J_{CP}$ 7.7), 126.55 (d, $^4J_{CP}$ 3.8), 114.24, 55.53; IR ν (cm^{-1}) 1514,

1434; TOF MS ES+ m/z: 382.4 $[M+Na]^+$; HRMS calc. $[C_{21}H_{18}N_3OPNa]^+$ 382.1080, obs. 382.1078.

Synthesis of 1-(2,6-dimethoxyphenyl)-5-(diphenylphosphanyl)-1H-1,2,3-triazole (93e)

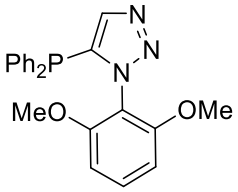

93e

Prepared following *General Procedure 4* on a 0.2 mmol scale. Obtained as a white (63 mg, 82%); mp. 136-138 °C; ^{1}H NMR (400 MHz, $CDCl_3$) δ 7.48 (d, *J* 0.7, 1H, Trz*H*), 7.40-7.27 (m, 11H), 6.55 (d, *J* 8.5, 2H, C*H*CHC*H*), 3.53 (s, 6H, OC*H*$_3$); ^{31}P NMR (122 MHz, $CDCl_3$) δ -36.36; ^{13}C NMR (126 MHz, $CDCl_3$) δ 156.22, 139.17, 137.82 (d, $^1J_{CP}$ 13.2), 134.44 (d, $^1J_{CP}$ 6.7), 133.42 (d, $^2J_{CP}$ 20.7), 131.74, 129.21, 128.46 (d, $^3J_{CP}$ 7.5), 114.20, 103.92, 55.65; IR ν (cm^{-1}) 2921, 1600, 1482. 1261; TOF MS ES+ m/z: 390.1 $[M+H]^+$, 412.1 $[M+Na]^+$; HRMS calc. $[C_{22}H_{21}N_3O_2P]^+$ 390.1366, obs. 390.1370.

Synthesis of 5-(diisopropylphosphanyl)-1-(2,6-dimethoxyphenyl)-1H-1,2,3-triazole (93f)

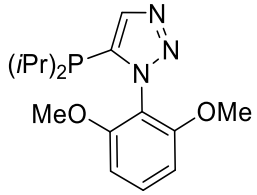

93f

Prepared following *General Procedure 4* on a 0.2 mmol scale. Obtained as a white solid (57 mg, 88%); mp. 113-115 °C; ^{1}H NMR (400 MHz, $CDCl_3$) δ 7.85 (s, 1H, Trz*H*), 7.44 (t, *J*

8.5, 1H, CHC*H*CH), 6.66 (d, *J* 8.5, 2H, C*H*CHC*H*), 3.71 (s, 6H, OCH_3), 2.04 (sept, *J* 7.0, 2H, PC*H*), 1.07-0.88 (m, 12H,2 × CH(CH_3)$_2$). ^{31}P NMR (121 MHz, $CDCl_3$) δ -20.89 (m). ^{13}C NMR (126 MHz, $CDCl_3$) δ 156.12, 137.61 (d, $^2J_{CP}$ 5.8), 135.83 (d, $^1J_{CP}$ 21.5), 131.64, 114.84, 103.85, 55.59, 23.69 (d, $^1J_{CP}$ 8.7), 19.41 (d, J_{CP} 18.2), 18.70 (d, J_{CP} 7.8); IR ν (cm^{-1}) 2951, 1599, 1482, 1461; TOF MS ES+ m/z: 322.2 $[M+H]^+$; HRMS calc. $[C_{16}H_{25}N_3O_2P]^+$ 322.1679 obs. 322.1682.

Synthesis of 5-(dicyclohexylphosphanyl)-1-(2,6-dimethoxyphenyl)-1H-1,2,3-triazole (93g)

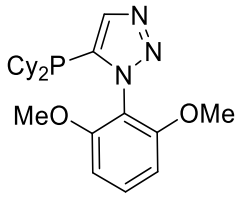

93g

Prepared following *General Procedure 4* on a 0.2 mmol scale. Obtained as a white solid (361 mg, 90%); mp. 116-118 °C; ^{1}H NMR (400 MHz, $CDCl_3$) δ 7.84 (s, 1H, Trz*H*), 7.43 (t, *J* 8.5, 1H, Ar CHC*H*CH), 6.65 (d, *J* 8.5, 2H, Ar C*H*CHC*H*), 3.71 (s, 6H, OCH_3), 1.89-1.54 (m, 12H), 1.35-0.83 (m, 10H); ^{31}P NMR (121 MHz, $CDCl_3$) δ -29.52; ^{13}C NMR (126 MHz, $CDCl_3$) δ 156.14, 137.66 (d, $^2J_{CP}$ 5.8), 135.99 (d, $^1J_{CP}$ 22.4), 131.59, 114.87, 103.82, 55.60, 33.07 (d, $^1J_{CP}$ 9.0), 29.61 (d, J_{CP} 15.8), 28.84 (d, J_{CP} 6.9), 27.13 (d, J_{CP} 12.7), 26.92 (d, J_{CP} 7.7), 26.30; IR ν (cm^{-1}) 2923, 2849, 1600, 1482; TOF MS ES+ m/z: 402.2 $[M+H]^+$; HRMS calc. $[C_{22}H_{33}N_3O_2P]^+$ 402.2305, obs. 402.2308.

Synthesis of 5-(dicyclohexylphosphanyl)-1-(2,6-dimethoxyphenyl)-1H-1,2,3-triazole (93h)

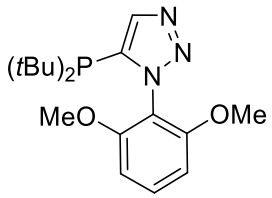

93h

Prepared following *General Procedure 4* on a 1.0 mmol scale. Obtained as a white solid (251 mg, 72%); m.p. 170-173 °C; ^{1}H NMR (300 MHz, $CDCl_3$) δ 8.06 (s, 1H, Trz*H*), 7.43 (t, *J* 8.5, 1H, CHC*H*CH), 6.65 (d, *J* 8.5, 2H, C*H*CHC*H*), 3.68 (s, 6H, OCH_3), 1.15 (d, $^{3}J_{HP}$ 12.4, 18H, CCH_3); ^{31}P {^{1}H}NMR (121 MHz, $CDCl_3$) δ 2.04; ^{31}P NMR (121 MHz, $CDCl_3$) δ 2.04 ; ^{13}C NMR (126 MHz, $CDCl_3$) δ 156.16, 138.11 (d, $^{2}J_{CP}$ 6.2), 136.07 (d, $^{1}J_{CP}$ 27.7), 131.58, 115.09, 103.81, 55.39, 32.34 (d, $^{1}J_{CP}$ 18.2), 30.11 (d, $^{2}J_{CP}$ 14.8); IR ν (cm^{-1}) 2941, 2860, 1596, 1481; TOF MS ES+ m/z: 350.2 $[M+H]^+$, 372.2 $[M+Na]^+$; HRMS calc. $[C_{18}H_{29}N_3O_2P]^+$ 350.1992, obs. 350.1996.

Synthesis of 1-([1,1'-biphenyl]-2-yl)-5-(diphenylphosphanyl)-1H-1,2,3-triazole (93i)

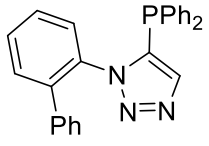

93i

Prepared following *General Procedure 4* on a 0.2 mmol scale. Obtained as a white solid (75 mg, 90%); mp. 94-95 °C; ^{1}H NMR (400 MHz, $CDCl_3$) δ 7.65-7.49 (m, 2H), 7.43-7.11 (m, 14H), 7.04-6.84 (br, 4H); ^{31}P NMR (121 MHz, $CDCl_3$) δ -37.87 (t, *J* 8.0); ^{13}C NMR (101 MHz, $CDCl_3$) δ 139.80, 139.65, 137.75, 137.57, 134.35, 133.97 (d, $^{1}J_{CP}$ 7.6), 132.99 (d,

$^{2}J_{CP}$ 20.7), 130.90, 130.61, 129.27, 128.89, 128.64, 128.57, 128.30, 128.00, 127.62; IR ν (cm^{-1}) 3052, 1728, 1482, 1435; TOF MS ES+ m/z: 406.1 $[M+H]^+$, 428.1 $[M+Na]^+$; HRMS calc. $[C_{26}H_{21}N_3P]^+$ 406.1468, obs. 406.1475.

Synthesis of 5-(diphenylphosphanyl)-1-(naphthalen-1-yl)-1H-1,2,3-triazole (93j)

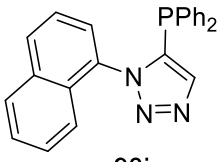

93j

Prepared following *General Procedure 4* on a 0.6 mmol scale. Obtained as a white solid (208 mg, 91%); m.p. 135-136 °C; ^{1}H NMR (300 MHz, $CDCl_3$) δ 7.95 (d, *J* 8.0, 1H), 7.89 (d, *J* 8.0, 1H), 7.57-7.48 (m, 2H), 7.46-7.13 (m, 14H); ^{31}P NMR (121 MHz, $CDCl_3$) δ -36.21; ^{13}C NMR (101 MHz, $CDCl_3$) δ 139.39, 138.54 (d, $^{1}J_{CP}$ 18.4), 133.98, 133.64, 133.59, 133.38, 130.69, 129.77, 129.67, 128.76 (d, $^{3}J_{CP}$ 7.6), 127.99, 127.57, 126.88, 125.41 (d, $^{1}J_{CP}$ 3.0), 124.49, 122.66. IR ν (cm^{-1}) 3054, 1478, 1434; TOF MS ES+ m/z: 380.1 $[M+H]^+$, 402.1 $[M+Na]^+$, 481.3 $[M+H+TEA]^+$, HRMS calc. $[C_{30}H_{34}N_4P]^+$ 481.2516, obs. 481.2522.

Synthesis of 5-(diphenylphosphanyl)-1-(4-(trifluoromethyl)phenyl)-1H-1,2,3-triazole (93k)

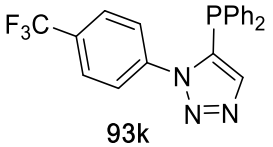

93k

Prepared following *General Procedure 4* on a 0.2 mmol scale. Obtained as a white solid (54 mg, 68%); mp. 105-107 °C; ^{1}H NMR (300 MHz, $CDCl_3$) δ 7.70 (d, *J* 8.7, 2H), 7.60 (d, *J* 8.7, 2H), 7.46-7.29 (m, 11H). ^{19}F NMR (282 MHz, $CDCl_3$) δ -62.70; ^{31}P NMR (121 MHz,

$CDCl_3$) δ -35.08(t, *J* 7.6); 13C NMR (101 MHz, $CDCl_3$) δ 141.07, 139.68, 136.12 (d, $^1J_{CP}$ 22.3), 133.56 (d, $^2J_{CP}$ 20.9), 133.13 (d, $^1J_{CP}$ 6.6), 131.35 (q, $^2J_{CF}$ 34.4), 130.10, 129.10 (d, $^3J_{CP}$ 7.7), 126.44 (q, $^3J_{CF}$ 3.8), 125.16 (d, $^4J_{CP}$ 5.1), 123.50 (q, $^1J_{CF}$ 272.1); IR ν (cm^{-1}) 3055, 1617, 1323; TOF MS ES+ m/z: 398.1 $[M+H]^+$, 420.1 $[M+Na]^+$; HRMS calc. $[C_{21}H_{16}N_3PF_3]^+$ 398.1028, obs. 398.1041.

Synthesis of 1-(3,5-dimethoxyphenyl)-5-(diphenylphosphanyl)-1H-1,2,3-triazole (93l)

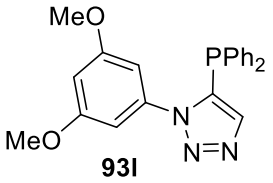

93l

Prepared following *General Procedure 4* on a 0.2 mmol scale. Obtained as a white solid (56 mg, 72%); mp 145-147 °C; ^{1}H NMR (300 MHz, $CDCl_3$) δ 7.47-7.29 (m, 10H), 7.25 (d, *J* 0.9, 1H, Trz*H*), 6.57-6.53 (m, 2H), 6.49 (t, *J* 2.3, 1H, Ar MeOCC*H*COMe), 3.61 (s, 6H, OC*H*$_3$). ^{31}P NMR (121 MHz, $CDCl_3$) δ -35.33; ^{13}C NMR (101 MHz, $CDCl_3$) δ 160.89, 140.86, 138.28, 135.59 (d, $^1J_{CP}$ 20.0), 133.89 (d, $^1J_{CP}$ 6.9), 133.61 (d, $^2J_{CP}$ 20.9), 129.85, 128.99 (d, $^3J_{CP}$ 7.8), 103.10 (d, J_{CP} 4.2), 102.39, 55.42; IR ν (cm^{-1}) 2921, 1612, 1463; TOF MS ES+ m/z: 390.1 $[M+H]^+$; HRMS calc. $[C_{22}H_{21}N_3O_2P]^+$ 390.1366, obs. 390.1374.

Synthesis of 5-(dicyclohexylphosphanyl)-1-(2,6-diisopropylphenyl)-1H-1,2,3-triazole (93m)

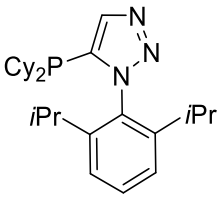

93m

Prepared following *General Procedure 4* on a 0.2 mmol scale. Obtained as a white solid (76 mg, 89%); mp. 138-140 °C; ^{1}H NMR (400 MHz, $CDCl_3$) δ 7.88 (s, 1H, Trz*H*), 7.49 (t, *J* 7.8, 1H, Ar CHC*H*CH), 7.27 (d, *J* 7.8, 2H, Ar C*H*CHC*H*), 2.06 (sept, *J* 6.8, 2H, C*H*$(CH_3)_2$), 1.86-1.63 (m, 12H, Cy*H*), 1.30-1.03 (m, 22H, Cy*H,* 2 x CH(C*H*$_3)_2$). ^{31}P NMR (121 MHz, $CDCl_3$) δ -30.65; ^{13}C NMR (101 MHz, $CDCl_3$) δ 146.22, 137.89 (d, $^{2}J_{CP}$ 5.0), 135.97 (d, $^{1}J_{CP}$ 25.3), 132.73, 130.70, 123.57, 33.85 (d, $^{1}J_{CP}$ 10.8), 30.04 (d, J_{CP} 12.0), 29.52 (d, J_{CP} 12.7), 28.89, 27.13 (d, J_{CP} 26.5), 27.13 (d, J_{CP} 5.7), 26.18, 26.07, 22.19; IR ν (cm^{-1}) 2925, 2850, 1446; TOF MS ES+ m/z: 426.3 $[M+H]^+$, 448.3 $[M+Na]^+$; HRMS calc. $[C_{26}H_{41}N_3P]^+$ 426.3033, obs. 426.3039.

Synthesis of 5-(di-tert-butylphosphanyl)-1-(2,6-diisopropylphenyl)-1H-1,2,3-triazole (93n)

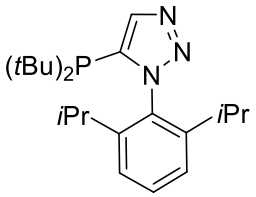

93n

Prepared following *General Procedure 4* on a 0.4 mmol scale. Obtained as a white solid (132 mg, 88%); mp. 93-95 °C; ^{1}H NMR (400 MHz, $CDCl_3$) δ 8.11 (d, *J* 0.5, 1H, Trz*H*), 7.48 (t, *J* 7.8, 1H, CHC*H*CH), 7.28 (d, *J* 7.8, 2H,C*H*CHC*H*), 2.18 (sept, *J* 6.8, 2H, 2 x C*H*$(CH_3)_2$), 1.22 (d, *J* 6.8, 6H, 2 x CH_3CHC*H*$_3$), 1.16 (d, $^{3}J_{HP}$ 12.3, 18H, 2 x C(C*H*$_3)_3$), 1.08 (d, *J* 6.8, 6H, 2 x C*H*$_3$CHCH_3; ^{31}P{^{1}H} NMR (121 MHz, $CDCl_3$) δ 2.14; ^{31}P NMR (121 MHz, $CDCl_3$) δ 2.14 (11 sub-peaks of the signal clearly defined, $^{3}J_{PH}$ 12.4); ^{13}C NMR (126 MHz, $CDCl_3$) δ 146.30, 138.67 (d, $^{2}J_{CP}$ 5.4), 135.57 (d, $^{1}J_{CP}$ 35.3), 133.09, 130.58, 123.57, 32.74 (d, $^{1}J_{CP}$

19.7), 30.45 (d, $^{2}J_{CP}$ 14.5), 29.11, 26.58, 21.73; IR ν (cm^{-1}) 2962, 2866, 1468, 1364; TOF MS ES+ m/z: 374.3 $[M+H]^{+}$; HRMS calc. $[C_{22}H_{37}N_3P]^{+}$ 374.2720, obs. 374.2726.

2,2',4,6,6'-Pentamethyl-1,1'-biphenyl (96)

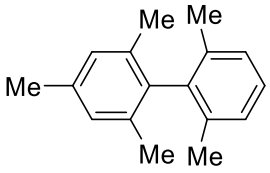

96

Product of catalysed reaction, see *General Procedure 7* for analysis protocol, data collected are consistent with that reported in the literature:[215]

Isolated from Table *4*, entry 1. Colourless oil. ^{1}H NMR (400MHz, CDCl3) δ 7.19-7.09 (m, 4H), 6.94 (s, 2H), 2.33 (s, 3H), 1.90 (s, 6H), 1.86 (s, 6H). ^{13}C NMR (101MHz, $CDCl_3$) δ 140.02 [-], 136.96 [-], 136.15 [-], 135.73 [-], 135.47 [-], 135.25 [-], 128.26 [+], 127.37 [+], 126.69 [+], 21.14 [+], 19.92 [+], 19.75 [+]. TOF MS EI+ m/z: 224.0 $[M]^{+}$, 209.0 $[M\text{-}CH_3]^{+}$.

4-Methyl-1,1'-biphenyl (101)

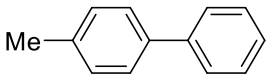

101

Product of catalysed reaction, see *General Procedure 7* for analysis protocol, data collected are consistent with that reported in the literature:[216]

Isolated from **Scheme *26***, using **93g** as ligand. Off white solid. ^{1}H NMR (400MHz, CDCl3) δ 7.57 (d, *J* 7.9, 2H), 7.49 (d, *J* 7.9, 2H), 7.41 (t, *J* 7.3, 2H), 7.31 (td, *J* 7.3, 1.3, 1H), 7.24 (d, *J* 7.3, 2H), 2.39 (s, 3H). ^{13}C NMR (101MHz, $CDCl_3$) δ 141.19[-], 138.39[-], 137.06[-],

129.52[+], 128.79[+], 127.21[+], 127.03[+], 127.01[+], 21.15[+]. TOF MS EI+ m/z: 168.1 $[M]^+$.

Synthesis of 2,4-dimethoxy-5-(1-methyl-1H-pyrazol-4-yl)pyrimidine (105a)

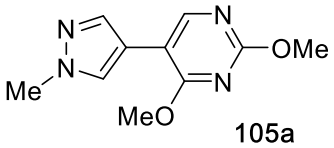

105a

Prepared following *General Procedure 5* on a 0.4 mmol scale. Obtained as an off white solid (67 mg, 76%); mp. 96-97 °C; ^{1}H NMR (400 MHz, $CDCl_3$) δ 8.40 (s, 1H), 7.80 (s, 1H), 7.74(s, 1H), 4.09 (s, 3H, OC*H*$_3$), 4.01(s, 3H, OC*H*$_3$), 3.95 (s, 3H, NC*H*$_3$); ^{13}C NMR (101 MHz, $CDCl_3$) δ 167.07 [-], 163.58 [-], 154.63 [+], 137.05 [+], 128.66 [+], 113.72 [-], 108.19 [-], 54.78 [+], 54.10 [+], 39.06 [+]; IR ν (cm^{-1}) 1611, 1557, 1370, 1087, 1015. TOF MS ES+ m/z: 221.1 $[M+H]^+$; HRMS calc. $[C_{10}H_{13}N_4O_2]^+$, 221.1033 obs. 221.1040.

Synthesis of 1-methyl-4-(4-(methylsulfonyl)phenyl)-1H-pyrazole (105b)

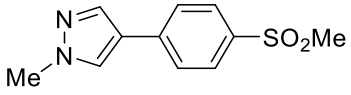

105b

Prepared following *General Procedure 5* on a 0.4 mmol scale. Obtained as a colourless crystalline solid (26 mg, 31%); mp. 223-224 °C; ^{1}H NMR (300 MHz, $CDCl_3$) δ 7.92 (d, *J* 8.6, 2H), 7.83 (s, 1H), 7.73(s, 1H), 7.64 (d, *J* 8.6, 2H), 3.80(s, 3H, NC*H*$_3$), 3.07 (s, 3H, SC*H*$_3$); ^{13}C NMR (101 MHz, $CDCl_3$) δ 138.35 [-], 137.82 [u], 137.18 [+], 128.15 [+], 127.83 [+], 125.81 [+], 122.17 [u], 44.65 [+], 39.30 [+]; IR ν (cm^{-1}) 1297, 1149; TOF MS EI+ m/z: 236.1 $[M]^+$, 221.1 $[M\text{-}CH_3]^+$; HRMS calc. $[C_{11}H_{12}N_2O_2S]^+$ 236.0614, obs. 236.0615.

Synthesis of 2,4-dimethoxy-5-(pyrazin-2-yl)pyrimidine (105c)

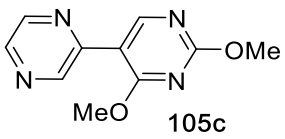

105c

Prepared following *General Procedure 5* on a 0.4 mmol scale. Obtained as a colourless crystalline solid (105 mg, 98%); mp. 109-110 °C; ^{1}H NMR (400 MHz, $CDCl_3$) δ 9.17 (d, *J* 1.5, 1H), 8.98 (s, 1H), 8.64-8.62 (dd, *J* 2.5, 1.5, 1H), 8.50 (d, *J* 2.5, 1H), 4.13 (s, 3H, OC*H*$_3$), 4.08(s, 3H, OC*H*$_3$); ^{13}C NMR (101 MHz, $CDCl_3$) δ 168.21 [-], 165.69 [-], 160.33 [+], 147.91 [-], 145.06 [+], 144.11 [+], 142.78 [+], 111.70 [-], 55.17 [+], 54.36 [+]; IR ν (cm^{-1}) 1398, 1090; TOF MS ES+ m/z: 219.1 $[M+H]^+$; HRMS calc. $[C_{10}H_{11}N_4O_2]^+$ 219.0877, obs. 219.0884.

Synthesis of 2-(4-(methylsulfonyl)phenyl)pyrazine (105d)

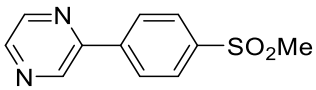

105d

Prepared following *General Procedure 5* on a 0.4 mmol scale. Obtained as a colourless crystalline solid (57 mg, 61%); mp. 167-168 °C; ^{1}H NMR (300 MHz, $CDCl_3$) δ 9.04(s, 1H), 8.64-8.62 (m, 1H), 8.57 (d, *J* 2.3, 1H), 8.17 (d, *J* 8.7, 2H), 8.03 (d, *J* 8.7, 2H), 3.04 (s, 3H, SC*H*$_3$); ^{13}C NMR (101 MHz, $CDCl_3$) δ 150.72 [-], 144.53 [+], 144.30 [+], 142.49 [+], 141.56 [-], 141.48 [-], 128.14 [+], 127.84 [+], 44.52 [+]; IR ν (cm^{-1}) 1301, 1149. TOF MS ES+ m/z: 235.1 $[M+H]^+$, 257.0 $[M+Na]^+$, 286.2 $[M+K]^+$; HRMS calc. $[C_{11}H_{11}N_2O_2S]^+$ 235.0536, obs. 235.0540

Synthesis of 2,4-dimethoxy-5-(4-(trifluoromethyl)phenyl)pyrimidine (105e)

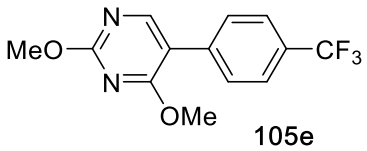

105e

Prepared following *General Procedure 5* on a 0.4 mmol scale. Obtained as a colourless crystalline solid (85 mg, 75%); mp. 102-103 °C; ^{1}H NMR (400 MHz, $CDCl_3$) δ 8.20 (s, 1H), 7.60 (d, *J* 8.2, 2H), 7.54 (d, *J* 8.2, 2H), 3.97(s, 3H, OC*H*$_3$), 3.96 (s, 3H, OC*H*$_3$); ^{13}C NMR (101 MHz, $CDCl_3$) δ 168.08, 164.99, 157.87, 137.06, 129.85(q, $^{2}J_{CF}$ 32.7), 129.06, 125.46-125.26 (m), 124.13(q, $^{1}J_{CF}$ 276.8), 114.92, 54.98, 54.23. ^{19}F NMR (282 MHz, $CDCl_3$) δ -62.60; IR ν (cm^{-1}) 1326, 1067; TOF MS ES+ m/z: 285.1 $[M+H]^+$; HRMS calc. $[C_{13}H_{12}N_2O_2F_3]^+$ 285.0845, obs. 285.0853.

Synthesis of 5-(3,5-bis(trifluoromethyl)phenyl)-2,4-dimethoxypyrimidine (105f)

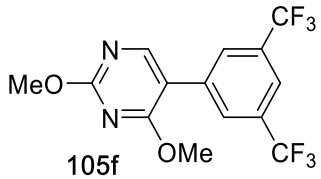

105f

Prepared following *General Procedure 5* on a 0.4 mmol scale. Obtained as a colourless crystalline solid (107 mg, 76%); mp. 64-65 °C; ^{1}H NMR (400 MHz, $CDCl_3$) δ 8.25 (s, 1H), 7.88 (s, 2H), 7.79 (s, 1H), 4.00 (s, 3H, OC*H*$_3$), 3.99(s, 3H, OC*H*$_3$); ^{13}C NMR (101 MHz, $CDCl_3$) δ 167.99 [-], 165.38 [-], 158.05 [+], 135.60 [-], 131.86 (q, $^{2}J_{CF}$ 33.5) [-], 128.93-128.66 (m) [+], 123.26 (d, $^{1}J_{CF}$ 272.7) [-], 121.49-121.22 (m) [+], 113.57 [-], 55.16 [+], 54.47 [+]. ^{19}F NMR (282 MHz, $CDCl_3$) δ -62.85; IR ν (cm^{-1}) 1366, 1277, 1129; TOF MS ES+ m/z: 353.1 $[M+H]^+$; HRMS calc. $[C_{14}H_{11}N_2O_2F_6]^+$ 353.0719, obs. 353.0728.

Synthesis of 2,4-difluoro-2',6'-dimethoxy-1,1'-biphenyl (105g)

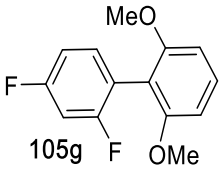

105g

Prepared following *General Procedure 5* on a 0.4 mmol scale. Obtained as a colourless crystalline solid (53 mg, 53%) isolated yield; mp. 108-109 °C; ^{1}H NMR (400 MHz, $CDCl_3$) δ 7.32 (t, *J* 8.4, 1H, CHC*H*CH), 7.28-7.20 (m, 1H), 6.94-6.83 (m, 2H), 6.65 (d, *J* 8.4, 2H, C*H*CHC*H*), 3.75 (s, 6H, OCH_3); ^{13}C NMR (101 MHz, $CDCl_3$) δ 162.32 (dd, *J* 247.3 & 11.9) [-], 160.41 (dd, 249.1 & 12.1) [-], 158.08 [-], 133.54, (dd, *J* 9.2 & 5.7) [+], 129.74 [+], 117.89 [u], (dd, *J* 17.1 & 3.6), 112.39 [u], 110.64 (dd, *J* 21.0 & 3.2) [+], 104.51 [+], 103.95-103.44 (m) [+], 55.94 [+]; ^{19}F NMR (282 MHz, $CDCl_3$) δ -109.04 (d, $^{4}J_{FF}$ 7.7), -112.22 (d, $^{4}J_{FF}$ 7.7); IR ν (cm^{-1}) 1471, 1249, 1108; TOF MS EI+ m/z: 250.1 $[M]^+$; HRMS calc. $[C_{14}H_{12}O_2F_2]^+$ 250.0800, obs. 250.0798.

Synthesis of 2',6'-dimethoxy-[1,1'-biphenyl]-2-carbonitrile (105h)

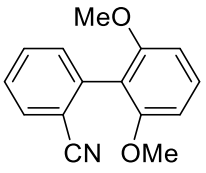

105h

Prepared following *General Procedure 5* on a 0.4 mmol scale. Obtained as a colourless crystalline solid (61 mg, 64 %); mp. 102-103 °C; ^{1}H NMR (400 MHz, $CDCl_3$) δ 7.71 (d, *J* 7.8, 1H, COCHC*H*CHCO), 7.63-7.56 (m, 1H), 7.43-7.31 (m, 3H), 6.67 (d, *J* 8.4, 2H, MeOCC*H*CHC*H*COMe), 3.76 (s, 6H, OCH_3); ^{13}C NMR (101 MHz, $CDCl_3$) δ 157.59 [-], 138.80 [-], 132.51 [+], 132.19 [+], 131.93 [+], 130.42 [+], 127.16 [+], 118.71 [-], 115.69

[-], 114.49 [-], 104.21 [+], 55.87 [+]; IR ν (cm^{-1}) 2227, 1248, 1105; TOF MS ES+ m/z: 240.1 $[M+H]^+$, 262.1 $[M+Na]^+$, 275.1 $[M+K]^+$; HRMS calc. $[C_{15}H_{14}NO_2]^+$ 240.1019, obs. 240.1024.

Synthesis of 2-(benzofuran-2-yl)benzonitrile (105i)

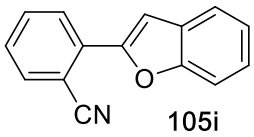

105i

Prepared following *General Procedure 5* on a 0.4 mmol scale. Obtained as a colourless crystalline solid (53 mg, 61 %); mp. 71-72 °C; ^{1}H NMR (300 MHz, $CDCl_3$) δ 8.09 (dd, *J* 8.1, 0.6,2H), 7.78-7.63 (m, 4H), 7.57-7.50 (m, 1H), 7.43-7.31 (m, 2H), 7.30-7.24 (m,1H); ^{13}C NMR (101 MHz, $CDCl_3$) δ 154.67 [-], 151.21 [-], 134.40 [+], 133.04 [+], 132.95 [-], 128.76 [-], 128.16 [+], 127.03 [+], 125.73 [+], 123.40 [+], 121.95 [+], 118.87 [-], 111.29 [+], 108.08 [-], 106.79 [+]; IR ν (cm^{-1}) 1256, 1022; TOF MS EI+ m/z: $[M]^+$, HRMS calc. $[C_{15}H_9NO]^+$ 219.0679, obs. 219.0685.

Synthesis of 1-(4-(benzofuran-2-yl)phenyl)ethan-1-one (105j)

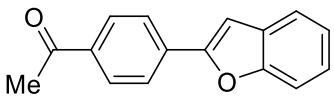

105j

Prepared following *General Procedure 5* on a 0.4 mmol scale. Obtained as a colourless crystalline solid (61 mg, 65 %); mp. 177-179 °C; ^{1}H NMR (400 MHz, $CDCl_3$) δ 8.04 (d, *J* 8.7, 2H), 7.95 (d, *J* 8.6, 2H), 7.62 (d, *J* 7.6, 1H), 7.55 (d, *J* 8.4, 1H), 7.33 (td, *J* 7.7, 1.4, 1H), 7.28-7.21 (m, 2H), 2.64 (s, 3H, C*H*$_3$); ^{13}C NMR (101 MHz, $CDCl_3$) δ 197.33 [u], 155.23 [-], 154.56 [-], 136.65 [-], 134.61 [-], 128.95 [+], 128.90 [u], 125.16 [+], 124.80 [+], 123.27

[+], 121.33 [+], 111.37 [+], 103.66 [+], 26.63 [+]; IR ν (cm^{-1}) 1678, 1272, 1034; TOF MS EI+ m/z: 236.1 $[M]^+$, 221.1 $[M\text{-}CH_3]^+$; HRMS calc. $[C_{16}H_{12}O_2]^+$ 236.0832, obs. 236.0833.

Synthesis of (105)

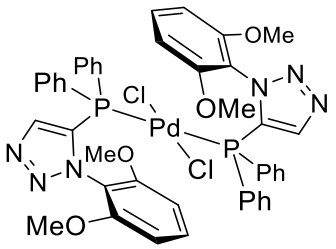

106

Prepared following *General Procedure 6*, and crystallised from dichloromethane/hexane, 30 mg, 63%. Yellow solid MP 230 °C (decomp.). ^{1}H NMR (400 MHz, $CDCl_3$) δ 8.23 (s, 2H, Trz*H*), 7.55-7.49 (m, 8H), 7.42-7.38 (m, 5H), 7.33-7.24 (m, 7H), 7.08 (t, *J* 8.5, 2H, CHC*H*CH), 6.23 (d, *J* 8.5, 4H, C*H*CHC*H*), 3.30 (s, 12H, OC*H*$_3$). ^{31}P NMR (162 MHz, $CDCl_3$) δ -2.02. ^{13}C NMR (101 MHz, $CDCl_3$) δ 155.99, 144.02, 143.94, 135.15, 135.09, 135.03, 133.54, 133.33, 131.57, 130.78, 129.24, 128.52, 128.43, 127.65, 12.49, 127.44, 127.38, 127.14, 126.87, 126.61, 114.42, 103.69, 55.26, 53.45 [signal complexity observed due to P-C splitting]. IR 2940, 2841,1602, 1603, 1483, 1262, 1113, 910.

Synthesis of (107)

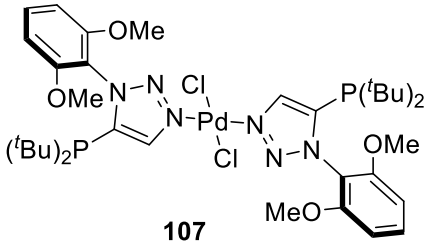

107

Prepared following *General Procedure 6*, and crystallised from dichloromethane/hexane, 38 mg, 88%. Yellow solid, mp. 205 °C (decomp.). ^{1}H NMR (400 MHz, $CDCl_3$) δ 8.48 (s, 2H, Trz*H*), 7.43 (t, *J* 8.5, 2H, CHC*H*CH), 6.61 (d, *J* 8.5, 4H, C*H*CHC*H*), 3.68 (s, 12H, OC*H*$_3$), 1.13 (d, J 12.6, 36H). ^{31}P NMR (121 MHz, $CDCl_3$) δ 3.55. ^{13}C NMR (101 MHz, $CDCl_3$) δ 156.10 140.87 (d,$^{2}J_{CP}$ 7.2), 137.98 (d, $^{1}J_{CP}$ 34.6), 132.24, 114.37, 103.91, 55.61, 32.67 (d, $^{1}J_{CP}$ 18.7), 30.05 (d,$^{2}J_{CP}$ 14.9). IR 2941, 2896, 1603, 1482, 1435, 1261, 1113.

6.3Experimental for Chapter 3

General procedure 8: Preparation of Phosphine compound 109a-b

Under anhydrous conditions and protected from air, a solution of the triazole **92a** (1 equiv.) in tetrahydrofuran (0.04 M) was stirred at -78 °C. To which *n*-butyl lithium (1.2 equiv., 2.0 M in tetrahydrofuran) was added dropwise. The reaction mixture was stirred for two hours at this temperature, and then the phenyl- or cyclohexyl- phosphine dichloride (0.5 equiv.) was carefully added. After addition was complete, the reaction mixture was allowed to slowly warm to room temperature. After stirring at room temperature for a further ten hours, the volatiles were removed *in vacuo* to afford a crude residue. The residue thus obtained, was purified by flash chromatography (*Isco CombiFlash,* silica 50-60 μm, or *Interchim XS 420*, 20 μm, 4 or 12 g column, gradient elution; hexane (100%) to hexane (20%): ethyl acetate (80%), detection absorption at 254 and 288 nm) to afford the corresponding products.

General procedure 9: Preparation of Tris-triazole phosphine ligand 110a-c, 110g

Under anhydrous conditions and protected from air, a solution of corresponding triazole **92** (1.0 mmol) in tetrahydrofuran (0.04 M) was stirred at -78 °C. To which *n*-butyl lithium (1.2 equiv., 2.0 M in tetrahydrofuran) was added dropwise. The reaction mixture was stirred for two hours at this temperature, and then phosphorus trichloride (0.33 equiv.) was carefully added. After addition was complete, the reaction mixture was allowed to slowly warm to room temperature. After stirring at room temperature for a further ten hours, the volatiles were removed *in vacuo* to afford a crude residue. The residue thus obtained, was purified by flash chromatography (*Isco CombiFlash,* silica 50-60 μm, gradient elution hexane (100%) to hexane (0%): ethyl acetate (100%), detection 254 and 288 nm absorption) to afford the corresponding product.

General procedure 10: Preparation of Phosphine Gold(I) Chloride Complexes

Dimethylsulfide gold(I)chloride and corresponding phosphine (1 equiv.) were added to a dried flask. Dichloromethane was added and the solution thus obtained (to achieve a concentration of 0.1 M), which was stirred at room temperature, under argon, for two hours. After this time an at least 4 equal volume amount of hexane was added resulting formation a white precipitate. The precipitate was collected *via* filtration and washed with cold hexane to yield the desired complexes.

General procedure 11: Hydration of terminal alkyne to prepare 118a-118l and 118m'

To a 10 ml sealed tube reactor, 1 mmol alkyne **117a-t** was dissolved in 1.3 ml methanol, 36 μl (2 mmol, 2 euqiv.) water was added *via* micro-syringe.0.5 ml of AgOTf methanol

(0.01 M) solution was added, followed by 0.2 ml of **115** DCM (0.0125M) solution (0.05M **115** DCM solution was used in reaction with **117j-117l**). The vial was capped and heat at 80 °C for 2 hours. After reaction completed, the reaction was filtered *via* Celite, and the volatiles were removed *in vacuo* to afford a crude residue. The residue thus obtained, was purified by flash chromatography (*Isco CombiFlash,* silica 50-60 μm, or *Interchim XS 420*, 20 μm, 4 or 12 g column, gradient elution; hexane (100%) to hexane (20%): ethyl acetate (80%), detection absorption at 254 and 288 nm) to afford the corresponding products

General procedure 12: Analysis of hydration of terminal alkyne (Table 10)

For 0.5 mol% gold complex loading reaction, to a 10 ml sealed tube reactor, 1 mmol alkyne **117a** was dissolved in 1.3 ml methanol, 36 μl (2 mmol, 2 euqiv.) water was added *via* micro-syringe, 0.5 ml of AgOTf methanol (0.02 M) solution was added, followed by 0.2 ml of corresponding phosphine-gold complexes in methanol (0.025M) solution (DCM was used for complex **114**). For lower catalysts loading reaction, the concentration of AgOTf-methanol solution and phosphine-gold complex methanol solution have been diluted into 0.01M and 0.0125M for 0.25 mol% loading reaction, 0.002M and 0.0025M for 0.05 mol% loading. The volume of the reaction solvent has not changed in all cases.

The vial was capped and heat at 80 °C for 2 hours. After the reaction completed, the reaction was filtered *via* Celite. The conversions were determined by GC analysis using the same method in each case. Internal standard *n*-dodecane in toluene, injection temperature 260 °C, oven temperature gradient from 100 to 200 °C over 20 min

maintain temperature for another 5 min (minimum), column ZB-5. Typical run time 25 min, peaks determined using FID.

General procedure 13: Analysis of hydration of internal alkyne (Table 11)

To a 10 ml sealed tube reactor, 1 mmol alkyne **119** was dissolved in 1.3 ml methanol, 36 μl (2 mmol, 2 euqiv.) water was added *via* micro-syringe, 0.5 ml of AgOTf methanol (0.04 M) solution was added, followed by 0.2 ml of corresponding phosphine-gold complexes in methanol (0.05M) solution (DCM was used for complex **114**). The vial was capped and heat at 80 °C for 2 hours. After the reaction completed, the reaction mixture was filtered *via* Celite, and the volatiles were removed *in vacuo* to afford a crude residue. The crude residue was then analysed via ^{1}H-NMR or GC to determine the ratio of **120a** and **120b**.

Synthetic Protocols and Experimental Details

Synthesis of dimethylsulfide gold(I)chloride

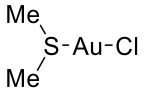

Under anhydrous conditions and protected from air, a solution of the potassium tetrachloroaurate (377 mg, 1.0 mmol 1 equiv.) in methanol (1 mL) was added to a solution of dimethyl sulfide (0.22 mL, 3.0 mmol 3 equiv.) in methanol (4 mL). The resulting mixture was stirred at room temperature, protected from light, for two hours. The resulting white solid was collected by filtration and washed with cold methanol (~2 mL) to deliver the desired product as a white solid (248 mg, 84%).

Synthesis of 5,5'-(penylphosphanediyl)bis(1-phenyl-1H-1,2,3-triazole) (109a)

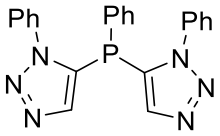

109a

Prepared following *General Procedure 8* on a 1.0 mmol scale. White solid (104 mg, 54%); m.p. 165-167 °C; ^{1}H NMR (400 MHz, $CDCl_3$) δ 7.47-7.38 (m, 12H, Ar*H*), 7.28-7.24 (m, 5H, Ar*H*);^{31}P NMR (121 MHz, $CDCl_3$) δ 64.31; ^{13}C NMR (126 MHz. $CDCl_3$) δ 140.64, 136.32, 133.69 d, J_{CP} 23.0), 132.63 (d, J_{CP} 12.2), 131.27, 129.95, 129.60, 129.53, 129.42, 125.00 (d, J_{CP} 4.3); IR ν (cm^{-1}) 3107, 3058, 1596, 1498, 1436, 1286, 1229; TOF MS ES+ m/z: 397.1 $[M+H]^+$, 419.1 $[M+Na]^+$; $[C_{22}H_{18}N_6P]^+$ 397.1325 obs. 397.1330. Structure corroborated by single crystal X-ray diffraction determination.

Synthesis of 5,5'-(cyclohexylphosphanediyl)bis(1-phenyl-1H-1,2,3-triazole) (109b)

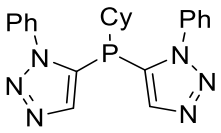

109b

Prepared following *General Procedure 8* on a 1.47 mmol scale. White solid (143 mg, 71%); m.p. 169-171 °C; ^{1}H NMR (400 MHz, $CDCl_3$) δ 7.78 (d, *J* 0.7, 2H, Trz*H*), 7.53-7.48 (m, 2H), 7.44 (t, *J* 7.4, 4H), 7.21-7.18 (m, 4H), 2.40-2.30 (m, 1H), 1.73-1.59 (m, 5H), 1.28-1.03 (m, 6H); ^{31}P NMR (121 MHz, $CDCl_3$) δ 65.94; ^{13}C NMR (101 MHz. $CDCl_3$) δ 139.04, 136.38, 132.79 (d, $^{1}J_{CP}$ 19.2), 129.96, 129.29, 125.87 (d, $^{4}J_{CP}$ 4.0), 37.82 (d, $^{1}J_{CP}$ 4.4), 29.42 (d, J_{CP} 16.1), 26.10 (d, J_{CP} 12.5), 25.74; IR ν (cm^{-1}) 3112, 3062, 2927, 2852, 1596, 1498, 1450; TOF MS ES+ m/z: 403.2 $[M+H]^+$, 375.2 $[M+H-2N]^+$; HR-MS calc. $[C_{22}H_{24}N_6P]^+$ 403.1795 obs. 403.1799. Structure corroborated by single crystal X-ray diffraction determination.

Synthesis of tris(1-phenyl-1H-1,2,3-triazol-5-yl)phosphane (110a)

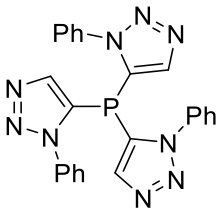

110a

Prepared following *General Procedure 9* on a 1.0 mmol scale. White solid (108 mg, 77%); mp. 186-188 °C; ^{1}H NMR (400 MHz, $CDCl_3$) δ 7.63 (d, $^{3}J_{HP}$ 0.9, 3H, Trz*H*), 7.49 (tt, *J* 7.4, 1.2, 3H), 7.42 (t, *J* 7.9, 6H), 7.17-7.14 (m, 6H); ^{31}P NMR (121 MHz, $CDCl_3$) δ -93.52; ^{13}C NMR (101 MHz, $CDCl_3$) δ 141.07, 135.72, 130.45, 129.72, 129.43 (d, $^{1}J_{CP}$ 4.2), 124.90 (d,

$^{4}J_{CP}$ 4.3); IR ν (cm^{-1}) 3105, 1595, 1497; TOF MS ES+ m/z: 464.2 $[M+H]^+$, 486.1 $[M+Na]^+$, 949.3 $[2M+Na]^+$; HR-MS calc. $[C_{24}H_{18}N_9PNa]^+$ 486.1315, obs. 486.1323. Structure corroborated by single crystal X-ray diffraction determination.

Synthesis of tris(1-(p-tolyl)-1H-1,2,3-triazol-5-yl)phosphane (110bb)

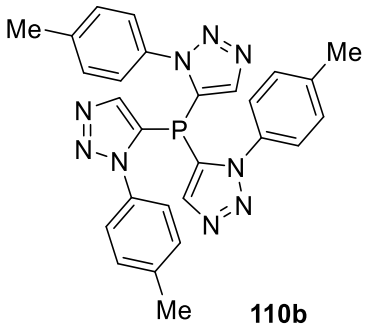

110b

Prepared following *General Procedure 9* on a 0.5 mmol scale. White solid (28mg, 34%); m.p. 210-212 °C; ^{1}H NMR (400 MHz, $CDCl_3$) δ 7.60 (d, $^{3}J_{HP}$ 0.8, 3H, Trz*H*), 7.20 (d, *J* 8.1, 6H, Ar*H*), 7.02 (d, *J* 8.1, 6H, Ar*H*), 2.40 (s, 9H, C*H*$_3$); ^{31}P NMR (121 MHz, $CDCl_3$) -93.60; ^{13}C NMR (101 MHz, $CDCl_3$) δ 140.89 [+], 140.71 [-], 133.25 [-], 130.14 [+], 129.53 (d, $^{1}J_{CP}$ 3.7) [-], 124.62 (d, $^{4}J_{CP}$ 4.2) [+], 21.20 [+]; IR ν (cm^{-1}) 2921, 2853, 1514, 1467, 1290; TOF MS ES+ m/z: 506.2 $[M+H]^+$, 528.2 $[M+Na]^+$; HR-MS calc. $[C_{27}H_{25}N_9P]^+$ 506.1965, obs. 506.1972. Structure corroborated by single crystal X-ray diffraction determination.

Synthesis of tris(1-(4-methoxyphenyl)-1H-1,2,3-triazol-5-yl)phosphane (110c)

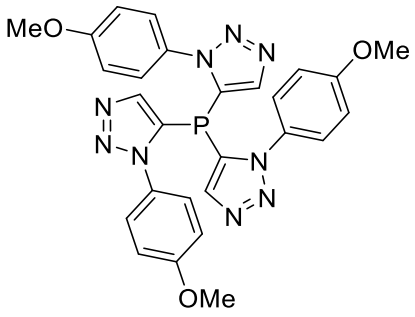

110c

Prepared following *General Procedure 9* on a 1.0 mmol scale. White solid (13mg, 7%); m.p. 216-218 °C; ^{1}H NMR (400 MHz, $CDCl_3$) δ 7.60 (d, $^{3}J_{HP}$ 0.9, 3H, Trz*H*), 7.05 (d, *J* 9.0, 6H, Ar*H*), 6.88 (d, *J* 9.0, 6H, Ar*H*), 3.84 (s, 9H, OCH_3); ^{31}P NMR (121 MHz, $CDCl_3$) -94.32; ^{13}C NMR (101 MHz, $CDCl_3$) δ 160.85 [-], 140.74 [+], 129.74 (d, $^{1}J_{CP}$ 3.0) [-], 128.47 [-], 126.34 (d, $^{4}J_{CP}$ 3.9) [+], 114.67 [+], 55.65 [-]; IR ν (cm^{-1}) 2925, 2853, 1607, 1514, 1463, 1255; TOF MS ES+ m/z: 554.2 $[M+H]^+$, 576.2 $[M+Na]^+$; HR-MS calc. $[C_{27}H_{24}N_9O_3PNa]^+$ 576.1632, obs. 576.1636. Structure corroborated by single crystal X-ray diffraction determination.

Synthesis of tris(1-(4-(trifluoromethyl)phenyl)-1H-1,2,3-triazol-5-yl)phosphane (110g)

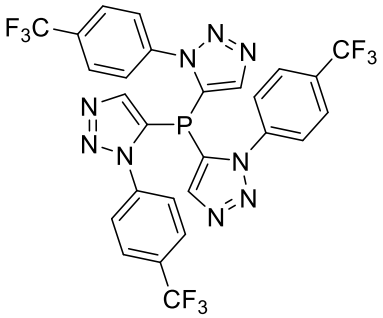

110g

Prepared following *General Procedure 9* on a 0.5 mmol scale. White solid (95mg, 89%); m.p. 215-217 °C; ^{1}H NMR (400 MHz, $CDCl_3$) δ 7.74-7.70 (m, 9H), 7.33 (d, *J* 8.3, 6H, Ar*H*); ^{31}P NMR (121 MHz, $CDCl_3$) -92.54; ^{13}C NMR (101 MHz, $CDCl_3$) δ 141.56, 138.20, 132.84 (q, $^{2}J_{CF}$ 33.9), 128.81 (d, $^{1}J_{CP}$ 3.6), 127.16 (q, $^{3}J_{CF}$ 3.4), 125.11 (d, $^{4}J_{CP}$ 4.7), 123.03 (q, $^{1}J_{CF}$ 272.6); ^{19}F NMR (282 MHz, $CDCl_3$) δ -62.89; IR ν (cm^{-1}) 3121, 1617, 1520. 1419, 1326; TOF MS ES+ m/z: 668.1 $[M+H]^+$; HR-MS calc. $[C_{27}H_{16}N_9F_9P]^+$ 668.1117, obs. 6688.1124. Structure corroborated by single crystal X-ray diffraction determination.

Synthesis of chloro[5-(diphenylphosphanyl)-1-phenyl-1H-1,2,3-triazole] gold(I) (112a)

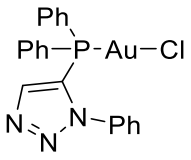

112a

Prepared following *General Procedure 10* on a 0.1 mmol scale. White solid (43 mg, 86%); m.p. 230 °C (decomp); ^{1}H NMR (400 MHz, $CDCl_3$) δ 7.68-7.51 (m, 12H), 7.44 (t, *J* 7.9, 2H), 7.19 (d, *J* 7.4, 2H); ^{31}P NMR (121 MHz, $CDCl_3$) δ 8.61; ^{13}C NMR (101 MHz. $CDCl_3$) δ 141.53 (d, J_{CP} 10.6), 135.55, 133.97 (d, J_{CP} 15.2), 133.15 (d, J_{CP} 2.5), 131.23, 129.86, 129.82, 129.73, 126.33, 126.55 (d, J_{CP} 67.3); IR ν (cm^{-1}) 3056, 2923, 1595, 1498, 137, 1287, 1102; TOF MS ES+ m/z: 562.06 $[M+H]^+$; HR-MS calc. $[C_{20}H_{17}AuClN_3P]^+$ 562.0509 obs. 562.0499. Structure corroborated by single crystal X-ray diffraction determination.

Synthesis of chloro[5-(dicyclohexylphosphanyl)-1-phenyl-1H-1,2,3-triazole] gold(I) (112b)

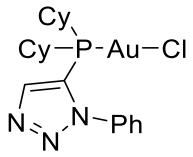

112b

Prepared following *General Procedure 10* on a 0.1 mmol scale. White solid (48 mg, 83%); m.p. >250 °C; ^{1}H NMR (400 MHz, $CDCl_3$) δ 7.99 (s, 1H, Trz*H*), 7.73 (t, *J* 7.51, 1H), 7.63 (t, *J* 7.8, 2H), 7.35 (d, *J* 7.6, 2H), 2.21-2.07 (m, 2H), 2.01-1.92 (m, 2H), 1.92-1.80 (m, 4H), 1.79-1.64 (m, 4H), 1.43-1.10 (m, 10H); ^{31}P NMR (121 MHz, $CDCl_3$) δ 22.14; ^{13}C NMR (101 MHz. $CDCl_3$) δ 139.18 (d, J_{CP} 7.2), 135.78, 131.65, 130.15, 127.54, 126.17 (d, J_{CP} 52.8), 35.63 (d, J_{CP} 35.8), 29.78 (d, J_{CP} 3.5), 28.58, 26.28 (d, J_{CP} 5.0), 26.13, 25.41; IR ν (cm^{-1}) 2927, 2852, 1595, 1497, 1448, 1287; TOF MS ES+ m/z: 574.10 $[M+H]^+$; HR-MS calc. $[C_{20}H_{29}AuClN_3P]^+$ 574.1448 obs. 574.1445. Structure corroborated by single crystal X-ray diffraction determination

Synthesis of chloro[5,5'-(penylphosphanediyl)bis(1-phenyl-1H-1,2,3-triazole)] gold(I) (113a)

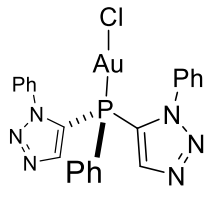

113a

Prepared following *General Procedure 10* on a 0.1 mmol scale. White solid (37 mg, 58%); m.p. 176-178 °C; ^{1}H NMR (400 MHz, $CDCl_3$) δ 7.91-7.44 (m, 13H, Ar*H*), 7.19-7.02 (m, 4H,

Ar*H*); ^{31}P NMR (121 MHz, $CDCl_3$) δ -16.87; ^{13}C NMR (126 MHz. $CDCl_3$) δ 141.43 (d, J_{CP} 10.8), 135.04, 134.40, 133.99 (d, J_{CP} 17.3), 131.70, 131.40 (d, J_{CP} 13.6), 130.10, 127.09, 126.49, 126.28; IR ν (cm^{-1}) 3111, 3059, 1594, 1467, 1438, 1289; TOF MS ES+ m/z: 397.10 $[M\text{-}Au\text{-}Cl+H]^+$, 629.01 $[M+H]^+$; HR-MS calc. $[C_{22}H_{18}AuClN_6P]^+$ 629.0679 obs. 629.0688; elemental analysis calc. $C_{22}H_{17}AuClN_6P$: C 42.02, H 2.73, N 13.37%, found C 42.25, H 2.69, N 13.52%. Structure corroborated by single crystal X-ray diffraction determination.

Synthesis of chloro [5,5'-(cyclohexylphosphanediyl)bis(1-phenyl-1H-1,2,3-triazole)] gold(I) (113b)

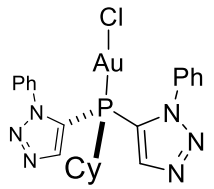

113b

Prepared following *General Procedure 10* on a 0.1 mmol scale White solid (51 mg, 80%); m.p. 235-237 °C; ^{1}H NMR (400 MHz, $CDCl_3$) δ 7.84 (s, 2H, Trz*H*), 7.69 (t, *J* 7.6, 2H), 7.55 (t, *J* 7.9, 4H), 7.08 (d, *J* 7.3), 2.50-2.39 (m, 1H), 1.97-1.86 (m, 2H), 1.82-1.73 (m, 3H), 1.49-1.24 (m, 5H); ^{31}P NMR (121 MHz, $CDCl_3$) δ -11.87; ^{13}C NMR (101 MHz. $CDCl_3$) δ 140.42 (d, $^2J_{CP}$ 13.3), 135.01, 131.88, 130.16, 126.97, 125.74 (d, J_{CP} 67.1), 38.15 (d, J_{CP} 41.0), 29.40 (d, J_{CP} 4.6), 25.79 (d, J_{CP} 16.7), 25.03; IR ν (cm^{-1}) 3110, 3063, 2932, 2854, 1594, 1496, 1452; TOF MS ES+ m/z: 635.07 $[M+H]^+$; HR-MS calc. $[C_{22}H_{24}AuClN_6P]^+$ 635.1149 obs. 635.1143. Structure corroborated by single crystal X-ray diffraction determination.

Synthesis of chloro[tris(1-phenyl-1H-1,2,3-triazol-5-yl)phosphane] gold(I) (114)

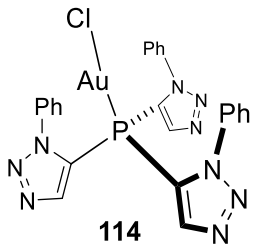

114

Prepared following *General Procedure 10* on a 0.1 mmol scale. White solid (63 mg, 91%); m.p. 230 °C (deco); ^{1}H NMR (400 MHz, $CDCl_3$) δ 7.91 (s, 3H, Trz*H*), 7.61 (t, *J* 7.6, 3H), 7.47 (t, *J* 7.94, 6H), 7.62 (d, *J* 7.6, 6H); ^{31}P NMR (121 MHz, $CDCl_3$) δ -44.19; ^{13}C NMR (101 MHz. $CDCl_3$) δ 141.75 (d, $^{2}J_{CP}$ 12.0), 134.45, 132.16, 130.34, 126.22, 124.87 (d, J_{CP} 89.32); IR ν (cm^{-1}) 2923, 2853, 1759, 1496; TOF MS ES+ m/z: 464.11 $[M\text{-}Au\text{-}Cl+H]^+$, 696.03 $[M+H]^+$; HR-MS calc. $[C_{24}H_{19}AuClN_9P]^+$ 696.0850 obs. 696.0866. Structure corroborated by single crystal X-ray diffraction determination.

Synthesis of chloro[5-(dicyclohexylphosphanyl)-1-(2,6-dimethoxyphenyl)-1H-1,2,3-triazole] gold(I) (115)

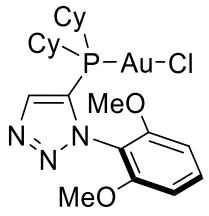

115

Prepared following *General Procedure 10* on a 0.1 mmol scale. White solid (48 mg, 86%); m.p. 260 °C; ^{1}H NMR (500 MHz, $CDCl_3$) δ 7.97 (s, 1H), 7.60 (t, *J* 8.6, 1H), 6.72(d, *J* 8.6), 3.75 (s, 6H), 2.15-2.07 (m, 2H), 1.94-1.68 (m, 10H), 1.37-1.17 (m, 10H); ^{31}P NMR (121 MHz, $CDCl_3$) δ 22.03; ^{13}C NMR (126 MHz, $CDCl_3$) δ 156.17, 138.23 (d, *J* 7.2), 133.07,

127.11 (d, *J* 58.6), 113.41, 104.78, 55.72, 35.53 (d, *J* 36.4), 29.34 (d, *J* 3.5), 28.53, 26.44 (d, *J* 3.9), 26.33, 25.52 (d, *J* 1.5); IR ν (cm^{-1}); 2928, 2852, 1600, 1483, 1447, 1262; TOF MS ES+ m/z: 634.11 $[M+H]^+$; HR-MS calc. $[C_{22}H_{33}AuClN_3O_2P]^+$ 634.1659 obs. 634.1657. Structure corroborated by single crystal X-ray diffraction determination.

Analysis of materials resulting from substrate screening in catalysis

Analysis of decan-2-one (118a)

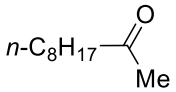

118a

Prepared following *General Procedure 11.* Colourless oil (123mg, 79%); ^1H NMR (400 MHz, $CDCl_3$) δ 2.41 (t, *J* 7.5, 2H), 2.13 (s, 3H), 1.62-1.52 (m, 2H), 1.28 (brs, 10H), 0.88 (t, *J* 6.9, 3H); ^{13}C NMR (101 MHz, $CDCl_3$) δ 209.43[-], 43.84[-], 31.82[-], 29.86[+], 29.37[-], 29.20[-], 29.14[-], 23.89[-], 22.65[-], 14.10[+]; IR ν (cm^{-1}) 2924, 2854, 1716, 1464, 1358, 1162; TOF MS EI+ m/z: 156.2 $[M]^+$. Data are consistent with those described in the literature.[217]

Analysis of 1-cyclohexylethan-1-one (118b)

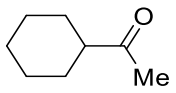

118b

Prepared following *General Procedure 11.* Colourless oil (81mg, 64%); ^1H NMR (400 MHz, $CDCl_3$) δ 2.37-2.28 (m, 1H), 2.13 (s, 3H, C*H*$_3$), 1.93-1.58 (m, 5H), 1.40-1.13 (m,5H); ^{13}C NMR (101 MHz, $CDCl_3$) δ 212.15[-], 51.38[+], 28.39[-], 27.80[+], 25.82[-], 25.59[-]; IR ν (cm^{-1}) 2927, 285, 1705, 1448, 1351, 1166; TOF MS EI+ m/z: 126.1 $[M]^+$.

Analysis of 1-(cyclohex-1-en-1-yl)ethan-1-one (118c)

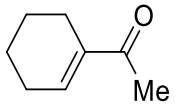

118c

Prepared following *General Procedure 11.* Yellowish oil (86mg, 69%); ^{1}H NMR (400 MHz, $CDCl_3$) δ 6.95-6.86 (m, 1H), 2.30-2.18 (m, 7H), 1.68-1.57 (m, 4H); ^{13}C NMR (101 MHz, $CDCl_3$) δ 199.30[-], 140.89[+], 139.63[-], 26.07[-], 25.12[+], 22.92[-], 21.89[-], 21.50[-] ; IR ν (cm^{-1}) 2932, 2860, 1662, 1432, 1224; TOF MS EI+ m/z: 124.1 $[M]^+$.

Analysis of acetophenone (118d)

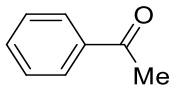

118d

Prepared following *General Procedure 11.* Pale yellow oil (70mg, 58%); ^{1}H NMR (400 MHz, $CDCl_3$) δ 7.99 (dd, *J* 8.4, 1.3, 2H, Ar*H*), 7.56 (tt, *J* 7.3, 1.3, 1H, Ar*H*), 7.45 (t, *J* 7.3, 2H, Ar*H*), 2.59 (s, 3H, C*H*$_3$); ^{13}C NMR (101 MHz, $CDCl_3$) δ 198.12[-], 137.13[-], 133.10[+], 128.57[+], 128.30[+], 26.60[+]; IR ν (cm^{-1}) 1680, 1598, 1448, 1358, 1263; TOF MS EI+ m/z: 120.1 $[M]^+$. Data are consistent with those described in the literature.[218]

Analysis of 1-(2-methylnaphthalen-1-yl)ethan-1-one (107e)

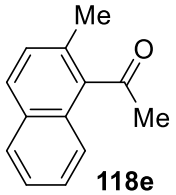

118e

Prepared following *General Procedure 11*. Colourless oil(147mg, 80%); ^{1}H NMR (400 MHz, $CDCl_3$) δ 7.82 (d, *J* 7.5, 1H), 7.76 (d, *J* 8.5, 1H), 7.60 (d, *J* 8.5, 1H), 7.50-7.42 (m, 2H), 7.29 (d, *J* 8.4, 1H), 2.62 (s, 3H), 2.43 (s, 3H); ^{13}C NMR (101 MHz, $CDCl_3$) δ 208.25[-], 138.78[-], 131.76[-], 129.94[-], 128.90[-], 128.77[+], 128.60[+], 128.29[+], 126.91[+], 125.48[+], 123.91[+], 32.93[+], 19.39[+]; IR ν (cm^{-1}) 1697, 1508, 1419, 1350, 1209; TOF MS EI+ m/z: 184.1 $[M]^+$, 169.1 $[M\text{-}CH_3]^+$.

Analysis of 4-phenylbutan-2-one (118f)

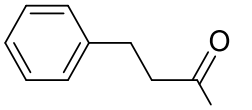

118f

Prepared following *General Procedure 11*. Colourless oil(131mg, 89%); ^{1}H NMR (400 MHz, $CDCl_3$) δ 7.32-7.25 (m, 2H) 7.23-7.16 (m, 3H), 2.90 (t, *J* 7.7, 2H), 2.76 (t, *J* 7.5, 2H), 2.14 (s, 3H, C*H*$_3$); ^{13}C NMR (101 MHz, $CDCl_3$) δ 207.9[-], 141.0[-], 128.5[+], 128.3[+], 126.1[+], 45.2[-], 30.1[+], 29.8[-]; IR ν (cm^{-1}) 2924, 1714, 1496, 1357, 1161; TOF MS EI+ m/z: 148.1 $[M]^+$. Data are consistent with those described in the literature.[217]

Analysis of 1-(4-methoxyphenyl)ethan-1-one (118g) [218]

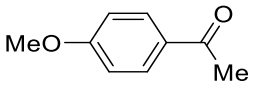

118g

Prepared following *General Procedure 11.* Yellow solid(132mg, 88%)(literature reported as yellow oil); ^{1}H NMR (400 MHz, $CDCl_3$) δ 7.92 (d, *J* 9.0, 2H, Ar*H*), 6.91 (d, *J* 8.9, 2H, Ar*H*), 3.84 (s, 3H, OC*H*$_3$), 2.53 (s, 3H, C*H*$_3$); ^{13}C NMR (101 MHz, $CDCl_3$) δ 196.7[-],

163.4[-], 130.5[+], 130.2[-], 113.6[+], 55.4[+], 26.3[+]; IR ν (cm^{-1}) 1671, 1597, 1509, 1459, 1417, 1356, 1247, 1169; TOF MS EI+ m/z: 150.1 $[M]^+$.

Analysis of 1-(4-(4,4,5,5-tetramethyl-1,3,2-dioxaborolan-2-yl)phenyl)ethan-1-one (118h)

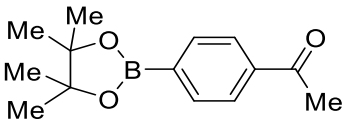

118h

Prepared following *General Procedure 11.* White solid (199mg, 81%); ^{1}H NMR (400 MHz, $CDCl_3$) δ 7.93 (d, *J* 8.4, Ar*H*), 7.89 (d, *J* 8.4, Ar*H*), 2.61 (s, 3H, C*H*$_3$), 1.36 (s, 12H, C(C*H*$_3$)$_2$); ^{13}C NMR (101 MHz, $CDCl_3$) δ 198.5[-], 139.0[-], 134.9[+], 127.3[+], 84.2[-], 26.8[+], 24.9[+]; IR ν (cm^{-1}) 2979, 1686, 1507, 1397, 1356, 1265; TOF MS EI+ m/z: 246.2 $[M]^+$.

Analysis of 1-(thiophen-3-yl)ethan-1-one (107i)

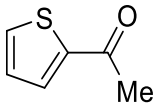

118i

Prepared following *General Procedure 11.* White solid (76mg 61%); ^{1}H NMR (400 MHz, $CDCl_3$) δ 8.31 (dd, *J* 2.9, 1.3, 1H), 7.54 (dd, *J* 5.1, 1.3, 1H), 7.31 (dd, *J* 5.1, 2.9), 2.53 (s, 3H, C*H*$_3$); ^{13}C NMR (101 MHz, $CDCl_3$) δ 192.3[-], 142.6[-], 132.4[+], 132.4[+], 127.0[+], 126.4[+], 27.6[+]; IR ν (cm^{-1}) 3103, 1667, 1510, 1410, 1352, 1254; TOF MS ES+ m/z: 126.0 $[M]^+$

Analysis of 3-methyl-3-(2-oxopropyl)indolin-2-one (118j)

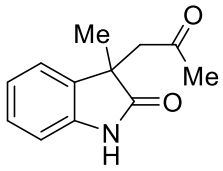

118j

Prepared following *General Procedure 11.* White solid (54mg, 27%); m.p. 150-152 °C; ^{1}H NMR (400 MHz, $CDCl_3$) δ 7.96 (brs, 1H, N*H*), 7.18 (td, *J* 7.7, 1.3, 1H, Ar*H*), 7.12 (dt, *J* 7.4, 0.6, 1H, Ar*H*), 6.99 (td, *J* 7.5, 1.0, 1H, Ar*H*), 6.90 (d, *J* 7.7, 1H, Ar*H*), 3.12 (ABq, *J* 17.8, 2H, CH_2), 2.02 (s, 3H, COCH_3), 1.35 (s, 3H, CCH_3); ^{13}C NMR (101 MHz, $CDCl_3$) δ 204.7[-], 182.1[-], 140.7[-], 133.9[-], 127.9[+], 122.3[+], 122.2[+], 109.9[+], 50.4[-], 45.6[-], 30.0[+], 24.6[+]; IR ν (cm^{-1}) 1709, 1620, 1472, 1196; TOF MS EI+ m/z: 203.1 $[M]^+$; HRMS calc. $[C_{12}H_{13}NO_2]^+$ 203.0940, obs. 203.0945.

Analysis of 1-benzyl-3-methyl-3-(2-oxopropyl)indolin-2-one (118k)

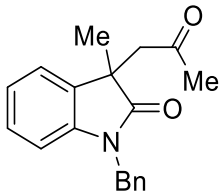

118k

Prepared following *General Procedure 11.* White solid (249mg, 85%); m.p. 115-117 °C; ^{1}H NMR (400 MHz, $CDCl_3$) δ 7.39 (d, *J* 7.6, 2H), 7.33 (t, *J* 7.3, 2H), 7.24(t, *J* 7.1, 1H), 7.15-7.08 (m, 2H), 6.96 (td, *J* 7.5, 1.0, 1H), 6.69, (d, *J* 7.8, 1H), 4.97 (ABq, *J* 15.9, 2H, PhCH_2), 3.16 (ABq, *J* 17.8, 2H, CH_2CO), 2.01 (s, 3H, COCH_3), 1.39 (s, 3H, CCH_3); ^{13}C NMR (101 MHz, $CDCl_3$) δ 204.5[-], 180.4[-], 142.8[-], 136.2[-], 133.5[-], 128.7[+], 127.8[+], 127.4[+], 127.3[+], 122.3[+], 121.8[+], 109.4[+], 50.4[-], 45.3[-], 44.0[-], 30.0[+], 25.1[+]; IR ν (cm^{-}

[1]) 1704, 1611, 1489, 1355, 1176; TOF MS EI+ m/z: 293.2 $[M]^+$; HRMS calc. $[C_{19}H_{19}NO_2]^+$ 293.1410, obs. 293.1417.

Analysis of tert-butyl 3-methyl-2-oxo-3-(2-oxopropyl)indoline-1-carboxylate (118l)

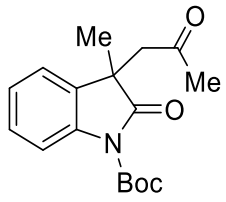

118l

Prepared following *General Procedure 11.* White solid (91mg, 30%); ^{1}H NMR (400 MHz, $CDCl_3$) δ 7.88 (d, *J* 8.2, 1H), 7.30-7.24 (m, 1H), 7.13-7.08 (m, 2H), 3.17 (ABq, *J* 17.8, 2H), 2.00 (s, 3H, COC*H*$_3$), 1.66 (s, 9H, C(C*H*$_3$)$_3$), 1.36 (s, 3H, CC*H*$_3$);^{13}C NMR (101 MHz, $CDCl_3$) δ 204.2[-], 178.9[-], 149.5[-], 139.7[-], 132.4[-], 128.1[+], 124.2[+], 121.3[+], 115.4[+], 84.1 [-], 51.6[-], 45.5[-], 29.7[+], 28.2[+], 25.6[+]; IR ν (cm^{-1}) 1764, 1717, 1601, 1480, 1297, 1148. TOF MS ES+ m/z: 326.1 $[M+Na]^+$; HRMS calc. $[C_{17}H_{21}NO_4Na]^+$ 326.1363, obs. 326.1368.

Analysis of 3,3-dimethoxy-1-phenylpropan-1-one (118m')

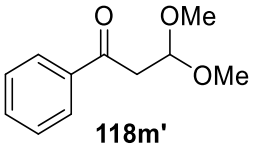

118m'

Prepared following *General Procedure 11.* Light yellow oil (182mg, 94%); ^{1}H NMR (400 MHz, $CDCl_3$) δ 7.95 (d, *J* 8.5, 2H), 7.59 (tt, *J* 7.3, 1.3, 1H), 7.46 (t, *J* 7.6, 2H), 5.01 (t, *J* 5.5, 1H, CH_2CH), 3.41 (s, 6H, OC*H*$_3$), 3.28 (d, *J* 5.5, 2H, C*H*$_2$CH); ^{13}C NMR (101 MHz, $CDCl_3$) δ

196.9[-], 137.1[-], 133.3[+], 128.6[+], 128.3[+], 102.2[+], 54.2[+], 42.6[-]; IR ν (cm^{-1}) 2935, 1683, 1597, 1448, 1186, 1118; TOF MS EI+ m/z: 194.1 $[M]^+$, 179.1 $[M\text{-}CH_3]^+$.

6.4Experimental for Chapter 4

Synthesis of 1-Azido-2-methylnaphthalene (125)

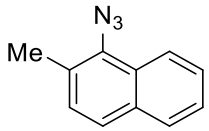

125

Prepared following *General Procedure 1* on a 5 mmol scale. Orange oil (583 mg, 63% yield); ^{1}H NMR (400 MHz, $CDCl_3$) δ 8.16 (d, *J* 8.6, 1H), 7.78 (d, *J* 8.0, 1H), 7.63 (d, *J* 8.4, 1H), 7.56-7.51 (m, 1H), 7.49-7.45 (m, 1H), 7.28 (d, *J* 8.4, 1H), 2.58 (s, 3H); ^{13}C NMR (101 MHz, $CDCl_3$) δ 133.19 [-], 133.30 [-], 129.24[+], 128.71[-], 128.24[-], 127.94[+], 126.60[+], 125.95[+], 125.76[+], 122.50[+], 18.09[+]; IR ν (cm^{-1}) 3053, 2102, 1598, 1506, 1449, 1371, 1340, 1281;TOF MS EI+ m/z: 183 $[M]^+$;

Synthesis of 1-(2-methylnaphthalen-1-yl)-1H-1,2,3-triazole (126)

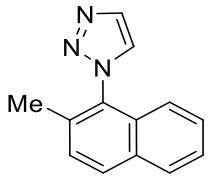

126

Prepared following *General Procedure 3* on a 3.2 mmol scale. Light red solid (430 mg, 64% yield); m.p. 112-113 °C; ^{1}H NMR (400 MHz, $CDCl_3$) δ 8.01 (d, *J* 1.0, 1H), 7.94 (d, *J* 8.5, 1H), 7.90 (d, *J* 7.4, 1H), 7.80 (d, *J* 1.0, 1H), 7.53-7.43 (m, 3H), 7.01 (d, *J* 8.6, 1H), 2.20

(s, 3H); ^{13}C NMR (101 MHz, $CDCl_3$) δ 133.79[+], 133.50[-], 132.42[-], 130.52[-], 130.22[+], 128.24[+], 127.87[+], 126.47[+], 126.16[+], 121.72[+], 17.60[+] (11 of 13 expected signals observed). IR ν (cm^{-1}) 31244, 1599, 1510, 1449, 13731228; TOF MS EI+ m/z: 209.1 $[M]^+$, HR-MS calc. $[C_{13}H_{11}N_3]^+$209.0947, obs. 209.0946.

Synthesis of Rac-5-(Di-tert-butylphosphanyl)-1-(2-methylnaphthalen-1-yl)-1H-1,2,3-triazole(127a)

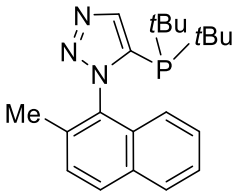

rac-127a

Prepared following *General Procedure 4* on a 0.5 mmol scale. White solid (104 mg, 65% yield); White solid; m.p. 134-136 °C; ^{1}H NMR (300 MHz, $CDCl_3$) δ 8.22 (s, 1H), 7.93 (d, *J* 8.5, 1H), 7.86 (d, *J* 7.7, 1H), 7.48-7.41 (m, 2H), 7.40-7.33 (m, 1H), 6.87 (d, *J* 8.5, 1H), 2.21 (s. 3H), 1.19 (d, *J* 12.3, 9H), 1.04 (d, *J* 12.3, 9H); ^{31}P{H} NMR (121 MHz, $CDCl_3$) δ 2.57; ^{13}C NMR (101 MHz, $CDCl_3$) δ 139.03 (d, $^2J_{CP}$ 5.8), 136.86 (d, $^1J_{CP}$ 35.4), 133.98, 132.31, 131.65, 131.16, 130.17, 128.21, 127.75, 126.90, 125.86, 123.42, 32.70 (d, $^1J_{CP}$ 19.6), 32.60 (d, $^1J_{CP}$ 19.6), 30.64 (d, $^2J_{CP}$ 14.7), 30.55 (d, $^2J_{CP}$ 14.6), 19.26, 19.23; IR ν (cm^{-1}) 2940, 2898, 2863, 1473, 1406, 1365; TOF MS ES+ m/z: 354.21 $[M+H]^+$, HR-MS calc. $[C_{20}H_{25}N_3O_2P]^+$ 354.2094, obs. 354.2102.

Synthesis of Rac-5-(Diphenylphosphanyl)-1-(2-methylnaphthalen-1-yl)-1H-1,2,3-triazole (127b)

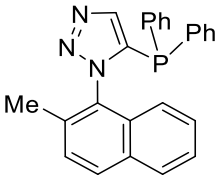

rac-127b

Prepared following *General Procedure 4* on a 1 mmol scale. White solid (256 mg, 65% yield); m.p. 141-143 °C; ^{1}H NMR (400 MHz, $CDCl_3$) δ 7.88 (d, *J* 8.4, 1H), 7.81 (d, *J* 8.2, 1H), 7.70 (d, *J* 0.7, 1H), 7.41-7.16 (m, 13H), 6.72 (d, *J* 8.5, 1H), 1.97 (s, 3H); ^{31}P{H} NMR (121 MHz, $CDCl_3$) δ -36.91; ^{13}C NMR (101 MHz, $CDCl_3$) δ 139.25, 138.98, 138.81, 134.36, 133.65, 133.58, 133.53, 133.44, 133.411, 133.37, 133.34, 132.28, 130.91, 130.62, 130.43, 129.68, 129.54, 128.83, 128.75, 128.64, 128.57, 128.05, 127.69, 127.40, 125.86, 122.01, 17.79, 17.76. (complexity observed due to the phosphine coupling and diastereotopic carbon); IR ν (cm^{-1}) 3053, 1600, 1508, 1479, 1435, 1415; TOF MS EI+ m/z: 394.15 $[M+H]^+$; 416.13 $[M+Na]^+$, HR-MS calc. $[C_{25}H_{21}N_3P]^+$ 394.1468, obs. 394.1478

Synthesis of Rac-5-(Diisopropylphosphanyl)-1-(2-methylnaphthalen-1-yl)-1H-1,2,3-triazole (127c)

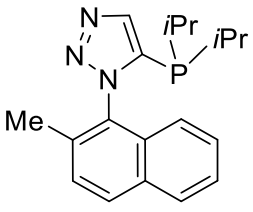

rac-127c

Prepared following *General Procedure 4* on a 0.5 mmol scale. Obtained as white solid (68 mg, 42% yield); m.p. 104-106 °C; ^{1}H NMR (400 MHz, $CDCl_3$) δ 8.00 (s, 1H), 7.94 (d, *J*

8.5, 1H), 7.87 (d, *J* 8.0, 1H), 7.48-7.44 (m, 2H), 7.42-7.37 (m, 1H), 6.88 (d, *J* 8.4, 1H), 2.19 (s, 3H), 2.14 (sept, d, *J* 7.0, 2.7$_{(HP)}$, 1H), 1.88 (sept, d, *J* 7.1, 1.2$_{(HP)}$, 1H), 1.10-0.97 (m, 9H), 0.75 (dd, *J* 15.3$_{(HP)}$, 7.1, 3H); ^{31}P{H} NMR (121 MHz, $CDCl_3$) δ -20.42; ^{13}C NMR (101 MHz, $CDCl_3$) δ 138.46 (d, $^2J_{CP}$ 5.3), 136.78 (d, $^1J_{CP}$ 28.0), 133.79, 132.35, 131.35, 131.00, 130.26, 128.16, 127.84, 127.26, 125.95, 122.65, 23.80 (d, $^1J_{CP}$ 10.8), 23.59 (d, $^1J_{CP}$ 9.1), 19.81 (pseudo t, *J* 11.2), 19.58 (d, $^2J_{CP}$ 8.7), 19.18 (d, $^2J_{CP}$ 7.7), 18.54, 18.50; IR ν (cm^{-1}) 2954, 295, 2866, 1601, 1509, 1460, 1411, 1383, 1279, 1224; TOF MS EI+ m/z: 326.18 $[M+H]^+$, 348.16 $[M+Na]^+$, HR-MS calc. $[C_{19}H_{25}N_3P]^+$ 326. 1781, obs. 326.1785.

Synthesis of chloro[(S)-5-(Di-tert-butylphosphanyl)-1-(2-methylnaphthalen-1-yl)-1H-1,2,3-triazole]gold(I) (S)-128

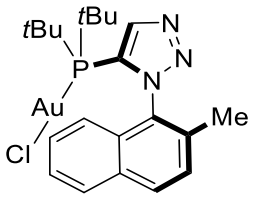

(S)-**128**

Prepared following *General Procedure 10* on a 0.43 mmol scale. White solid (208mg, 82%); m.p. 276 °C (decom.); ^{1}H NMR (500 MHz, $CDCl_3$) δ 8.36 (s, 1H), 8.14 (d, *J* 8.5, 1H), 7.96 (d, *J* 8.2, 1H), 7.52-7.47 (m, 2H), 7.38-7.33 (m, 1H), 6.65 (d, *J* 8.4, 1H), 2.18 (s, 3H), 1.41 (d, *J* 16.8, 9H), 1.31 (d, *J* 16.8, 9H); ^{31}P[H] NMR (202 MHz, $CDCl_3$) δ 46.72; ^{13}C NMR (126 MHz, $CDCl_3$) δ 139.0 (d, $^2J_{CP}$ 6.2, triazole *C*-4), 135.0, 132.8, 131.9, 131.2, 130.3, 128.7 (d, $^1J_{CP}$ 44.5), 128.8, 128.5, 127.2, 126.3, 121.9, 37.9 (d, $^1J_{CP}$ 28.1), 37.6 (d, $^1J_{CP}$ 28.0, , 30.5 (d, $^2J_{CP}$ 6.7), 30.3 (d, $^2J_{CP}$ 6.7), 19.1; IR ν (cm^{-1}) 2959, 1601, 1508, 1473, 1402, 1370, 1278; $[\alpha]_D^{25}$ +63.1° ($CHCl_3$, c 0.5 gdm^{-3}). Identity confirmed and absolute

configuration determined by single crystal XRD structure determination. Flack parameter -0.034(4).

Synthesis of Rac-5-(tert-butyl(phenyl)phosphanyl)-1-(2,6-dimethoxyphenyl)-1H-1,2,3-triazole (130)

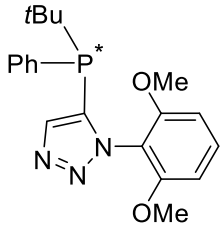

rac-**130**

Prepared following *General Procedure 4* on a 1 mmol scale. Obtained as white solid (151 mg, 74% yield); ^{1}H NMR (400 MHz, $CDCl_3$) δ 8.23 (d, *J* 0.5, 1H), 7.39 -7.26 (m, 6H), 6.67 (dd, *J* 8.5, 0.8), 6.42 (dd, *J* 8.6, 0.8) 3.78 (s, 3H), 3.09 (s, 3H), 1.10 (d, *J* 13.5, 9H); ^{31}P{H} NMR (162 MHz, $CDCl_3$) δ -14.53; ^{13}C NMR (101 MHz, $CDCl_3$) δ 156.22 (d, J_{CP} 10.1), 137.84 (d, J_{CP} 4.4), 135.02 (d, J_{CP} 19.4), 134.31 (d, J_{CP} 21.1), 133.23 (d, J_{CP} 15.0), 131.56, 128.78, 127.78 (d, J_{CP} 7.87), 114.76, 104.09, 103.57, 56.04, 55.02, 30.30 (d, J_{CP} 9.8), 28.03 (d, J_{CP} 15.3); IR ν (cm^{-1}) 2940, 1600, 1483, 1434, 1261, 1113; TOF MS ES+ m/z: 370.17 $[M+H]^+$, 392.15 $[M+Na]^+$ HR-MS calc. $[C_{20}H_{25}N_3O_2P]^+$ 370.1679, obs. 370.1686.

Synthesis of chloro[(S)-5-(tert-butyl(phenyl)phosphanyl)-1-(2,6-dimethoxyphenyl)-1H-1,2,3-triazole]gold(I)-131

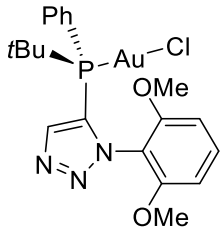

(*S*)-**131**

Prepared following *General Procedure 10* on a 0.27 mmol scale. White solid (152mg, 94%); m.p. 180-182 °C; ^{1}H NMR (400 MHz, $CDCl_3$) δ 8.41 (s,1H), 7.61-7.42 (m, 6H), 6.75 (dd, *J* 8.6, 0.9), 6.38 (dd, *J* 8.6, 0.9) 3.85 (s, 3H), 2.95 (s, 3H), 1.34(d, *J* 18.2, 9H); ^{31}P NMR (162 MHz, $CDCl_3$) δ 30.2; ^{13}C NMR (126 MHz, $CDCl_3$) δ 156.3, 155.9, 138.3 (d, J_{CP} 5.0), 135.1 (d, J_{CP} 14.4), 133.0, 132.2 (d, J_{CP} 2.8), 128.6 (d, J_{CP} 12.1), 126.5 (d, J_{CP} 63.1), 125.3 (d, J_{CP} 57.9), 113.1, 105.4, 103.5, 56.1, 54.8, 34.5 (d, *J* 36.9), 27.8 (d, *J* 7.5); IR ν (cm^{-1}) 2967, 1600, 1484, 1436, 1263, 1113; $[\alpha]_D^{25}$ +25.7° (0.5 in $CHCl_3$); Identity confirmed and absolute configuration determined by single crystal XRD structure determination. Flack parameter -0.050(5).

Synthesis of 1-(2,6-dimethoxyphenyl)-5-((11bS)-dinaphtho[2,1-d:1',2'-f][1,3,2]dioxaphosphepin-4-yl)-1H-1,2,3-triazole [(S)-132]

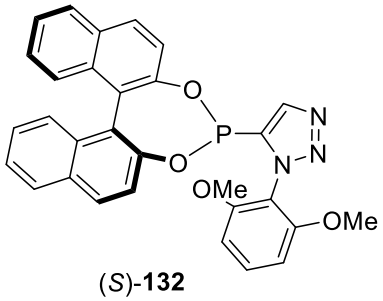

(*S*)-**132**

Prepared following *General Procedure 4* on a 0.57 mmol. White solid (77 mg, 26%); mp. 116 - 121 °C; ^{1}H NMR (400 MHz, $CDCl_3$) δ 7.99 (d, *J* 8.9, 1H, Ar*H*), 7.93 (t, *J* 7.0, 2H, Ar*H*), 7.83 (d, *J* 8.7, 1H, Ar*H*), 7.52-7.28 (m, 8H, Ar*H*), 7.15 (d, *J* 0.7, 1H, Ar*H*), 6.92 (d, *J* 8.9, 1H, Ar*H*), 6.74 (t, *J* 7.6, 2H, Ar*H*), 3.95 (s, 3H, CH_3), 3.82 (s, 3H, CH_3); ^{31}P NMR (121 MHz, $CDCl_3$) δ +161.12; ^{13}C NMR (101 MHz, $CDCl_3$) 155.98,155.94, 149.05, 148.22 (d, $^{2}J_{CP}$ 5.6), 137.91 (d, $^{1}J_{CP}$ 49.2), 136.43, 132.80, 132.42, 132.10, 131.73, 131.35, 130.83, 130.00, 128.55, 128.46, 127.48, 126.90, 126.83, 126.49, 126.36, 125.30, 125.21, 124.94, 124.89, 124.02, 123.43, 121.65, 120.97, 114.10, 104.56, 104.15, 56.26, 56.12; IR ν (cm^{-1}) 3059, 2926, 1600, 1484, 1261.5, 1226.9, 1112.5, 949.9; TOF MS EI+ m/z: 520.19 $[M]^+$, 552.22 $[M+MeOH]^+$; HRMS calc. $[C_{30}H_{23}N_3O_4P]^+$ 520.1426, obs. 520.1428, $[C_{31}H_{27}N_3O_5P]^+$ 552.1688, obs. 552.1689

Synthesis of chloro[1-(2,6-dimethoxyphenyl)-5-((11bS)-dinaphtho[2,1-d:1',2'-f][1,3,2]dioxaphosphepin-4-yl)-1H-1,2,3-triazole] [(S)-133]

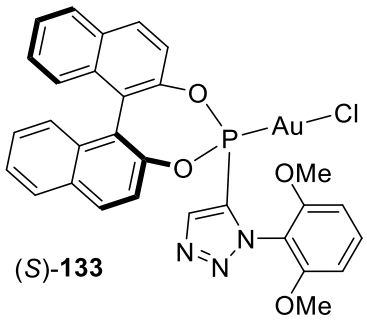

(*S*)-**133**

Prepared following *General Procedure 10* on a 0.11 mmol scale. white solid (71mg, 87%); m.p. 253-255 °C; ^{1}H NMR (400 MHz, $CDCl_3$) δ 8.11 (d, *J* 8.9, 1H, Ar*H*), 8.00 (d, *J* 8.3, 1H, Ar*H*), 7.98 (d, *J* 8.2, 1H, Ar*H*), 7.93 (d, *J* 8.9, 1H, Ar*H*), 7.64-7.60 (m, 2H, Ar*H*), 7.59-7.53 (m, 2H, Ar*H*), 7.46-7.34 (m, 5H, Ar*H*), 7.01 (dd, *J* 8.8, 1.0, 1H, Ar*H*), 6.82 (d, *J* 8.6, 1H,

Ar*H*), 6.80 (t, *J* 8.6, 1H, Ar*H*), 3.99 (s, 3H, OCH_3), 3.88 (s, 3H, OCH_3); ^{31}P NMR (161 MHz, $CDCl_3$) δ +133.44; ^{13}C NMR δ *due to restricted rotation and ^{31}P coupling, aromatic signals are not fully assigned yet, more detailed assignment to follow* 156.4, 156.1, 146.4, 146.3, 146.0 (d, $^1J_{CP}$ 13.1), 138.9 (d, $^2J_{CP}$ 9.2), 133.5, 132.4, 132.4, 132.4, 132.2, 132.0, 131.3, 130.9, 128.8, 128.8, 127.3, 127.3, 127.0, 126.9, 126.4, 123.4 (d, J_{CP} 3.5) 122.8 (d, J_{CP} 3.8), 120.1, 120.0, 112.9 (*C*COCH$_3$), 105.5, 104.3, 56.3, 56.3; IR ν (cm^{-1}) 1600, 1484, 1263, 1218, 1112; $[\alpha]_D^{25}$ +76.5° (0.5 in $CHCl_3$). Absolute configuration was confirmed by single crystal XRD structure determination. Flack parameter -0.038(3).

Synthesis of 5,5'-(((2'-(dinaphtho[2,1-d:1',2'-f][1,3,2]dioxaphosphepin-4-yloxy)-[1,1'-binaphthalen]-2-yl)oxy)phosphanediyl)bis(1-(2,6-diisopropylphenyl)-1H-1,2,3-triazole) [(S,S)-135

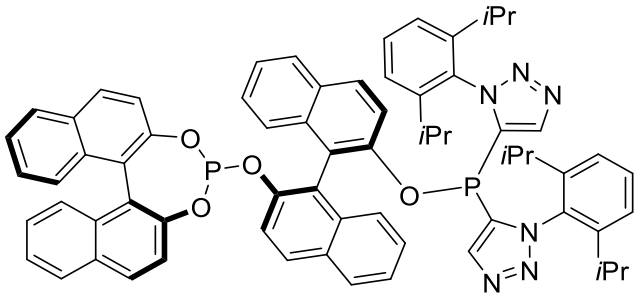

(*S*,*S*)-**135**

Prepared following *General Procedure 4* on a 0.57 mmol. Obtained as a white solid (177 mg, 56%); m.p. 285 °C (decom.); ^{1}H NMR (400 MHz, $CDCl_3$) δ; 8.02-7.89 (m, 4H, Ar*H*), 7.85-7.82 (m, 2H, Ar*H*), 7.63 (d, *J* 9.0, 2H, Ar*H*), 7.55 (t, *J* 7.8, 1H, Ar*H*), 7.50-7.41 (m, 3H, Ar*H*), 7.40-7.33 (m, 3H, Ar*H*), 7.30-7.27 (m, 2H, Ar*H*), 7.25-7.16 (m, 8H, Ar*H*), 7.05 (m, 2H, Ar*H*), 6.87-6.85 (m, 2H, Ar*H*), 6.79 (dd, *J* 3.0, 1H, Ar*H*), 6.74 (s, 1H, Ar*H*), 5.72 (dd, *J* 3.8, 1H, Ar*H*), 1.82 (sept, *J* 6.5, 1H, C*H*(CH$_3$)$_2$), 1.76 (sept, *J* 6.5, 1H, C*H*(CH$_3$)$_2$), 1.67 (sept,

J 6.5, 1H, C*H*(CH_3)$_2$), 1.59 (sept, *J* 6.8, 1H, C*H*(CH_3)$_2$), 1.01 (d, *J* 6.8, 3H, C*H*$_3$), 0.93 (d, *J* 6.8, 3H, C*H*$_3$), 0.90-0.86 (m, 6H, (C*H*$_3$)$_2$), 0.74 (d, *J* 6.8, 3H, C*H*$_3$), 0.59 (d, *J* 6.8, 3H, C*H*$_3$), 0.57 (d, *J* 6.8, 3H, C*H*$_3$), 0.44 (d, *J* 6.8, 3H, C*H*$_3$); ^{31}P NMR (121 MHz, $CDCl_3$) δ +140.91, +58.26; ^{13}C NMR (101 MHz, $CDCl_3$) Not assigned due to complexity of product 151.62, 151.47, 148.03, 147.49, 147.44, 147.33, 146.69, 146.58, 146.30, 146.09, 138.75, 138.40, 136.18, 136.11, 135.92, 135.83, 133.81, 133.45, 132.65, 132.47, 131.47, 131.39, 131.29, 131.18, 131.09, 130.58, 130.43, 130.20, 130.02, 129.77, 129.64, 128.37, 128.22, 128.08, 127.85, 127.18, 126.92, 126.41, 126.36, 126.23, 125.98, 125.36, 125.28, 125.10, 124.85, 124.53, 124.32, 124.15, 124.10, 123.82, 123.42, 122.34, 121.62, 121.47, 121.33, 121.22, 118.13, 117.94, 28.95, 28.34, 28.00, 25.68, 25.60, 25.43, 24.66, 22.31, 21.68, 21.57; IR ν (cm^{-1}) 3068, 2964, 1587, 1506, 1463, 1209, 973, 951, 931; TOF MS EI+ m/z: 1125.42 $[M+K]^+$; HRMS calc. $[C_{68}H_{60}N_6O_4P_2K]^+$ 1125.3788, obs. 1125.3787. Absolute configuration was confirmed by single crystal XRD structure determination. Flack parameter 0.02(3).

7. Appendix 2 Crystal structure data

The datasets were measured on an Agilent SuperNova diffractometer using an Atlas detector. The data collections were driven and processed and absorption corrections were applied using CrysAlisPro.[219] The structures of **76a**, **106**, **93g, 110b, 110c** were solved using ShelXS[220] while **75a, 107, 109a, 109b, 110a, 110g, 112a, 112b, 113a, 113b, 114, 115, 116, *rac*-127a, *rac*-127b, *(R)*-127a, *(R)*-128, *(S)*-128, 129, (*R*)-131, *(S)*-133, *(S,S)*-135** were solved using ShelXT.[221] All structures were refined by a full-matrix least-squares procedure on F^2 in ShelXL.[222] All non-hydrogen atoms were refined with anisotropic displacement parameters. All hydrogen atoms were added at calculated positions and refined by use of a riding model with isotropic displacement parameters based on the equivalent isotropic displacement parameter (U_{eq}) of the parent atom. Reports were produced using OLEX2.[223]

The CIFs for **75a**, **76a**, **93g**, **106** and **107** have been deposited with the CCDC and have been given the deposition numbers CCDC 1856208-1856212 respectively. The CIFs for **109b, 109a, 110a, 112b, 112a, 113b, 113a, 114, 115, 116** have been deposited with the CCDC and have been given the deposition numbers 1922101-1922110 respectively. These numbers contain the supplementary crystallographic data for this paper. These data can be obtained free of charge from The Cambridge Crystallographic Data Centre *via* www.ccdc.cam.ac.uk/data_request/cif.

*Crystal structure of **75a***

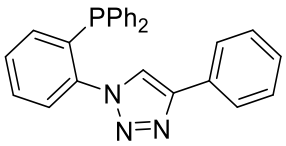

75a

$C_{26}H_{20}N_3P$ (M= 405.42 g/mol): Triclinic, space group P-1 (no. 2), *a*= 7.3987(2)Å, *b*= 15.1176(7)Å, *c*= 19.3877(9)Å, *α*= 71.909(4), *β*= 87.593(3), *γ*= 85.945(3), *V*= 2055.70(15)Å^3, *Z*= 4, *T*= 100.01(10) K, μ(MoKα)= 0.152 mm^{-1}, *Dcalc*= 1.310g/cm^3, 21339 reflections measured (5.422° ≤ 2Θ ≤ 59.096°), 9782 unique (R_{int} = 0.0230, R_{sigma} = 0.0376) which were used in all calculations. The final R_1 was 0.0440 (I > 2σ(I)) and wR_2 was 0.1106 (all data). This structure has been published previously by Choubey *et al.* from a twinned dataset (two domains related by 180° about unit cell axis *a*) measured at 150 K.[108] The structure presented here is refined from a dataset measured at 100 K from a single crystal.

*Crystal structure of **76a***

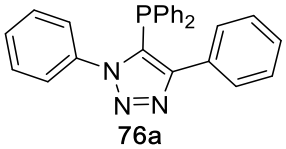

76a

$C_{26}H_{20}N_3P$ (*M*= 405.42 g/mol): Monoclinic, space group $P2_1/c$ (no. 14), *a*= 13.3005(6)Å, *b*= 11.1770(4)Å, *c*= 14.6857(6)Å, *β*= 108.847(5)°, *V*= 2066.13(16)Å^3, *Z*= 4, *T*= 100.01(10)K, μ(MoKα)= 0.151 mm^{-1}, *Dcalc*= 1.303g/cm^3, 10700 reflections measured (6.774° ≤ 2Θ ≤ 52.742°), 4217 unique (R_{int} = 0.0256, R_{sigma} = 0.0332) which were used in all calculations. The final R_1 was 0.0387 (I > 2σ(I)) and wR_2 was 0.0896 (all data). The

substituted nitrogen atom and the opposite carbon of the triazole ring (N(1), C(2) and N(1'), C(2')) are disordered such that the ring occupies two opposing orientations, related by a 180° rotation about an axis through C(1) and the midpoint of the N(2)-N(3) bond. The refined percentage occupancy ratio of the two positions are 59.7 (15): 40.3 (15). Rings C(3)-C(8) and C(21)-C(26) form an intermolecular π-π stacking interaction with the angle between the planes being 13.9° and the perpendicular distance from the first ring to the centroid of the latter being 3.5 Å. This structure has been published previously by Choubey *et al.* from a dataset also measured at 100 K with no disorder in the triazole ring modelled (although inspection of the relevant anisotropic thermal parameters indicate that it may also be possible to model disorder of this nature in that structure).[108]

*Crystal structure of **93g***

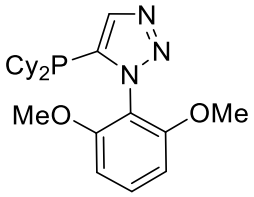

93g

$C_{22}H_{32}N_3O_2P$ (M=401.47 g/mol): Monoclinic, space group $P2_1/n$ (no. 14), *a*= 10.7237(2)Å, *b*= 18.9356(3)Å, *c*= 10.8968(2)Å, *β*= 90.5390(10)°, *V*= 2212.60(7)Å^3, *Z*= 4, *T*= 100.01(10)K, μ(CuKα)= 1.267 mm^{-1}, *Dcalc*= 1.205g/cm^3, 8826 reflections measured (9.342° ≤ 2Θ ≤ 144.238°), 4287 unique (R_{int} = 0.0217, R_{sigma} = 0.0266) which were used in all calculations. The final R_1 was 0.0337 (I > 2σ(I)) and wR_2 was 0.0893 (all data).

*Crystal structure of **106***

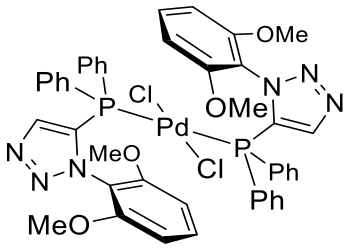

106

$C_{44}H_{40}Cl_2N_6O_4P_2Pd$, $2(CH_2Cl_2)$ (*M*=1125.91 g/mol): Monoclinic, space group $P2_1/n$ (no. 14), *a*= 12.4148(3)Å, *b* = 13.3900(3)Å, *c*= 14.0922(3)Å, *β*= 92.115(2)°, *V*= 2341.03(10)Å^3, *Z*= 2, *T*= 100.01(10)K, μ(MoKα)= 0.859 mm^{-1}, *Dcalc*= 1.597g/cm^3, 10705 reflections measured (6.538° ≤ 2Θ ≤ 51.358°), 4433 unique (R_{int} = 0.0260, R_{sigma} = 0.0365) which were used in all calculations. The final R_1 was 0.0437 (I > 2σ(I)) and wR_2 was 0.1279 (all data).

*Crystal structure of **107***

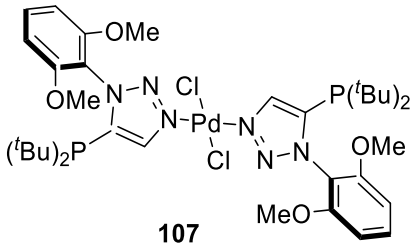

107

$C_{36}H_{56}Cl_2N_6O_4P_2Pd$, $2(CH_2Cl_2)$ (M=1045.96 g/mol): Triclinic, space group P-1 (no. 2), *a*= 8.44710(10)Å, *b*= 12.2836(2)Å, *c*= 24.1667(4)Å, *α*= 93.8190(10)°, *β*= 98.2470(10)°, *γ*= 106.000(2)°, *V*= 2370.60(7)Å^3, *Z*= 2, *T*= 100.00(10)K, μ(CuKα)= 7.265 mm^{-1}, *Dcalc*= 1.465g/cm^3, 44055 reflections measured (7.534° ≤ 2Θ ≤ 140.148°), 9007 unique (R_{int} = 0.0360, R_{sigma} = 0.0228) which were used in all calculations. The final R_1 was 0.0338 (I > 2σ(I)) and wR_2 was 0.0859 (all data).

*Crystal structure of **109a***

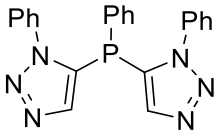

109a

$C_{22}H_{17}N_6P$ (*M* =396.38 g/mol): triclinic, space group P-1 (no. 2), *a* = 8.8796(11) Å, *b* = 10.1744(12) Å, *c* = 11.6292(13) Å, *α* = 74.241(10)°, *β* = 75.180(10)°, *γ* = 87.296(10)°, *V* = 977.2(2) Å^3, *Z* = 2, *T* = 100.00(10) K, μ(MoKα) = 0.162 mm^{-1}, *Dcalc* = 1.347 g/cm^3, 7802 reflections measured (6.762° ≤ 2Θ ≤ 52.742°), 3983 unique (R_{int} = 0.0301, R_{sigma} = 0.0495) which were used in all calculations. The final R_1 was 0.0481 (I > 2σ(I)) and wR_2 was 0.1300 (all data).

*Crystal structure of **109b***

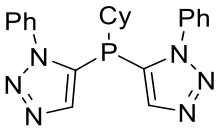

109b

$C_{22}H_{23}N_6P$ (*M* =402.43 g/mol): monoclinic, space group $P2_1/n$ (no. 14), *a* = 8.5878(6) Å, *b* = 30.5588(18) Å, *c* = 8.7236(7) Å, *β* = 115.922(9)°, *V* = 2059.0(3) Å^3, *Z* = 4, *T* = 100.01(10) K, μ(CuKα) = 1.343 mm^{-1}, *Dcalc* = 1.298 g/cm^3, 7580 reflections measured (11.584° ≤ 2Θ ≤ 143.892°), 3925 unique (R_{int} = 0.0346, R_{sigma} = 0.0518) which were used in all calculations. The final R_1 was 0.0467 (I > 2σ(I)) and wR_2 was 0.1327 (all data).

*Crystal structure of **110a***

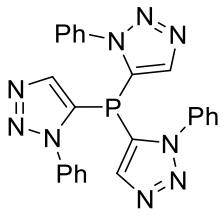

110a

$C_{24}H_{18}N_9P$, (CH_3COCH_3) (M =521.52 g/mol): triclinic, space group P-1 (no. 2), a = 10.2901(4) Å, b = 10.5099(5) Å, c = 13.7597(7) Å, α = 101.908(4)°, β = 110.581(4)°, γ = 93.969(4)°, V = 1346.71(11) Å^3, Z = 2, T = 100.01(10) K, μ(MoKα) = 0.140 mm^{-1}, Dcalc = 1.286 g/cm^3, 10967 reflections measured (5.394° ≤ 2Θ ≤ 59.17°), 6298 unique (R_{int} = 0.0248, R_{sigma} = 0.0448) which were used in all calculations. The final R_1 was 0.0454 (I > 2σ(I)) and wR_2 was 0.1080 (all data).

*Crystal structure data of **110b***

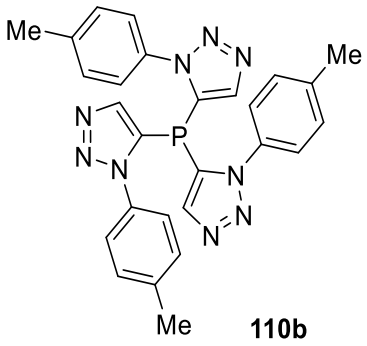

110b

$C_{27}H_{24}N_9P$ (CH_3COCH_3) (*M* =563.60 g/mol): triclinic, space group P-1 (no. 2), *a* = 11.3460(5) Å, *b* = 12.0485(5) Å, *c* = 12.7145(5) Å, *α* = 66.936(4)°, *β* = 74.573(4)°, *γ* = 63.382(4)°, *V* = 1421.01(12) Å^3, *Z* = 2, *T* = 100.00(10) K, μ(MoKα) = 0.138 mm^{-1}, *Dcalc* = 1.317 g/cm^3, 12412 reflections measured (6.632° ≤ 2Θ ≤ 52.746°), 5789 unique (R_{int} =

0.0211, R_{sigma} = 0.0334) which were used in all calculations. The final R_1 was 0.0395 (I > 2σ(I)) and wR_2 was 0.0969 (all data).

Crystal structure data of ***110c***

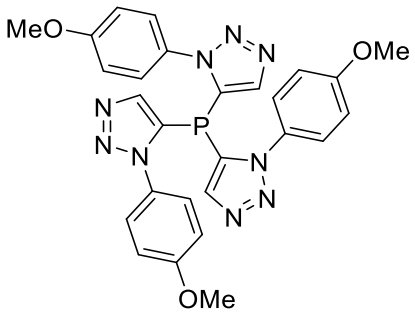

110c

$C_{27}H_{24}N_9O_3P$ (M =553.52 g/mol): monoclinic, space group $P2_1/c$ (no. 14), a = 11.14711(12) Å, b = 15.90434(17) Å, c = 14.72198(15) Å, β = 99.8060(10)°, V = 2571.89(5) Å^3, Z = 4, T = 100.01(10) K, μ(CuKα) = 1.367 mm^{-1}, *Dcalc* = 1.430 g/cm^3, 10477 reflections measured (8.05° ≤ 2Θ ≤ 144.258°), 5001 unique (R_{int} = 0.0219, R_{sigma} = 0.0261) which were used in all calculations. The final R_1 was 0.0309 (I > 2σ(I)) and wR_2 was 0.0803 (all data).

Crystal structure data of ***110g***

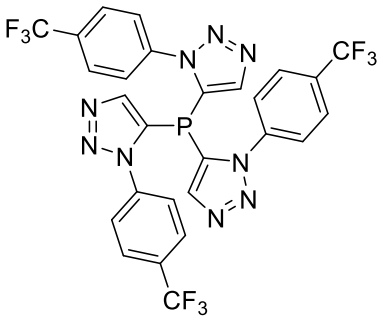

110g

$C_{27}H_{15}N_9F_9P$ (*M* =667.45 g/mol): triclinic, space group P-1 (no. 2), *a* = 8.1518(3) Å, *b* = 11.2723(5) Å, *c* = 14.7304(6) Å, *α* = 86.494(4)°, *β* = 89.039(4)°, *γ* = 86.056(4)°, *V* = 1347.73(10) Å^3, *Z* = 2, *T* = 100.01(10) K, μ(MoKα) = 0.203 mm^{-1}, *Dcalc* = 1.645 g/cm^3, 11289 reflections measured (4.43° ≤ 2Θ ≤ 59.028°), 6341 unique (R_{int} = 0.0234, R_{sigma} = 0.0449) which were used in all calculations. The final R_1 was 0.0405 (I > 2σ(I)) and wR_2 was 0.0988 (all data).

Crystal structure of ***112a***

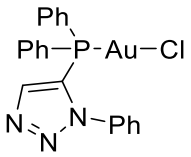

112a

$C_{20}H_{16}AuClN_3P$ (*M* =561.74 g/mol): triclinic, space group P-1 (no. 2), *a* = 9.1495(3) Å, *b* = 13.5665(5) Å, *c* = 15.9837(6) Å, *α* = 77.761(3)°, *β* = 82.352(3)°, *γ* = 79.954(3)°, *V* = 1899.64(12) Å^3, *Z* = 4, *T* = 100.01(10) K, μ(MoKα) = 7.978 mm^{-1}, *Dcalc* = 1.964 g/cm^3, 19415 reflections measured (5.242° ≤ 2Θ ≤ 58.738°), 9018 unique (R_{int} = 0.0251, R_{sigma} = 0.0395) which were used in all calculations. The final R_1 was 0.0342 (I > 2σ(I)) and wR_2 was 0.0621 (all data).

Crystal structure of ***112b***

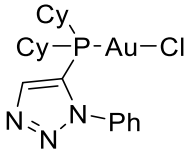

112b

$C_{20}H_{28}N_3PClAu$ (*M* =573.84 g/mol): triclinic, space group P-1 (no. 2), *a* = 9.3253(3) Å, *b* = 10.7200(5) Å, *c* = 11.7307(7) Å, *α* = 108.817(5)°, *β* = 98.520(4)°, *γ* = 103.935(4)°, *V* = 1044.28(9) Å^3, *Z* = 2, *T* = 100.01(10) K, μ(MoKα) = 7.257 mm^{-1}, *Dcalc* = 1.825 g/cm^3, 9349 reflections measured (6.726° ≤ 2Θ ≤ 58.854°), 4915 unique (R_{int} = 0.0334, R_{sigma} = 0.0513) which were used in all calculations. The final R_1 was 0.0277 (I > 2σ(I)) and wR_2 was 0.0538 (all data).

*Crystal structure of **113a***

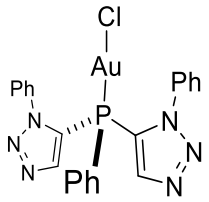

113a

$C_{22}H_{17}N_6PClAu$ (M =628.80 g/mol): monoclinic, space group $P2_1/c$ (no. 14), a = 8.2902(2) Å, b = 14.1064(4) Å, c = 19.1489(6) Å, β = 99.717(3)°, V = 2207.24(11) Å^3, Z = 4, T = 100.01(10) K, μ(CuKα) = 14.506 mm^{-1}, Dcalc = 1.892 g/cm^3, 8034 reflections measured (7.824° ≤ 2Θ ≤ 143.504°), 4217 unique (R_{int}= 0.0314, R_{sigma} = 0.0405) which were used in all calculations. The final R_1 was 0.0277 (I > 2σ(I)) and wR_2 was 0.0719 (all data).

*Crystal structure of **113b***

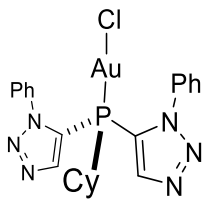

113b

$C_{22}H_{23}AuClN_6P$ (*M* =634.85 g/mol): monoclinic, space group $P2_1/n$ (no. 14), *a* = 15.1740(13) Å, *b* = 9.0970(5) Å, *c* = 17.9495(17) Å, *β* = 114.837(11)°, *V* = 2248.5(4) Å^3, *Z* = 4, *T* = 100.01(10) K, μ(CuKα) = 14.241 mm^{-1}, *Dcalc* = 1.875 g/cm^3, 25510 reflections measured (10.002° ≤ 2Θ ≤ 136.466°), 4116 unique (R_{int} = 0.0965, R_{sigma} = 0.0400) which were used in all calculations. The final R_1 was 0.0366 (I > 2σ(I)) and wR_2 was 0.1032 (all data).

*Crystal structure of **114***

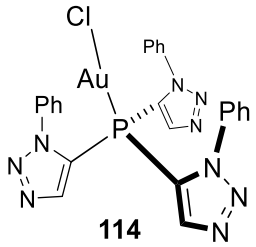

114

$C_{24}H_{18}AuClN_9P[CH_2Cl_2]$ (*M* =780.79 g/mol): triclinic, space group P-1 (no. 2), *a* = 10.2434(4) Å, *b* = 14.6032(6) Å, *c* = 19.0803(7) Å, *α* = 92.986(3)°, *β* = 93.407(3)°, *γ* = 100.172(3)°, *V* = 2798.63(19) Å^3, *Z* = 4, *T* = 100.00(10) K, μ(MoKα) = 5.634 mm^{-1}, *Dcalc* = 1.853 g/cm^3, 28543 reflections measured (4.508° ≤ 2Θ ≤ 59.02°), 13281 unique (R_{int} = 0.0252, R_{sigma} = 0.0392) which were used in all calculations. The final R_1 was 0.0253 (I > 2σ(I)) and wR2 was 0.0544 (all data).

*Crystal structure of **115***

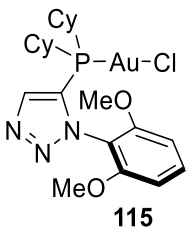

115

$C_{22}H_{32}AuClN_3O_2P[CHCl_3]$ (*M* =753.26 g/mol): monoclinic, space group $P2_1/c$ (no. 14), *a* = 16.3596(7) Å, *b* = 19.1615(7) Å, *c* = 9.1916(4) Å, *β* = 94.769(4)°, *V* = 2871.4(2) Å^3, *Z* = 4, *T* = 100.01(10) K, μ(CuKα) = 13.785 mm^{-1}, *Dcalc* = 1.742 g/cm^3, 10995 reflections measured (7.12° ≤ 2Θ ≤ 140.136°), 5404 unique (R_{int} = 0.0587, R_{sigma} = 0.0713) which were used in all calculations. The final R_1 was 0.0527 (I > 2σ(I)) and wR_2 was 0.1441 (all data).

Crystal structure of ***116***

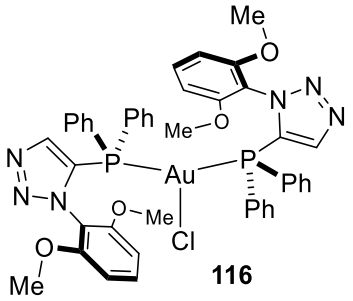

116

$C_{44}H_{40}AuClN_6O_4P_2$, $3(CH_2Cl_2)$ (*M* =1265.95 g/mol): monoclinic, space group $P2_1/c$ (no. 14), *a* = 11.7669(5) Å, *b* = 41.4044(10) Å, *c* = 11.5627(4) Å, *β* = 115.166(5)°, *V* = 5098.6(4) Å^3, *Z* = 4, *T* = 100.01(10) K, μ(MoKα) = 3.364 mm^{-1}, *Dcalc* = 1.649 g/cm^3, 28129 reflections measured (4.362° ≤ 2Θ ≤ 52.742°), 10437 unique (R_{int} = 0.0360, R_{sigma} = 0.0493) which were used in all calculations. The final R_1 was 0.0320 (I > 2σ(I)) and wR_2 was 0.0575 (all data).

Crystal structure of ***rac-127a***

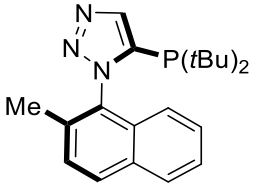

***(R)*-127a**

$C_{21}H_{28}N_3P$ (*M* =353.43 g/mol): orthorhombic, space group Pbca (no. 61), *a* = 15.9440(10) Å, *b* = 10.4374(9) Å, *c* = 23.1495(17) Å, *V* = 3852.4(5) Å^3, *Z* = 8, *T* = 100.01(10) K, μ(MoKα) = 0.151 mm^{-1}, *Dcalc* = 1.219 g/cm^3, 16163 reflections measured (6.668° ≤ 2Θ ≤ 52.74°), 3925 unique (R_{int} = 0.0309, R_{sigma} = 0.0264) which were used in all calculations. The final R_1 was 0.0362 (I > 2σ(I)) and wR_2 was 0.0954 (all data).

Crystal structure of ***(R)-127a***

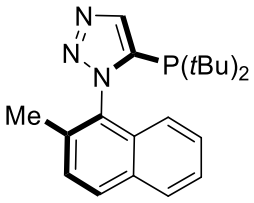

***(R)*-127a**

$C_{21}H_{28}N_3P$ (*M* =353.43 g/mol): orthorhombic, space group $P2_12_12_1$ (no. 19), *a* = 9.0290(2) Å, *b* = 11.9982(2) Å, *c* = 18.6439(3) Å, *V* = 2019.73(6) Å^3, *Z* = 4, *T* = 100.01(10) K, μ(CuKα) = 1.249 mm^{-1}, *Dcalc* = 1.162 g/cm^3, 18927 reflections measured (8.764° ≤ 2Θ ≤ 140.14°), 3823 unique (R_{int} = 0.0298, R_{sigma} = 0.0207) which were used in all calculations. The final R_1 was 0.0411 (I > 2σ(I)) and wR_2 was 0.1011 (all data).

Crystal structure of ***rac-127b***

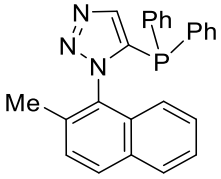

rac-127b

$C_{25}H_{20}N_3P$ (*M* =393.41 g/mol): triclinic, space group P-1 (no. 2), *a* = 9.2372(6) Å, *b* = 10.6106(6) Å, *c* = 11.6193(6) Å, *α* = 89.641(5)°, *β* = 69.061(6)°, *γ* = 68.694(6)°, *V* =

980.88(11) Å^3, Z = 2, T = 100.01(10) K, μ(MoKα) = 0.157 mm^{-1}, *Dcalc* = 1.332 g/cm^3, 8769 reflections measured (7.196° ≤ 2Θ ≤ 53.458°), 4145 unique (R_{int} = 0.0259, R_{sigma} = 0.0384) which were used in all calculations. The final R_1 was 0.0452 (I > 2σ(I)) and wR_2 was 0.1138 (all data).

Crystal structure of ***(R)-128***

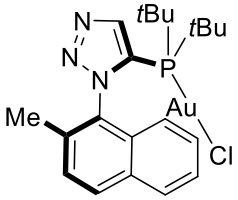

(R)-**128**

$C_{21}H_{28}AuClN_3P$ (CH_2Cl_2) (M =670.77 g/mol): orthorhombic, space group $P2_12_12_1$ (no. 19), a = 9.7882(4) Å, b = 15.6836(8) Å, c = 16.3587(8) Å, V = 2511.3(2) Å^3, Z = 4, T = 100.01(10) K, μ(MoKα) = 6.256 mm^{-1}, *Dcalc* = 1.774 g/cm^3, 10227 reflections measured (6.992° ≤ 2Θ ≤ 51.36°), 4640 unique (R_{int} = 0.0353, R_{sigma} = 0.0497) which were used in all calculations. The final R_1 was 0.0328 (I > 2σ(I)) and wR_2 was 0.0803 (all data).

Crystal structure of ***(S)-128***

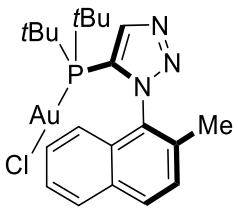

(S)-**128**

$C_{21}H_{28}AuClN_3P$ (CH_2Cl_2) (*M* =670.77 g/mol): orthorhombic, space group $P2_12_12_1$ (no. 19), *a* = 9.81680(10) Å, *b* = 15.7486(2) Å, *c* = 16.4137(2) Å, *V* = 2537.57(5) Å^3, *Z* = 4, *T* = 100.00(10) K, μ(CuKα) = 14.505 mm^{-1}, *Dcalc* = 1.756 g/cm^3, 24197 reflections measured (7.78° ≤ 2Θ ≤ 144.148°), 4962 unique (R_{int} = 0.0263, R_{sigma} = 0.0174) which were used in all calculations. The final R_1 was 0.0149 (I > 2σ(I)) and wR_2 was 0.0365 (all data).

Crystal structure of ***129***

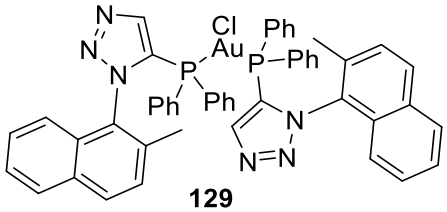

129

$C_{50}H_{40}AuClN_6P_2$ (CH_2Cl_2) (*M* =1104.16 g/mol): monoclinic, space group $P2_1/c$ (no. 14), *a* = 12.0536(4) Å, *b* = 20.6590(7) Å, *c* = 18.3903(6) Å, *β* = 90.835(3)°, *V* = 4579.0(3) Å^3, *Z* = 4, *T* = 100.01(10) K, μ(MoKα) = 3.502 mm^{-1}, *Dcalc* = 1.602 g/cm^3, 26819 reflections measured (4.85° ≤ 2Θ ≤ 51.362°), 8687 unique (R_{int} = 0.0392, R_{sigma} = 0.0473) which were used in all calculations. The final R_1 was 0.0376 (I > 2σ(I)) and wR_2 was 0.0838 (all data).

Crystal structure of ***(S)-131***

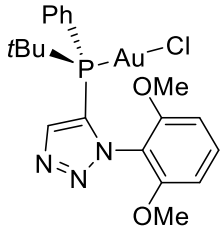

(*S*)-**131**

$C_{20}H_{24}AuClN_3O_2P$ (*M* =601.81 g/mol): orthorhombic, space group $P2_12_12_1$ (no. 19), *a* = 9.6058(2) Å, *b* = 13.4116(3) Å, *c* = 16.9131(3) Å, *V* = 2178.90(8) Å^3, *Z* = 4, *T* = 100.00(10) K, μ(CuKα) = 14.679 mm^{-1}, *Dcalc* = 1.835 g/cm^3, 20694 reflections measured (8.414° ≤ 2Θ ≤ 144.184°), 4276 unique (R_{int} = 0.0357, R_{sigma} = 0.0245) which were used in all calculations. The final R_1 was 0.0185 (I > 2σ(I)) and wR_2 was 0.0432 (all data).

Crystal structure of ***(S)-133***

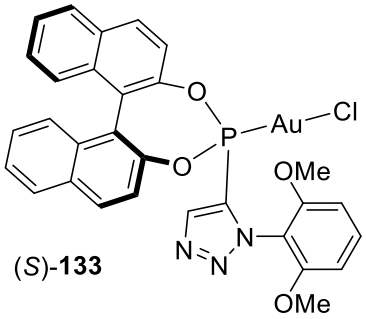

(*S*)-**133**

$C_{30}H_{22}AuClN_3O_4P$ (CH_2Cl_2)(*M* =836.82 g/mol): monoclinic, space group C2 (no. 5), *a* = 26.2701(5) Å, *b* = 8.49110(10) Å, *c* = 14.8812(3) Å, *β* = 106.340(2)°, *V* = 3185.36(10) Å^3, *Z* = 4, *T* = 100.00(10) K, μ(CuKα) = 11.809 mm^{-1}, *Dcalc* = 1.745 g/cm^3, 30626 reflections measured (7.014° ≤ 2Θ ≤ 144.216°), 6231 unique (R_{int} = 0.0344, R_{sigma} = 0.0238) which were used in all calculations. The final R_1 was 0.0202 (I > 2σ(I)) and wR_2 was 0.0526 (all data).

Crystal structure of ***(S,S)-124***

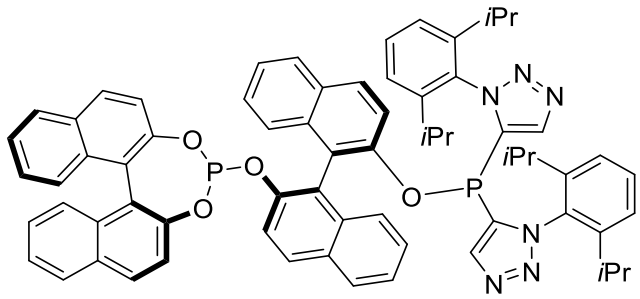

(*S*,*S*)-**135**

$C_{68}H_{60}N_6O_4P_2$ (*M* =1087.16 g/mol): orthorhombic, space group $P2_12_12_1$ (no. 19), *a* = 10.6019(5) Å, *b* = 21.2960(8) Å, *c* = 25.1476(11) Å, *V* = 5677.8(4) Å^3, *Z* = 4, *T* = 100.01(10) K, μ(CuKα) = 1.139 mm^{-1}, *Dcalc* = 1.272 g/cm^3, 13068 reflections measured (7.03° ≤ 2Θ ≤ 140.15°), 9248 unique (R_{int} = 0.0528, R_{sigma} = 0.0744) which were used in all calculations. The final R_1 was 0.0767 (I > 2σ(I)) and wR_2 was 0.2300 (all data).

8. References

1. H. C. Kolb, M. G. Finn and K. B. Sharpless, *Angew. Chem. Int. Ed.*, 2001, **40**, 2004-2021.
2. C. D. Hein, X.-M. Liu and D. Wang, *Pharm. Res.*, 2008, **25**, 2216-2230.
3. Y. Sohma and Y. Kiso, *ChemBioChem*, 2006, **7**, 1549-1557.
4. Y. Fu, L. Mi, M. Sanda, S. Silverstein, M. Aggarwal, D. Wang, P. Gupta, R. Goldman, D. H. Appella and F. L. Chung, *RSC Adv*, 2014, **4**, 3920-3923.
5. P. Thirumurugan, D. Matosiuk and K. Jozwiak, *Chem. Rev.*, 2013, **113**, 4905-4979.
6. P. Wu, A. K. Feldman, A. K. Nugent, C. J. Hawker, A. Scheel, B. Voit, J. Pyun, J. M. Frechet, K. B. Sharpless and V. V. Fokin, *Angew. Chem. Int. Ed.*, 2004, **43**, 3928-3932.
7. J. Thundimadathil, *Chimica Oggi-Chemistry Today*, 2013, **31**, 34-37.
8. D. Pasini, *Molecules*, 2013, **18**, 9512-9530.
9. D. Tanner, A. Almario and T. Högberg, *Tetrahedron*, 1995, **51**, 6061-6070.
10. P.-y. Lin, K. Bellos, H. Stamm and A. Onistschenko, *Tetrahedron*, 1992, **48**, 2359-2372.
11. J. Vincent, P. Schipper, A. de Groot and H. Buck, *Tetrahedron Lett.*, 1975, **16**, 1989-1992.
12. M. S. Berridge, M. P. Franceschini, E. Rosenfeld and T. J. Tewson, *J. Org. Chem.*, 1990, **55**, 1211-1217.
13. K. Bellos and H. Stamm, *J. Org. Chem.*, 1995, **60**, 5661-5666.
14. T.-H. Chuang and K. B. Sharpless, *Org. Lett.*, 1999, **1**, 1435-1437.
15. D. Seebach, J. D. Aebi, M. Gandercoquoz and R. Naef, *Helv. Chim. Acta*, 1987, **70**, 1194-1216.
16. M. Jung and S. Lee, *Bioorg. Med. Chem. Lett.*, 1998, **8**, 1003-1006.
17. P. Deslongchamps, Y. L. Dory and S. G. Li, *Tetrahedron*, 2000, **56**, 3533-3537.
18. Y. Y. Fan, K. S. Ramos and R. S. Chapkin, *Prostaglandins, Leukotrienes Essent. Fatty Acids*, 1996, **54**, 101-107.
19. V. V. Rostovtsev, L. G. Green, V. V. Fokin and K. B. Sharpless, *Angew. Chem. Int. Ed.*, 2002, **41**, 2596-2599.
20. Y. Zhao, H. van Nguyen, L. Male, P. Craven, B. R. Buckley and J. S. Fossey, *Organometallics*, 2018, **37**, 4224-4241.
21. R. Huisgen, *Proc. Chem. Soc.*, 1961, 357-396.
22. H. C. Kolb and K. B. Sharpless, *Drug Discov Today*, 2003, **8**, 1128-1137.
23. R. Huisgen, *Angew. Chem. Int. Ed. Engl.*, 1963, **2**, 565-598.
24. L. Liang and D. Astruc, *Coord. Chem. Rev.*, 2011, **255**, 2933-2945.
25. B. C. Boren, S. Narayan, L. K. Rasmussen, L. Zhang, H. Zhao, Z. Lin, G. Jia and V. V. Fokin, *J. Am. Chem. Soc.*, 2008, **130**, 8923-8930.
26. N. J. Agard, J. A. Prescher and C. R. Bertozzi, *J. Am. Chem. Soc.*, 2004, **126**, 15046-15047.
27. I. Kii, A. Shiraishi, T. Hiramatsu, T. Matsushita, H. Uekusa, S. Yoshida, M. Yamamoto, A. Kudo, M. Hagiwara and T. Hosoya, *Org Biomol Chem*, 2010, **8**, 4051-4055.

28. S. Yoshida, Y. Hatakeyama, K. Johmoto, H. Uekusa and T. Hosoya, *J. Am. Chem. Soc.*, 2014, **136**, 13590-13593.
29. L. S. Campbell-Verduyn, L. Mirfeizi, A. K. Schoonen, R. A. Dierckx, P. H. Elsinga and B. L. Feringa, *Angew. Chem. Int. Ed.*, 2011, **50**, 11117-11120.
30. M. Meldal and C. W. Tornøe, *Chem. Rev.*, 2008, **108**, 2952-3015.
31. C. W. Tornoe, C. Christensen and M. Meldal, *J. Org. Chem.*, 2002, **67**, 3057-3064.
32. A. Krasiński, V. V. Fokin and K. B. Sharpless, *Org. Lett.*, 2004, **6**, 1237-1240.
33. A. Akao, T. Tsuritani, S. Kii, K. Sato, N. Nonoyama, T. Mase and N. Yasuda, *Synlett*, 2007, **1**, 0031-0036.
34. G. Himbert, D. Frank and M. Regit, *Chem. Ber.*, 1976, **109**, 370-394.
35. S. W. Kwok, J. R. Fotsing, R. J. Fraser, V. O. Rodionov and V. V. Fokin, *Org. Lett.*, 2010, **12**, 4217-4219.
36. W. G. Kim, M. E. Kang, J. B. Lee, M. H. Jeon, S. Lee, J. Lee, B. Choi, P. M. S. D. Cal, S. Kang, J.-M. Kee, G. J. L. Bernardes, J.-U. Rohde, W. Choe and S. Y. Hong, *J. Am. Chem. Soc.*, 2017, **139**, 12121-12124.
37. F. Himo, T. Lovell, R. Hilgraf, V. V. Rostovtsev, L. Noodleman, K. B. Sharpless and V. V. Fokin, *J. Am. Chem. Soc.*, 2005, **127**, 210-216.
38. B. T. Worrell, J. A. Malik and V. V. Fokin, *Science*, 2013, **340**, 457-460.
39. C. Iacobucci, S. Reale, J.-F. Gal and F. De Angelis, *Angew. Chem. Int. Ed.*, 2015, **54**, 3065-3068.
40. L. Jin, D. R. Tolentino, M. Melaimi and G. Bertrand, *Sci Adv*, 2015, **1**, e1500304.
41. B. R. Buckley, S. E. Dann and H. Heaney, *Chem. Eur. J.*, 2010, **16**, 6278-6284.
42. J. S. Oakdale, V. V. Fokin, S. Umezaki and T. Fukuyama, *Organic Synth*, 2013, **90**, 96-104.
43. J. E. Moses and A. D. Moorhouse, *Chem. Soc. Rev.*, 2007, **36**, 1249-1262.
44. W. G. Lewis, L. G. Green, F. Grynszpan, Z. Radić, P. R. Carlier, P. Taylor, M. G. Finn and K. B. Sharpless, *Angew. Chem. Int. Ed.*, 2002, **41**, 1053-1057.
45. E. Saxon and C. R. Bertozzi, *Science*, 2000, **287**, 2007-2010.
46. J. Gierlich, G. A. Burley, P. M. E. Gramlich, D. M. Hammond and T. Carell, *Org. Lett.*, 2006, **8**, 3639-3642.
47. K. Sivakumar, F. Xie, B. M. Cash, S. Long, H. N. Barnhill and Q. Wang, *Org. Lett.*, 2004, **6**, 4603-4606.
48. T. S. Seo, Z. Li, H. Ruparel and J. Ju, *J. Org. Chem.*, 2003, **68**, 609-612.
49. E. M. Larin and M. Lautens, *Angew. Chem. Int. Ed.*, 2019, **58**, 13438-13442.
50. A. Capci, M. M. Lorion, H. Wang, N. Simon, M. Leidenberger, M. C. Borges Silva, D. R. M. Moreira, Y. Zhu, Y. Meng, J. Y. Chen, Y. M. Lee, O. Friedrich, B. Kappes, J. Wang, L. Ackermann and S. B. Tsogoeva, *Angew. Chem. Int. Ed.*, 2019, **58**, 13066-13079.
51. R. He, Z. Yu, Y. He, L. F. Zeng, J. Xu, L. Wu, A. M. Gunawan, L. Wang, Z. X. Jiang and Z. Y. Zhang, *ChemMedChem*, 2010, **5**, 2051-2056.
52. X. P. He, Q. Deng, L. X. Gao, C. Li, W. Zhang, Y. B. Zhou, Y. Tang, X. X. Shi, J. Xie, J. Li, G. R. Chen and K. Chen, *Bioorg. Med. Chem.*, 2011, **19**, 3892-3900.
53. C. Li, X. P. He, Y. J. Zhang, Z. Li, L. X. Gao, X. X. Shi, J. Xie, J. Li, G. R. Chen and Y. Tang, *Eur. J. Med. Chem.*, 2011, **46**, 4212-4218.

54. P. B. Reddy, S. K. Agrawal, S. Singh, B. A. Bhat, A. K. Saxena, H. M. S. Kumar and G. N. Qazi, *Chemistry & Biodiversity*, 2008, **5**, 1792-1802.
55. G. C. Tron, T. Pirali, R. A. Billington, P. L. Canonico, G. Sorba and A. A. Genazzani, *Med Res Rev*, 2008, **28**, 278-308.
56. R. Srinivasan, M. Uttamchandani and S. Q. Yao, *Org. Lett.*, 2006, **8**, 713-716.
57. W. Phetsang, M. A. T. Blaskovich, M. S. Butler, J. X. Huang, J. Zuegg, S. K. Mamidyala, S. Ramu, A. M. Kavanagh and M. A. Cooper, *Biorg. Med. Chem.*, 2014, **22**, 4490-4498.
58. V. Aucagne, K. D. Hänni, D. A. Leigh, P. J. Lusby and D. B. Walker, *J. Am. Chem. Soc.*, 2006, **128**, 2186-2187.
59. R. Y. Zhu, M. E. Farmer, Y. Q. Chen and J. Q. Yu, *Angew. Chem. Int. Ed.*, 2016, **55**, 10578-10599.
60. L. Ackermann, R. Vicente and A. Althammer, *Org. Lett.*, 2008, **10**, 2299-2302.
61. K. D. Yamajala, M. Patil and S. Banerjee, *J. Org. Chem.*, 2015, **80**, 3003-3011.
62. X. Tian, F. Yang, D. Rasina, M. Bauer, S. Warratz, F. Ferlin, L. Vaccaro and L. Ackermann, *Chem. Commun.*, 2016, **52**, 9777-9780.
63. L. Ackermann, H. K. Potukuchi, D. Landsberg and R. Vicente, *Org. Lett.*, 2008, **10**, 3081-3084.
64. I. Guerrero and A. Correa, *Eur. J. Org. Chem.*, 2018, **44**, 6034-6049.
65. H. Li, F. Cheng, A. M. Duft and A. Adronov, *J. Am. Chem. Soc.*, 2005, **127**, 14518-14524.
66. Y. Liu, W. Zhao, C. H. Chen and A. H. Flood, *Science*, 2019, **365**, 159-161.
67. P. Wu, A. K. Feldman, A. K. Nugent, C. J. Hawker, A. Scheel, B. Voit, J. Pyun, J. M. J. Fréchet, K. B. Sharpless and V. V. Fokin, *Angew. Chem. Int. Ed.*, 2004, **43**, 3928-3932.
68. W. Zhai, L. Male and J. S. Fossey, *Chem. Commun.*, 2017, **53**, 2218-2221.
69. W. Zhai, B. M. Chapin, A. Yoshizawa, H.-C. Wang, S. A. Hodge, T. D. James, E. V. Anslyn and J. S. Fossey, *Organic Chemistry Frontiers*, 2016, **3**, 918-928.
70. P. I. P. Elliott, in *Organometallic Chemistry: Volume 39*, The Royal Society of Chemistry, 2014, vol. 39, pp. 1-25.
71. K. O. Marichev, S. A. Patil and A. Bugarin, *Tetrahedron*, 2018, **74**, 2523-2546.
72. B. M. Suijkerbuijk, B. N. Aerts, H. P. Dijkstra, M. Lutz, A. L. Spek, G. van Koten and R. J. Klein Gebbink, *Dalton Trans*, 2007, **13**, 1273-1276.
73. B. S. Uppal, R. K. Booth, N. Ali, C. Lockwood, C. R. Rice and P. I. P. Elliott, *Dalton Transactions*, 2011, **40**, 7610-7616.
74. H. Struthers, T. L. Mindt and R. Schibli, *Dalton Transactions*, 2010, **39**, 675-696.
75. H. Rensmo, S. Lunell and H. Siegbahn, *J. Photochem. Photobiol., A*, 1998, **114**, 117-124.
76. U. Monkowius, S. Ritter, B. König, M. Zabel and H. Yersin, *Eur. J. Inorg. Chem.*, 2007, **29**, 4597-4606.
77. J. T. Fletcher, B. J. Bumgarner, N. D. Engels and D. A. Skoglund, *Organometallics*, 2008, **27**, 5430-5433.
78. B. Happ, C. Friebe, A. Winter, M. D. Hager, R. Hoogenboom and U. S. Schubert, *Chem Asian J*, 2009, **4**, 154-163.

79. M. Obata, A. Kitamura, A. Mori, C. Kameyama, J. A. Czaplewska, R. Tanaka, I. Kinoshita, T. Kusumoto, H. Hashimoto, M. Harada, Y. Mikata, T. Funabiki and S. Yano, *Dalton Trans*, 2008, **25**, 3292-3300.
80. T. R. Chan, R. Hilgraf, K. B. Sharpless and V. V. Fokin, *Org. Lett.*, 2004, **6**, 2853-2855.
81. C. Dai, Y. Cheng, J. Cui and B. Wang, *Molecules*, 2010, **15**, 5768-5781.
82. H. A. Michaels and L. Zhu, *Chem Asian J*, 2011, **6**, 2825-2834.
83. B. Beyer, C. Ulbricht, D. Escudero, C. Friebe, A. Winter, L. González and U. S. Schubert, *Organometallics*, 2009, **28**, 5478-5488.
84. E. A. B. Kantchev, C. J. O'Brien and M. G. Organ, *Angew. Chem. Int. Ed.*, 2007, **46**, 2768-2813.
85. P. Mathew, A. Neels and M. Albrecht, *J. Am. Chem. Soc.*, 2008, **130**, 13534-13535.
86. A. J. Arduengo, R. L. Harlow and M. Kline, *J. Am. Chem. Soc.*, 1991, **113**, 361-363.
87. M. Albrecht, *Chem. Commun.*, 2008, **31**, 3601-3610.
88. K. F. Donnelly, A. Petronilho and M. Albrecht, *Chem. Commun.*, 2013, **49**, 1145-1159.
89. S. Hohloch, C.-Y. Su and B. Sarkar, *Eur. J. Inorg. Chem.*, 2011, **2011**, 3067-3075.
90. T. Nakamura, T. Terashima, K. Ogata and S.-i. Fukuzawa, *Org. Lett.*, 2011, **13**, 620-623.
91. R. Saravanakumar, V. Ramkumar and S. Sankararaman, *Organometallics*, 2011, **30**, 1689-1694.
92. K. J. Kilpin, U. S. D. Paul, A.-L. Lee and J. D. Crowley, *Chem. Commun.*, 2011, **47**, 328-330.
93. L. Casarrubios, M. C. de la Torre and M. A. Sierra, *Chem. Eur. J*, 2013, **19**, 3534-3541.
94. T. Nakamura, K. Ogata and S.-i. Fukuzawa, *Chem. Lett.*, 2010, **39**, 920-922.
95. T. Terashima, S. Inomata, K. Ogata and S.-i. Fukuzawa, *Eur. J. Inorg. Chem.*, 2012, **2012**, 1387-1393.
96. J. Bouffard, B. K. Keitz, R. Tonner, G. Guisado-Barrios, G. Frenking, R. H. Grubbs and G. Bertrand, *Organometallics*, 2011, **30**, 2617-2627.
97. B. K. Keitz, J. Bouffard, G. Bertrand and R. H. Grubbs, *J. Am. Chem. Soc.*, 2011, **133**, 8498-8501.
98. J. Cai, X. Yang, K. Arumugam, C. W. Bielawski and J. L. Sessler, *Organometallics*, 2011, **30**, 5033-5037.
99. A. Petronilho, M. Rahman, J. A. Woods, H. Al-Sayyed, H. Muller-Bunz, J. M. Don MacElroy, S. Bernhard and M. Albrecht, *Dalton Trans*, 2012, **41**, 13074-13080.
100. R. Lalrempuia, N. D. McDaniel, H. Müller-Bunz, S. Bernhard and M. Albrecht, *Angew. Chem. Int. Ed.*, 2010, **49**, 9765-9768.
101. N. V. Dubrovina, L. Domke, I. A. Shuklov, A. Spannenberg, R. Franke, A. Villinger and A. Börner, *Tetrahedron*, 2013, **69**, 8809-8817.
102. E. M. Schuster, G. Nisnevich, M. Botoshansky and M. Gandelman, *Organometallics*, 2009, **28**, 5025-5031.
103. E. M. Schuster, M. Botoshansky and M. Gandelman, *Angew. Chem. Int. Ed.*, 2008, **47**, 4555-4558.

104. F. Dolhem, M. J. Johansson, T. Antonsson and N. Kann, *J. Comb. Chem.*, 2007, **9**, 477-486.
105. D. Liu, W. Gao, Q. Dai and X. Zhang, *Org. Lett.*, 2005, **7**, 4907-4910.
106. Q. Dai, W. Gao, D. Liu, L. M. Kapes and X. Zhang, *J. Org. Chem.*, 2006, **71**, 3928-3934.
107. D. M. Zink, T. Baumann, M. Nieger and S. Bräse, *Eur. J. Org. Chem.*, 2011, **8**, 1432-1437.
108. B. Choubey, L. Radhakrishna, J. T. Mague and M. S. Balakrishna, *Inorg. Chem.*, 2016, **55**, 8514-8526.
109. J. E. Glover, D. J. Martin, P. G. Plieger and G. J. Rowlands, *Eur. J. Org. Chem.*, 2013, **2013**, 1671-1675.
110. H. Oki, I. Oura, T. Nakamura, K. Ogata and S.-i. Fukuzawa, *Tetrahedron: Asymmetry*, 2009, **20**, 2185-2191.
111. C. Laborde, M.-M. Wei, A. van der Lee, E. Deydier, J.-C. Daran, J.-N. Volle, R. Poli, J.-L. Pirat, E. Manoury and D. Virieux, *Dalton Trans*, 2015, **44**, 12539-12545.
112. U. Christmann and R. Vilar, *Angew. Chem. Int. Ed.*, 2005, **44**, 366-374.
113. W. A. Herrmann, *Angew. Chem. Int. Ed.*, 2002, **41**, 1290-1309.
114. N. T. S. Phan, M. Van Der Sluys and C. W. Jones, *Adv. Synth. Catal.*, 2006, **348**, 609-679.
115. S. L. Buchwald, *Adv. Synth. Catal.*, 2004, **346**, 1524-1524.
116. R. Martin and S. L. Buchwald, *Acc. Chem. Res.*, 2008, **41**, 1461-1473.
117. Y. Zhou, X. Zhang, H. Liang, Z. Cao, X. Zhao, Y. He, S. Wang, J. Pang, Z. Zhou, Z. Ke and L. Qiu, *ACS Catalysis*, 2014, **4**, 1390-1397.
118. C. C. C. Johansson Seechurn, M. O. Kitching, T. J. Colacot and V. Snieckus, *Angew. Chem. Int. Ed.*, 2012, **51**, 5062-5085.
119. J. Uenishi, J. M. Beau, R. W. Armstrong and Y. Kishi, *J. Am. Chem. Soc.*, 1987, **109**, 4756-4758.
120. G. Bringmann, A. J. Price Mortimer, P. A. Keller, M. J. Gresser, J. Garner and M. Breuning, *Angew. Chem. Int. Ed.*, 2005, **44**, 5384-5427.
121. P. S. Kutchukian, J. F. Dropinski, K. D. Dykstra, B. Li, D. A. DiRocco, E. C. Streckfuss, L. C. Campeau, T. Cernak, P. Vachal, I. W. Davies, S. W. Krska and S. D. Dreher, *Chem. Sci.*, 2016, **7**, 2604-2613.
122. P. W. Glunz, *Bioorg. Med. Chem. Lett.*, 2018, **28**, 53-60.
123. S. R. LaPlante, P. J. Edwards, L. D. Fader, A. Jakalian and O. Hucke, *ChemMedChem*, 2011, **6**, 505-513.
124. C. Wolf, in *Dynamic Stereochemistry of Chiral Compounds: Principles and Applications*, The Royal Society of Chemistry, 2008, pp. 136-179.
125. P. Wipf, E. M. Skoda and A. Mann, in *The Practice of Medicinal Chemistry (Fourth Edition)*, eds. C. G. Wermuth, D. Aldous, P. Raboisson and D. Rognan, Academic Press, San Diego, 2015, pp. 279-299.
126. A. Zask, J. Murphy and G. A. Ellestad, *Chirality*, 2013, **25**, 265-274.
127. S. R. LaPlante, P. J. Edwards, L. D. Fader, A. Jakalian and O. Hucke, *ChemMedChem*, 2011, **6**, 505-513.
128. G. Bringmann and D. Menche, *Angew. Chem. Int. Ed.*, 2001, **40**, 1687-1690.

129. G. Bringmann, A. J. Price Mortimer, P. A. Keller, M. J. Gresser, J. Garner and M. Breuning, *Angew. Chem. Int. Ed.*, 2005, **44**, 5384-5427.
130. Y. Fukuyama and Y. Asakawa, *J. Chem. Soc., Perkin Trans. 1*, 1991, 2737-2741.
131. A. Zask, J. Murphy and G. A. Ellestad, *Chirality*, 2013, **25**, 265-274.
132. J. M. Brunel, *Chem. Rev.*, 2005, **105**, 857-898.
133. E. Zhou, B. Liu and C. Dong, *Tetrahedron: Asymmetry*, 2014, **25**, 181-186.
134. S. Akutagawa, *Appl. Catal., A*, 1995, **128**, 171-207.
135. C. Chen, X. Li and S. L. Schreiber, *J. Am. Chem. Soc.*, 2003, **125**, 10174-10175.
136. E. Fernández, P. J. Guiry, K. P. T. Connole and J. M. Brown, *J. Org. Chem.*, 2014, **79**, 5391-5400.
137. S. Shirakawa and K. Maruoka, *Angew. Chem. Int. Ed.*, 2013, **52**, 4312-4348.
138. J. Winn, A. Pinczewska and S. M. Goldup, *J. Am. Chem. Soc.*, 2013, **135**, 13318-13321.
139. S. Kumar, F. Saleem and A. K. Singh, *Dalton Trans.*, 2016, **45**, 11445-11458.
140. G. Zhang, Y. Wang, X. Wen, C. Ding and Y. Li, *Chem. Commun.*, 2012, **48**, 2979-2981.
141. S. Hohloch, D. Schweinfurth, M. G. Sommer, F. Weisser, N. Deibel, F. Ehret and B. Sarkar, *Dalton Trans*, 2014, **43**, 4437-4450.
142. E. P. McCarney, C. S. Hawes, S. Blasco and T. Gunnlaugsson, *Dalton Trans*, 2016, **45**, 10209-10221.
143. I. Bratsos, D. Urankar, E. Zangrando, P. Genova-Kalou, J. Kosmrlj, E. Alessio and I. Turel, *Dalton Trans*, 2011, **40**, 5188-5199.
144. B. Chowdhury, S. Khatua, R. Dutta, S. Chakraborty and P. Ghosh, *Inorg. Chem.*, 2014, **53**, 8061-8070.
145. D. Schweinfurth, R. Pattacini, S. Strobel and B. Sarkar, *Dalton Trans*, 2009, **42**, 9291-9297.
146. J. M. Fernández-Hernández, C. H. Yang, J. I. Beltrán, V. Lemaur, F. Polo, R. Fröhlich, J. Cornil and L. De Cola, *J. Am. Chem. Soc.*, 2011, **133**, 10543-10558.
147. K. N. Swanick, S. Ladouceur, E. Zysman-Colman and Z. Ding, *Chem. Commun.*, 2012, **48**, 3179-3181.
148. S. Ladouceur, D. Fortin and E. Zysman-Colman, *Inorg. Chem.*, 2011, **50**, 11514-11526.
149. N. C. Bruno, M. T. Tudge and S. L. Buchwald, *Chem. Sci.*, 2013, **4**, 916-920.
150. N. C. Bruno, N. Niljianskul and S. L. Buchwald, *J. Org. Chem.*, 2014, **79**, 4161-4166.
151. R. B. Bedford, C. S. J. Cazin and D. Holder, *Coord. Chem. Rev.*, 2004, **248**, 2283-2321.
152. A. Zapf, R. Jackstell, F. Rataboul, T. Riermeier, A. Monsees, C. Fuhrmann, N. Shaikh, U. Dingerdissen and M. Beller, *Chem Commun (Camb)*, 2004, 38-39.
153. T. E. Pickett, F. X. Roca and C. J. Richards, *J. Org. Chem.*, 2003, **68**, 2592-2599.
154. J. F. Jensen and M. Johannsen, *Org. Lett.*, 2003, **5**, 3025-3028.
155. S. Y. Liu, M. J. Choi and G. C. Fu, *Chem. Commun.*, 2001, **23**, 2408-2409.
156. A. H. Christian, Z. L. Niemeyer, M. S. Sigman and F. D. Toste, *ACS Catal.*, 2017, **7**, 3973-3978.

157. M. J. Barrett, G. F. Khan, P. W. Davies and R. S. Grainger, *Chem. Commun.*, 2017, **53**, 5733-5736.
158. M. Dos Santos and P. W. Davies, *Chem. Commun.*, 2014, **50**, 6001-6004.
159. C. A. Tolman, *Chem. Rev.*, 1977, **77**, 313-348.
160. H. Clavier and S. P. Nolan, *Chem. Commun.*, 2010, **46**, 841-861.
161. A. C. Hillier, W. J. Sommer, B. S. Yong, J. L. Petersen, L. Cavallo and S. P. Nolan, *Organometallics*, 2003, **22**, 4322-4326.
162. A. Poater, B. Cosenza, A. Correa, S. Giudice, F. Ragone, V. Scarano and L. Cavallo, *Eur. J. Inorg. Chem.*, 2009, **13**, 1759-1766.
163. F. Lovering, J. Bikker and C. Humblet, *J. Med. Chem.*, 2009, **52**, 6752-6756.
164. I. Colomer, C. J. Empson, P. Craven, Z. Owen, R. G. Doveston, I. Churcher, S. P. Marsden and A. Nelson, *Chem. Commun.*, 2016, **52**, 7209-7212.
165. R. A. Arthurs and C. J. Richards, *Org. Lett.*, 2017, **19**, 702-705.
166. S. Chuprakov, N. Chernyak, A. S. Dudnik and V. Gevorgyan, *Org. Lett.*, 2007, **9**, 2333-2336.
167. C. Adamo, C. Amatore, I. Ciofini, A. Jutand and H. Lakmini, *J. Am. Chem. Soc.*, 2006, **128**, 6829-6836.
168. E. Vitaku, D. T. Smith and J. T. Njardarson, *J. Med. Chem.*, 2014, **57**, 10257-10274.
169. R. D. Taylor, M. MacCoss and A. D. G. Lawson, *J. Med. Chem.*, 2014, **57**, 5845-5859.
170. S. Badèche, J.-C. Daran, J. Ruiz and D. Astruc, *Inorg. Chem.*, 2008, **47**, 4903-4908.
171. A. J. Kendall, L. N. Zakharov and D. R. Tyler, *Inorg. Chem.*, 2016, **55**, 3079-3090.
172. M. Su and S. L. Buchwald, *Angew. Chem. Int. Ed.*, 2012, **51**, 4710-4713.
173. R. A. Altman and S. L. Buchwald, *Nat. Protoc.*, 2007, **2**, 3115-3121.
174. L. Chen, P. Ren and B. P. Carrow, *J. Am. Chem. Soc.*, 2016, **138**, 6392-6395.
175. N. Marion, R. S. Ramón and S. P. Nolan, *J. Am. Chem. Soc.*, 2009, **131**, 448-449.
176. L. Falivene, R. Credendino, A. Poater, A. Petta, L. Serra, R. Oliva, V. Scarano and L. Cavallo, *Organometallics*, 2016, **35**, 2286-2293.
177. Z. L. Niemeyer, A. Milo, D. P. Hickey and M. S. Sigman, *Nat. Chem.*, 2016, **8**, 610-617.
178. A. S. K. Hashmi, *Chem. Rev.*, 2007, **107**, 3180-3211.
179. N. C. Baenziger, W. E. Bennett and D. M. Soborofe, *Acta Crystallogr., Sect. B: Struct. Crystallogr. Cryst. Chem.*, 1976, **32**, 962-963.
180. J. A. Muir, M. M. Muir, L. B. Pulgar, P. G. Jones and G. M. Sheldrick, *Acta Crystallogr., Sect. C: Cryst. Struct. Commun.*, 1985, **41**, 1174-1176.
181. N. C. Baenziger, W. E. Bennett and D. M. Soborofe, *Acta Crystallographica Section B*, 1976, **32**, 962-963.
182. J. A. Muir, M. M. Muir, L. B. Pulgar, P. G. Jones and G. M. Sheldrick, *Acta Crystallographica Section C*, 1985, **41**, 1174-1176.
183. N. C. Baenziger, K. M. Dittemore and J. R. Doyle, *Inorg. Chem.*, 1974, **13**, 805-811.
184. M. Gatto, A. Del Zotto, J. Segato and D. Zuccaccia, *Organometallics*, 2018, **37**, 4685-4691.
185. P. W. Davies and C. Detty-Mambo, *Org Biomol Chem*, 2010, **8**, 2918-2922.

186. R. E. Ebule, D. Malhotra, G. B. Hammond and B. Xu, *Adv. Synth. Catal.*, 2016, **358**, 1478-1481.
187. F. Sanchez-Cantalejo, J. D. Priest and P. W. Davies, *Chem. Eur. J*, 2018, **24**, 17215-17219.
188. Y. Zhao, M. G. Wakeling, F. Meloni, T. J. Sum, H. van Nguyen, B. R. Buckley, P. W. Davies and J. S. Fossey, *Eur. J. Org. Chem.*, 2019, **31-32**, 5540-5548.
189. Y.-M. Li, F.-Y. Kwong, W.-Y. Yu and A. S. C. Chan, *Coord. Chem. Rev.*, 2007, **251**, 2119-2144.
190. W. Tang and X. Zhang, *Chem. Rev.*, 2003, **103**, 3029-3070.
191. W. S. Knowles, M. J. Sabacky, B. D. Vineyard and D. J. Weinkauff, *J. Am. Chem. Soc.*, 1975, **97**, 2567-2568.
192. W. S. Knowles, *Angew. Chem. Int. Ed.*, 2002, **41**, 1998-2007.
193. B. L. Feringa, M. Pineschi, L. A. Arnold, R. Imbos and A. H. M. de Vries, *Angew. Chem. Int. Ed.*, 1997, **36**, 2620-2623.
194. W. D. G. Brittain, *unpublished data*.
195. N. G. Andersen, P. D. Ramsden, D. Che, M. Parvez and B. A. Keay, *J. Org. Chem.*, 2001, **66**, 7478-7486.
196. B. D. Vineyard, W. S. Knowles, M. J. Sabacky, G. L. Bachman and D. J. Weinkauff, *J. Am. Chem. Soc.*, 1977, **99**, 5946-5952.
197. T. Imamoto, *ISSN 1349-4848 CODEN: TCIMDW*, 2017, 2.
198. U. Eggenberger and G. Bodenhausen, *Angew. Chem., Int. Ed. Engl.*, 1990, **29**, 374-383.
199. M. Piotto, M. Bourdonneau, K. Elbayed, J. M. Wieruszeski and G. Lippens, *Magn. Reson. Chem.*, 2006, **44**, 943-947.
200. J. A. Parkinson, *Emagres*, 2015, **4**, 69-81.
201. L. L. Landucci, *Holzforschung*, 1991, **45**, 425-432.
202. H. E. Gottlieb, V. Kotlyar and A. Nudelman, *J. Org. Chem.*, 1997, **62**, 7512-7515.
203. S. G. Zhou, H. M. Liao, M. M. Liu, G. B. Feng, B. L. Fu, R. J. Li, M. S. Cheng, Y. F. Zhao and P. Gong, *Biorg. Med. Chem.*, 2014, **22**, 6438-6452.
204. F. Alonso, Y. Moglie, G. Radivoy and M. Yus, *Eur. J. Org. Chem.*, 2010, **10**, 1875-1884.
205. W. J. Ye, X. Xiao, L. Wang, S. C. Hou and C. Hu, *Organometallics*, 2017, **36**, 2116-2125.
206. J. J. Gu, Z. Fang, Z. Yang, X. Li, N. Zhu, L. Wan, P. Wei and K. Guo, *Rsc Advances*, 2016, **6**, 89073-89079.
207. Y. Li, L. X. Gao and F. S. Han, *Chem. Eur. J*, 2010, **16**, 7969-7972.
208. I. T. Alt and B. Plietker, *Angew. Chem. Int. Ed. Engl.*, 2016, **55**, 1519-1522.
209. H. J. Yang, Y. Li, M. Jiang, J. M. Wang and H. Fu, *Chem. Eur. J*, 2011, **17**, 5652-5660.
210. C. C. Ciocoiu, N. Nikolic, H. H. Nguyen, G. H. Thoresen, A. J. Aasen and T. V. Hansen, *Eur. J. Med. Chem.*, 2010, **45**, 3047-3055.
211. K. Yamamoto, T. Bruun, J. Y. Kim, L. Zhang and M. Lautens, *Org. Lett.*, 2016, **18**, 2644-2647.
212. G. Guisado-Barrios, J. Bouffard, B. Donnadieu and G. Bertrand, *Angew. Chem. Int. Ed. Engl.*, 2010, **49**, 4759-4762.

213. C. Song, Y. Ma, Q. Chai, C. Ma, W. Jiang and M. B. Andrus, *Tetrahedron*, 2005, **61**, 7438-7446.
214. P. Eisenberger, B. P. Bestvater, E. C. Keske and C. M. Crudden, *Angew. Chem. Int. Ed.*, 2015, **54**, 2467-2471.
215. C. M. So, W. K. Chow, P. Y. Choy, C. P. Lau and F. Y. Kwong, *Chem. Eur. J*, 2010, **16**, 7996-8001.
216. I. J. S. Fairlamb, A. R. Kapdi and A. F. Lee, *Org. Lett.*, 2004, **6**, 4435-4438.
217. S. A. Van Arman, A. J. Zimmet and I. E. Murray, *J. Org. Chem.*, 2016, **81**, 3528-3532.
218. D. A. Chaudhari and R. A. Fernandes, *J. Org. Chem.*, 2016, **81**, 2113-2121.
219. CrysAlisPro, 2013, **Version 1.171.36.28**, Agilent Technologies.
220. G. M. Sheldrick, *Acta Crystallogr. Sect. A: Found. Crystallogr.*, 2008, **64**, 112-122.
221. G. M. Sheldrick, *Acta Crystallogr., Sect. A: Found. Adv.*, 2015, **71**, 3-8.
222. G. M. Sheldrick, *Acta Crystallogr., Sect. C: Struct. Chem.*, 2015, **71**, 3-8.
223. O. V. Dolomanov, L. J. Bourhis, R. J. Gildea, J. A. K. Howard and H. Puschmann, *J. Appl. Crystallogr.*, 2009, **42**, 339-341.